
Doctoral Dissertations

Student Theses and Dissertations

Fall 2013

Shear and fracture behavior of high performance concretes

Mahdi Arezoumandi

Follow this and additional works at: https://scholarsmine.mst.edu/doctoral_dissertations



Part of the [Civil Engineering Commons](#)

Department: Civil, Architectural and Environmental Engineering

Recommended Citation

Arezoumandi, Mahdi, "Shear and fracture behavior of high performance concretes" (2013). *Doctoral Dissertations*. 2258.

https://scholarsmine.mst.edu/doctoral_dissertations/2258

This thesis is brought to you by Scholars' Mine, a service of the Missouri S&T Library and Learning Resources. This work is protected by U. S. Copyright Law. Unauthorized use including reproduction for redistribution requires the permission of the copyright holder. For more information, please contact scholarsmine@mst.edu.

SHEAR AND FRACTURE BEHAVIOR OF HIGH PERFORMANCE
CONCRETES

by

MAHDI AREZOUMANDI

A DISSERTATION

Presented to the Faculty of the Graduate School of the
MISSOURI UNIVERSITY OF SCIENCE AND TECHNOLOGY

In Partial Fulfillment of the Requirements for the Degree

DOCTOR OF PHILOSOPHY

in

CIVIL ENGINEERING

2013

Approved by:

Jeffery S. Volz, Advisor
John J. Myers
David N. Richardson
Mohamed A. Elgawady
K. Chandrashekhara

© 2013

MAHDI AREZOUMANDI
All Rights Reserved

PUBLICATION DISSERTATION OPTION

This dissertation has been prepared in the style such that the individual sections may be submitted for publication in the *Journal of Structural Engineering* and the *Journal of Materials in Civil Engineering*, both published by the American Society of Civil Engineers (ASCE).

Paper I, pages 23-55, manuscript entitled “Shear Behavior of High-Volume Fly Ash Concrete versus Conventional Concrete - Experimental Study” was accepted for publication in the *Journal of Structural Engineering*. Paper II, pages 56-84, manuscript entitled “Shear Behavior of High-Volume Fly Ash Concrete versus Conventional Concrete” and paper III, pages 85-113, manuscript entitled “Shear Strength of Chemically-Based Self-Consolidating Concrete Beams – Fracture Mechanics Approach vs. Modified Compression Field Theory” were both accepted for publication in the *Journal of Materials in Civil Engineering*.

Three companion papers investigating the bond behavior of both high-volume fly ash concrete and self-consolidating concrete are included in the Appendices. The testing that served as the background for these manuscripts was completed by other researchers at Missouri S&T, but the author analyzed and evaluated the results and served as the primary/secondary author for these papers.

ABSTRACT

Concrete is the most widely used man-made material in the world. Like other materials, it has been improved over time. Nowadays, with continued development of science and technology, a new generation of concretes is produced and is termed high performance concretes. A review of previously published work indicates that very few studies (in some cases none) have addressed the structural behavior of full-scale, high performance concrete elements. This study investigated the shear and fracture behavior of two types of high performance concrete – high-volume fly ash concrete (HVFAC) and self-consolidating concrete (SCC). The HVFAC incorporates up to 70% cement replacement with fly ash, and the SCC is based on using only chemical admixtures to convert a conventional concrete (CC) mix to a SCC mix with all of the necessary passing, filling, flowability, and stability requirements typically found in SCC.

This experimental program consisted of 16 shear beams (12 without shear reinforcing and four with shear reinforcing in the form of stirrups) and also 16 fracture mechanics beams for each type of concrete investigated (HVFAC and SCC). Additionally, three different longitudinal reinforcement ratios were evaluated within the test matrix of shear beams. The shear beams were tested under a simply supported four-point loading condition. Results of this study showed that the HVFAC had higher shear strength and fracture energy compared with the CC, while the SCC showed higher fracture energy, but the same shear strength as the CC.

ACKNOWLEDGMENTS

My advisor, Dr. Jeffery Volz, is an outstanding professor and excellent researcher. Words cannot express how grateful I am to have such an amazing advisor. He is higher than every standard you can consider for a teacher or researcher. I thank him for all that he taught me and undoubtedly, he is one of my best friends.

I would like to express my sincere gratitude to my lovely wife, Sara Tabatabaei. I owe her a lot, since I was in my office or High-Bay lab most of the weekends in the last two years, instead of spending time with her.

I would like to express my everlasting love to my parents, brother, and sisters for their supports.

Special thanks to my advisory committee members, Dr. John J. Myers (for his valuable comments in our papers), Dr. David Richardson, Dr. Mohamed A. ElGawady, Dr. K. Chandrashekhara, and my advisor, Dr. Jeffery S. Volz, for their time to review this document.

My thanks to my wonderful colleagues Amanda Steele, Ben Gliha, Brian Tucker Carlos Ortega, Eric Sells, Hesham Tuwair, Ish Keener, Jonathan Drury, Krista Porterfield, Kyle Holman, Mostafa Fakharifar, Nichole Podhorsky, Trevor Looney, Wei Wang, and Zach Carter.

My sincere appreciation to Gary Abbott, John Bullock, Jason Cox, Michael Lusher, Scott Parker, and Brian Swift for their technical assistance and help.

Last but not least, I would like to thank our sponsors MoDOT and BASF company.

TABLE OF CONTENTS

	Page
PUBLICATION DISSERTATION OPTION	iii
ABSTRACT.....	iv
ACKNOWLEDGMENTS	v
LIST OF ILLUSTRATIONS.....	x
LIST OF TABLES.....	xi
NOMENCLATURE	xii
SECTION	
1. INTRODUCTION	1
1.1. BACKGROUND	1
1.2. OBJECTIVE AND SCOPE OF WORK.....	2
1.3. DISSERTATION OUTLINE	2
2. LITERATURE REVIEW	4
2.1. HIGH-VOLUME FLY ASH CONCRETE	4
2.1.1. General	4
2.1.2. Shear Behavior	5
2.1.3. Fracture Energy	6
2.2. CHEMICALLY-BASED SELF CONSOLIDATING CONCRETE.....	6
2.2.1. General	6
2.2.2. Shear Behavior	7
2.2.3. Fracture Energy	8
2.3. SHEAR IN CONVENTIONAL CONCRETE	8
2.3.1. Factors Effecting Shear Behavior.....	8
2.3.2. Basic Shear Transfer Mechanisms	10
2.3.3. Shear Design Principles.....	11
2.3.3.1. Truss model.....	11
2.3.3.2. Strut and tie model.....	13
2.3.3.3. Modified compression field theory.....	15
2.3.3.4. Fracture mechanics approach.....	16
REFERENCES	18

PAPER

I. SHEAR BEHAVIOR OF HIGH-VOLUME FLY ASH CONCRETE VERSUS CONCRETE – EXPERIMENTAL STUDY	23
Abstract	23
Introduction.....	24
Research Significance.....	26
Experimental Program	26
Specimen Design	26
Materials	27
Mixture Proportions.....	27
Fabrication and Curing of Test Specimens.....	28
Test Setup and Procedure	28
Test Results, Analysis, and Discussion	28
Test Results.....	28
General Behavior (Cracking and Failure Mode)	29
Comparison of Test Results with Shear Provisions of Applicable Standards	30
Comparison of Test Results with Shear Test Database	32
Statistical Data Analysis	32
Fracture Mechanics Testing and Discussion	34
Comparison of Reinforcement Strains from Experiment and AASHTO LRFD (2010)	35
Conclusions and Recommendations	35
Acknowledgment.....	37
References.....	37
II. SHEAR BEHAVIOR OF HIGH-VOLUME FLY ASH CONCRETE VERSUS CONVENTIONAL CONCRETE	56
Abstract	56
Introduction.....	57
Experimental Program	58
Specimen Design	58
Materials	59
Mixture Proportions.....	59
Fabrication and Curing of Test Specimens.....	60

Fresh and Hardened Properties	60
Test Setup and Procedure	60
Test Results and Discussion	61
General Behavior (Cracking and Failure Mode)	61
Standard Provisions for the Shear Capacity of Concrete Beams.....	62
American Concrete Institute (ACI 318 (2008)).....	62
American Association of State Highway Transportation Officials, Load and Resistance Factor Design (AASHTO LRFD (2007))	63
Comparison of Test Results with Shear Provisions of ACI 318 (2008) and AASHTO LRFD (2007).....	63
Statistical Data Analysis	64
Parametric Test	64
Nonarametric Test.....	65
Comparison of Test Results with Shear Test Database	65
Comparison of Reinforcement Strains from Experiment and AASHTO LRFD (2007)	66
Conclusions and Recommendations	66
Acknowledgment	67
References.....	68
III. SHEAR STRENGTH OF CHEMICALLY-BASED SELF-CONSOLIDATING CONCRETE BEAMS –FRACTURE MECHANICS APPROACH VS. MODIFIED COMPRESSION FIELD THEORY	85
Abstract	85
Introduction.....	85
Experimental Program	87
Specimen Design	87
Materials and Concrete Mixture Proportions.....	88
Fabrication and Curing of Test Specimens.....	89
Test Setup and Procedure	89
Test Results and Discussion	89
General Behavior (Cracking and Failure Mode)	90
Comparison of Test Results with Shear Provisions of Applicable Standards	92
Comparison of Test Results with Fracture Mechanics Approaches	93
Comparison of Test Results with MCFT Method	94

Comparison of Test Results with Shear Test Database	95
Conclusions and Recommendations	95
Acknowledgment	96
References.....	97
SECTION	
3. SUMMARY, CONCLUSIONS AND RECOMMENDATIONS	114
3.1. SUMMARY OF RESEARCH WORK.....	114
3.2. CONCLUSIONS	114
3.2.1. Shear Behavior of HVFAC	114
3.2.2. Shear Behavior of SCC	115
3.2.3. Fracture Energy of HVFAC	117
3.2.4. Fracture Energy of SCC	117
3.3. RECOMMENDATIONS.....	117
APPENDICES	
A. AN EXPERIMENTAL STUDY ON BOND STRENGTH OF REINFORCING STEEL IN HIGH-VOLUME FLY ASH CONCRETE	118
B. AN EXPERIMENTAL STUDY ON BOND STRENGTH OF REINFORCING STEEL IN SELF-CONSOLIDATING CONCRETE.....	150
C. A COMPARATIVE STUDY OF THE BOND STRENGTH OF REINFORCING STEEL IN HIGH-VOLUME FLY ASH CONCRETE AND CONVENTIONAL CONCRETE	177
D. MECHANICAL PROPERTIES OF HVFAC.....	201
E. MECHANICAL PROPERTIES OF SCC	206
F. SHEAR TEST DATA OF HVFAC.....	213
G. SHEAR TEST DATA OF SCC	223
H. FRACTURE ENERGY TEST DATA OF HVFAC	233
I. FRACTURE ENERGY TEST DATA OF SCC.....	239
J. STATISTICAL DATA ANALYSIS OF HVFAC	245
K. STATISTICAL DATA ANALYSIS OF SCC.....	249
VITA	253

LIST OF ILLUSTRATIONS

Figure	Page
PAPER I	
1- Cross sections and reinforcement layout of the beams.....	50
2- Load pattern and location of strain gauges on the test beams	51
3- Crack pattern of the beams at shear failure (Study B).....	52
4- Load-deflections of the beams (Study B).....	53
5- Shear strength vs. longitudinal reinforcement ratio; results from (Reineck et al. 2003) and test results of this study.....	54
6- Shear strength vs. longitudinal reinforcement ratio; results from (Reineck et al. 2003) ($2.9 \leq \frac{a}{d} \leq 3.4$) and test results of this study	55
PAPER II	
1- Cross sections and reinforcement layout of the beams.....	79
2- Load pattern and location of strain gauges on the test beams	80
3- Crack pattern of the beams at shear failure	81
4- Load-deflections of the beams.....	82
5- Shear strength vs. longitudinal reinforcement ratio; results from (Reineck 2003) and test results of this study	83
6- Shear strength vs. longitudinal reinforcement ratio; results from (Reineck et al. 2003) ($2.9 \leq \frac{a}{d} \leq 3.4$) and test results of this study.....	84
PAPER III	
1- Load pattern, cross sections, reinforcement layout, and location of strain gauges on the test beams.....	108
2- Crack pattern of the beams at shear failure	109
3- Load-deflections of the beams.....	110
4- Comparison of shear strength of experiment with fracture mechanics approaches and MCFT method.....	111
5- Load-deflections of the beams (test and MCFT method).....	112
6- Shear strength vs. longitudinal reinforcement ratio; results from (Reineck 2003) and test results of this study	113

LIST OF TABLES

Table	Page
PAPER I	
1- Shear beams test matrix	41
2- Physical properties and chemical compositions of cement and fly ash.....	42
3- Mechanical properties of reinforcing steel	43
4- Mixture proportions of concrete	44
5- Fresh and hardened concrete properties	45
6- Test results summary	46
7- Comparison of shear strength of experiment and codes (Study A).....	47
8- Comparison of shear strength of experiment and codes (Study B).....	48
9- Comparison of reinforcement strain from experiment and AASHTO-LRFD (2010) equation (μ strain).....	49
PAPER II	
1- Shear beams test matrix	71
2- Physical properties of cement and fly ash	72
3- Chemical composition of cement and fly ash.....	73
4- Mixture proportions of concrete	74
5- Fresh and hardened concrete properties	75
6- Test results summary	76
7- Comparison of shear strength of experiment and codes.....	77
8- Comparison of reinforcement strain from experiment and AASHTO-LRFD-07 equation.....	78
PAPER III	
1- Shear beams test matrix	101
2- Mechanical properties of reinforcing steel	102
3- Mixture proportions of concrete	103
4- Fresh mixture properties	104
5- Test results summary	105
6- Maximum strains of longitudinal reinforcement at shear failure (μ mm/mm)	106
7- Comparison of shear strength of experiment and codes.....	107

NOMENCLATURE

Symbol	Description
A_s	Area of longitudinal reinforcement
A'_s	Area of compression reinforcement
A_v	Steel vertical reinforcement area
$A_{v,min}$	Minimum shear reinforcement area
a	Aggregate size
a	Shear span
\underline{a}	Critical crack length
a/d	Shear span-to-depth ratio
a_0	Notch depth
a_0/d	Notch depth-to-depth ratio
a_g	Aggregate size (AASHTO LRFD, 2004)
a_s	Shear span
b	Width of cross-section
b_v	Effective width of cross-section
b_w	Width of cross-section
D_{max}	Aggregate size
d	Effective depth of cross-section
d_{agg}	Aggregate size
d_v	Effective shear depth
E_c	Modulus of elasticity of the concrete
E_s	Modulus of elasticity of the steel
f'_c	Compressive strength of the concrete
f_{ct}	Tensile strength of the concrete
f_t	Splitting tensile strength of the concrete
f_y	Yield stress of steel
f_{yt}	Yield stress of transverse steel reinforcement
G_F	Fracture energy (Work-of-fracture method)

h	Height of cross-section
L	Length of the beam
M_n	Nominal moment capacity
M_u	Factored shear moment
P	Maximum load at failure
s	Center-to-center spacing of steel stirrups
V	External shear force
V_c	Concrete contribution to shear strength
V_{cr}	Ultimate shear force
V_s	Steel contribution to shear strength
V_{test}	Experimentally determined total shear resistance
V_u	Factored shear force
v	Shear stress
v_{ci}	Shear transferred by aggregate interlock
$v_{ci,max}$	Maximum shear transferred by aggregate interlock
w/c	Water-to-cement ratio
w/cm	Water-to-cementitious material ratio
α_0	Aggregate shape factor
ϵ_c	Compressive strain in the concrete
ϵ_s	Measured longitudinal strain at the center of gravity at the bottom steel reinforcement
ϵ_s	Strain in the tension reinforcement
θ	Shear crack angle
θ_c	Shear crack angle
ρ_L	Longitudinal reinforcement ratio
ρ_s	Longitudinal reinforcement ratio
ρ_v	Transverse reinforcement ratio
ρ_w	Longitudinal reinforcement ratio
ρ_x	Longitudinal reinforcement ratio

1. INTRODUCTION

1.1. BACKGROUND

Concrete is the most widely used man-made material in the world. Like other materials, it has been improved over time. Nowadays, with continued development of science and technology, a new generation of concretes is produced and is termed high performance concretes. A review of previously published work indicates that very few studies (in some cases none) have addressed the structural behavior of full-scale, high performance concrete elements. This project intends to investigate the shear and fracture behavior of two types of high performance concrete – high-volume fly ash concrete (HVFAC) and self-consolidating concrete (SCC).

Recently, there has been an increasing trend toward the use of sustainable materials. Sustainability helps the environment by reducing the consumption of non-renewable natural resources. Concrete uses a significant amount of non-renewable resources. Cement production – the essential ingredient in the production of concrete – also accounts for a significant amount of global carbon dioxide emissions from industry. One of the solutions for this global concern is the use of supplementary cementitious materials as replacement of cement, such as fly ash. Using fly ash in concrete not only helps the environment but also makes the concrete more economical, and, in many instances, more durable. HVFAC is generally defined as a concrete with at least 50% fly ash as a cement replacement.

SCC is a highly workable concrete that can spread under its own weight without segregation and bleeding, and it thus has the potential to significantly reduce costs associated with concrete construction. In general, SCC has the following advantages over conventional concrete (CC):

- decreased labor and equipment costs during concrete placement;
- decreased potential for (and costs to repair) honeycombing and voids;
- increased production rates of precast and cast-in-place elements; and
- improved finish and appearance of cast and free concrete surfaces.

However, SCC is not without its problems, which can include increased creep and shrinkage, as well as decreased bond and shear strength depending on the approach used to develop the particular mix design.

1.2. OBJECTIVE AND SCOPE OF WORK

The main *objective* of this research study was to evaluate the shear and fracture behavior of two high performance concretes – HVFAC and SCC – and determine if a possible correlation exists between these two engineering properties. The HVFAC test program included shear and fracture specimens constructed with a concrete mix that used 70% cement replacement with Class C fly ash. The SCC test program included shear and fracture specimens constructed with an SCC mix design that used only chemically admixtures to obtain the necessary passing, filling, flowability, and stability requirements typically found in SCC.

The following scope of work was implemented in an effort to attain this objective: (1) review applicable literature; (2) develop a research plan; (3) design, construct, and test full scale beam shear test specimens; (4) compare beam shear test results with design standards and shear test database; (5) design, construct, and test fracture mechanics test specimens; (6) compare fracture mechanics test results with design standards and fracture mechanics database; (7) evaluate correlation between fracture energy and shear strength; (8) perform detailed statistical analyses of test data; (9) summarize findings and develop conclusions and recommendations; (10) prepare this thesis in order to document the information obtained during this study.

1.3. DISSERTATION OUTLINE

This thesis includes three sections and nine appendices. Section 1 gives a brief introduction to the subject area and explains the need for the current research study. The first section also presents the objective and scope of work of the study, as well as a detailed literature review to establish the state-of-the-art on the proposed topic.

Section 2 presents three published journal papers discussing the shear response and fracture energy of HVFAC and SCC.

Section 3 summarizes the findings and conclusions of this study and proposes future research.

The appendices include three companion papers on bond and fracture energy also published by the author as well as detailed test data from the research study.

2. LITERATURE REVIEW

The purpose of this task is to conduct a comprehensive literature review of previous research on two types of high performance concrete – HVFAC and SCC – with particular attention on the structural behavior.

2.1. HIGH-VOLUME FLY ASH CONCRETE

2.1.1. General. Concrete is the most widely used man-made material in the world, and cement is an essential ingredient in the production of Portland cement concrete. The cement industry plays a key role in the world, from both an economic and an environmental perspective. In 2011, world cement output was estimated at 3.4 billion metric tons (USGS 2012). Cement production is also a relatively significant source of global carbon dioxide (CO₂) emissions, accounting for approximately 4.5% of global CO₂ emissions from industry in 2007 (Marland et al. 2008). According to the World Business Council for Sustainable Development (WBCSD), emissions from cement manufacturing vary across worldwide regions from 0.73 to 0.99 kg (lb) of CO₂ for each kilogram (pound) of cement produced (Hanle et al. 2012).

One of the solutions for this global concern is the use of supplementary cementitious materials as replacement of cement. The most available supplementary cementitious material worldwide is fly ash, a by-product of coal-burning thermal power stations (Bilodeau et al. 2000). ASTM C618 (2012) defines fly ash as “the finely divided residue that results from the combustion of ground or powdered coal and that is transported by flue gasses.” Fly ash is categorized in three classes: class N, F, and C based on the chemical compositions (ACI 232.2R 2003).

Fly ash has been used in the U.S. since 1930; Davis et al. (1937) were the first researchers to publish their results about using fly ash in concrete (ACI 232.2R 2003). Initially, fly ash was used in massive structures like the Thames Barrage in the U.K. and the Upper Stillwater Dam in the U.S., with about 30 to 75% mass replacement of hydraulic cement to reduce heat generation (ACI 232.2R 2003). Subsequent research

(Dunstan 1976, 1980, 1984) has shown several beneficial aspects of using fly ash in concrete such as low permeability and high durability.

Traditionally, fly ash used in structural concrete as a replacement or supplementary material has been limited to 15% to 25% cement replacement (ACI Committee 211, 1993; Berry et al. 1994), except in high strength concrete (HSC) where replacement levels of Portland cement at 35% are more common to control peak hydration temperature development (Myers et al. 1999). When a significant amount of fly ash is used, how it contributes to the strength development of the concrete and the hydration characteristics of this type of material are of significant research interest. High-volume fly ash concrete (HVFAC) is a concrete generally defined as that with at least 50% of the Portland cement replaced with fly ash. In 1986, the Canadian Centre for Mineral and Energy Technology (CANMET) developed HVFAC for structural applications. The investigations by CANMET (Malhotra 1986) and also other researchers (Gopalan 1993) have shown that HVFAC has lower shrinkage, creep and water permeability and higher modulus of elasticity compared with conventional concrete (CC).

2.1.2. Shear Behavior. Comprehensive research has been completed on both the fresh and hardened properties of HVFAC, but very little research has been performed on the structural behavior of HVFAC. Rao et al. (2011) performed tests on four beams constructed with 50% Class F fly ash replacement of cement. The beams had no shear reinforcement, longitudinal steel ratios of 0.6%, 1.0%, 2.0%, and 2.9%, and shear span-to-depth ratios of 2.5. The results indicated shear strengths approximately 5% lower than conventional concrete. However, the specimens used by Rao et al. measured only 4 in. x 8 in. in cross section, significantly less than what would be termed full-scale specimens, and unlike many other materials, the shear performance of reinforced concrete is affected by what is termed the “size effect,” meaning that results are not generally scalable. Koyama et al. (2008) studied shear behavior of beams with 25% and 50% fly ash replacement of the fine aggregate, which corresponds to 46% and 61% equivalent replacement of cement with fly ash. The beams had a cross section of 10 in. x 16 in. and span lengths ranging from 14 in. to 28 in. For the 46% fly ash replacement level, the test results indicated shear strengths ranging from 91% to 110% of design code predicted strengths for conventional concrete, while for the 61% fly ash replacement level, the test

values ranged from 92% to 135% of design code predicted strengths. However, the beams had shear span-to-depth values of 1.0, 1.5, and 2.0, classifying them all as “deep beams” with respect to shear behavior, and the majority of actual structures have beam depths that result in diagonal tension (beam shear) behavior. In 2005, Cross et al. investigated the performance of three simply supported reinforced concrete beams measuring 6 in. x 10 in. in cross section and constructed with a mixture containing 100% fly ash replacement of cement. However, all of the beams were designed to fail in flexure.

2.1.3. Fracture Energy. Lam et al. (1998) evaluated the effects of replacing cement with fly ash and silica fume on fracture behavior of concrete. Their investigation contained high volumes of fly ash with or without the addition of small amounts of silica fume. HVFAC showed similar or higher fracture energy compared with CC. A relatively small amount of silica fume increased the brittleness of the concrete but had a positive effect on fracture toughness (K_{IC}) although it did not necessarily produce higher work of fracture (G_F) values.

Wong et al. (1999) investigated the effect of fly ash on fracture properties of concrete with fly ash replacements from 15 to 55% by mass of cement. They reported that a 15% fly ash replacement increased the fracture toughness. However, fly ash replacements at higher levels (45 and 55%) reduced the fracture toughness at 28 days, but recovered almost all the reduction at later age (90 days) and at times even went higher. Fly ash replacement at all levels studied increased the interfacial fracture energy.

2.2. CHEMICALLY-BASED SELF CONSOLIDATING CONCRETE

2.2.1. General. Self-consolidating concrete (SCC) is a highly workable concrete that can spread under its own weight without segregation and bleeding. SCC was developed in Japan in the early 1980's by Okamura and colleagues at Tokyo University (Ozawa et al. 1989). The motivation for this development was a lack of skilled workers for consolidating concrete to form durable concrete structures (Daczko et al. 2006).

Like many new products, SCC was slow to gain popularity. It was used for the first time on a large scale for the Akashi-Kaikyo bridge in Japan in 1998 (Okamura

1997). It began to spread in Asian and European countries before the United States, where it finally gained acceptance around the year 2000 (Daczko et al. 2006). SCC has become more popular because of several advantages including reduced labor, equipment, job noise, and time of construction. The enhanced flowability also aids in filling densely reinforced members and very complex formwork shapes (ACI 237R-07).

2.2.2. Shear Behavior. Comprehensive research has been done on both fresh and hardened properties of SCC, but relatively little research have been performed on the structural behavior of SCC. With regard to shear behavior, results from multiple researchers have shown somewhat conflicting results. Das et al. (2005) found that SCC beams had higher shear strength compared to conventional concrete (CC). Wilson et al. (2005) reported, however, that shear provisions as included in ACI 318-11 did not always yield conservative results for SCC beams. Test results from Burgueno and Bendert (2005, 2006A, 2006B) showed that the shear behavior of both SCC and CC beams are very similar to each other. In addition, the ultimate shear strength of SCC and CC beams were almost the same. Hassan et al. (2008, 2010) and also Choulli (2005) reported there was no significant difference between the shear behavior of SCC and CC beams, and that the ultimate shear strength of SCC beams was only slightly lower than CC beams. Dymond (2007) tested a single, precast bulb-tee bridge girder and concluded that the theoretical prediction of the simplified method was conservative compared with experimental test results of the beam. These somewhat conflicting results are likely due to the wide range of potential mix designs available for SCC, and with only limited information provided by the researchers cited above, it is impossible to determine what lead to these particular results. However, with aggregate interlock playing such a critical role in shear behavior (Taylor 1970, 1972), SCC mixes that rely on material-based changes – higher paste contents and smaller rounded aggregates – may result in substantially reduced shear strengths.

The potential for significant variation in shear strength between different SCC mixes has to do with the variety of approaches available to obtain the necessary flowability of the concrete. In general, there are three different approaches to developing an SCC mix. The first is material-based, the second is chemically-based, and the third is a hybrid of the first two. The first approach focuses on modifying the aggregate types and

amounts. Typically, the coarse aggregate content is reduced and also rounder aggregate is used to improve the flowability of the SCC mix (ACI 237R-07). The main disadvantage of this approach is that with a lower coarse aggregate content, aggregate interlock, and as a result shear strength, is potentially reduced. To avoid this issue, the second approach was developed and, in this approach, the coarse aggregate and paste contents are kept the same as in a CC mix. To improve the flowability and stability of this type of mix, high-range water-reducing admixtures (HRWRA) and viscosity-modifying admixtures (VMA) are used (ACI 237R (2007)). The third approach combines both modifications to the aggregate type or amount as well as the addition of HRWRA and possibly VMA to obtain the desired behavior.

All of the aforementioned previous researchers studied shear behavior of SCC that used the first or third approaches for SCC mix design. The current study presents the results of an experimental investigation that examines the shear strength of full-scale SCC beams constructed with a chemically-based mix.

2.2.3. Fracture Energy. Fava et al. (2003) tested the fracture energy of both SCC and CC using the traditional notched specimen tested in three point bending. They reported similar fracture behavior in terms of fracture energy in the SCC and CC specimens.

Zhao et al. (2005) measured the toughness and fracture toughness for four different SCC mixes. They obtained similar toughness values for the SCC mixes and CC.

2.3. SHEAR IN CONVENTIONAL CONCRETE

2.3.1. Factors Effecting Shear Behavior. Shear strength is controlled by the presence of web reinforcement, longitudinal reinforcement, coarse aggregate size, presence of axial loads, depth of the member, tensile strength of the concrete, and shear span to depth ratio (a/d). Some of these parameters are included in design equations and others are not.

Web reinforcement, typically called stirrups, is used to increase the shear strength of concrete beams and to ensure flexural failure. This is necessary due to the explosive and sudden nature of shear failures, compared with flexural failures which tend to be

more ductile. Web reinforcement is normally provided as vertical stirrups and is spaced at varying intervals along a beam depending on the shear requirements. Alternatively, this reinforcement may be provided as inclined longitudinal bars. In general, small sized bars such as #3 and #4 are used in a U-shaped configuration that may be open or closed, or used as multiple legs.

Shear reinforcement has very little effect prior to the formation of diagonal cracks. However after cracking, the web reinforcement enhances the beam in the following ways (Nilson et al., 2004):

- The stirrups crossing the crack help in resisting the shear force.
- The stirrups restrict the growth of the cracks and reduce their penetration further into the compression zone.
- The stirrups oppose widening of the cracks, which helps to maintain aggregate interlock within the concrete.
- The presence of stirrups provides extra restraint against the splitting of concrete along the longitudinal bars due to their confinement effect.

The longitudinal reinforcement ratio (ρ_L) affects the extent and the width of the flexural cracks. If this ratio is small, the flexural cracks extend higher into the beam and open wider. When the crack width increases, the components of shear decrease, because they are transferred either by dowel action or by shear stresses on the crack surfaces.

The coarse aggregate type and size noticeably affect the shear capacity, especially for beams without stirrups. Lightweight aggregate has a lower tensile strength than normal aggregate. The shear capacity of a concrete beam with no stirrups is directly related to the tensile strength, therefore, the failure due to mortar cracking, which is more desirable, could be preceded by aggregate failure instead. The aggregate size also affects the amount of shear stresses transferred across the cracks. Large diameter aggregate increases the roughness of the crack surfaces, allowing higher shear stresses to be transferred (Wight and MacGregor, 2009).

Researchers have concluded that axial compression serves to increase the shear capacity of a beam while axial tension greatly decreases the strength. As the axial compressive force is increased, the onset of flexural cracking is delayed, and the flexural cracks do not penetrate as far as into the beam (Wight and MacGregor, 2009).

The size of the beam affects the shear capacity at failure. If the overall depth of a beam is increased, it could result in a smaller shear force at failure. The reasoning is that when the overall depth of a beam increases, so do the crack width and crack spacing, causing loss of aggregate interlock. This condition is known as a size effect.

The tensile strength of the concrete (f_{ct}) also affects the shear strength. Because of the low tensile strength of the concrete, diagonal cracking develops along planes perpendicular to the planes of principal tensile stress. The shear strength of an RC beam increases as the concrete material strength increases. The tensile strength of the concrete is known to have a great influence on the shear strength, but the concrete compressive strength (f'_c) is used instead in most shear strength formulas. This approach is used because tensile tests are more difficult to conduct and usually show greater scatter than compression tests.

The shear span to depth ratio (a/d) does not considerably affect the diagonal cracking for values larger than 2.5. The shear capacity increases as the shear span to depth ratio decreases. This phenomenon is quite significant in deep beams ($a/d \leq 2.5$) because a portion of shear is transmitted directly to the support by an inclined strut or arch action. For deep beams, the initial diagonal cracking develops suddenly along almost the entire length of the test region (Wight and MacGregor, 2009).

2.3.2. Basic Shear Transfer Mechanisms. The 1973 ASCE-ACI Committee 426 Report concluded that shear is transferred by the following four mechanisms: shear stress in the uncracked concrete, interface shear transfer, dowel action, and arch action. In a RC beam, after the development of flexural cracks, a certain amount of shear is carried by the concrete in the compression zone. The shear force carried by the uncracked concrete in the compression zone can be represented by the compressive strength of concrete and the longitudinal reinforcement ratio. Shear may continue to be transferred across a crack in the concrete by interface shear transfer, also known as aggregate interlock. Since the flexural crack width is approximately proportional to the strain of the tension reinforcement, the crack width at failure becomes smaller as the longitudinal reinforcement ratio is increased. It is also expected that the interlocking force will be increased when the compressive strength of the concrete is high. If longitudinal reinforcing bars cross a crack, dowel forces in the bars will resist shear displacement. The

dowel force induces tension in the surrounding concrete that may produce splitting cracks along the longitudinal reinforcement. Although there is some contribution in dowel action by the number and arrangement of longitudinal bars, spacing of flexural cracks, and the concrete cover, the main factors influencing this mechanism are the flexural rigidity of the longitudinal bars and the strength of the surrounding concrete. Arch action occurs where shear flow cannot be transmitted. Arch action is dominant in deep beams. For this mechanism to be developed, a tie is required to restrain the thrust developed as a result of the arch. For deep beams, failure is often due to anchorage failure of the bars restraining this thrust.

Shear can be carried through beam action, arch action or any combination of the two. When shear is carried through beam action, the tensile force in the reinforcement varies through bond stresses and plane sections remain plane. These are the normal assumptions of elastic beam theory.

The 1998 ASCE-ACI Committee 445 Report highlights a new mechanism, residual tensile stresses, which are transmitted directly across cracks. The basic explanation of residual tensile stresses is that when concrete first cracks, small pieces of concrete bridge the crack and continue to transmit tensile force as long as cracks do not exceed 0.00197-0.0059 in. in width. The application of fracture mechanics to shear design is based on the premise that residual tensile stress is the primary mechanism of shear transfer.

2.3.3. Shear Design Principles. The following section explains about different shear design principles.

2.3.3.1. Truss model. The truss method of analysis has for some time been accepted as an appropriate method for the design of structural concrete members comprising both reinforced and prestressed concrete elements, and now forms the basis of many design standard recommendations. The truss model was presented by the Swiss engineer Ritter (1899) to explain the flow of forces in cracked reinforced concrete. The principle of the truss model is based on the following assumptions: (1) the longitudinal tension reinforcement acts as a tension chord of the truss while the flexural compressive zone of the beam acts as the compression chord, and (2) the diagonal compressive

stresses act as diagonal members, and the stirrups are considered as vertical tension members.

Mörsch (1902), a German engineer, pointed out that the compression diagonals do not need to extend from the top of one stirrup to the bottom of the next stirrup, and that the stirrups represent a continuous field of stresses rather than discrete diagonal compressive struts. Mörsch and Ritter neglected the tensile stress in cracked concrete assuming that only after cracking the diagonal compression stresses would remain at 45 degrees. Mörsch also proposed truss models to explain the behavior of beams detailed with bent-up longitudinal reinforcing bars. He also used the principal stress trajectories as an indication of how tensile reinforcement should be proportioned and detailed in a region where the internal stress flow is complex.

The truss model is derived using the equilibrium condition between the external and internal forces. The shear stresses are assumed to be uniformly distributed over an effective shear area \mathbf{b}_w wide and \mathbf{d} deep. Between the external shear force \mathbf{V} , and the total diagonal compressive force, from which the principal compressive stress can be determined assuming a crack angle of 45 degrees.

The variable-angle truss model is derived from the Mörsch truss model. This model adds a concrete contribution to shear strength to compensate for the conservative nature of the model based on a variable angle of the crack (θ). In this model, the required magnitude of the principal compressive stress is determined from the equality between the resultant of the diagonal stresses and the projection of the shear force. The tensile force in the longitudinal reinforcement due to shear will be equal to the horizontal projection of the shear force.

Proportioning and detailing of the transverse reinforcement in members with a complex flow of internal stresses was a main aspect of structural concrete research in central Europe during the 1960s and 1970s. Leonhardt, from the University of Stuttgart in Germany, and Thürlimann and Müeller, from the Swiss Federal Institute of Technology in Zürich, were instrumental in the development of analysis and design methods for structural concrete regions with complex internal stress flows. Leonhardt focused mainly on the analysis and design of deep beams and anchorage end regions in post-tensioned beams. In most of his work, the detailing of the reinforcing steel closely followed the

principal tensile stress trajectories found from an elastic analysis of a homogeneous isotropic element. Thürlimann focused mainly on the application of the theory of plasticity in reinforced and prestressed concrete, with practical applications to the design for shear and torsion.

In the mid-1970s, Park and Paulay, from the University of Canterbury, extended many of the analytical and design concepts developed by Leonhardt to include, for the first time, the detailing of regions having a complex flow of stresses and subjected to cyclic load reversals caused by earthquake excitation (Park and Paulay, 1975). One of these regions is the joint between the beam and column in a moment resisting frame. In the analysis and design of beam-column joints, Park and Paulay deviated from Leonhardt's method by proposing a simple mechanism of shear transfer that did not follow the principal tensile stress trajectories shown by an elastic analysis. This model requires vertical and horizontal reinforcement to sustain the diagonal compressive field introduced into the joint as a result of bond forces from the outermost longitudinal column and beam bars.

The truss model is also the starting point of the shear friction model, also known as Loov's theory (1998), in which the shear forces are carried by stirrups and shear friction across the concrete crack. The method comprises the calculation of the shear capacity from all possible crack angles by identifying the weakest plane of failure. The force that holds the two surfaces together is equal to the yield stress multiplied by the cross-sectional area of any steel crossing the crack for bars perpendicular to the failure plane. In addition to the friction of the failure plane surface, the model accounts for shearing of the reinforcement and the dowel action that they generate. The main drawback to the use of the shear friction models for beam shear is that the critical failure plane is typically unknown, so an interactive approach must be conducted to find the weakest or most critical failure plane.

2.3.3.2. Strut and tie model. The Strut and Tie Model (STM) was developed in the late 1980s. It was formalized and popularized by Schlaich et al. in a comprehensive paper published in 1987. Reinforced concrete theory hinges on various assumptions of simple beam theory such as plane sections remaining plane. However, regions near a discontinuity do not satisfy this assumption and are called D-regions, which stand for

disturbed regions that do not follow simple beam theory. These regions extend approximately a distance h away from the discontinuity which may include concentrated loads, openings, or changes in the cross section. Entire beams consisting of a D-region are called deep beams. Regions in between these areas are subjected to typical beam behavior and are called B-regions. The STM was developed based on the truss model to account for these D-regions. They consist of struts, ties, and nodal zones.

Struts are internal concrete compression members which may be rectangular or bottle-shaped. Bottle-shaped struts swell throughout their depth, and are wider at the center than at the ends. Ties are tension members within the model and consist of steel reinforcement, plus the portion of concrete surrounding the steel. However, the model assumes that the steel carries all of the tension force. Nodal zones are regions where struts, ties, and concentrated loads meet. Nodes are classified by the types of forces passing into them, which create four types: (a) C-C-C, (b) C-C-T, (c) C-T-T, and (d) T-T-T, where C represents compression and T represents tension.

The following procedure is used to develop a STM:

- Defining of the D-region; borders and forces within these boundaries.
- Drawing a STM based on the assumed node geometry.
- Solving for the truss member forces.
- Calculating the reinforcement layout providing the required tied capacity and enough anchorage length for the bars to ensure the correct behavior at the nodes.
- Dimensioning nodes using truss member forces obtained previously.
- Repeating analysis for the new geometry in order to find a converged solution.

The STM method is not always trouble-free and has many uncertainties. There are four major problems in developing STM, and these are:

- Uncertainties in obtaining dimensions, stiffness, and effective strength of strut, ties, and nodes for the truss models.
- Need to select the optimal STM and iteratively adjust and refine the truss geometry.
- Need to combine different load cases.
- Multiple potential solutions for statically indeterminate models.

The creation of the strut and tie model offers no unique solution, and more than one admissible model may be valid for a given problem. The STM must be statically admissible, thus, in equilibrium with the external loads, reactions and nodes. Design takes place by selecting the amount of steel for the tension ties, effective width of the strut, and shape of the nodal zone such that the strength is adequate.

Previous researchers (Kani, 1967) have found that beams with shear span-to-depth ratios greater than 2.5 are governed by conditions away from the disturbed regions adjacent to the support and the loads. In this range, the strength of the beam is not influenced by details such as the size of the bearing plates, and the strength decreases by only a small amount as the shear span increases. Collins and Mitchell (1997). This study shows that a beam can resist a higher shear force if the shear is produced by a load that is closer to the support. This series of beams was tested by Kani (1967), and based on the observation of the results, it was concluded that the shear strength was reduced by a factor of about 6 as the shear span-to-depth ratio decreased from 1 to 7 (Collins and Mitchell, 1997). This result can be explained by the fact that deep beams carry the load by strut-and-tie action, and as the applied load moves closer to the support, the angle of the compression strut increases, reducing the force (stress) in the strut, and thus increasing the capacity of a given cross section. Typical failure mode of these beams involves crushing of the concrete strut.

2.3.3.3. Modified compression field theory. The Modified Compression Field Theory (MCFT) was developed by Vecchio and Collins in 1986, and is a further development of the Compression Field Theory (CFT) derived by Collins and Mitchell in 1980. In the CFT it is assumed that the principal tensile stress is zero after the concrete has cracked while in the MCFT the effect of the residual stress in the concrete between the cracks is taken into account. Tensile stresses across the diagonal struts increase from zero at the cracks to a maximum in the middle of the strut.

The MCFT model consists of strain compatibility and equilibrium equations which can be used to predict the complete shear deformation response. All the compatibility equations are expressed in terms of average strains measured over base lengths long enough to include several cracks.

Collins and Mitchell (1991) noted that expresses shear resistance in terms of the sum of the concrete and steel contributions, as the traditional or classical method. The concrete contribution depends on the average tensile stresses in the concrete, and the steel contribution depends on the tensile stresses in the stirrups. It must be clarified that although the MCFT and the truss model approaches might seem to be similar, the concrete contribution from the concrete suggested by the MCFT is not constant as assumed in the classical truss model. The shear contribution of the concrete (V_c) in the MCFT is not equal to the shear strength of a similar member without shear reinforcement. According to the MCFT, the contribution of the concrete is a function primarily of the crack width. Increasing the number of stirrups reduces the crack spacing, this decreases the crack width and thus increases the concrete contribution.

One of the most important features of the MCFT is the average strain-stress relationships derived from the tests of reinforced panels subjected to pure shear (Vecchio and Collins, 1986). The concrete compressive strength is reduced to take into account softening due to transverse tensile strain (ε_1).

The stress and strain formulations adopted in the MCFT use average values, so local variations are not considered. In this methodology, a check must be done to ensure that the reinforcement can take the increment in tensile stress at the crack.

The MCFT can provide accurate predictions of shear strength and deformation. The first and most important assumption made in the MCFT is that of a rotating crack model in which previous cracks are assumed to be inactive. The MCFT assumes that the angles of the axes for the principal strains and principal stresses coincide (θ). The crack in which all the checks are performed is assumed to be oriented at the same angle, θ , as the compressive stress field.

2.3.3.4. Fracture mechanics approach. Numerous researchers (Bazant et al. 1984, 1987, 2005, Gustafsson et al. 1988, Jeng et al. 1989, So et al. 1993, Gastebled et al. 2001, Xu et al. 2012) have used fracture mechanics approaches to predict shear strength of reinforced concrete members without stirrups. Between 1984 and 2005, Bazant et al. (1984, 1987, 2005) developed different formulas based on fracture mechanics to predict the shear capacity of reinforced concrete members without stirrups. Bazant et al. (2005) proposed Equation 2 for shear strength of reinforced concrete

members without stirrups. Furthermore, Gasteblet et al. (2001) presented an analytical model (Equation 3) based on the required fracture energy for splitting tensile crack propagation that releases longitudinal reinforcement from surrounding concrete (Mode I fracture energy). More recently, Xu et al. (2012) proposed Equation 4 based on the required fracture energy to release interface bond resistance between steel and concrete (Mode II fracture energy).

$$V_c = 10\rho^{\frac{3}{8}} \left(1 + \frac{d}{a_s}\right) \sqrt{\frac{f'_c}{d}} b_w d \sqrt{1 + \frac{f_c'^{-\frac{2}{3}} 3800 \sqrt{d_a}}{d}} \quad (2)$$

$$V_c = \frac{1.109}{\sqrt{d}} \left(\frac{d}{a_s}\right)^{\frac{1}{3}} \rho^{\frac{1}{6}} (1 - \sqrt{\rho})^{\frac{2}{3}} f_c'^{0.35} \sqrt{E_s} b_w d \quad (3)$$

$$V_c = \frac{1.018}{\sqrt{d}} \left(\frac{d}{a_s}\right)^{\frac{1}{3}} \rho^{\frac{1}{6}} (1 - \sqrt{\rho})^{\frac{2}{3}} (0.0255f'_c + 1.024) b_w d \quad (4)$$

REFERENCES

- ACI Committee 211 (1993). "Guide for Selecting Proportions for High-strength Concrete with Portland Cement and Fly Ash," ACI 226.4R, ACI Material Journal, V. 90, pp. 272-283.
- ACI Committee 232 (2003). "Use of Fly Ash in Concrete" (ACI 232.2R-03). Farmington Hills, MI: American Concrete Institute.
- American Concrete Institute ACI Committee. (2007). "Self –Consolidating Concrete" ACI 237R-07, Farmington Hills, MI: American Concrete Institute.
- ASCE-ACI Task Committee 426, (1973). The Shear Strength of Reinforced Concrete Members. ASCE Journal of the Structural Division, Vol. 99, No. 6, pp. 1091-1187.
- ASCE-ACI Task Committee 445, (1998). Recent Approaches to Shear Design of Structural Concrete. ASCE Journal of Structural Engineering, Vol. 124, No. 12, pp. 1375-1417.
- ASTM C 618, (2012). "Standard Specification for Coal Fly Ash and Raw or Calcined Natural Pozzolan for Use in Concrete" ASTM, West Conshohocken, PA, 3 pp.
- Bažant, Z.P., and Yu, Q., (2005) "Design against Size Effect on Shear Strength of Reinforced Concrete Beams without Stirrups," Journal of Structural Engineering, ASCE, V. 131, No. 12, pp. 1877-1885.
- Bendert, D.A. and Burgueño, R. (2006A). "Report on the Experimental Evaluation of Prestressed Box beams for SCC Demonstration Bridge." Research Report CEE-RR-2006-01, Department of Civil and Environmental Engineering, Michigan State University, East Lansing, MI.
- Bendert, D.A. and Burgueño, R. (2006B). "Report on the Production of Prestressed Box beams for SCC Demonstration Bridge." Research Report CEE-RR-2006-02, Department of Civil and Environmental Engineering, Michigan State University, East Lansing, MI.
- Berry, E.E., Hemmings, R.T. , Zhang, M.H. , Cornelious, B.J. , Golden, D.M. (1994). "Hydration in High-volume Fly Ash Binders," ACI Materials Journal, V. 91, pp. 382-389.

Bilodeau, A. and Malhotra, V. M., (2000). "High-Volume Fly Ash System: Concrete Solution for Sustainable Development, ACI Materials Journal, V. 97, pp. 41-48.

Burgueño, R. and Till, R. (2005). "Special Provision for Production of Prestressed Beams with Self-Consolidating Concrete," Internal Report, Michigan Department of Transportation, Lansing, MI.

Choulli, Y. and Mari, A.R. (2005). "Shear Behaviour of full scale prestressed I beams made with Self Compacting Concrete," Proceedings Second North American Conference on the Design and Use of Self-Consolidating Concrete and the Fourth International RILEM Symposium on Self-Compacting Concrete, (CD-ROM), Chicago, Illinois.

Collins, M.P., and Mitchell, D., (1991). Prestressed Concrete Structures. Response Publications.

Cross, D., Stephens, J., and Vollmer, J., (2005). "Structural Applications of 100 Percent Fly Ash Concrete, Proceedings of the 2005 World of Coal Ash (WOCA), Lexington, KY, pp. 1-19.

Daczko, J. and Vachon, M. (2006). "Self Consolidating Concrete (SCC), Significance of Tests and Properties of Concrete and Concrete-Making Materials," STP 169D, ASTM International West Conshohocken, PA., pp. 637-645.

Das, D, Kaushik, S.K., Gupta V.K. (2005). "Shear Resistance of Self-Compacting concrete," Proceedings Second North American Conference on the Design and Use of Self-Consolidating Concrete and the Fourth International RILEM Symposium on Self-Compacting Concrete, (CD-ROM), Chicago, Illinois.

Dunstan, E. R. (1976). "Performance of Lignite and Sub-Bituminous Fly Ash in Concrete," Report No. REC-ERC-76, U.S. Bureau of Reclamation, Denver, Colo., 23 pp.

Dunstan, E. R. (1980). "A Possible Method for Identifying Fly Ashes That Will Improve the Sulfate Resistance of Concretes," Cement, Concrete, and Aggregates, V. 2, No. 1, Summer, pp. 20-30.

Dunstan, E. R. (1984). "Fly Ash and Fly Ash Concrete," Report No. REC-ERC-82-1, Bureau of Reclamation, Denver, Colo., 42 pp.

Dymond, B.Z. (2007). "Shear Strength of A PCBT-53 Girder Fabricated with Lightweight, Self-Consolidating Concrete," MS Thesis, Virginia Tech, Blacksburg, VA.

European Committee for Standardization. Eurocode No. 2 (2005). "Design of concrete structures. Part 1: General rules and rules for buildings."

Fava C, Bergol L, Fornasia G, Giangrasso F, Rocco C. (2003) "Fracture behaviour of self compacting concrete." In: Wallevik O, Nielsson I, editors. Proceedings of third RILEM international symposium on self compacting concrete Reykjavik Iceland. Bagnaux, France: RILEM Publications, PRO 33; 2003. p. 628–36.

Gastebled, O.J., and May, I.M., (2001) "Fracture Mechanics Model Applied to Shear Failure of Reinforced Concrete Beams without Stirrups," ACI Structural Journal, V. 98, No. 2, pp. 184-190.

Gopalan, M.K. (1993). "Nucleation and Pozzolanic Factors in Strength Development of Class F Fly Ash Concrete," ACI Materials Journal, V. 90, pp. 117-121.

Hanle, L., Jayaraman, K., and Smith, J. (2012) "CO₂ Emissions Profile of the U.S. Cement Industry," <http://infohouse.p2ric.org/ref/43/42552.pdf>, [March 2012].

Hassan, A.A.A., Hossain, K.M.A., and Lachemi, M. (2008). "Behavior of Full-Scale Self-Consolidating Concrete Beams in Shear," Cement & Concrete Composites. V. 30, No. 7, pp.588-596.

Hassan, A.A.A., Hossain, K.M.A., and Lachemi, M. (2010). "Strength, Cracking and Deflection Performance of Large-Scale Self-Consolidating Concrete Beams Subjected to Shear Failure," Engineering Structures, V. 32, No. 5, pp. 1262-1271.

Okamura, H. (1997). "Self-Compacting High-Performance Concrete," Concrete International, pp. 50-54.

Koyama, T., Sun, Y.P., Fujinaga, T., Koyamada, H., and Ogata, F. (2008). "Mechanical Properties of Concrete Beam Made of a Large Amount of Fine Fly Ash," Proceedings for the 14th World Conference on Earthquake Engineering, http://www.iitk.ac.in/nicee/wcee/article/14_05-03-0040.pdf, [March 2012].

Lam, L., Y. L. Wong, and C. S. Poon. (1998) "Effect of fly ash and silica fume on compressive and fracture behaviors of concrete." Cement and Concrete research 28.2, 271-283.

Malhotra, V.M. (1986). "Superplasticized Fly Ash Concrete for Structural Applications," Concrete International, V. 8, pp. 28- 31.

Marland, G., T.A. Boden, and R.J. Andres. (2008). "Global, Regional, and National Fossil Fuel CO₂ Emissions. In Trends: A Compendium of Data on Global Change," Carbon Dioxide Information Analysis Center, Oak Ridge National Laboratory, United States Department of Energy, Oak Ridge, Tenn., <http://cdiac.ornl.gov/trends/emis/overview.html>, [March 2012].

Myers, J.J., Carrasquillo, R.L., (1999) "Mix Proportioning for High-Strength HPC Bridge Beams," American Concrete Institute, Detroit, MI, American Concrete Institute Special Publication 189, pp. 37-56.

Nilson, A.H., Darwin, D., and Dolan, C.W., (2004). Design of Concrete Structures (13th Ed.). McGraw Hill.

Ozawa, K, Maekawa, K, Kunishima, M, and Okamura, H. (1989). "Development of High Performance Concrete Based on the Durability Design of Concrete Structures." In Proceedings of the Second East-Asia and Pacific Conference on Structural Engineering and Construction (EASEC-2), Vol. 1, pp. 445-450.

Park, R., and Paulay, T., (1975). Reinforced Concrete Structures. John Wiley & Sons.

Rao, R. M., Mohan, S., and Sekar, .S.K, (2011). "Shear Resistance of High Volume Fly ash Reinforced Concrete Beams without Web Reinforcement," International Journal of Civil and Structural Engineering, V. 1, No. 4, pp. 986-993.

Taylor, HPJ. (1970). "Investigation of the forces carried across cracks in reinforced concrete beams in shear by interlock of aggregate," Cement and Concrete Association, London, Technical report 42.447.

Taylor, HPJ. (1972). "Shear Strength of Large Beams," Journal of the Structural Division, ASCE, V. 98, No. ST11, Nov., pp. 2473-2489.

USGS (2012). "Minerals Yearbook, Cement, U.S. Geological Survey," United States Department of the Interior, pp. 38-39.

Vecchio, F.J., and Collins, M.P., (1986). The Modified Compression Field Theory for Reinforced Concrete Elements Subjected to Shear. ACI Journal Proceedings, Vol. 83, No. 2, pp. 219-231.

Vecchio, F.J., and Collins, M.P., (1993). Compression Response of Cracked Reinforced Concrete. Journal of Structural Engineering, Vol. 119, No. 12, pp. 3590-3610.

Wong, Y. L., Lam, L., Poon, C. S., & Zhou, F. P. (1999) "Properties of fly ash-modified cement mortar-aggregate interfaces." *Cement and Concrete Research*, 29(12), 1905-1913.

Wight, J.K., and MacGregor, J.G., (2009). *Reinforced Concrete Mechanics and Design* (5th Ed.). Pearson-Prentice Hall.

Wilson, ND, Kioussis, P. (2005) "High-Strength SCC in Shear," *Proceedings Second North American Conference on the Design and Use of Self-Consolidating Concrete and the Fourth International RILEM Symposium on Self-Compacting Concrete, (CDROM)*, Chicago, Illinois.

Xu, S., Zhang, X., and Reinhardt, H.W., (2012) "Shear Capacity Prediction of Reinforced Concrete Beams without Stirrups Using Fracture Mechanics Approach," *ACI Structural Journal*, V. 109, No. 5, pp. 705-714.

Zhao Y, Ma J, Wu Z, Xu S, Gao H. (2005) "Study of fracture properties of self-compacting concrete using wedge splitting test." In: *Proceedings of first international symposium on design, performance and use of self consolidating concrete, China 2005, Hunan China, RILEM Publications, PRO 42, May 2005, p. 421-8.*

PAPER

I. SHEAR BEHAVIOR OF HIGH-VOLUME FLY ASH CONCRETE VERSUS CONVENTIONAL CONCRETE – EXPERIMENTAL STUDY

Mahdi Arezoumandi, Jeffery S. Volz, Carlos A. Ortega, and John J. Myers

Abstract

The production of portland cement – the key ingredient in concrete – generates a significant amount of carbon dioxide. However, due to its incredible versatility, availability, and relatively low cost, concrete is the most consumed man-made material on the planet. One method of reducing concrete's contribution to greenhouse gas emissions is the use of fly ash to replace a significant amount of the cement.

This paper compares two experimental studies that were conducted to investigate the shear strength of full-scale beams constructed with both high-volume fly ash concrete (HVFAC) – concrete with at least 50% of the cement replaced with fly ash – and conventional concrete (CC). The primary difference between the two studies involved the amount of cementitious material, with one mix having a relatively high total cementitious content (502 kg/m³ [850 lb/yd³]) and the other mix having a relatively low total cementitious content (337 kg/m³ [570 lb/yd³]). Both HVFAC mixes utilized a 70% replacement of portland cement with Class C fly ash. Each of these experimental programs consisted of 16 beams – 8 constructed from HVFAC and 8 constructed from CC – with three different longitudinal reinforcement ratios. The beams were tested under a simply supported four-point loading condition. The experimental shear strengths of the beams were compared with both the shear provisions of selected standards (U.S., Australia, Canada, Europe, and Japan) and a shear database of CC specimens. This comparison indicates that HVFAC beams possess comparable shear strength as CC beams.

Keywords:

Reinforced concrete, Fly ash, Experimentation, Structural behavior, Shear strength

Introduction

Concrete is the most widely used man-made material in the world, and cement is an essential ingredient in the production of Portland cement concrete. The cement industry plays a key role in the world, from both an economic and an environmental perspective. In 2011, world cement output was estimated at 3.4 billion metric tons (USGS 2012). Cement production is also a relatively significant source of global carbon dioxide (CO₂) emissions, accounting for approximately 4.5% of global CO₂ emissions from industry in 2007 (Marland et al. 2008). According to the World Business Council for Sustainable Development (WBCSD), emissions from cement manufacturing vary across worldwide regions from 0.73 to 0.99 kg (lb) of CO₂ for each kilogram (pound) of cement produced (Hanle et al. 2012).

One of the solutions for this global concern is the use of supplementary cementitious materials as replacement of cement. The most available supplementary cementitious material worldwide is fly ash, a by-product of coal-burning thermal power stations (Bilodeau et al. 2000). ASTM C618 (2012) defines fly ash as “the finely divided residue that results from the combustion of ground or powdered coal and that is transported by flue gasses.” Fly ash is categorized in three classes: class N, F, and C based on the chemical compositions (ACI 232.2R 2003).

Fly ash has been used in the U.S. since 1930; Davis et al. (1937) were the first researchers to publish their results about using fly ash in concrete (ACI 232.2R 2003). Initially, fly ash was used in massive structures like the Thames Barrage in the U.K. and the Upper Stillwater Dam in the U.S., with about 30 to 75% mass replacement of hydraulic cement to reduce heat generation (ACI 232.2R 2003). Subsequent research (Dunstan 1976, 1980, 1984) has shown several beneficial aspects of using fly ash in concrete such as low permeability and high durability.

Traditionally, fly ash used in structural concrete as a replacement or supplementary material has been limited to 15% to 25% cement replacement (ACI Committee 211, 1993; Berry et al. 1994), except in high strength concrete (HSC) where replacement levels of Portland cement at 35% are more common to control peak hydration temperature development (Myers et al. 1999). When a significant amount of fly ash is used, how it contributes to the strength development of the concrete and the

hydration characteristics of this type of material are of significant research interest. High-volume fly ash concrete (HVFAC) is a concrete generally defined as that with at least 50% of the Portland cement replaced with fly ash. In 1986, the Canadian Centre for Mineral and Energy Technology (CANMET) developed HVFAC for structural applications. The investigations by CANMET (Malhotra 1986) and also other researchers (Gopalan 1993) have shown that HVFAC has lower shrinkage, creep and water permeability and higher modulus of elasticity compared with conventional concrete (CC).

Comprehensive research has been completed on both the fresh and hardened properties of HVFAC, but very little research has been performed on the structural behavior of HVFAC. Rao et al. (2011) performed tests on four beams constructed with 50% Class F fly ash replacement of cement. The beams had no shear reinforcement, longitudinal steel ratios of 0.6%, 1.0%, 2.0%, and 2.9%, and shear span-to-depth ratios of 2.5. The results indicated shear strengths approximately 5% lower than conventional concrete. However, the specimens used by Rao et al. measured only 100 mm x 200 mm (4 in. x 8 in.) in cross section, significantly less than what would be termed full-scale specimens, and unlike many other materials, the shear performance of reinforced concrete is affected by what is termed the “size effect,” meaning that results are not generally scalable. Koyama et al. (2008) studied shear behavior of beams with 25% and 50% fly ash replacement of the fine aggregate, which corresponds to 46% and 61% equivalent replacement of cement with fly ash. The beams had a cross section of 250 mm x 400 mm (10 in. x 16 in.) and span lengths ranging from 360 mm to 720 mm (14 in. to 28 in.). For the 46% fly ash replacement level, the test results indicated shear strengths ranging from 91% to 110% of design code predicted strengths for conventional concrete, while for the 61% fly ash replacement level, the test values ranged from 92% to 135% of design code predicted strengths. However, the beams had shear span-to-depth values of 1.0, 1.5, and 2.0, classifying them all as “deep beams” with respect to shear behavior, and the majority of actual structures have beam depths that result in diagonal tension (beam shear) behavior. In 2005, Cross et al. investigated the performance of three simply supported reinforced concrete beams measuring 152 mm × 254 mm (6 in. x 10 in.) in cross section and constructed with a mixture containing 100% fly ash replacement of cement. However, all of the beams were designed to fail in flexure.

Research Significance

Based on a review of the existing literature, there is a lack of full-scale shear testing of HVFAC specimens. Without this background, there is no quantitative basis for safely implementing HVFAC in structural design. Consequently, the authors, in conjunction with the Missouri Department of Transportation (MoDOT), developed a testing plan to evaluate shear strength of HVFAC (70% replacement of portland cement with a Class C fly ash). The investigators developed two HVFAC mixes that covered the range of potential mix designs used by MoDOT in the construction of transportation-related infrastructure. One mix design had a relatively low total cementitious content of 337 kg/m^3 (570 lb/yd^3), while the other had a relatively high total cementitious content of 502 kg/m^3 (850 lb/yd^3). The experimental program, test results, and analyses for this study are presented in the following discussion.

Experimental Program

Specimen Design

Study A consisted of the high cementitious content mix while Study B consisted of the low cementitious content mix, with each study consisting of 16 beams – 8 constructed from HVFAC and 8 constructed from CC – for a total of 32 specimens. The beams contained three different longitudinal reinforcement ratios designed to preclude flexural failure and satisfy the minimum and maximum longitudinal reinforcement requirements of ACI 318 (2011). All beams of both studies had a rectangular cross section with a width of 305 mm (12 in.), a height of 457 mm (18 in.) (see Table 1 and Figure 1), and shear span-to-depth ratios of 3.0 or greater. The beam designation included a combination of letters and numbers: NS and S stand for no stirrups and stirrups, respectively. The numbers 4, 5, 6, and 8 indicate the number of #22 (#7) longitudinal reinforcement bars within the tension area of the beam section. For example, NS-6 indicates a beam with no stirrups and 6 #22 (#7) bars within the bottom of the beam (Table 1). Although Study A used closed stirrups and Study B used U-shaped stirrups, no differences were noted between the behavior of these beams, and for both studies, when stirrups were used within the shear test regions, they yielded at failure.

Materials

Both concrete mixtures used the same basic constituents and reinforcing steel. The cement was an ASTM Type I/II portland cement (Lafarge), and the fly ash was an ASTM Class C fly ash from the Ameren Labadie Power Plant (Labadie, MO). The powder activators used in the HVFAC mixtures consisted of recycled gypsum wallboard from USA Gypsum (Reinholds, PA) and calcium hydroxide from Mississippi Lime Company (Sainte Genevieve, MO). The coarse aggregate was a crushed limestone from Jefferson City Dolomite (Jefferson City, MO) with a maximum nominal aggregate size of 19 mm (0.75 in.), while the fine aggregate was natural sand from Missouri River Sand (Jefferson City, MO). The longitudinal steel consisted of ASTM A615 (2012), Grade 60, 414 MPa material while the shear reinforcement was ASTM A615 (2012), Grade 40, 276 MPa (to ensure a shear failure prior to a flexural failure). Table 3 contains the tested mechanical properties of the reinforcing steel.

Mixture Proportions

A local ready-mix concrete supplier (Rolla, MO) delivered the concrete mixtures with a target compressive strength of 28 MPa (4000 psi). The purpose of using the ready-mix supplier was to validate the HVFAC concept in actual concrete production runs. The mixture proportions are given in Table 4. The HVFAC mixes used a 70% replacement of cement with fly ash – with Study A containing a relatively high total cementitious content (502 kg/m³ [850 lb/yd³]) and Study B containing a relatively low total cementitious content (337 kg/m³ [570 lb/yd³]). For the HVFAC mixes, the gypsum was used to maintain the initial hydration stage by preventing sulfate depletion, while the calcium hydroxide ensured a more complete hydration of the fly ash with the low content of portland cement in the mix (Bentz 2010). The drums were charged at the ready-mix facility with the required amounts of cement, fly ash, sand, coarse aggregate, and water, while the powder activators (gypsum and lime) were added when the truck arrived at the lab, approximately 5 minutes later. After the gypsum and lime were added, the HVFAC was mixed at high speed for 10 minutes. For the CC mixes, all of the constituents were added at the ready-mix facility.

Fabrication and Curing of Test Specimens

Specimens were constructed and tested in the Structural Engineering High-Bay Research Laboratory (SERL) at Missouri University of Science and Technology. After casting, the beam specimens and the quality control/quality assurance companion cylinders (ASTM C39 (2012) and C496 (2011)) and beams (ASTM C78 (2010)) were covered with both wet burlap and a plastic sheet. All of the beams and companion cylinders were moist cured for three days and, after formwork removal, were stored in the laboratory until they were tested. Table 5 presents the fresh and hardened strength properties of the CC and HVFAC mixes.

Test Setup and Procedure

A load frame was assembled and equipped with two 490-kN (110-kips), servo-hydraulic actuators intended to apply the two point loads to the beams. The load was applied in a displacement control method at a rate of 0.50 mm/min. The shear beams were supported on a roller and a pin support, 300 mm from each end of the beam, creating a four-point loading situation with the two actuators. Linear variable differential transformer (LVDT) and strain gauges were used to measure the deflection at the beam center and strain in the reinforcement, respectively. The strain gauges were installed on the lower layer of the bottom longitudinal reinforcement at midspan (maximum flexural moment location) and quarter point along the span (middle of the shear test region). For the sections with stirrups within the shear test region, strain gauges were also installed on these stirrups. Figure 2 shows both the beam loading pattern and the location of the strain gauges. During the test, any cracks that formed on the surface of the beam were marked at load increments of approximately 22 kN (5 kips), and both the deformation and strains were monitored until the beam reached failure.

Test Results, Analysis, and Discussion

Test Results

Table 6 summarizes the compressive strength at time of testing, shear force at failure, V_{test} , average shear stress at failure, V_{test}/bwd , ratio of the average shear stress

to compressive strength, v_{test} / f'_c , and ratio of the average shear stress to square root of the compressive strength, $v_{\text{test}} / \sqrt{f'_c}$. The average shear stress of the CC beams varies from 3.4% to 5.6% of the compressive strength for Study A and from 3.4% to 4.8% of the compressive strength for Study B. However, for the HVFAC beams, the average shear stress increased to 4.4% to 6.8% of the compressive strength for Study A and 3.6% to 8.5% of the compressive strength for Study B. Another useful comparison is to examine the last column in Table 6 relative to ACI 318 (2011) Equation 11-3, rewritten in terms of average shear stress for normal weight concrete and shown as Equation 1. The ratio of experimental shear stress to square root of compressive strength for the beams without stirrups exceeded the ACI value of 0.17 for all of the beams tested, both CC and HVFAC, even at low longitudinal reinforcement ratios.

$$v_c = 0.17\sqrt{f'_c} \quad (\text{MPa}) \quad v_c = 2\sqrt{f'_c} \quad (\text{psi}) \quad (1)$$

General Behavior (Cracking and Failure Mode)

In terms of crack morphology, crack progression, and load-deflection response, the behavior of the HVFAC and CC beams was virtually identical. All of the beams failed in shear. For the beams without shear reinforcing, failure occurred when the inclined flexure-shear crack penetrated to the compression zone of the beam near the loading plate prior to yielding of the longitudinal reinforcement, as observed in Figure 3. For the beams with shear reinforcing, failure occurred when the stirrups crossing the critical flexure-shear crack reached yield. Based upon data collected from the strain gauges, none of the longitudinal reinforcement reached yield at failure, as expected, all of the stirrups yielded.

Crack progression in the beams began with the appearance of flexural cracks in the maximum moment region, followed by additional flexural cracks forming between the load and support regions as the load was increased. Upon further increasing the applied load, the majority of the flexural cracks developed vertically and, after that, inclined flexure-shear cracks began to appear. As the load increased further, the inclined cracks progressed both upward toward the applied load plate and horizontally along the

longitudinal reinforcement toward the support (see Figure 3). Figure 3 offers a direct visual comparison of the crack shape and distribution at failure for both the HVFAC and CC beams, which are indistinguishable from each other.

Figure 4 shows the load-deflection behavior for the beams without shear reinforcing and with different longitudinal reinforcement ratios (the deflection was measured at midspan). Before the first flexural cracks occurred (point A), all of the beams displayed a steep linear elastic behavior. After additional application of load, the beams eventually developed the critical flexure-shear crack, which resulted in a drop in load and redistribution of the internal shear in the majority of specimens (point B for example). After this redistribution, the beams were able to support additional load until reaching failure. As expected, sections with a higher percentage of longitudinal reinforcement had a higher shear capacity, which can be attributed to a combination of additional dowel action (Taylor 1972, 1974), tighter shear cracks and thus an increase in aggregate interlock, and a larger concrete compression zone due to a downward shift of the neutral axis.

Comparison of Test Results with Shear Provisions of Applicable Standards

In the following section, the experimental shear strengths of the beams are compared with the shear provisions of the following standards: AASHTO LRFD (2010), ACI 318 (2011), AS 3600 (2009), CSA (2004), Eurocode 2 (2005), and JSCE (2007). For this comparison, all of the material resistance factors of the standards were set equal to one, all ultimate moments and shear forces were calculated without load factors, and all of the measured material properties and beam dimensions were used to calculate the capacities.

Tables 7 and 8 present the ratio of experimental-to-code predicted capacity (V_{test}/V_{code}) for the selected design standards for Study A and Study B, respectively. In comparing the two studies, the ratios are very similar, particularly given the wide scatter normally associated with shear testing of reinforced concrete. Most importantly, the ratios for the vast majority of the beams in all the selected standards are greater than one. This result indicates that existing code provisions conservatively predict the shear strength of HVFAC beams.

For the CC beams without stirrups, the ratios range from 0.96 to 1.48 for Study A and 0.91 to 1.41 for Study B. For the HVFAC beams without stirrups, the ratios range from 1.01 to 1.92 for Study A and 1.06 to 1.85 for Study B. On average, the ratios for the HVFAC beams were higher than those for the CC beams, indicating that the HVFAC beams exceeded the code predicted strengths by a larger margin. For the beams with stirrups, the ratios were in much closer agreement between the two concrete types, most likely due to the greater predictability of the stirrup capacity portion of the shear strength, with ratios ranging from 1.16 to 1.60 for the CC and 1.24 to 1.60 for the HVFAC. For both studies and both concrete types, the AASHTO LRFD, AS-3600, CSA, and Eurocode 2 offered the closest agreement between experimental and code predicted strengths.

All of the design codes attempt to quantify the complex and highly variable nature of shear behavior of reinforced concrete in different ways, balancing conservativeness with complexity. With regard to the concrete contribution to shear strength, the design code provisions are generally a function of the depth, compressive strength of the concrete and longitudinal reinforcement ratio of the section. However, the codes define the aforementioned factors differently, for instance some provisions use effective flexural depth as effective depth (e.g., ACI 318) while some use effective shear depth (e.g., AASHTO LRFD). Furthermore, the relative influence of different factors are not the same in all the codes as, for example, AASHTO LRFD, ACI 318, CSA, and JSCE use the square root of the compressive strength of the concrete while others use the cube root. Also, most of the code provisions are empirical, but some of them are semi empirical such as AASHTO LRFD (2010) and CSA (2004) that are based on the modified compression field theory. With regard to the shear contribution of stirrups, some design codes use a constant truss angle model (e.g., ACI 318, JSCE) while others use a variable truss angle model (AASHTO LRFD, CSA). As shown in the following section, the extensive database of shear test results has an extremely high degree of variability due to the complex nature of this brittle failure mode. As a result, some codes, such as ACI 318, use a more simplified yet conservative approach to shear strength while others, such as AASHTO LRFD, use a more complex and generally less conservative approach. The most important point to note with regard to the code comparisons presented in this paper is how the two concrete types compare within a given code.

Comparison of Test Results with Shear Test Database

Figure 5 presents the normalized shear strength versus longitudinal reinforcement ratio for the beams of this study as well as the wealth of shear test data available in the literature (Reineck et al. 2003). Given the significant scatter of the database of previous shear test results, it is somewhat difficult to draw definitive conclusions on the current test values. Nonetheless, visually, Figure 5 seems to indicate that the CC and HVFAC test results fall within the central portion of the data and follow the same general trend of increasing shear strength as a function of the longitudinal reinforcement ratio. In addition, statistical analysis of the data indicates that the CC and HVFAC test results fall within a 95% confidence interval of a nonlinear regression curve fit of the database. Furthermore, a significant majority of the HVFAC test results fall at or above the nonlinear regression curve fit. This result indicates that the test values are very consistent with the wealth of shear test data available in the literature and that, in general, the normalized HVFAC test results tend to be greater than CC.

Since span-to-depth ratio plays a significant role in the shear strength of beams (Taylor 1972, 1974), Figure 6 shows the normalized shear strength for the beams of this study with the portion of the database that had similar span-to-depth ratios of the current study (span-to-depth ratio $\pm 5\%$ [2.9-3.4]). It can be seen from Figure 6 that the test results of this current study are within a 95% confidence interval of a nonlinear regression curve fit of this subset of the shear database, with the majority falling above the curve fit. As a result, it would appear that the shear strength of HVFAC is higher than CC for the beams tested in this investigation.

Statistical Data Analysis

Statistical tests were used to evaluate whether there is any statistically significant difference between the normalized shear strengths of the HVFAC and the CC beams. To compare the test results of both the HVFAC and the CC beams, the results must be adjusted to reflect the different compressive strengths of the specimens. The shear strength of a beam is generally a function of the square root of the compressive strength of the concrete (see Equations 1). Therefore, to normalize the data for comparison, the

shear strengths were divided by the square root of compressive strength. Both parametric and nonparametric test methods were used to analyze the data.

The paired t-test is a statistical technique used to compare two population means. This test assumes that the differences between pairs are normally distributed. If this assumption is violated, the paired t-test may not be the most powerful test. As mentioned earlier, since the shear strength of HVFAC appears higher than that of the CC beams, the following hypothesis is used for the paired t-test.

Ho: The means of the shear capacity of the HVFAC is higher than the CC beams.

Ha: The means of the shear capacity of the HVFAC is not higher than the CC beams.

The statistical computer program Minitab 15 was employed to perform these statistical tests. Both Kolmogorov-Smirnov and Anderson-Darling tests showed the data – the differences between the shear capacities of the HVFAC and the CC beams – follows a normal distribution. Therefore, the paired t-tests could be performed. The result of the paired t-test showed that the p-values were 0.879 and 0.963 (>0.05) for studies A and B, respectively. This confirms the null hypothesis at the 0.05 significance level. In other words, the shear capacity of the HVFAC is statistically higher than the CC beams tested in this investigation and not within the variation of the results.

Unlike the parametric tests, nonparametric tests are referred to as distribution-free tests. These tests have the advantage of requiring no assumption of normality, and they usually compare medians rather than means. The Wilcoxon signed-rank test is usually identified as a nonparametric alternative to the paired t-test. The hypothesis for this test is the same as those for the paired t-test. The Wilcoxon signed rank test assumes that the distribution of the difference of pairs is symmetrical. This assumption can be checked; if the distribution is normal, it is also symmetrical. As mentioned earlier, the data follows normal distribution and the Wilcoxon signed ranks test can be used. The p-values for the Wilcoxon signed rank were 0.860 and 0.995 (>0.05), which confirmed the null hypothesis at the 0.05 significance level. Interestingly, the p-values for both the paired t-

tests (parametric test) and the Wilcoxon signed rank test (nonparametric test) are very close to each other.

Overall, results of the statistical data analyses showed that the normalized shear capacity of the HVFAC is statistically higher than the CC for the beams tested in this investigation.

Fracture Mechanics Testing and Discussion

Some researches (Bazant et al. 2005; Gasteble and May 2001; Xu et al. 2012) have used fracture mechanics approaches to predict the shear strength of reinforced concrete members without stirrups. Bazant et al. (2005) proposed size effect equations for shear strength of reinforced concrete members without stirrups. Gasteble and May (2001) presented an analytical model based on the fracture energy for splitting tensile crack propagation that releases longitudinal reinforcement from surrounding concrete (Mode I fracture energy). More recently, Xu et al. (2012) proposed an equation based on the required fracture energy to release interface bond resistance between the steel and concrete (Mode II fracture energy).

As a result, the authors performed fracture energy tests on both the CC and HVFAC mixes to determine the potential cause of the increased shear strengths for the HVFAC. The fracture energy tests were performed on both the CC and HVFAC using the standard three-point, notched specimen, bend test. The beam specimens measured 150×150×600 mm (6×6×24 in.) with a span length of 450 mm (18 in.). The notch – which was cast into the concrete as opposed to being saw cut after the concrete hardened – had a depth of 40 mm (1.5 in.) and a thickness of 6 mm (0.25 in.). A clip gauge measured the crack mouth opening displacement (CMOD), two linear variable differential transformers (LVDTs) measured deflection at midspan of the beam, and self-weight compensation was provided through lever arms. The tests were performed using a closed loop, servo-controlled MTS machine at a loading rate of 0.002 mm/s (0.00008 in./s).

Results of the fracture energy tests were normalized in terms of concrete compressive strength using relationships developed by Bazant (2002). On average, the HVFAC mixes of Studies A and B had normalized fracture energies 12% and 17% higher

than the CC mix, respectively. In comparison, for the full-scale shear specimen tests, the HVFAC mixes of Studies A and B had average, normalized shear strengths 14% and 21% higher than the CC mix, respectively. It would appear that the cementitious matrix formed by the HVFAC results in higher fracture energies than a conventional portland cement matrix, leading to a corresponding increase in shear strength.

Comparison of Reinforcement Strains from Experiment and AASHTO LRFD (2010)

According to the AASHTO LRFD standard (2010), strain in the longitudinal tension reinforcement can be determined by

$$\varepsilon_s = \frac{\left(\frac{|M_u|}{d_v} + |V_u| \right)}{E_s A_s} \quad (2)$$

Table 9 presents the tensile strain in the longitudinal tension reinforcement at the quarter-point of the span (middle of the shear test region) obtained from both the experiments (strain gauges) and the AASHTO LRFD (2010) equation. The AASHTO LRFD equation estimates the strain for both the HVFAC and CC beams very well for low and medium reinforcement ratios (NS-4 and NS-6), but it underestimates the strain for the sections with higher reinforcement ratios (NS-8 and S-8). As it can be seen from Table 9, Equation 2 predicts the longitudinal steel strain for the HVFAC beams slightly better than the CC beams.

Conclusions and Recommendations

To evaluate the shear capacity of HVFAC, this paper compares the results of two experimental studies, each with a different mix design based on a 70% replacement of portland cement with Class C fly ash. Each study included 16 full-scale beams constructed with three different longitudinal reinforcement ratios. The behavior of the HVFAC was examined in terms of crack morphology and progression, load-deflection response, failure mechanism, predicted strengths from design standards, comparison with

a CC shear test database, a fracture mechanics evaluation, and reinforcement strains at failure. Based on the results, the following conclusions are presented:

In terms of crack morphology, crack progression, and load-deflection response, the behavior of the HVFAC and CC beams was virtually identical.

Existing design standards conservatively predicted the capacity of the HVFAC beams.

In general, the HVFAC beams exceeded the code predicted shear strengths by a larger margin than the CC beams.

The total cementitious content had little effect on the shear behavior of the HVFAC beams.

The HVFAC and CC test results fall within a 95% confidence interval of a nonlinear regression curve fit of a CC shear test database.

A significant majority of the HVFAC test results fall at or above the nonlinear regression curve fit of the CC shear test database.

It would appear that the cementitious matrix formed by the HVFAC results in higher fracture energies than a conventional portland cement matrix, leading to a corresponding increase in shear strength.

The AASHTO LRFD equation estimates strain in the longitudinal steel very well for low and medium reinforcement ratios, but it underestimates the strain for sections with higher reinforcement ratios for both the HVFAC and CC beams.

In general, the AASHTO LRFD equation estimates strain in the longitudinal steel for the HVFAC slightly better than the CC.

Based on the specimens investigated, it would appear that existing design codes for conventional concrete are equally applicable to high-volume fly ash concrete. However, although very promising, the two studies examined only two potential variables – total cementitious content and longitudinal reinforcement ratio. Existing design codes for conventional reinforced concrete are based on a significant database of test results that also examined variables such as size effect, shear span-to-depth ratio, aggregate type and content, and compressive strength. The effect of these same variables on the shear behavior of high-volume fly ash concrete must also be investigated to arrive at the same level of reliability for this new sustainable material.

Acknowledgment

The authors gratefully acknowledge the financial support provided by the Missouri Department of Transportation (MoDOT) and the National University Transportation Center at Missouri University of Science and Technology. The conclusions and opinions expressed in this paper are those of the authors and do not necessarily reflect the official views or policies of the funding institutions.

Notation

A_s = area of nonprestressed tension reinforcement

d_v = effective shear depth

E_s = modulus of elasticity of reinforcing bars

f_c' = specified compressive strength of concrete for use in design

M_u = factored moment at section

V_u = factored shear force at section

v_c = nominal shear stress provided by concrete

ϵ_s = strain in nonprestressed longitudinal tension reinforcement

References

American Association of State and Highway Transportation Officials (AASHTO). (2010). AASHTO LRFD bridge design specifications, 4th Ed., Washington, D.C., pp. 5-(72-84).

ACI Committee 211 (1993). "Guide for Selecting Proportions for High-strength Concrete with Portland Cement and Fly Ash," ACI 226.4R, ACI Material Journal, V. 90, pp. 272-283.

ACI Committee 232 (2003). "Use of Fly Ash in Concrete" (ACI 232.2R-03). Farmington Hills, MI: American Concrete Institute.

American Concrete Institute ACI Committee (2011). "Building code requirements for structural concrete ACI 318-08 and commentary 318R-08." ACI 318-08/318R-08, Farmington Hills, MI: American Concrete Institute, pp. 155-168.

AS 3600 (2009). Concrete Structures, Standards Australia, Sydney, pp. 105-109.

ASTM C 618, (2012). "Standard Specification for Coal Fly Ash and Raw or Calcined Natural Pozzolan for Use in Concrete" ASTM, West Conshohocken, PA, 3 pp.

ASTM A 615/A 615-12, (2012). "Standard Specification for Deformed and Plain Carbon-Steel Bars for Concrete Reinforcement," ASTM, West Conshohocken, PA, 6 pp.

ASTM C 39/C 39M-12, (2012). "Standard Test Method for Compressive Strength of Cylindrical Concrete Specimens," ASTM, West Conshohocken, PA, 7 pp.

ASTM C 78/C 78M-10, (2010). "Standard Test Method for Flexural Strength of Concrete (Using Simple Beam with Third-Point Loading)," ASTM, West Conshohocken, PA, 4 pp.

ASTM C 496/C 496M-11, (2011). "Standard Test Method for Splitting Tensile Strength of Cylindrical Concrete," ASTM, West Conshohocken, PA, 5 pp.

Bazant, Z.P., and Becq-Giraudon, E., (2002), Statistical prediction of fracture parameters of concrete and implications for choice of testing standards. *Cement and Concrete Research Journal*, Vol. 32, No. 4, pp. 529-556.

Bazant, Z. P., and Yu, Q., (2005) "Design against Size Effect on Shear Strength of Reinforced Concrete Beams without Stirrups," *Journal of Structural Engineering*, ASCE, V. 131, No. 12, pp. 1877-1885.

Bentz, D.P. (2010). "Powder Additions to Mitigate Retardation in High-Volume Fly Ash Mixtures," *ACI Materials Journal*, V. 107, No. 5, pp. 508-514.

Berry, E.E., Hemmings, R.T. , Zhang, M.H. , Cornelious, B.J. , Golden, D.M. (1994). "Hydration in High-volume Fly Ash Binders," *ACI Materials Journal*, V. 91, pp. 382-389.

Bilodeau, A. and Malhotra, V. M., (2000). "High-Volume Fly Ash System: Concrete Solution for Sustainable Development, *ACI Materials Journal*, V. 97, pp. 41-48.

CSA CAN3-A23.3 (2004). *Design of Concrete Standards for Buildings*, Rexdale, Ontario, pp. 53-61.

Cross, D., Stephens, J., and Vollmer, J., (2005). "Structural Applications of 100 Percent Fly Ash Concrete, *Proceedings of the 2005 World of Coal Ash (WOCA)*, Lexington, KY, pp. 1-19.

Dunstan, E. R. (1976). "Performance of Lignite and Sub-Bituminous Fly Ash in Concrete," Report No. REC-ERC-76, U.S. Bureau of Reclamation, Denver, Colo., 23 pp.

Dunstan, E. R. (1980). "A Possible Method for Identifying Fly Ashes That Will Improve the Sulfate Resistance of Concretes," *Cement, Concrete, and Aggregates*, V. 2, No. 1, Summer, pp. 20-30.

Dunstan, E. R. (1984). "Fly Ash and Fly Ash Concrete," Report No. REC-ERC-82-1, Bureau of Reclamation, Denver, Colo., 42 pp.

European Committee for Standardization, Eurocode No. 2 (2005). Design of concrete structures. Part 1: General rules and rules for buildings, pp. 84-92.

Gastebled, O. J., and May, I. M., (2001) "Fracture Mechanics Model Applied to Shear Failure of Reinforced Concrete Beams without Stirrups," *ACI Structural Journal*, V. 98, No. 2, pp. 184-190.

Gopalan, M.K. (1993). "Nucleation and Pozzolanic Factors in Strength Development of Class F Fly Ash Concrete," *ACI Materials Journal*, V. 90, pp. 117-121.

Hanle, L., Jayaraman, K., and Smith, J. (2012) "CO2 Emissions Profile of the U.S. Cement Industry," <http://infohouse.p2ric.org/ref/43/42552.pdf>, [March 2012].

Japan Society of Civil Engineers (2007) Standard Specification for concrete structure, JSCE No. 15, Tokyo, pp. 154-159.

Koyama, T., Sun, Y.P., Fujinaga, T., Koyamada, H., and Ogata, F. (2008). "Mechanical Properties of Concrete Beam Made of a Large Amount of Fine Fly Ash," Proceedings for the 14th World Conference on Earthquake Engineering, http://www.iitk.ac.in/nicee/wcee/article/14_05-03-0040.pdf, [March 2012].

Malhotra, V.M. (1986). "Superplasticized Fly Ash Concrete for Structural Applications," *Concrete International*, V. 8, pp. 28- 31.

Marland, G., T.A. Boden, and R.J. Andres. (2008). "Global, Regional, and National Fossil Fuel CO2 Emissions. In Trends: A Compendium of Data on Global Change," Carbon Dioxide Information Analysis Center, Oak Ridge National Laboratory, United States Department of Energy, Oak Ridge, Tenn., <http://cdiac.ornl.gov/trends/emis/overview.html>, [March 2012].

Myers, J.J., Carrasquillo, R.L., (1999) "Mix Proportioning for High-Strength HPC Bridge Beams," American Concrete Institute, Detroit, MI, American Concrete Institute Special Publication 189, pp. 37-56.

Rao, R. M., Mohan, S., and Sekar, .S.K, (2011). "Shear Resistance of High Volume Fly ash Reinforced Concrete Beams without Web Reinforcement," International Journal of Civil and Structural Engineering, V. 1, No. 4, pp. 986-993.

Reineck, KH, Kuchma, DA, Kim, KS, and Marx, S., (2003). "Shear Database for Reinforced Concrete Members without Shear Reinforcement," ACI Structural Journal, V. 100, No. 2, pp. 240-249.

Taylor, HPJ. (1972). "Shear Strength of Large Beams," Journal of the Structural Division, ASCE, V. 98, No. ST11, Nov., pp. 2473-2489.

Taylor, HPJ. (1974). "The Fundamental Behavior of Reinforced Concrete Beams in Bending and Shear," American Concrete Institute, Shear in Reinforced Concrete, SP-42, pp. 43-77.

USGS (2012). "Minerals Yearbook, Cement, U.S. Geological Survey," United States Department of the Interior, pp. 38-39.

Xu, S., Zhang, X., and Reinhardt, H.s W., (2012) "Shear Capacity Prediction of Reinforced Concrete Beams without Stirrups Using Fracture Mechanics Approach," ACI Structural Journal, V. 109, No. 5, pp. 705-714.

Table 1-Shear beams test matrix

Study	Section	Bottom reinforcement	Top reinforcement	ρ	Stirrup
A	NS-5	5#22	4 #13	0.0159	-
	NS-6	6#22	4 #13	0.0203	-
	NS-8	8#22	4#13	0.0271	-
	S-8	8#22	4#13	0.0271	#10@180 mm
B	NS-4	4#22	2#13	0.0127	-
	NS-6	6#22	2#13	0.0203	-
	NS-8	8#22	2#22	0.0271	-
	S-8	8#22	2#22	0.0271	#10@180 mm

#3(U.S.): #10(SI); #4(U.S.): #13(SI); #7(U.S.): #22(SI)

1 ft = 304.8 mm

1 in. = 25.4 mm

Table 2 - Physical properties and chemical compositions of cement and fly ash

Physical properties		
Property	Type I Cement	Class C Fly Ash
Fineness: Blaine, m ² /kg	347	not measured
+325 mesh (+44 μm)	4.1%	14.4%
Specific gravity	3.15	2.73
Chemical compositions		
Component	Type I Cement (%)	Class C Fly Ash (%)
SiO ₂	21.98	33.46
Al ₂ O ₃	4.35	19.53
Fe ₂ O ₃	3.42	6.28
CaO	63.97	26.28
MgO	1.87	5.54
SO ₃	2.73	2.40
Na ₂ O	0.52 equivalent	1.43 equivalent
LOI	0.60	0.34

Table 3 - Mechanical properties of reinforcing steel

Bar No.	Modulus of elasticity	Yielding strength	Elongation
	MPa	MPa	%
10	196,800	380	12
22	208,300	475	16

#3(U.S.): #10(SI); #7(U.S.): #22(SI)

Table 4 -Mixture proportions of concrete

Study	Mix	Water kg/m ³	Cement kg/m ³	Fly ash kg/m ³	Fine aggregate kg/m ³	Coarse aggregate kg/m ³	Gypsum kg/m ³	Calcium Hydroxide kg/m ³	HRWR liter/m ³
A	CC	201	502	-	655	1033	-	-	-
	HVFAC	201	136	317	655	1033	14	35	-
B	CC	134	337	-	735	1103	-	-	0.66
	HVFAC	134	92	213	735	1103	9	23	0.66

$$1 \text{ kg/m}^3 = 1.686 \text{ lb/yd}^3$$

Table 5 - Fresh and hardened concrete properties

Property	Study A		Study B	
	CC	HVFAC	CC	HVFAC
Slump ¹ (mm)	114	127	114	139
Air content ² (%)	1.5	1.5	5.5	3.5
Unit weight ³ (kg/m ³)	2390	2340	2306	2451
Split cylinder strength ^{*4}	3.3	3.2	2.9	2.8
Compressive strength ^{*5}	38.7	30.5	29.0	30.7

*: Values represent the average of three cylinders

¹ ASTM C143 (2010)

² ASTM C173 (2012)

³ ASTM C138 (2012)

⁴ ASTM C496 (2011)

⁵ ASTM C39 (2012)

1 in. = 25.4 mm

1MPa = 145 psi

1 kg/m³=1.686 lb/yd³

Table 6 - Test results summary

Study	Section	f'_c ¹ MPa	V_{test}^2 kN	$v_{test}=V_{test}/b_wd$ MPa	v_{test}/f'_c %	$v_{test}/\sqrt{f'_c}$	
Study A - CC	NS-5	1	34.5	140.6	1.2	3.4	0.20
		2	32	138.1	1.1	3.6	0.20
	NS-6	1	34.5	174.1	1.5	4.4	0.26
		2	32	143.9	1.3	3.9	0.22
	NS-8	1	34.5	219.5	1.9	5.6	0.33
		2	32	146.8	1.3	4.0	0.23
	S-8	1	34.6	367.8	3.2	-	-
		2	34.6	352.5	3.1	-	-
Study A - HVFAC	NS-5	1	22.0	140.7	1.2	4.8	0.25
		2	21.6	114.9	1.0	4.4	0.20
	NS-6	1	22.0	131.9	1.2	5.2	0.25
		2	21.6	121.5	1.1	4.9	0.23
	NS-8	1	22.0	170.9	1.5	6.8	0.32
		2	21.6	162.9	1.4	6.6	0.31
	S-8	1	24.4	328.6	2.9	-	-
		2	24.4	332.7	2.9	-	-
Study B - CC	NS-4	1	29.0	119.7	1.0	3.4	0.18
		2	26.5	113.9	0.90	3.5	0.18
	NS-6	1	29.0	153.5	1.3	4.6	0.25
		2	26.5	144.6	1.3	4.8	0.25
	NS-8	1	29.0	147.7	1.3	4.5	0.24
		2	26.5	143.7	1.3	4.8	0.24
	S-8	1	29.0	299.8	2.6	-	-
		2	26.5	319.8	2.8	-	-
Study B - HVFAC	NS-4	1	30.7	134.3	1.1	3.6	0.20
		2	20.7	122.8	1.0	4.9	0.22
	NS-6	1	30.7	150.4	1.3	4.3	0.24
		2	20.7	168.1	1.5	7.1	0.32
	NS-8	1	30.7	162.4	1.4	4.6	0.26
		2	20.7	201.5	1.8	8.5	0.39
	S-8	1	34.7	328.7	2.9	-	-
		2	34.7	337.2	3.0	-	-

¹: Specimens with the same f'_c were cast from the same batch of concrete.

²: Includes part of the load frame not registered by the load cells and also the beam self weight at a distance d from the interior face of the support plate.

1kN = 0.225 kips

1MPa = 145 psi

Table 7 - Comparison of shear strength of experiment and codes (Study A)

Section		AASHTO	ACI	AS-3600	CSA	Eurocode 2	JSCE		
CC	NS-5	1	1.08	1.12	1.07	1.09	1.07	1.21	
		2	1.09	1.14	1.08	1.10	1.08	1.22	
	NS-6	1	1.31	1.48	1.27	1.31	1.19	1.45	
		2	1.04	1.26	1.08	1.04	1.01	1.23	
	NS-8	1	1.61	1.86	1.46	1.62	1.50	1.66	
		2	0.96	1.26	1.00	0.97	1.03	1.14	
	Ave.		1.18	1.35	1.16	1.19	1.15	1.32	
	COV (%)		20.19	20.57	14.89	20.19	16.21	14.99	
	S-8	1	1.55	1.58	1.39	1.44	1.49	1.60	
		2	1.46	1.51	1.33	1.37	1.43	1.53	
	Ave.		1.51	1.54	1.36	1.41	1.46	1.57	
	COV (%)		4.22	3.08	3.01	3.99	3.01	3.01	
	HVFAC	NS-5	1	1.18	1.36	1.13	1.19	1.13	1.28
			2	1.01	1.22	1.02	1.02	1.02	1.15
NS-6		1	1.11	1.48	1.12	1.11	1.05	1.27	
		2	1.00	1.38	1.04	1.01	0.97	1.18	
NS-8		1	1.42	1.92	1.32	1.43	1.36	1.50	
		2	1.34	1.85	1.26	1.35	1.30	1.43	
Ave.		1.18	1.54	1.15	1.19	1.14	1.30		
COV (%)		14.69	18.53	10.40	14.65	13.92	10.59		
S-8		1	1.42	1.58	1.32	1.33	1.32	1.41	
		2	1.45	1.60	1.34	1.35	1.34	1.43	
Ave.		1.44	1.59	1.33	1.34	1.33	1.42		
COV (%)		1.48	0.89	1.06	1.06	1.06	1.00		

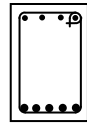
Table 8 - Comparison of shear strength of experiment and codes (Study B)

Section		AASHTO	ACI	AS-3600	CSA	Eurocode 2	JSCE	
CC	NS-4	1	0.93	1.04	1.04	0.94	0.96	1.18
		2	0.91	1.02	1.02	0.91	0.94	1.15
	NS-6	1	1.19	1.41	1.19	1.20	1.11	1.35
		2	1.15	1.38	1.16	1.15	1.08	1.31
	NS-8	1	1.02	1.33	1.04	1.03	1.07	1.18
		2	1.03	1.34	1.04	1.03	1.07	1.18
	Ave.		1.04	1.25	1.08	1.04	1.04	1.23
	COV (%)		10.87	14.02	6.68	10.86	6.78	6.80
	S-8	1	1.20	1.32	1.16	1.13	1.21	1.30
		2	1.31	1.41	1.24	1.23	1.29	1.39
Ave.		1.25	1.36	1.20	1.18	1.25	1.35	
COV (%)		6.30	4.70	4.57	6.00	4.57	4.57	
HVFAc	NS-4	1	1.07	1.14	1.15	1.08	1.06	1.30
		2	1.14	1.25	1.19	1.15	1.10	1.35
	NS-6	1	1.13	1.34	1.14	1.13	1.07	1.30
		2	1.60	1.82	1.46	1.61	1.36	1.65
	NS-8	1	1.12	1.43	1.12	1.13	1.16	1.27
		2	1.84	2.15	1.59	1.85	1.64	1.80
	Ave.		1.32	1.52	1.28	1.33	1.23	1.45
	COV (%)		24.49	25.36	15.63	24.42	18.56	15.47
	S-8	1	1.32	1.40	1.24	1.24	1.32	1.42
		2	1.37	1.44	1.27	1.28	1.35	1.45
Ave.		1.35	1.42	1.26	1.26	1.34	1.44	
COV (%)		2.63	1.99	1.69	2.24	1.59	1.48	

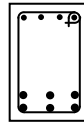
Table 9 - Comparison of reinforcement strain from experiment and AASHTO-LRFD (2010) equation (μ strain)

Section		CC			HVFAC				
		ϵ_s quarter-point	ϵ_s quarter-point	$\frac{\epsilon_{s-Eq.}}{\epsilon_{s-Ex.}}$	ϵ_s quarter-point	ϵ_s quarter-point	$\frac{\epsilon_{s-Eq.}}{\epsilon_{s-Ex.}}$		
		Equation	Experiment		Equation	Experiment			
Study A	NS-5	1	1179	*		1077	*		
		2	1159	*		962	*		
	NS-6	1	1013	1004	1.01	766	591	1.30	
		2	837	692	1.21	706	661	1.07	
	NS-8	1	1457	1526	0.95	745	974	0.76	
		2	573	641	0.89	709	737	0.96	
	S-8	1	1602	2098	0.76	1430	1658	0.86	
		2	1536	2038	0.75	1448	1866	0.78	
	Ave.					0.93			0.96
	COV (%)					18.53			21.27
Study B	NS-4	1	1004	*		1127	1211	0.93	
		2	954	844	1.13	1029	730	1.41	
	NS-6	1	892	989	0.90	875	943	0.93	
		2	840	906	0.93	977	1148	0.85	
	NS-8	1	645	726	0.89	707	780	0.91	
		2	626	818	0.77	878	1483	0.59	
	S-8	1	1305	1648	0.79	1431	1700	0.84	
		2	1392	1791	0.78	1468	1847	0.79	
	Ave.					0.88			0.91
	COV (%)					14.39			25.45

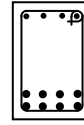
*: No usable data



NS-5

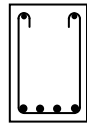


NS-6

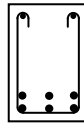


NS-8 & S-8

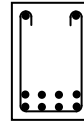
a) Study A



NS-4



NS-6

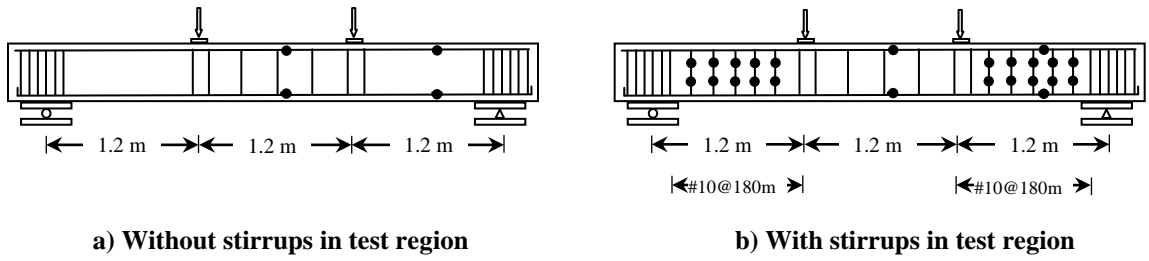


NS-8 & S-8

b) Study B

Figure 1- Cross sections and reinforcement layout of the beams

#3(U.S.): #10(SI); #4(U.S.): #13(SI); #7(U.S.): #22(SI)



- : Strain gauge

Figure 2 - Load pattern and location of strain gauges on the test beams

#3(U.S.): #10(SI); #4(U.S.): #13(SI); #7(U.S.): #22(SI)

1 ft = 304.8 mm

1 in. = 25.4 mm

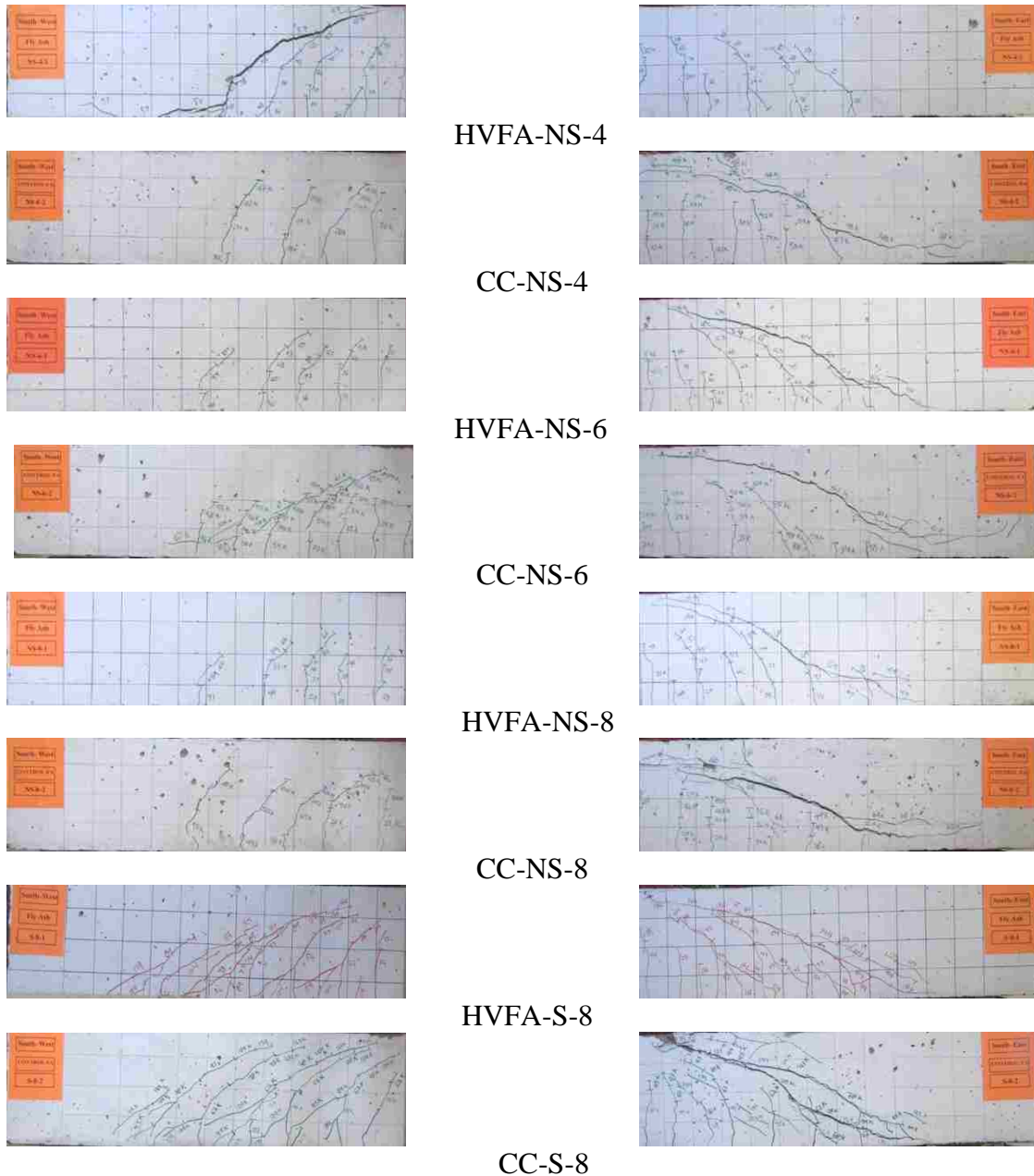
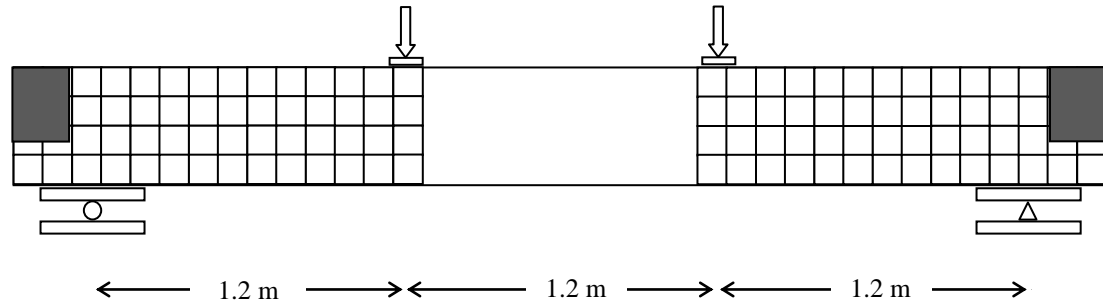


Figure 3 - Crack pattern of the beams at shear failure (Study B)

1 ft = 304.8 mm

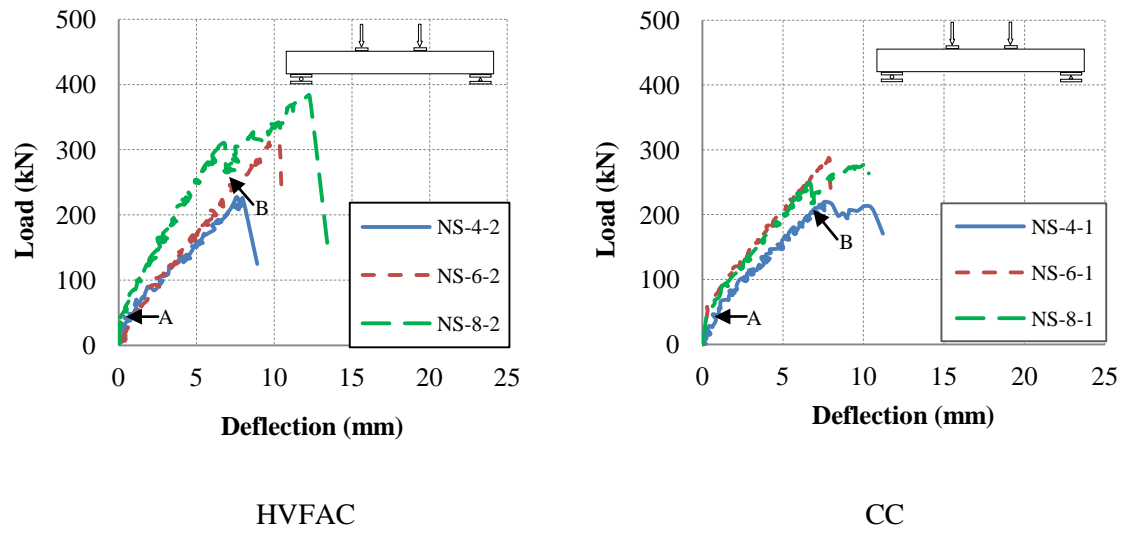


Figure 4 - Load-deflections of the beams (Study B)

1kN = 0.2248 kips

1 in. = 25.4 mm

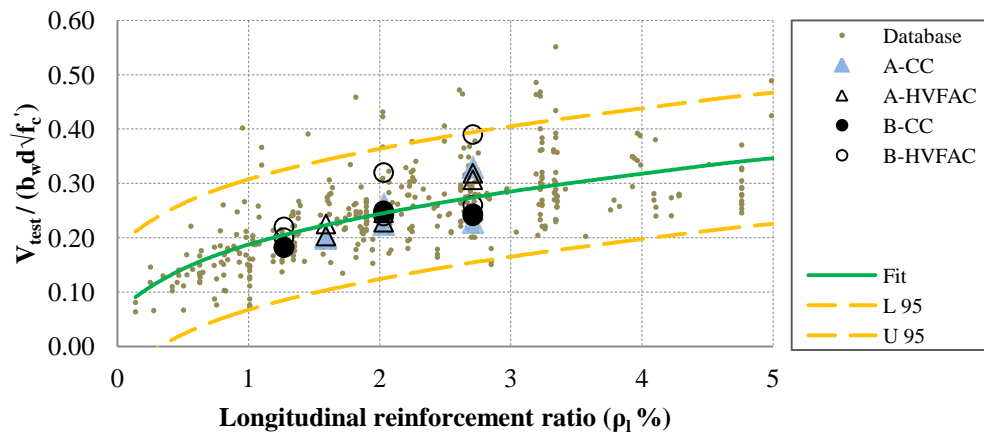


Figure 5 - Shear strength vs. longitudinal reinforcement ratio;
 results from Reineck (2003) and test results of this study

1 MPa = 145 psi

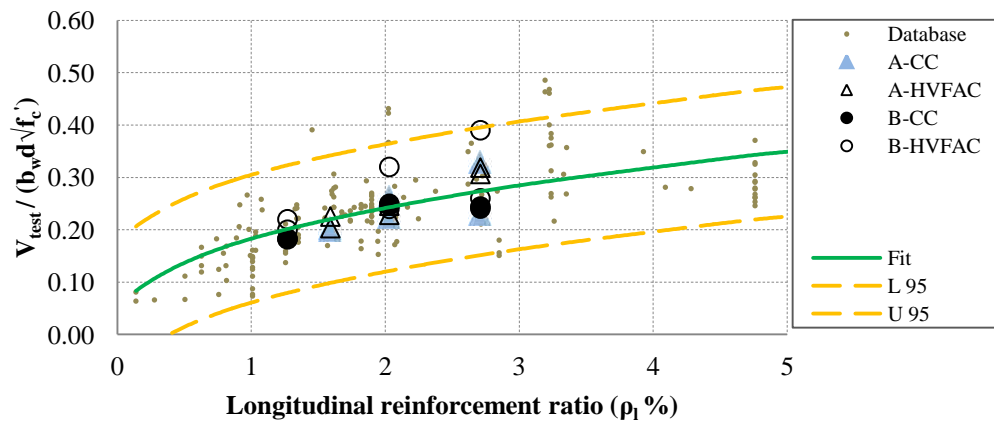


Figure 6 - Shear strength vs. longitudinal reinforcement ratio; results from (Reineck et al. 2003) ($2.9 \leq \frac{a}{d} \leq 3.4$) and test results of this study

1MPa = 145 psi

II. SHEAR BEHAVIOR OF HIGH-VOLUME FLY ASH CONCRETE VERSUS CONVENTIONAL CONCRETE

Mahdi Arezoumandi, Jeffery S. Volz, and John J. Myers

Abstract

The production of portland cement – the key ingredient in concrete – generates a significant amount of carbon dioxide. However, due to its incredible versatility, availability, and relatively low cost, concrete is the most consumed man-made material on the planet. One method of reducing concrete’s contribution to greenhouse gas emissions is the use of fly ash to replace a significant amount of the cement.

An experimental investigation was conducted to study the shear strength of full-scale beams constructed with both high-volume fly ash concrete (HVFAC) – concrete with at least 50% of the cement replaced with fly ash – and conventional concrete (CC). This experimental program consisted of 16 beams (12 without shear reinforcing and four with shear reinforcing in the form of stirrups). Additionally, three different longitudinal reinforcement ratios were evaluated within the test matrix. The beams were tested under a simply supported four-point loading condition. The experimental shear strengths of the beams were compared with the shear provisions of both ACI 318 (2008) and AASHTO LRFD (2007). Furthermore, statistical data analyses (both parametric and non-parametric) were performed to evaluate whether or not there is any statistically significant difference between the shear strength of the HVFAC and the CC beams. Results of these statistical tests show that the normalized shear capacity of the HVFAC is higher than the CC for the beams tested in this investigation.

Keywords:

High-Volume Fly Ash Concrete, Conventional Concrete, Shear Strength, Experimental Study

Introduction

Concrete is the most widely used man-made material in the world, and cement is an essential ingredient in the production of Portland cement concrete. The cement industry plays a key role in the world, from both an economic and an environmental perspective. In 2011, world cement output was estimated at 3.4 billion metric tons (USGS 2012). Cement production is also a relatively significant source of global carbon dioxide (CO₂) emissions, accounting for approximately 4.5 percent of global CO₂ emissions from industry in 2007 (Marland et al. 2008). According to the World Business Council for Sustainable Development (WBCSD), the manufacture of cement emissions varies across worldwide regions from 0.73 to 0.99 kg of CO₂ for each kilogram of cement produced (Hanle et al. 2012).

One of the solutions for this global concern is the use of supplementary cementitious materials as replacement of cement. The most available supplementary cementitious material worldwide is fly ash, a by-product of coal-burning thermal power stations (Bilodeau et al. 2000). ASTM C618 (2012) defines fly ash as “the finely divided residue that results from the combustion of ground or powdered coal and that is transported by flue gasses.” Fly ash is categorized in three classes: class N, F, and C based on the chemical compositions (ACI 232.2R 2003).

Fly ash has been used in the U.S. since 1930; Davis et al. (1937) were the first researchers to publish their results about using fly ash in concrete (ACI 232.2R 2003). Initially, fly ash was used in massive structures like the Thames Barrage in the U.K. and the Upper Stillwater Dam in the U.S., with about 30% to 75% mass replacement of hydraulic cement to reduce heat generation (ACI 232.2R 2003). Subsequent research (Dunstan, 1976, 1980, 1984) has shown some beneficial aspects of using fly ash in concrete such as low permeability and high durability.

Traditionally, fly ash used in structural concrete as a replacement or supplementary material is limited to 15% to 25% cement replacement (ACI Committee 211, 1993; Berry et al. 1994) except in high strength concrete (HSC) where replacement levels of Portland cement at 35% are more common to control peak hydration temperature development (Myers et al. 1999). Strength development and hydration characteristics of concrete mixtures with significant amounts of fly ash are relevant

research topics. High-volume fly ash concrete (HVFAC) is a concrete generally defined as that with at least 50% of the Portland cement replaced with fly ash. In 1986, the Canadian Centre for Mineral and Energy Technology (CANMET) developed HVFAC for structural applications. The investigations by CANMET (Malhotra 1986) and also other researchers (e.g., Gopalan 1993) have shown that HVFAC has lower drying shrinkage, creep, and water permeability as well as higher modulus of elasticity compared with CC.

Comprehensive research has been done on both the fresh and hardened properties of HVFAC, but very little research has been performed on the structural behavior of HVFAC. Koyama et al. (2008) used fly ash as a replacement of fine aggregate in their specimens and concluded that beams using 50% replacement of the fine aggregate had higher shear strength compared with conventional concrete. However, the beams had shear span-to-depth values of 1.0, 1.5, and 2.0, classifying them all as deep beams with respect to shear behavior. Rao et al. (2011) studied shear behavior of beams with 50% Class F fly ash as a replacement of cement with four different longitudinal reinforcement ratios (ranging between 0.5% and 2.94%). They reported that the shear strength of HVFAC beams was slightly lower than conventional concrete. However, the beam cross-section measured only 100 mm x 200 mm (4 in. x 8 in.).

Particular interest in this study is to present the results of an experimental investigation that compares the shear strength of full-scale HVFAC beams with CC beams, as well as comparing both with the shear provisions of ACI 318 (2008) and AASHTO LRFD (2007).

Experimental Program

Specimen Design

Sixteen beams (12 without shear reinforcing and four with shear reinforcing in the form of stirrups) with three different longitudinal reinforcement ratios were designed to preclude flexural failure and satisfy the minimum and maximum longitudinal reinforcement requirements of ACI 318 (2008). All beams tested in this program had a rectangular cross section with a width of 305 mm (12 in.) and a height of 457 mm (18 in.) (see Table 1 and Figure 1). The beam designation included a combination of letters and

numbers: NS and S stand for no stirrups and stirrups, respectively. The numbers 4, 6, and 8 indicate the number of #22 (#7) longitudinal reinforcement bars within the tension area of the beam section. For example, NS-6 indicates a beam with no stirrups and 6 #22 (#7) bars within the bottom of the beam (Table 1).

Materials

The cementitious materials used for this study were ASTM Type I Portland cement; ASTM Class C fly ash from the Ameren Labadie Power Plant (Labadie, MO); gypsum from USA Gypsum (Reinholds, PA); and calcium hydroxide from the Mississippi Lime company (Sainte Genevieve, MO). Tables 2 and 3 show the physical properties and chemical compositions of the cement and fly ash.

Crushed limestone with a maximum nominal aggregate size of 19 mm (3/4 in.) from Jefferson City Dolomite (Jefferson City, MO) was used as the coarse aggregate. The fine aggregate was natural sand from Missouri River Sand (Jefferson City, MO).

The longitudinal steel consisted of ASTM A615 (2012), Grade 60, 414 MPa (60 ksi) material while the shear reinforcement was ASTM A615 (2012), Grade 40, 276 MPa (40 ksi) (to ensure a shear failure prior to a flexural failure).

Mixture Proportions

The concrete mixtures with a target compressive strength of 28 MPa (4000 psi) were delivered by a ready-mix concrete supplier (Rolla, MO). Both mixes had a water-cementitious materials ratio (w/cm) of 0.40, with the HVFAC using a 70% replacement of cement with fly ash. The concrete mixture proportions are given in Table 4. The gypsum was used to maintain the initial hydration stage by preventing sulfate depletion, while the calcium hydroxide ensured a more complete hydration of the fly ash with the low content of cement in the mix. The drums were charged at the ready-mix facility with the required amounts of cement, fly ash, sand, coarse aggregate, and water, while the powder activators (gypsum and lime) were added when the truck arrived at the lab, approximately 5 minutes later. After the gypsum and lime were added, the HVFAC was mixed at high speed for 10 minutes.

Fabrication and Curing of Test Specimens

Specimens were constructed and tested in the Structural Engineering High-Bay Research Laboratory (SERL) at Missouri University of Science and Technology. After casting, the beam specimens and the quality control/quality assurance companion 100 mm x 200 mm (4 in. x 8 in.) cylinders (ASTM C39 (2012)) and C496 (2011)) and 150 mm x 150 mm x 600 mm (6 in. x 6 in. x 24 in.) beams (ASTM C78 (2010)) were covered with both wet burlap and a plastic sheet. All of the beams and companion cylinders were moist cured for three days and, after formwork removal, were stored in the laboratory until they were tested. The full-scale beam specimens and quality control/quality assurance companion specimens were always tested on the same day and after at least 28 days of curing.

Fresh and Hardened Properties

Table 5 presents the fresh and hardened strength properties of the CC and HVFAC mixes.

Test Setup and Procedure

A load frame was assembled and equipped with two 490-kN (110-kip), servo-hydraulic actuators intended to apply the two point loads to the beams. The load was applied in a displacement control method at a rate of 0.50 mm/min (0.02 in./min). The shear beams were supported on a roller and a pin support, 305 mm (12 in.) from each end of the beam, creating a four-point loading situation with the two actuators. Linear variable differential transformers (LVDT's) and strain gauges were used to measure the deflection at the beam center and strain in the reinforcement. The strain gauges were installed on the lower layer of the bottom longitudinal reinforcement at midspan (maximum flexural moment location) and quarter point along the span (middle of the shear test region). For the sections with stirrups, 10 additional strain gauges were installed on the stirrups. Figure 2 shows both the beam loading pattern and the location of the strain gauges. The diagonal pattern of the stirrup strain gauges followed the anticipated critical shear crack based on previous testing of similar specimens. During the

test, any cracks that formed on the surface of the beam were marked at 22 kN (5 kip) load increments, and both the deformation and strains were monitored until the beam reached failure.

Test Results and Discussion

Table 6 summarizes the failure load, P_{test} , shear force, V_{test} , average shear stress at failure, V_{test}/bwd , ratio of the average shear stress to compressive stress, V_{test}/f'_c , and ratio of the average shear stress to square root of the compressive strength, $V_{test}/\sqrt{f'_c}$, to compare with ACI 318 (2008) shear provisions, Equation 11-3, for shear strength of concrete, shown as Equation 1.

$$V_c = 0.17\lambda\sqrt{f'_c}b_wd \quad (1)$$

As can be seen from Table 6, the average shear stress of the beams varies from 3.4% to 8.5% of the compressive strength of the concrete. Also, comparison between the experimental shear strength and ACI 318 (2008) shear provisions (Equation 1) shows this equation is conservative in all cases, even at low longitudinal reinforcement ratios.

It is also worth noting that the higher tensile splitting strengths of the CC mix did not lead to higher shear strengths for the CC beams. This phenomenon may be due to the aggregate interlock (interface shear) mechanism after shear crack initiation, which is generally independent of concrete tensile strength.

General Behavior (Cracking and Failure Mode)

All of the beams failed in shear. Failure occurred when the inclined flexure-shear crack penetrated to the compression zone of the beam near the loading plate prior to yielding of the longitudinal reinforcement, as observed in Figure 3. Based upon data collected from the strain gauges, none of the longitudinal reinforcement reached yield at failure, as expected, all of the stirrups yielded.

Crack progression in the beams began with the appearance of flexural cracks in the maximum moment region, followed by additional flexural cracks forming between the load and support regions as the load was increased. Upon further increasing the

applied load, the majority of the flexural cracks developed vertically and, after that, inclined flexure-shear cracks began to appear. As the load increased further, the inclined cracks progressed both upward toward the applied load plate and downward along the longitudinal reinforcement toward the support (see Figure 3).

Figure 4 shows the load-deflection behavior for the beams with different longitudinal reinforcement ratios (the deflection was measured at midspan). Before the first flexural cracks occurred (point A), all of the beams displayed a steep linear elastic behavior. After additional application of load, the beams eventually developed the critical flexure-shear crack, which resulted in a drop in load and redistribution of the internal shear (point B for example). After this redistribution, the beams were able to support additional load until reaching failure. As expected, sections with a higher percentage of longitudinal reinforcement had a higher shear capacity, which can be attributed to a combination of additional dowel action (Taylor 1970, 1972, 1974), tighter shear cracks and thus an increase in aggregate interlock, and a larger concrete compression zone due to a downward shift of the neutral axis.

Standard Provisions for the Shear Capacity of Concrete Beams

In this section, the experimental shear strengths of the beams are compared with the shear provisions of the American Concrete Institute (ACI 318 (2008)) and American Association of State Highway Transportation Officials, Load and Resistance Factor Design (AASHTO LRFD (2007)).

American Concrete Institute (ACI 318 (2008))

According to the ACI 318 (2008), the nominal shear strength (V_n) shall be determined by

$$V_n = V_c + V_s \quad (2)$$

where :

V_c and V_s are the nominal shear strengths provided by the concrete and shear reinforcement, respectively, calculated in accordance with

$$V_c = (0.16\lambda\sqrt{f'_c} + 17\rho_w \frac{V_u d}{M_u})b_w d \quad (3)$$

and

$$V_s = \frac{A_v f_{yt} d}{s} \quad (4)$$

American Association of State Highway Transportation Officials, Load and Resistance Factor Design (AASHTO LRFD (2007))

The nominal shear strength (V_n) shall be determined by

$$V_n = V_c + V_s \quad (5)$$

in which:

$$V_c = 0.083\beta\sqrt{f'_c}b_v d_v \quad (6)$$

and

$$V_s = \frac{A_v f_y d_v \cot\theta}{s} \quad (7)$$

Comparison of Test Results with Shear Provisions of ACI 318 (2008) and AASHTO LRFD (2007)

For the following comparison of test results to code predicted values, all M_u and V_u values were calculated without load factors.

Table 7 presents the ratio of experimental-to-code predicted capacity (V_{test}/V_{code}) for both the ACI 318 (2008) and the AASHTO LRFD (2007) standards. As shown in Table 7, the ratios for the ACI 318 (2008) standard are higher than the ratios for the AASHTO LRFD (2007) standard. Also the V_{test} / V_{code} ratios for the HVFAC beams are higher than the CC beams for both standards. The average and coefficient of variation (COV) of the ratios for the CC beams are lower than the HVFAC beams for the sections without shear reinforcement, but for the sections with shear reinforcement, the CC beams have higher COV. Furthermore, the AASHTO LRFD (2007) standard overestimated the shear strengths of the CC beams for low longitudinal reinforcement ratios.

To compare the test results of both the HVFAC and the CC beams, the results must be adjusted to reflect the different compressive strengths of the beams. The shear

strength of a beam is a function of the square root of the compressive strength of the concrete (see Equations 3 and 6). Therefore, to normalize the data for comparison, the shear strengths were divided by the square root of compressive strength (see Table 7).

Statistical Data Analysis

Statistical tests were used to evaluate whether there is any statistically significant difference between the normalized shear strengths of the HVFAC and the CC beams. Because there were only 16 beams, a relatively small population, both parametric and nonparametric statistical tests were performed.

Parametric Test

The paired t-test is a statistical technique used to compare two population means. This test assumes that the differences between pairs are normally distributed. If this assumption is violated, the paired t-test may not be the most powerful test. As mentioned earlier, since the shear strength of HVFAC appears higher than that of the CC beams, the following hypothesis is used for the paired t-test.

Ho: The means of the shear capacity of the HVFAC is higher than the CC beams.

Ha: The means of the shear capacity of the HVFAC is not higher than the CC beams.

The statistical computer program Minitab 15 was employed to perform these statistical tests. Both Kolmogorov-Smirnov and Anderson-Darling tests showed the data – the differences between the shear capacities of the HVFAC and the CC beams – follows a normal distribution. Therefore, the paired t-tests could be performed. The result of the paired t-test showed that the p-value was 0.963 (>0.05). This confirms the null hypothesis at the 0.05 significance level. In other words, the normalized shear capacity of the HVFAC is higher than the CC beams tested in this investigation.

Nonparametric Test

Unlike the parametric tests, nonparametric tests are referred to as distribution-free tests. These tests have the advantage of requiring no assumption of normality, and they usually compare medians rather than means. The Wilcoxon signed-rank test is usually identified as a nonparametric alternative to the paired t-test. The hypothesis for this test is the same as those for the paired t-test. The Wilcoxon signed rank test assumes that the distribution of the difference of pairs is symmetrical. This assumption can be checked; if the distribution is normal, it is also symmetrical. As mentioned earlier, the data follows normal distribution and the Wilcoxon signed ranks test can be used. The p-value for the Wilcoxon signed rank was 0.995 (>0.05), that confirmed the null hypothesis at the 0.05 significance level. Interestingly, the p-values for both the paired t-tests (parametric test) and the Wilcoxon signed rank test (nonparametric test) are very close to each other.

Overall, results of the statistical data analyses showed that the normalized shear capacity of the HVFAC is higher than the CC for the beams tested in this investigation.

Comparison of Test Results with Shear Test Database

Figure 5 presents the normalized shear strength versus longitudinal reinforcement ratio for the beams of this study as well as the wealth of shear test data available in the literature (Reineck et al. 2003). Given the significant scatter of the database of previous shear test results, it is somewhat difficult to draw definitive conclusions on the current test values. Nonetheless, visually, Figure 5 seems to indicate that the CC and HVFAC test results fall within the central portion of the data and follow the same general trend of increasing shear strength as a function of the longitudinal reinforcement ratio. Furthermore, statistical analysis of the data indicates that the CC and HVFAC test results fall within a 95% confidence interval of a nonlinear regression curve fit of the database. This result indicates that the test values are very consistent with the wealth of shear test data available in the literature – even given the significant scatter – and that the results do indeed indicate that for the specimens tested, the shear strength of HVFAC beams is higher than the shear strength of the CC beams.

Since span-to-depth ratio plays a significant role in the shear strength of beams (Taylor 1970, 1972, 1974), Figure 6 shows the normalized shear strength for the beams of this study with the portion of the database that had similar span-to-depth ratios of the current study (span-to-depth ratio $\pm 5\%$ [2.9-3.4]). It can be seen from Figure 6 that the test results of this current study are within a 95% confidence interval of a nonlinear regression curve fit of this subset of the shear database. As a result, it would appear that the shear strength of HVFAC is higher than CC for the beams tested in this investigation.

Comparison of Reinforcement Strains from Experiment and AASHTO LRFD (2007)

According to the AASHTO LRFD (2007), the longitudinal tensile strain in the tension reinforcement can be determined by

$$\varepsilon_s = \frac{\left(\frac{|M_u|}{d_v} + |V_u| \right)}{E_s A_s} \quad (8)$$

Table 8 presents the tensile strain in the longitudinal tension reinforcement at the quarter-point of the span (middle of the shear test region) obtained from both the experimental (strain gauge) and the AASHTO LRFD (2007) equation. The AASHTO LRFD (2007) equation estimates the strain for both the HVFAC and the CC beams very well for low and medium reinforcement ratios (NS-4 and NS-6), but it underestimates the strain for the sections with higher reinforcement ratios (NS-8 and S-8).

Conclusions and Recommendations

To compare the shear strength of HVFAC and CC, 16 full-scale beams (eight from each concrete type) were assembled with different longitudinal reinforcement ratios. Based on the results of this study, the following conclusions can be made:

- No significant difference was observed between the HVFAC and CC beams in terms of crack patterns, load-deflection behavior, and failure mode.
- Shear provisions of the ACI 318 (2008) standard underestimates the shear capacity of both the HVFAC and CC beams compared with the AASHTO

LRFD (2007) standard. In other words, the AASHTO LRFD (2007) standard more accurately estimates the capacities of both concrete types.

- The HVFAC beams have higher V_{test} / V_{code} ratios than the CC beams for both standards.
- The ratio of V_{test} / V_{code} exceeded 1.0 for the HVFAC beams for both standards. In other words, the existing design provisions of ACI 318 (2008) and AASHTO LRFD (2007) conservatively predicted the strength of the HVFAC beam specimens.
- Statistical data analyses (parametric and non-parametric) indicated that the shear capacity of the HVFAC is higher than the CC for the beams tested in this investigation.
- The normalized shear strengths of both the HVFAC and CC beams fell within a 95% confidence interval of a nonlinear regression curve fit of the database of previous shear tests.
- The AASHTO LRFD (2007) equation used to calculate the tensile strain of the longitudinal reinforcement predicts the strain for both the HVFAC and CC beams very well at low and medium longitudinal reinforcement ratios.

However, due to the limited nature of the data set regarding aspect ratio, mix designs, aggregate type and content, etc., investigated, the researchers recommend further testing to increase the database of test results.

Acknowledgment

The authors gratefully acknowledge the financial support provided by the Missouri Department of Transportation (MoDOT) and the National University Transportation Center (NUTC) at Missouri University of Science and Technology (Missouri S&T). The authors would also like to thank the support staff in the Department of Civil, Architectural and Environmental Engineering and Center for Infrastructure Engineering Studies at Missouri S&T for their efforts. The conclusions and opinions expressed in this paper are those of the authors and do not necessarily reflect the official views or policies of the funding institutions.

Notation

A_s = area of nonprestressed tension reinforcement

A_v = area of shear reinforcement spacing s

b_v = effective web width taken as the minimum web width

b_w = web width

d = distance from extreme compression fiber to centroid of longitudinal tension reinforcement

d_v = effective shear depth

E_s = modulus of elasticity of reinforcing bars

f_c' = specified compressive strength of concrete for use in design

f_y = specified minimum yield strength of reinforcing bars

f_{yt} = specified yield strength of transverse reinforcement

M_u = factored moment at section

V_c = nominal shear strength provided by concrete

V_n = nominal shear strength

V_s = nominal shear strength provided by shear reinforcement

V_u = factored shear force at section

s = center-to-center spacing transverse reinforcement

β = factor indicating ability of diagonally cracked concrete to transmit tension and shear

ϵ_s = strain in nonprestressed longitudinal tension reinforcement

θ = factor indicating ability of diagonally cracked concrete to transmit tension and shear

λ = modification factor reflecting the reduced mechanical properties of lightweight concrete

ρ_w = ratio of A_s to $b_w d$

References

American Association of State and Highway Transportation Officials (AASHTO). (2007). AASHTO LRFD bridge design specifications, 4th Ed., Washington, D.C.

American Concrete Institute Committee 211 (1993). "Guide for Selecting Proportions for High-strength Concrete with Portland Cement and Fly Ash," ACI 226.4R, ACI Material Journal, V. 90, pp. 272-283.

American Concrete Institute Committee 232 (2003). "Use of Fly Ash in Concrete" (ACI 232.2R-03). Farmington Hills, MI: American Concrete Institute.

American Concrete Institute ACI Committee 318 (2008). "Building code requirements for structural concrete ACI 318-08 and commentary 318R-08." ACI 318-08/318R-08, Farmington Hills, MI: American Concrete Institute.

ASTM A 615/A 615-12, (2012). "Standard Specification for Deformed and Plain Carbon-Steel Bars for Concrete Reinforcement" ASTM, West Conshohocken, PA, 6 pp.

ASTM C 39/C 39M-12, (2012). "Standard Test Method for Compressive Strength of Cylindrical Concrete Specimens," ASTM, West Conshohocken, PA, 7 pp.

ASTM C 78/C 78M-10, (2010). "Standard Test Method for Flexural Strength of Concrete (Using Simple Beam with Third-Point Loading)" ASTM, West Conshohocken, PA, 4 pp.

ASTM C 496/C 496M-11, (2011). "Standard Test Method for Splitting Tensile Strength of Cylindrical Concrete," ASTM, West Conshohocken, PA, 5 pp.

ASTM C 618, (2012). "Standard Specification for Coal Fly Ash and Raw or Calcined Natural Pozzolan for Use in Concrete" ASTM, West Conshohocken, PA, 3 pp.

Berry, E.E., Hemmings, R.T., Zhang, M.H., Cornelious, B.J., Golden, D.M. (1994). "Hydration in High-volume Fly Ash Binders," ACI Materials Journal V.91, pp.382-389.

Bilodeau, A. and Malhotra, V. M., (2000). "High-Volume Fly Ash System: Concrete Solution for Sustainable Development, ACI Material Journal V.97, pp. 41-48.

Dunstan, E. R. (1976). "Performance of Lignite and Sub-Bituminous Fly Ash in Concrete," Report No. REC-ERC-76, U.S. Bureau of Reclamation, Denver, Colo., 23 pp.

Dunstan, E. R. (1980). "A Possible Method for Identifying Fly Ashes That Will Improve the Sulfate Resistance of Concretes," Cement, Concrete, and Aggregates, V. 2, No. 1, Summer, pp. 20-30.

Dunstan, E. R. (1984). "Fly Ash and Fly Ash Concrete," Report No. REC-ERC-82-1, Bureau of Reclamation, Denver, Colo., 42 pp.

Gopalan, M.K. (1993). "Nucleation and Pozzolanic Factors in Strength Development of Class F Fly Ash Concrete," ACI Material Journal, V.90, pp. 117-121.

Hanle, L., Jayaraman, K., and Smith, J. (2012) "CO2 Emissions Profile of the U.S. Cement Industry," <http://infohouse.p2ric.org/ref/43/42552.pdf>, [March 2012].

Koyama, T., Sun, Y.P., Fujinaga, T., Koyamada, H., and Ogata, F. (2008). "Mechanical Properties of Concrete Beam Made of a Large Amount of Fine Fly Ash," Proceedings for the 14th World Conference on Earthquake Engineering, http://www.iitk.ac.in/nicee/wcee/article/14_05-03-0040.pdf, [March 2012].

Malhotra, V.M. (1986). "Superplasticized Fly Ash Concrete for Structural Applications," Concrete International, V.8, pp. 28- 31.

Marland, G., T.A. Boden, and R.J. Andres. (2008). "Global, Regional, and National Fossil Fuel CO2 Emissions. In Trends: A Compendium of Data on Global Change," Carbon Dioxide Information Analysis Center, Oak Ridge National Laboratory, United States Department of Energy, Oak Ridge, Tenn., <http://cdiac.ornl.gov/trends/emis/overview.html>, [March 2012].

Myers, J.J., Carrasquillo, R.L., (1999) "Mix Proportioning for High-Strength HPC Bridge Beams," American Concrete Institute, Detroit, MI, American Concrete Institute Special Publication 189, pp. 37-56.

Rao, R. M., Mohan, S., and Sekar, .S.K, (2011). "Shear Resistance of High Volume Fly ash Reinforced Concrete Beams without Web Reinforcement," International Journal of Civil and Structural Engineering, V.1, No 4, pp. 986-993.

Reineck, KH, Kuchma, DA, Kim, KS; and Marx, S., (2003). "Shear Database for Reinforced Concrete Members without Shear Reinforcement," ACI Structural Journal, V. 100, No. 2, pp. 240-249.

USGS (2012). "Minerals Yearbook, Cement, U.S. Geological Survey," United States Department of the Interior, pp. 38-39.

Table 1- Shear beams test matrix

Section	Bottom reinforcement	Top reinforcement	ρ	Stirrup
NS-4	4 #22	2 #13	0.0127	-
NS-6	6 #22	2 #13	0.0203	-
NS-8	8 #22	2 #22	0.0271	-
S-8	8 #22	2 #22	0.0271	#10@180mm

Table 2 - Physical properties of cement and fly ash

Property	Type I Cement	Class C Fly Ash
Fineness: Blaine, m ² /kg	347	not measured
+325 mesh (+44 μm)	4.1%	14.4%
Specific gravity	3.15	2.73

Table 3 - Chemical composition of cement and fly ash

Component	Type I Cement, %	Class C Fly Ash, %
SiO ₂	21.98	33.46
Al ₂ O ₃	4.35	19.53
Fe ₂ O ₃	3.42	6.28
CaO	63.97	26.28
MgO	1.87	5.54
SO ₃	2.73	2.40
Na ₂ O	0.52 equivalent	1.43 equivalent
LOI	0.60	0.34

Table 4 - Mixture proportions of concrete

Material	Water kg/m ³	Cement kg/m ³	Fly ash kg/m ³	Fine aggregate kg/m ³	Coarse aggregate kg/m ³	Gypsum kg/m ³	Calcium Hydroxide kg/m ³	Glenium 7500 liter/m ³
HVFAC	134	92	213	735	1103	9	23	0.66
CC	134	335	-	735	1103	-	-	0.66

Table 5 - Fresh and hardened concrete properties

Property	CC	HVFAC
Slump (mm)	114	139
Air content (%)	5.5	3.5
Unit weight (kg/m ³)	2306	2451
Split cylinder strength* (MPa)	2.9	2.8
Compressive strength* (MPa)	29.0	30.7

*: Values represent the average of three cylinders.

Table 6 - Test results summary

Section			P_{test}	V_{test}^*	$v_{test}=V_{test}/b_wd$	v_{test}/f_c	$v_{test}/\sqrt{f_c}$	
			kN	kN	MPa	%		
CC	NS-4	1	222.4	119.7	1.0	3.4	0.18	
		2	210.4	113.9	0.90	3.5	0.18	
	NS-6	1	289.6	153.5	1.3	4.6	0.25	
		2	272.2	144.6	1.3	4.8	0.25	
	NS-8	1	278.5	147.7	1.3	4.5	0.24	
		2	270.0	143.7	1.3	4.8	0.24	
	S-8	1	582.3	299.8	2.6	-	-	
		2	622.3	319.8	2.8	-	-	
	HVFAc	NS-4	1	251.8	134.3	1.1	3.6	0.20
			2	228.2	122.8	1.0	4.9	0.22
NS-6		1	283.8	150.4	1.3	4.3	0.24	
		2	319.0	168.1	1.5	7.1	0.32	
NS-8		1	307.4	162.4	1.4	4.6	0.26	
		2	385.7	201.5	1.8	8.5	0.39	
S-8		1	640.1	328.7	2.9	-	-	
		2	657.0	337.2	3.0	-	-	

*: Includes part of the load frame not registered by the load cells and also the beam self weight at a distance d from the interior face of the support plate.

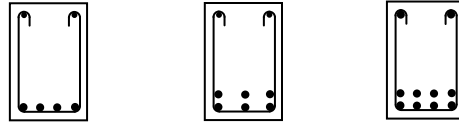
Table 7 - Comparison of shear strength of experiment and codes

Section		CC			HVFAC		
		$V_{\text{test}}/V_{\text{code}}$ AASHTO	$V_{\text{test}}/V_{\text{code}}$ ACI	$V_{\text{test}}/\sqrt{f'_c}$	$V_{\text{test}}/V_{\text{code}}$ AASHTO	$V_{\text{test}}/V_{\text{code}}$ ACI	$V_{\text{test}}/\sqrt{f'_c}$
NS-4	1	0.93	1.04	415.1	1.07	1.14	452.7
	2	0.91	1.02	412.3	1.14	1.25	503.0
NS-6	1	1.19	1.41	531.6	1.13	1.34	506.7
	2	1.15	1.38	524.5	1.60	1.82	689.2
NS-8	1	1.02	1.33	512.3	1.12	1.43	546.4
	2	1.03	1.34	520.4	1.84	2.15	771.4
Average		1.04	1.25		1.32	1.52	
COV (%)		10.90	14.00		24.49	25.36	
S-8	1	1.20	1.32		1.32	1.40	
	2	1.31	1.41		1.37	1.44	
Average		1.26	1.37		1.35	1.42	
COV (%)		6.20	4.66		2.63	1.99	

Table 8 - Comparison of reinforcement strain from experiment and AASHTO-LRFD-07 equation

Section		CC			HVFAC		
		ϵ_s quarter-point Equation	ϵ_s quarter-point Experiment	$\frac{\epsilon_{s-Eq.}}{\epsilon_{s-Ex.}}$	ϵ_s quarter-point Equation	ϵ_s quarter-point Experiment	$\frac{\epsilon_{s-Eq.}}{\epsilon_{s-Ex.}}$
NS-4	1	1004.0	*		1127.0	1211.0	0.93
	2	954.0	844.0	1.13	1029.0	730.0	1.41
NS-6	1	892.0	989.0	0.90	875.0	943.0	0.93
	2	840.0	906.0	0.93	977.0	1148.0	0.85
NS-8	1	645.0	726.0	0.89	707.0	780.0	0.91
	2	626.0	818.0	0.77	878.0	1483.0	0.59
S-8	1	1305.0	1648.0	0.79	1431.0	1700.0	0.84
	2	1392.0	1791.0	0.78	1468.0	1847.0	0.79
Average				0.88			0.91
COV (%)				14.39			25.45

*: No data



NS-4

NS-6

NS-8 & S-8

Figure 1 - Cross sections and reinforcement layout of the beams

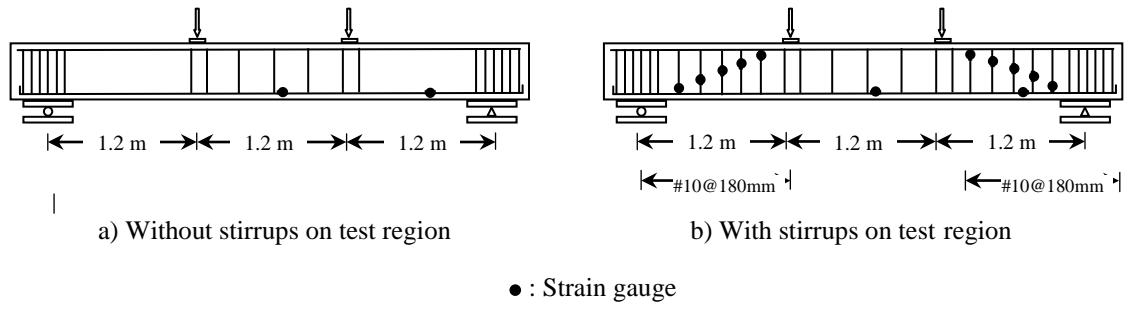


Figure 2 - Load pattern and location of strain gauges on the test beams

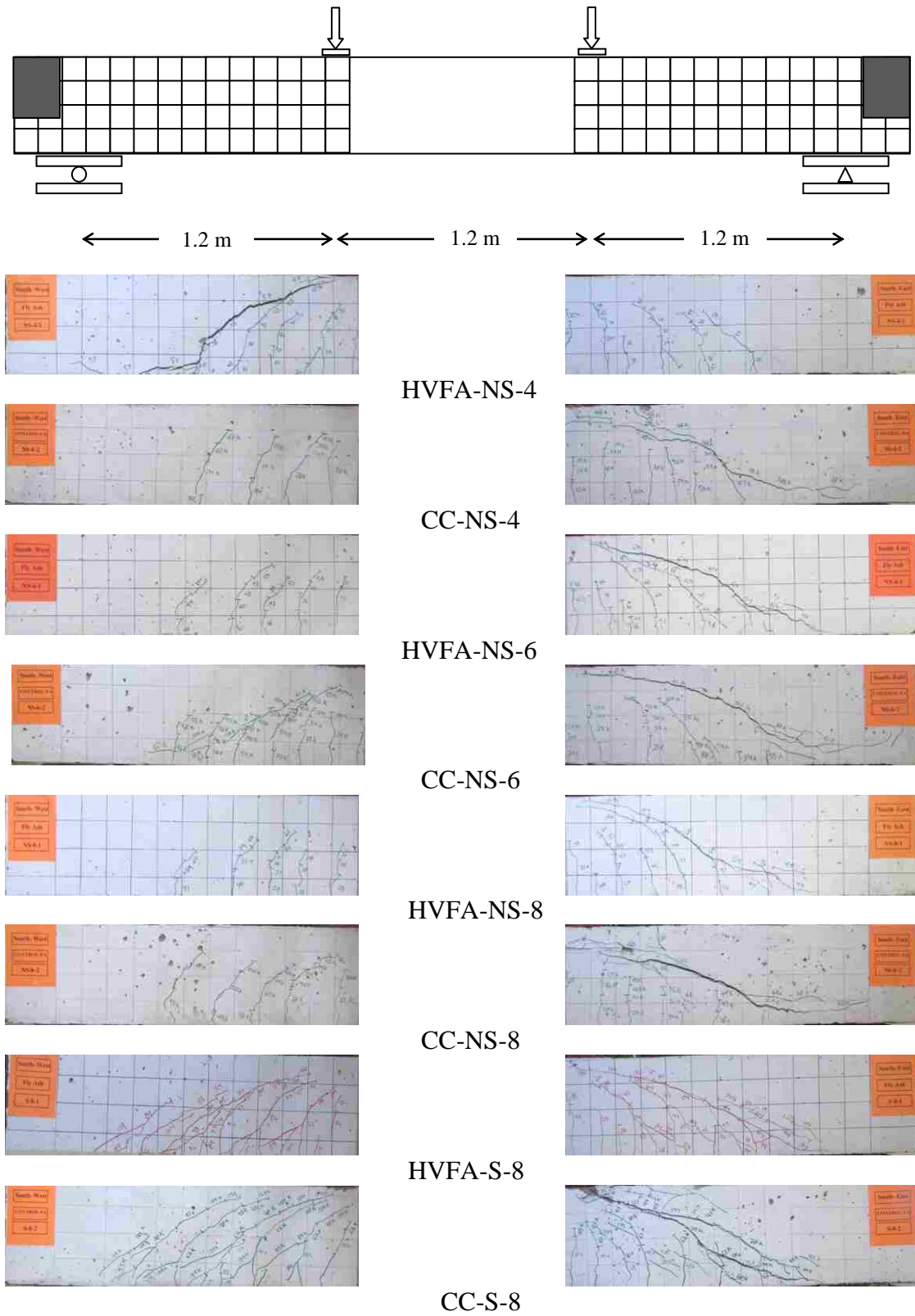
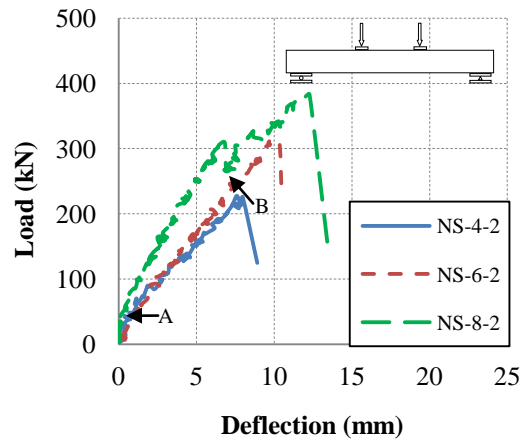
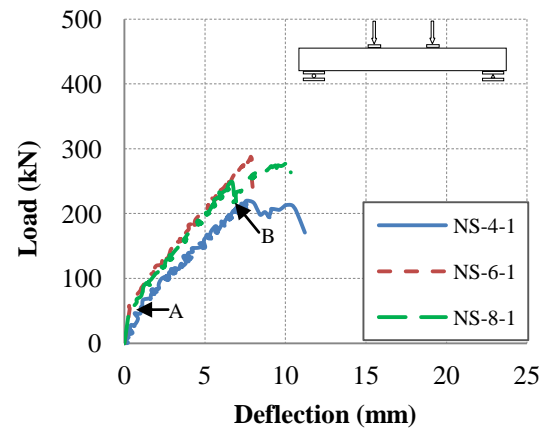


Figure 3 - Crack pattern of the beams at shear failure



HVFAC



CC

Figure 4 - Load-deflections of the beams

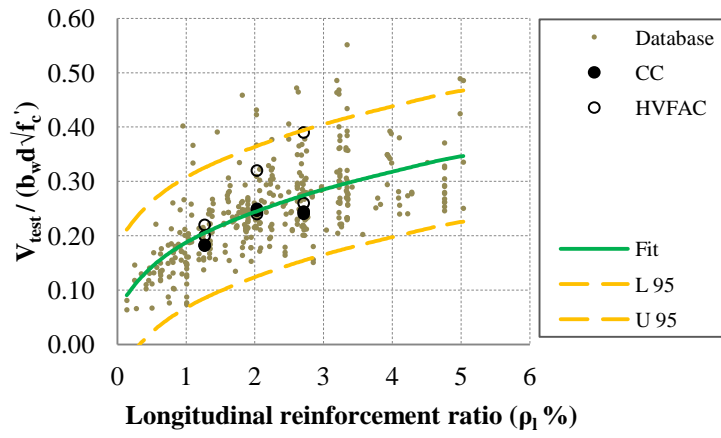


Figure 5 - Shear strength vs. longitudinal reinforcement ratio; results from (Reineck 2003) and test results of this study

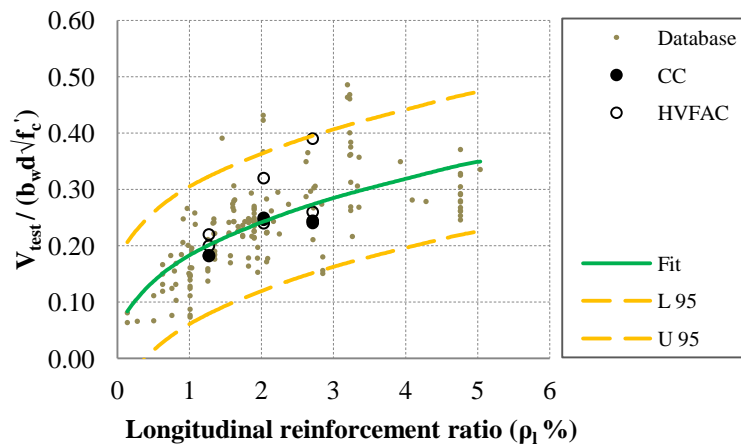


Figure 6 - Shear strength vs. longitudinal reinforcement ratio;

results from (Reineck 2003) ($2.9 \leq \frac{a}{d} \leq 3.4$) and test results of this study

III. SHEAR STRENGTH OF CHEMICALLY-BASED SELF-CONSOLIDATING CONCRETE BEAMS – FRACTURE MECHANICS APPROACH VS. MODIFIED COMPRESSION FIELD THEORY

Mahdi Arezoumandi and Jeffery S. Volz

Abstract

An experimental investigation was conducted to study the shear strength of full-scale beams constructed with both chemically-based self-consolidating concrete (SCC) and conventional concrete (CC). This experimental program consisted of 12 beams without stirrups with three different longitudinal reinforcement ratios. The beams were tested under a simply supported four-point loading condition. The experimental shear strengths of the beams were compared with the shear provisions of both U.S. and international design codes (U.S. [ACI-318 and AASHTO LRFD], Australia, Canada, Europe, and Japan). Furthermore, the shear strengths of the beams were evaluated based on fracture mechanics approaches, modified compression field theory (MCFT), and a shear database of CC specimens. Results of this study show that the SCC possesses comparable shear strength to the CC.

Keywords:

Admixtures, Self-Consolidating Concrete, Reinforced Concrete, Experimentation, Structural Behavior, Shear Strength

Introduction

Self-consolidating concrete (SCC) is a highly workable concrete that can spread under its own weight without segregation and bleeding. SCC was developed in Japan in the early 1980's by Okamura and colleagues at Tokyo University (Ozawa et al. 1989). The motivation for this development was a lack of skilled workers for consolidating concrete to form durable concrete structures (Daczko et al. 2006).

Like many new products, SCC was slow to gain popularity. It was used for the first time on a large scale for the Akashi-Kaikyo bridge in Japan in 1998 (Okamura 1997). It began to spread in Asian and European countries before the United States, where it finally gained acceptance around the year 2000 (Daczko et al. 2006). SCC has become more popular because of several advantages including reduced labor, equipment, job noise, and time of construction. The enhanced flowability also aids in filling densely reinforced members and very complex formwork shapes (ACI 237R-07).

Comprehensive research has been done on both fresh and hardened properties of SCC, but relatively little research have been performed on the structural behavior of SCC. With regard to shear behavior, results from multiple researchers have shown somewhat conflicting results. Das et al. (2005) found that SCC beams had higher shear strength compared to conventional concrete (CC). Wilson et al. (2005) reported, however, that shear provisions as included in ACI 318-11 did not always yield conservative results for SCC beams. Test results from Burgueno and Bendert (2005, 2006A, 2006B) showed that the shear behavior of both SCC and CC beams are very similar to each other. In addition, the ultimate shear strength of SCC and CC beams were almost the same. Hassan et al. (2008, 2010) and also Choulli (2005) reported there was no significant difference between the shear behavior of SCC and CC beams, and that the ultimate shear strength of SCC beams was only slightly lower than CC beams. Dymond (2007) tested a single, precast bulb-tee bridge girder and concluded that the theoretical prediction of the simplified method was conservative compared with experimental test results of the beam. These somewhat conflicting results are likely due to the wide range of potential mix designs available for SCC, and with only limited information provided by the researchers cited above, it is impossible to determine what lead to these particular results. However, with aggregate interlock playing such a critical role in shear behavior (Taylor 1970, 1972), SCC mixes that rely on material-based changes – higher paste contents and smaller rounded aggregates – may result in substantially reduced shear strengths.

The potential for significant variation in shear strength between different SCC mixes has to do with the variety of approaches available to obtain the necessary flowability of the concrete. In general, there are three different approaches to developing

an SCC mix. The first is material-based, the second is chemically-based, and the third is a hybrid of the first two. The first approach focuses on modifying the aggregate types and amounts. Typically, the coarse aggregate content is reduced and also rounder aggregate is used to improve the flowability of the SCC mix (ACI 237R-07). The main disadvantage of this approach is that with a lower coarse aggregate content, aggregate interlock, and as a result shear strength, is potentially reduced. To avoid this issue, the second approach was developed and, in this approach, the coarse aggregate and paste contents are kept the same as in a CC mix. To improve the flowability and stability of this type of mix, high-range water-reducing admixtures (HRWRA) and viscosity-modifying admixtures (VMA) are used (ACI 237R (2007)). The third approach combines both modifications to the aggregate type or amount as well as the addition of HRWRA and possibly VMA to obtain the desired behavior.

All of the aforementioned previous researchers studied shear behavior of SCC that used the first or third approaches for SCC mix design. The current study presents the results of an experimental investigation that examines the shear strength of full-scale SCC beams constructed with a chemically-based mix. In addition to comparing the results with control specimens constructed from CC, the study explored the behavior of the SCC beams relative to several existing design standards, fracture mechanics approaches to shear behavior, the modified compression field theory (MCFT), and an extensive shear database of CC test results.

Experimental Program

Specimen Design

Twelve beams without stirrups with three different longitudinal reinforcement ratios were designed to preclude flexural failure and satisfy the minimum and maximum longitudinal reinforcement requirements of ACI 318 (2008). All beams tested in this program had a rectangular cross section with a width of 300 mm, a height of 460 mm, and shear span-to-depth ratios of 3.0 or greater. The beam elevations and cross sections are shown in Figure 1 with the reinforcement also listed in Table 1. All beams used #22 (22 mm dia.) primary flexural reinforcement and #10 (10 mm dia.) stirrups. As shown in

Figure 1, the test region did not contain any stirrups although stirrups were located within the end regions and between the two load points to help support the reinforcing cage during construction and prevent any secondary failure mode such as local crushing. The beam designation included a combination of letters and numbers: NS stands for no stirrups within the test regions and numbers 4, 6, and 8 indicate the number of #22 (22 mm dia.) longitudinal reinforcement bars within the tension area of the beam section. For example, NS-6 indicates a beam with no stirrups within the test region and 6 #22 (22 mm dia.) bars within the bottom of the beam (Table 1).

Materials and Concrete Mixture Proportions

Both concrete mixtures used the same basic constituents and reinforcing steel. The cement was an ASTM Type I/II portland cement (Lafarge), and the fly ash was an ASTM Class C fly ash from the Ameren Labadie Power Plant (Labadie, MO). The coarse aggregate consisted of a crushed limestone from Jefferson City Dolomite (Jefferson City, MO) with a maximum nominal aggregate size of 19 mm, while the fine aggregate was natural sand from Missouri River Sand (Jefferson City, MO). For each individual bar size, all of the reinforcing was from the same heat of steel, used the same deformation pattern, and met the requirements of ASTM A615 (2009), Grade 60, 414 MPa material. Table 2 contains the tested mechanical properties of the reinforcing steel.

The intent of this research project was to determine whether a chemically-based SCC mix would experience a decrease in shear strength compared to CC. Consequently, the SCC mix design followed conventional proportioning in terms of aggregate type and content, cement content, air content, water-cementitious material ratio, and workability. Then, using only chemical admixtures, the authors converted this CC mix to an SCC mix with all of the necessary passing, filling, flowability, and stability requirements typically found in SCC. The high fluidity was achieved with a polycarboxylate-based HRWRA (Glenium 7500), while the enhanced stability was accomplished with an organic, polymer-based VMA (Rheomac 362). The concrete mixture proportions and fresh concrete properties are given in Tables 3 and 4, respectively. The air-entraining admixture was a rosin soap composition (MB-AE-90). A local ready-mix concrete

supplier (Rolla, MO) delivered the concrete mixture, which had a target compressive strength of 35 MPa.

Fabrication and Curing of Test Specimens

Specimens were constructed and tested in the Structural Engineering High-Bay Research Laboratory (SERL) at Missouri University of Science and Technology. After casting, the beam specimens and the quality control/quality assurance companion cylinders (ASTM C39 (2012) and C496 (2011)) and beams (ASTM C78 (2010)) were covered with both wet burlap and a plastic sheet. All of the beams and companion cylinders were moist cured for three days and, after formwork removal, were stored in a semi-controlled environment with a temperature range of 18 to 24°C and a relative humidity range of 30 to 50% until they were tested.

Test Setup and Procedure

A load frame was assembled and equipped with two 490-kN, servo-hydraulic actuators intended to apply the two point loads to the beams. The load was applied in a displacement control method at a rate of 0.50 mm/min. The shear beams were supported on a roller and a pin support, 300 mm from each end of the beam, creating a four-point loading situation with the two actuators. Linear variable differential transformer (LVDT) and strain gauges were used to measure the deflection at the beam center and strain in the reinforcement. The strain gauges were installed on the lower layer of the bottom longitudinal reinforcement at midspan (maximum flexural moment location) and quarter point along the span (middle of the shear test region). An LVDT was installed at the midspan of the beam to measure the deflection. Figure 1 shows both the beam loading pattern and the location of the strain gauges. During the test, any cracks that formed on the surface of the beam were marked at load increments of approximately 22 kN, and both the deformation and strains were monitored until the beam reached failure.

Test Results and Discussion

Table 5 summarizes the compressive strength at time of testing, shear force at failure, V_{test} , average shear stress at failure, V_{test}/bwd , ratio of the average shear stress

to compressive strength, v_{test} / f'_c , and ratio of the average shear stress to square root of the compressive strength, $v_{\text{test}} / \sqrt{f'_c}$. In order to compare results from specimens with different compressive strengths, it is convenient to normalize the results in terms of both compressive strength (ACI design codes prior to 1963) and square root of compressive strength (ACI design codes since 1963). The average shear stress of the CC beams varies from 2.6% to 4.9% of the compressive strength, while the average shear stress of the SCC beams varies from 2.7% to 4.1% of the compressive strength, with one value at 2.0%. Both sets are within a similar range and show the same trend of increasing average shear stress for increasing longitudinal steel ratio, indicating similar overall performance. Another useful comparison is to examine the last column in Table 5 with ACI 318 (2011) Equation 11-3, rewritten in terms of average shear stress for normal weight concrete and shown as Equation 1. The ratio of experimental shear stress to square root of compressive strength for the beams without stirrups exceeded the ACI value of 0.17 for all but one of the beams for each concrete type. This comparison shows that the ACI 318 shear provision (Equation 11-3) conservatively predicts the shear strength of the majority of beams in this study. The two instances where the test value fell below the ACI shear provisions corresponded to beams with the lowest amount of longitudinal reinforcement, which is a condition that has also been reported by other researchers (e.g., Collins et al. 1999).

$$v_c = 0.17\sqrt{f'_c} \quad (1)$$

General Behavior (Cracking and Failure Mode)

In terms of crack morphology, crack progression, and load-deflection response, the behavior of the SCC and CC beams was virtually identical. All of the beams failed in shear. Failure occurred when the inclined flexure-shear crack penetrated to the compression zone of the beam near the loading plate prior to yielding of the longitudinal reinforcement, as observed in Figure 2. Based upon data collected from the strain gauges,

as shown in Table 6, none of the longitudinal reinforcement reached yield at failure, as expected.

Crack progression in the beams began with the appearance of flexural cracks in the maximum moment region, followed by additional flexural cracks forming between the load and support regions as the load was increased. Upon further increasing the applied load, the majority of the flexural cracks developed vertically and, after that, inclined flexure-shear cracks began to appear. As the load increased further, the inclined cracks progressed both upward toward the applied load plate and horizontally along the longitudinal reinforcement toward the support (see Figure 2). Figure 2 offers a direct visual comparison of the crack orientation and distribution at failure for both the SCC and CC beams, which are indistinguishable from each other.

Figure 3 shows the load-deflection behavior for the beams with different longitudinal reinforcement ratios (the deflection was measured at midspan). Before the first flexural cracks occurred (point A), all of the beams displayed a steep linear elastic behavior. After additional application of load, the beams eventually developed the critical flexure-shear crack, which resulted in a drop in load and redistribution of the internal shear in two-thirds of the specimens (point B for example). The other one-third of the specimens failed to support additional load once the critical flexure-shear crack formed. For the remaining members, after this redistribution, the beams were able to support additional load until reaching failure. The ability to support and at other times not support additional load after formation of the critical flexure-shear crack has been noted by previous researchers (e.g., Collins et al. 1999) and is generally a function of the ability of interfacial crack stresses to develop. However, this inconsistent result is often why most design codes limit the concrete shear stress at failure to the load that initiates the critical flexure-shear crack. As expected, sections with a higher percentage of longitudinal reinforcement had a higher shear capacity, which can be attributed to a combination of additional dowel action (Taylor 1970, 1972), tighter shear cracks and thus an increase in aggregate interlock, and a larger concrete compression zone due to a downward shift of the neutral axis. The linear load-deflection behavior also confirms that the longitudinal steel did not yield prior to shear failure and that the bond between the reinforcement and surrounding concrete was maintained throughout loading.

Comparison of Test Results with Shear Provisions of Applicable Standards

In the following section, the experimental shear strengths of the beams are compared with the shear provisions of the following standards: AASHTO LRFD (2007), ACI 318 (2011), AS 3600 (2009), CSA (2004), Eurocode 2 (2005), and JSCE (2007). For this comparison, all of the material resistance factors of the standards were set equal to one, all ultimate moments and shear forces were calculated without load factors, and all of the measured material properties and beam dimensions were used to calculate the capacities.

Table 7 presents the ratio of experimental-to-code predicted capacity (V_{test}/V_{code}) for each of the selected design standards. In general, for a given standard, the ratios are very consistent between the two concrete types for beams with the same amount of longitudinal reinforcement. For example, for the AASHTO code, the ratios for the NS-6 CC beams are 1.12 and 1.22, while the ratios for the NS-6 SCC beams are 1.08 and 1.17. Overall, the ratios range from 0.73 to 1.72 for CC and 0.77 to 1.55 for SCC. There are two reasons for the noticeable differences between the different codes. First, in general, each design code uses a different approach to calculating the design capacity for a given section. For instance, ACI uses a set value for the shear strength as a function of the concrete compressive strength, while AASHTO, based on the Modified Compression Field Theory, uses a variable shear strength approach based on the inclination angle of the critical flexure-shear crack and associated longitudinal strains. Second, due to the brittle nature of shear failures, shear test results for reinforced concrete, particularly those without stirrups, have a significant amount of scatter and design codes must provide for a lower bound strength value.

The average of the ratios for each standard was slightly higher for the SCC compared to the CC beams. With regard to the ratios that fell below 1.0 – an unconservative result – this situation has been observed by other researchers (e.g., Collins et al. 1999), and it is important to note that the majority of standards do not allow sections without stirrups unless the factored shear force is significantly less than the concrete capacity in shear. It is also important to note that the code comparisons have been used to form a basis for comparing the results between the SCC and CC tests of this study. The results of applying the design equations show the relative consistency between

the two concrete types, but it is important to recognize that the results do not necessarily indicate a satisfactory target reliability for the SCC behavior as additional data would be required to arrive at that conclusion.

Comparison of Test Results with Fracture Mechanics Approaches

Numerous researchers (Bazant et al. 1984, 1987, 2005, Gustafsson et al. 1988, Jeng et al. 1989, So et al. 1993, Gastebled et al. 2001, Xu et al. 2012) have used fracture mechanics approaches to predict shear strength of reinforced concrete members without stirrups. Between 1984 and 2005, Bazant et al. (1984, 1987, 2005) developed different formulas based on fracture mechanics to predict the shear capacity of reinforced concrete members without stirrups. Bazant et al. (2005) proposed Equation 2 for shear strength of reinforced concrete members without stirrups. Furthermore, Gastebled et al. (2001) presented an analytical model (Equation 3) based on the required fracture energy for splitting tensile crack propagation that releases longitudinal reinforcement from surrounding concrete (Mode I fracture energy). More recently, Xu et al. (2012) proposed Equation 4 based on the required fracture energy to release interface bond resistance between steel and concrete (Mode II fracture energy).

$$V_c = 10\rho^{\frac{3}{8}} \left(1 + \frac{d}{a_s}\right) \sqrt{\frac{f'_c}{1 + \frac{d}{f'_c \cdot \frac{2}{3} 3800 \sqrt{d_a}}}} b_w d \quad (2)$$

$$V_c = \frac{1.109}{\sqrt{d}} \left(\frac{d}{a_s}\right)^{\frac{1}{3}} \rho^{\frac{1}{6}} (1 - \sqrt{\rho})^{\frac{2}{3}} f'_c{}^{0.35} \sqrt{E_s} b_w d \quad (3)$$

$$V_c = \frac{1.018}{\sqrt{d}} \left(\frac{d}{a_s}\right)^{\frac{1}{3}} \rho^{\frac{1}{6}} (1 - \sqrt{\rho})^{\frac{2}{3}} (0.0255f'_c + 1.024) b_w d \quad (4)$$

Figure 4 compares V_{test}/V_{EQ} for all the aforementioned fracture mechanics approaches. In general, all of the fracture mechanics approaches conservatively predict

the shear strength of the test beams. The only exception involves specimen NS-4-1 where the Xu et al. relationship underpredicts the shear strength for both the CC and SCC versions of this beam. In terms of accurately predicting the shear strength of the test specimens, there is a slight trend in that the Xu et al. relationship provides the closest agreement in 7 of the 12 tests, while the Bazant et al. equation provides a more accurate estimate for 3 of the specimens and the Gastebled et al. equation more accurately predicts the capacity of the remaining 2 specimens. More importantly, the results are very consistent between the CC and SCC, indicating that the existing approaches are equally valid for SCC.

Comparison of Test Results with MCFT Method

The Modified Compression Field Theory (MCFT) was developed by researchers at the University of Toronto (Vecchio et al. 1986). Several codes have incorporated simplified versions of the MCFT including the AASHTO-LRFD-10 and CSA A23.3-04. For this reason, the following section presents the shear strength of the specimens based on the MCFT method (Bentz 2000) and includes a comparison with the AASHTO-LRFD-10 approach.

Figure 4 also compares V_{test} / V_{MCFT} and V_{test} / V_{AASHTO} . As shown in Figure 4, the AASHTO-LRFD-10 equation is not always conservative compared with the MCFT method. For the beams of this study, the AASHTO-LRFD-10 equation overestimates the shear strength of the beams with the lowest amount of longitudinal steel (as well as one of the beams with the maximum amount of longitudinal steel) compared to the MCFT.

Figure 5 compares the load-deflection behavior between the experiments with those predicted by the MCFT method. As shown in the figure, plots based on the MCFT method show very good agreement with the experimental results. Also, in general, the MCFT method underestimates the shear strength of the beams for the specimens tested in this investigation as the plots fall either very close or slightly below the test result plots.

Comparison of Test Results with Shear Test Database

Figure 6 presents the normalized shear strength versus longitudinal reinforcement ratio for the beams of this study as well as the results from 527 previous shear tests of CC specimens (Reineck et al. 2003). Given the significant scatter of the database of previous shear test results, it is somewhat difficult to draw definitive conclusions on the current test values. Nonetheless, visually, Figure 6 indicates that the SCC test results fall within a 95% confidence interval of a nonlinear regression curve fit of the database and follow the same general trend of increasing shear strength as a function of the longitudinal reinforcement ratio. This result indicates that the test values are very consistent with the wealth of shear test data available in the literature – even given the significant scatter – and that the results do indeed indicate that for the specimens tested, the SCC shear strength is comparable to the shear strength of CC.

Since span-to-depth ratio plays a significant role in the shear strength of beams (Taylor 1970, 1972), Figure 7 shows the normalized shear strength for the beams of this study with the portion of the database that had similar span-to-depth ratios of the current study (span-to-depth ratio \pm 5% [2.9-3.4]). It can be seen from Figure 7 that the test results of this current study are within a 95% confidence interval of a nonlinear regression curve fit of this subset of the shear database. As a result, it would appear that there are no significant differences between the shear strength of chemically-based SCC and that of CC.

Conclusions and Recommendations

To evaluate the shear strength of chemically-based SCC, 12 full-scale beams (six for each concrete type) constructed with different longitudinal reinforcement ratios were tested to failure. Based on the results of this study, the following conclusions are presented:

- In terms of crack morphology, crack progression, and load-deflection response, the behavior of the SCC and CC beams was virtually identical.

- In general, for a given standard, the ratios of experimental-to-code predicted capacity are very consistent between the two concrete types for beams with the same amount of longitudinal reinforcement.
- The shear provisions of all selected standards except the JSCE-07 overestimated the shear capacity of the CC and SCC beams for low longitudinal reinforcement ratios.
- The fracture mechanics approaches underestimate the shear strength of both the CC and SCC beams, but appear to be equally applicable to both materials.
- The MCFT method somewhat overpredicts shear strength of both the CC and SCC beams, although in general offers very good agreement.
- The SCC and CC test results fall within a 95% confidence interval of a nonlinear regression curve fit of the CC shear test database.
- Based on a comparison of the test results of this study with the shear database available for CC specimens, it can be inferred that there is no significant difference between the shear strength of chemically-based SCC beams and that of CC.

Consequently, for chemically-based SCC reinforced concrete beams, the behavior is essentially identical to CC, indicating that existing design standards and approaches are equally valid for SCC. However, due to the limited nature of the data set regarding aspect ratio, mix designs, aggregate type and content, etc. investigated, the researchers recommend further testing to increase the database of test results for SCC.

Acknowledgment

The authors gratefully acknowledge the financial support provided by the BASF Corporation and the National University Transportation Center at Missouri University of Science and Technology (Missouri S&T). The conclusions and opinions expressed in this paper are those of the authors and do not necessarily reflect the official views or policies of the funding institutions.

Notation

a_s = shear span of beam

b_w = web width

d = distance from extreme compression fiber to centroid of longitudinal tension reinforcement

d_a = maximum aggregate size

E_s = modulus of elasticity of steel

f_c' = specified compressive strength of concrete for use in design

V_c = shear force provided by concrete

v_c = nominal shear stress provided by concrete

ρ = longitudinal reinforcement ratio

References

American Association of State and Highway Transportation Officials (AASHTO). (2007). AASHTO LRFD bridge design specifications, 4th Ed., Washington, D.C.

American Concrete Institute ACI Committee. (2007). "Self –Consolidating Concrete" ACI 237R-07, Farmington Hills, MI: American Concrete Institute.

American Concrete Institute ACI Committee. (2008). "Building code requirements for structural concrete ACI 318-08 and commentary 318R-08." ACI 318-08/318R-08, Farmington Hills, MI: American Concrete Institute.

AS 3600 (2009). "Concrete Structures," Standards Australia, Sydney.

ASTM A 615/A 615-12, (2012). "Standard Specification for Deformed and Plain Carbon-Steel Bars for Concrete Reinforcement," ASTM, West Conshohocken, PA, 6 pp.

ASTM C 39/C 39M-12, (2012). "Standard Test Method for Compressive Strength of Cylindrical Concrete Specimens," ASTM, West Conshohocken, PA, 7 pp.

ASTM C 78/C 78M-10, (2010). "Standard Test Method for Flexural Strength of Concrete (Using Simple Beam with Third-Point Loading)," ASTM, West Conshohocken, PA, 4 pp.

ASTM C 496/C 496M-11, (2011). "Standard Test Method for Splitting Tensile Strength of Cylindrical Concrete," ASTM, West Conshohocken, PA, 5 pp.

Bažant, Z.P., and Kim, J.K., (1984) "Size Effect in Shear Failure of Longitudinal Reinforced Beams," ACI Journal, Proceedings V. 81, No. 5, Sept.- Oct. pp. 456-468.

Bažant, Z.P., (1987) "Fracture Energy of Heterogeneous Materials and Similitude," Fracture of Concrete and Rock, S. P. Shah and S. E. Swartz, pp. 390-402.

Bažant, Z.P., and Yu, Q., (2005) "Design against Size Effect on Shear Strength of Reinforced Concrete Beams without Stirrups," Journal of Structural Engineering, ASCE, V. 131, No. 12, pp. 1877-1885.

Bentz, E.C. (2000). "Sectional Analysis of Reinforced Concrete Members" PhD thesis, University of Toronto.

Bentz, E.C., Vecchio, F.J., and Collins, M. P. (2006) "Simplified Modified Compression Field Theory for Calculating Shear Strength of Reinforced Concrete Elements", ACI Structural Journal V. 103, No. 4, pp. 614-624.

Bendert, D.A. and Burgueño, R. (2006A). "Report on the Experimental Evaluation of Prestressed Box beams for SCC Demonstration Bridge." Research Report CEE-RR-2006-01, Department of Civil and Environmental Engineering, Michigan State University, East Lansing, MI.

Bendert, D.A. and Burgueño, R. (2006B). "Report on the Production of Prestressed Box beams for SCC Demonstration Bridge." Research Report CEE-RR-2006-02, Department of Civil and Environmental Engineering, Michigan State University, East Lansing, MI.

Burgueño, R. and Till, R. (2005). "Special Provision for Production of Prestressed Beams with Self-Consolidating Concrete," Internal Report, Michigan Department of Transportation, Lansing, MI.

CEB-FIP Model Code 2010-fib (2012), Vol. 1, Comité Euro-Internationale du Bèton, Lausanne, Switzerland.

Collins, M.P. and Kuchma D. (1999). "How safe are our large, lightly reinforced concrete beams, slabs, and footings?" ACI Structural Journal, V. 96, No. 4, pp. 482-490.

Choulli, Y. and Mari, A.R. (2005). "Shear Behaviour of full scale prestressed I beams made with Self Compacting Concrete," Proceedings Second North American Conference on the Design and Use of Self-Consolidating Concrete and the Fourth International RILEM Symposium on Self-Compacting Concrete, (CD-ROM), Chicago, Illinois.

CSA CAN3-A23.3 (2004). "Design of Concrete Standards for Buildings," Rexdale, Ontario.

Daczko, J. and Vachon, M. (2006). "Self Consolidating Concrete (SCC), Significance of Tests and Properties of Concrete and Concrete-Making Materials," STP 169D, ASTM International West Conshohocken, PA., pp. 637-645.

Das, D, Kaushik, S.K., Gupta V.K. (2005). "Shear Resistance of Self-Compacting concrete," Proceedings Second North American Conference on the Design and Use of Self-Consolidating Concrete and the Fourth International RILEM Symposium on Self-Compacting Concrete, (CD-ROM), Chicago, Illinois.

Dymond, B.Z. (2007). "Shear Strength of A PCBT-53 Girder Fabricated with Lightweight, Self-Consolidating Concrete," MS Thesis, Virginia Tech, Blacksburg, VA.

European Committee for Standardization. Eurocode No. 2 (2005). "Design of concrete structures. Part 1: General rules and rules for buildings."

Gastebled, O.J., and May, I.M., (2001) "Fracture Mechanics Model Applied to Shear Failure of Reinforced Concrete Beams without Stirrups," ACI Structural Journal, V. 98, No. 2, pp. 184-190.

Gustafsson, P.J., and Hillerborg, A., (1988) "Sensitivity in Shear Strength of Longitudinally Reinforced Concrete Beams," ACI Structural Journal, V. 85, No. 3, pp. 286-294.

Hassan, A.A.A., Hossain, K.M.A., and Lachemi, M. (2008). "Behavior of Full-Scale Self-Consolidating Concrete Beams in Shear," Cement & Concrete Composites. V. 30, No. 7, pp.588-596.

Hassan, A.A.A., Hossain, K.M.A., and Lachemi, M. (2010). "Strength, Cracking and Deflection Performance of Large-Scale Self-Consolidating Concrete Beams Subjected to Shear Failure," Engineering Structures, V. 32, No. 5, pp. 1262-1271.

Japan Society of Civil Engineers (2007). "Standard Specification for concrete structure," JSCE No. 15, Tokyo.

Jenq, Y.S., and Shah, S.P., (1989) "Shear Resistance of Reinforced Concrete Beams—A Fracture Mechanics Approach," *Fracture Mechanics: Application to Concrete*, SP-118, V. Li and Z. P. Bažant, eds., American Concrete Institute, Farmington Hills, MI, pp. 237-258.

Okamura, H. (1997). "Self-Compacting High-Performance Concrete," *Concrete International*, pp. 50-54.

Ozawa, K, Maekawa, K, Kunishima, M, and Okamura, H. (1989). "Development of High Performance Concrete Based on the Durability Design of Concrete Structures." In *Proceedings of the Second East-Asia and Pacific Conference on Structural Engineering and Construction (EASEC-2)*, Vol. 1, pp. 445-450.

Reineck, K.H., Kuchma, D.A., Kim, KS; and Marx, S. (2003). "Shear Database for Reinforced Concrete Members without Shear Reinforcement," *ACI Structural Journal*, V. 100, No. 2, pp. 240-249.

So, K.O., and Karihaloo, B.L., (1993) "Shear Capacity of Longitudinally Reinforced Beams—A Fracture Mechanics Approach," *ACI Structural Journal*, V. 90, No. 6, pp. 591-600.

Taylor, HPJ. (1970). "Investigation of the forces carried across cracks in reinforced concrete beams in shear by interlock of aggregate," *Cement and Concrete Association*, London, Technical report 42.447.

Taylor, HPJ. (1972). "Shear Strength of Large Beams," *Journal of the Structural Division*, ASCE, V. 98, No. ST11, Nov., pp. 2473-2489.

Vecchio, F.J. and Collin, M.P. (1986). "The modified compression field theory for reinforced concrete elements subjected to shear" *ACI Structural Journal*, pp. 219-23.

Wilson, ND, Kiouisis, P. (2005) "High-Strength SCC in Shear," *Proceedings Second North American Conference on the Design and Use of Self-Consolidating Concrete and the Fourth International RILEM Symposium on Self-Compacting Concrete*, (CDROM), Chicago, Illinois.

Xu, S., Zhang, X., and Reinhardt, H.W., (2012) "Shear Capacity Prediction of Reinforced Concrete Beams without Stirrups Using Fracture Mechanics Approach," *ACI Structural Journal*, V. 109, No. 5, pp. 705-714.

Table 1- Shear beams test matrix

Section	Bottom reinforcement	Top reinforcement	ρ
NS-4	4#22	2#13	0.0127
NS-6	6#22	2#13	0.0203
NS-8	8#22	2#22	0.0271

Table 2 - Mechanical properties of reinforcing steel

Bar No.	Modulus of elasticity	Yielding stress	Elongation
	MPa	MPa	%
10	206,890	494	11.7
13	196,570	510	13.3
22	193,140	449	16.3

Table 3 - Mixture proportions of concrete

Material	Water kg/m ³	Cement kg/m ³	Fly ash kg/m ³	Fine aggregate kg/m ³	Coarse aggregate kg/m ³	AE l/m ³	HRWR l/m ³	VMA l/m ³
CC	179	336	112	576	1056	0.18	-	-
SCC	179	336	112	576	1056	0.18	1.75	2.34

Table 4 - Fresh mixture properties

Property	Air Content	Unit Weight	Slump	Slump Flow	J-Ring	Visual Stability Index	Static Segregation Column	L-Box
	%	kg/m ³	mm	mm	mm		%	%
CC	5.0	2370	100	-	-	-	-	-
SCC	5.9	2360	-	620 ¹	585	1 ²	3.5 ³	81.7 ⁴

¹A common range of slump flow for SCC is 450 to 760 mm (ACI 237R (2007)).

²1 = Stable with no evidence of segregation and slight bleeding observed as a sheen on the concrete mass (ASTM C1611 (2009)).

³SCC is generally considered to be acceptable if the percent segregation is less than 10% (ACI 237R (2007)).

⁴The minimum ratio of the L-Box value is considered to be 80% (ACI 237R (2007)).

Table 5 - Test results summary

Section			\bar{f}_c	V_{test}^*	$v_{test}=V_{test}/b_w d$	v_{test}/\bar{f}_c	$v_{test}/\sqrt{\bar{f}_c}$
			(MPa)	(kN)	(MPa)	%	
CC	NS-4	1	34.0	106.8	0.9	2.6	0.15
		2	34.5	123.2	1.0	2.9	0.18
	NS-6	1	34.0	155.7	1.4	4.0	0.24
		2	34.5	165.5	1.4	4.2	0.25
	NS-8	1	34.0	152.6	1.3	3.9	0.24
		2	34.5	191.3	1.7	4.9	0.29
SCC	NS-4	1	53.5	129.9	1.1	2.0	0.15
		2	39.6	128.1	1.1	2.7	0.17
	NS-6	1	53.5	177.9	1.6	2.9	0.22
		2	39.6	169.5	1.5	3.8	0.24
	NS-8	1	53.5	210.4	1.8	3.4	0.25
		2	39.6	185.5	1.6	4.1	0.25

*: Includes part of the load frame not registered by the load cells and also the beam self weight at a distance d from the interior face of the support plate.

Table 6 - Maximum strains of longitudinal reinforcement at shear failure (μ mm/mm) *

Section		CC	SCC
NS-4	1	1169	1644
	2	1441	1405
NS-6	1	1430	1782
	2	1378	1695
NS-8	1	1125	1660
	2	1202	1271

* $\epsilon_y = 2325 \mu \text{ mm/mm}$

Table 7 - Comparison of shear strength of experiment and codes

Section		AASHTO	ACI	AS-3600	CSA	Eurocode 2	JSCE		
CC	NS-4	1	0.73	0.91	0.88	0.74	0.81	0.99	
		2	0.89	1.04	1.01	0.89	0.93	1.14	
	NS-6	1	1.12	1.41	1.15	1.13	1.07	1.30	
		2	1.22	1.49	1.21	1.22	1.13	1.38	
	NS-8	1	0.98	1.38	1.02	0.99	1.05	1.16	
		2	1.33	1.72	1.27	1.34	1.31	1.44	
	Ave.		1.04	1.32	1.09	1.05	1.05	1.24	
	COV (%)		21.00	22.63	13.41	20.99	16.19	13.57	
	SCC	NS-4	1	0.77	0.88	0.92	0.78	0.85	1.04
			2	0.88	1.01	1.00	0.89	0.93	1.13
NS-6		1	1.08	1.28	1.26	1.09	1.17	1.28	
		2	1.17	1.42	1.18	1.18	1.11	1.34	
NS-8		1	1.22	1.52	1.33	1.22	1.25	1.37	
		2	1.18	1.55	1.18	1.19	1.21	1.34	
Ave.		1.05	1.28	1.15	1.06	1.09	1.25		
COV (%)		17.48	21.68	13.62	17.17	14.83	10.73		

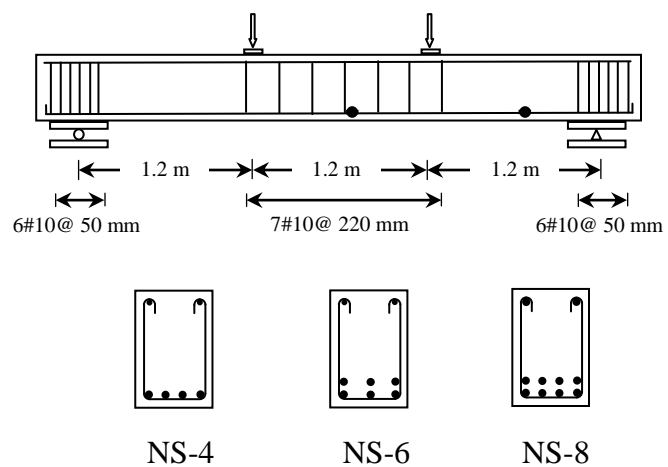
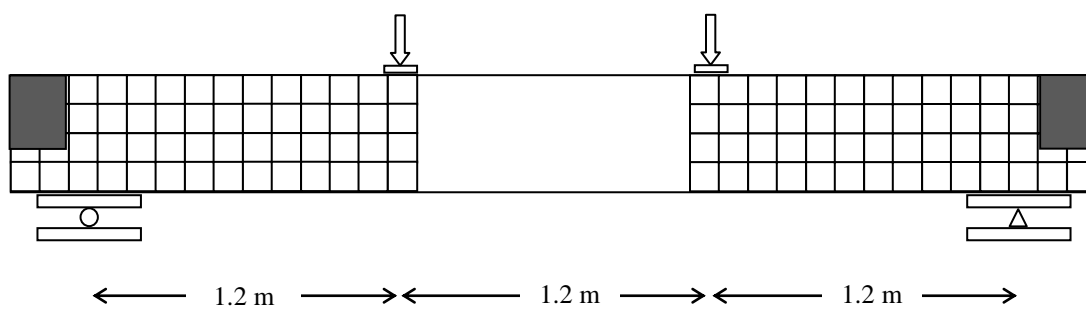


Figure 1 - Load pattern, cross sections, reinforcement layout, and location of strain gauges on the test beams



CC-NS-4



SCC-NS-4



CC-NS-6



SCC-NS-6



CC-NS-8



SCC-NS-8



Figure 2 - Crack pattern of the beams at shear failure

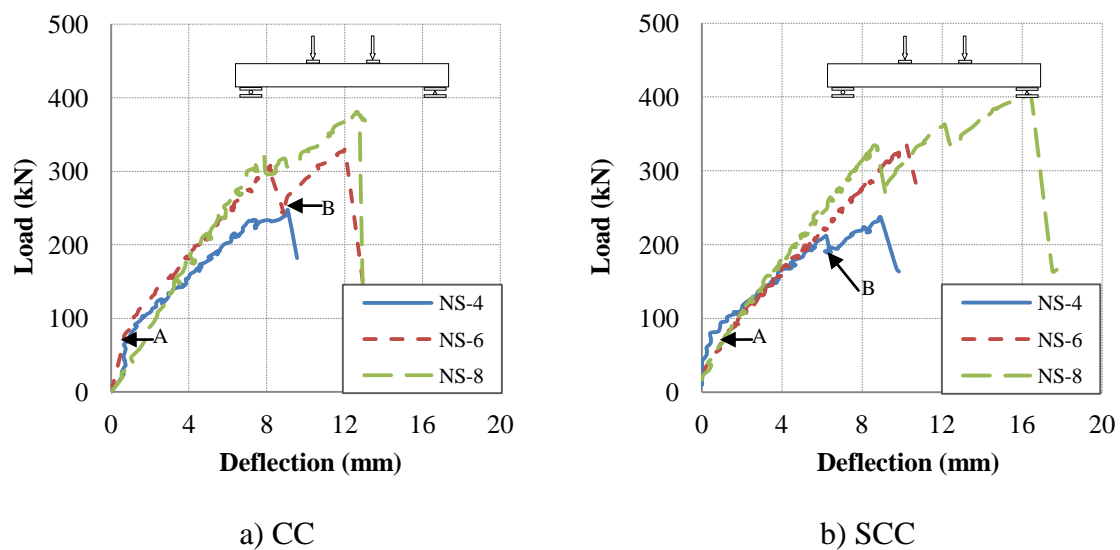


Figure 3 - Load-deflections of the beams

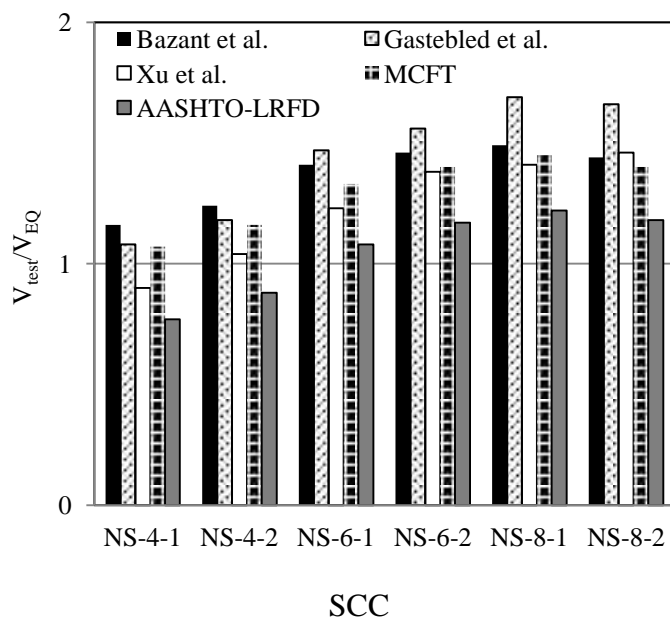
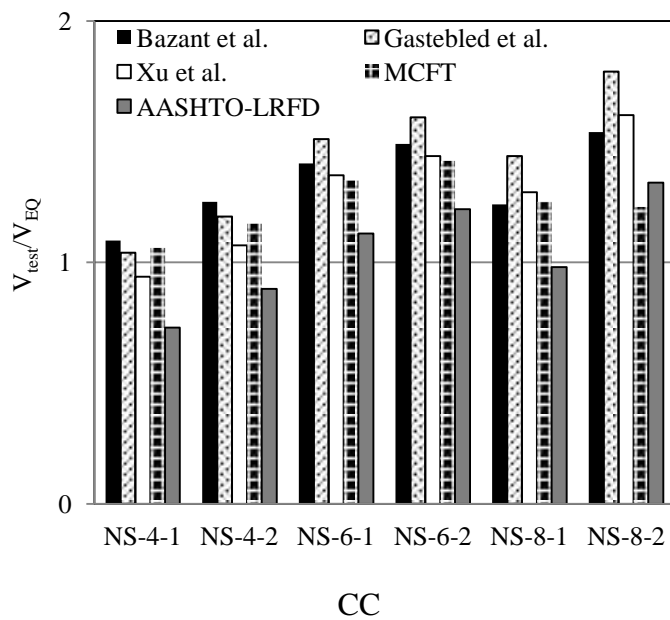


Figure 4 - Comparison of shear strength of experiment with fracture mechanics approaches and MCFT method

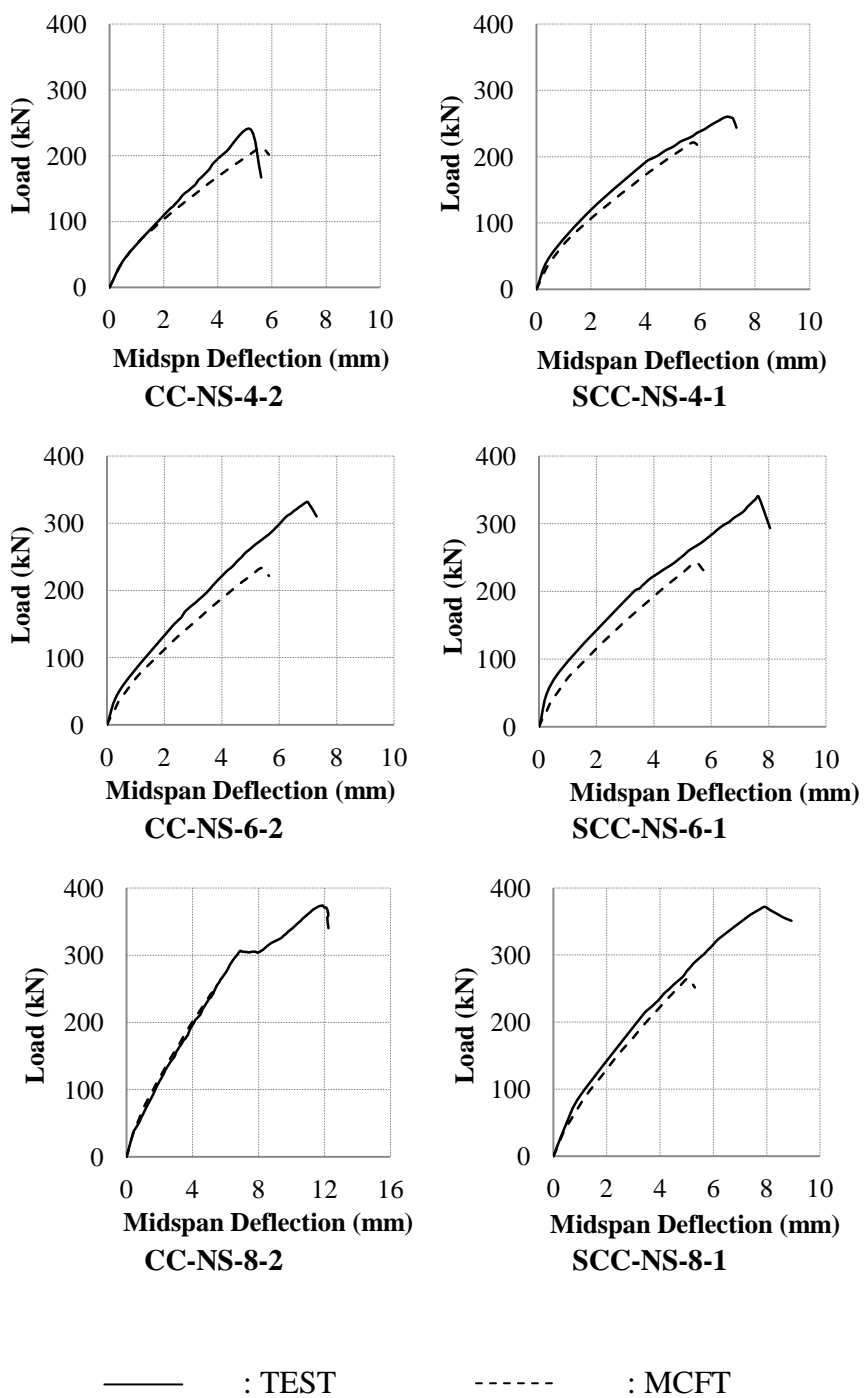


Figure 5 - Load-deflections of the beams (test and MCFT method)

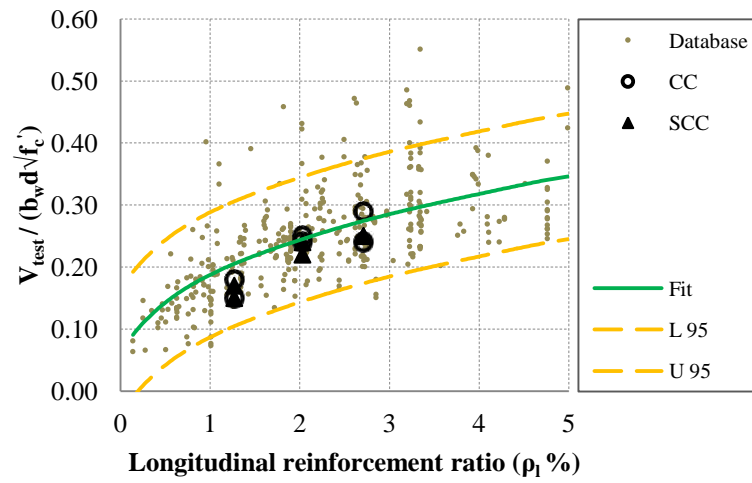


Figure 6 - Shear strength vs. longitudinal reinforcement ratio; results from (Reineck et al. 2003) and test results of this study

$$\text{Fit Equation: } \frac{V_{\text{test}}}{b_w d \sqrt{f_c}} = 0.1824 \rho^{0.3828}$$

SECTION

3. SUMMARY , CONCLUSIONS AND RECOMMENDATIONS

3.1. SUMMARY OF RESEARCH WORK

The purpose of this research was to evaluate the shear and fracture behavior of two high performance concretes – HVFAC and SCC – and determine their potential for success within the concrete industry. The test matrices for both studies were identical. Each study included 16 full-scale shear specimens, with 8 constructed from the respective high performance concrete (HVFAC or SCC) and 8 constructed from a conventional concrete to serve as a control. Three different longitudinal steel ratios were used in the construction of the 16 full-scale shear specimens. To investigate fracture energy, each study included 16 standard notched specimens, with 8 constructed from the respective high performance concrete (HVFAC or SCC) and 8 constructed from the conventional concrete control mix.

This chapter contains the conclusions from the full-scale shear tests, fracture energy results, and assessment of the shear design provisions of selected standards. Lastly, recommendations are presented.

3.2. CONCLUSIONS

The following section summarizes the conclusions from both the experimental and analytical studies of the two types of high performance concretes.

3.2.1. Shear Behavior of HVFAC. Based on the results of this study, the following conclusions can be made:

- In terms of crack morphology, crack progression, and load-deflection response, the behavior of the HVFAC and CC beams was virtually identical.
- In general, for a given standard, the ratios of experimental-to-code predicted capacity are higher for the HVFAC compared with the CC beams with the same amount of longitudinal reinforcement.

- Statistical data analyses (parametric and non-parametric) showed that the HVFAC beams had higher shear strength than the CC beams tested in this study.
- The HVFAC and CC test results fall within a 95% confidence interval of a nonlinear regression curve fit of the CC shear test database.
- Based on a comparison of the test results of this study with the shear database available for CC specimens, it can be inferred the HVFAC beams had greater shear capacity than the CC beams.
- The AASHTO LRFD estimations of the longitudinal tensile strain of the reinforcements were close to the actual strain for the low and medium longitudinal reinforcement ratio beams. However, the AASHTO LRFD equations underestimated strain of high longitudinal reinforcement ratio beams.
- The AASHTO LRFD equation predicts the diagonal shear crack angle of both the CC and HVFAC beams very well for beams without shear reinforcement, but it overestimates the values for beams with shear reinforcement.
- The fracture mechanics approaches underestimate the shear strength of both the CC and HVFAC beams, but appear to be equally applicable to both materials.
- The MCFT method somewhat overpredicts shear strength of both the CC and HVFAC beams, although in general offers very good agreement.

3.2.2. Shear Behavior of SCC. Based on the results of this study, the following conclusions can be made:

- In terms of crack morphology, crack progression, and load-deflection response, the behavior of the SCC and CC beams was virtually identical.
- In general, for a given standard, the ratios of experimental-to-code predicted capacity are very consistent between the two concrete types for beams with the same amount of longitudinal reinforcement.
- For beams without stirrups, the ratios of experimental-to-code predicted values for each standard were slightly higher for the SCC compared with the CC.

- For beams with stirrups, the ratios of experimental-to-code predicted values for each standard were slightly higher for the CC compared with the SCC.
- For beams without stirrups, shear provisions of all selected standards except the JSCE-07 overestimated the shear capacity of the CC and SCC beams for low longitudinal reinforcement ratios.
- For beams with stirrups, shear provisions of all selected standards underestimated the shear capacity of the CC and SCC beams, with values ranging from 1.19 to 1.42. Most importantly, the ratios were all well above 1.0, indicating a conservative result for the code predicted values.
- Statistical data analyses (parametric and non-parametric) showed that there is no statistically significant difference in the normalized shear strength of the SCC and CC beams tested in this study.
- The SCC and CC test results fall within a 95% confidence interval of a nonlinear regression curve fit of the CC shear test database.
- Based on a comparison of the test results of this study with the shear database available for CC specimens, it can be inferred that there is no significant difference between the shear strength of chemically-based SCC beams and that of CC.
- The AASHTO LRFD estimation of the longitudinal tensile strain of the reinforcements is less than the actual strain for the SCC beams. This higher strain in the reinforcements can be attributed to higher dowel action. Since both the SCC and the CC beams had the same crack patterns, it may be inferred that the SCC beams have lower aggregate interlock compared with the CC beams.
- The AASHTO LRFD equation predicts the diagonal shear crack angle of both the CC and SCC beams very well for beams with shear reinforcement, but it underestimates for the beams without shear reinforcement.
- The fracture mechanics approaches underestimate the shear strength of both the CC and SCC beams, but appear to be equally applicable to both materials.
- The MCFT method somewhat overpredicts shear strength of both the CC and SCC beams, although in general offers very good agreement.

3.2.3. Fracture Energy of HVFAC. Based on the results of this study, the following conclusions can be made:

- The Bazant and CEB-FIP Model Code 2010 equations underestimate the fracture energy of specimens except for one batch, while JSCE overestimates the fracture energy of specimens. The Bazant equation has the closest agreement with the fracture energy of specimens measured from tests.
- Statistical test results show the HVFAC mix possesses higher normalized fracture energy compared with the CC mix.

3.2.4. Fracture Energy of SCC. Based on the results of this study, the following conclusions can be made:

- The fracture energies for both mixes showed excellent agreement with both the Bazant and CEB-FIP equations, with most of the test values falling within 10% of the predicted fracture energies.
- Statistical analyses indicated that the normalized fracture energy for the SCC mix exceeded that for the CC mix.

3.3. RECOMMENDATIONS

Based on the conclusions stated in the previous sections, the following recommendations for future research were developed:

- Study the effect of depth of section, shear span to depth of section, compressive strength of concrete, and aggregate size on shear strength of HVFAC and SCC
- Perform shear tests on I shape girders for both HVFAC and SCC
- Investigate the shear strength of HVFAC and SCC columns
- Study cyclic load behavior of HVFAC and SCC on beams and columns

APPENDIX A
AN EXPERIMENTAL STUDY ON BOND STRENGTH OF REINFORCING STEEL
IN HIGH-VOLUME FLY ASH CONCRETE

AN EXPERIMENTAL STUDY ON BOND STRENGTH OF REINFORCING STEEL IN HIGH-VOLUME FLY ASH CONCRETE

Trevor J. Looney, Mahdi Arezoumandi, Jeffery S. Volz, John J. Myers

Abstract

The production of Portland cement – the key ingredient in concrete – generates a significant amount of carbon dioxide. However, due to its incredible versatility, availability, and relatively low cost, concrete is the most consumed man-made material on the planet. One method of reducing concrete's contribution to greenhouse gas emissions is the use of fly ash to replace a significant amount of the cement. An experimental investigation was conducted to compare the bond strength of reinforcing steel in high-volume fly ash concrete (HVFAC) – concrete with at least 50% of the cement replaced with fly ash – with conventional concrete (CC). This study investigated two HVFAC mixes (with one mix having a relatively high total cementitious content [502 kg/m³] and the other mix having a relatively low total cementitious content [337 kg/m³]) as well as a CC mix. Both HVFAC mixes utilized a 70% replacement of Portland cement with a Class C fly ash. This experimental program consisted of 18 pull-out specimens as well as 9 full-scale beams (three for each concrete type). The pull-out specimens were based on RILEM recommendations, and the beam specimens were tested under a simply supported four-point loading condition. The CC test results served as a control and were used to evaluate the results from the HVFAC pull-out and beam specimen tests. Furthermore, a comparison was performed between results of this study and a bond database of CC specimens. These comparisons indicate that HVFAC beams possess greater bond strength than CC beams.

Keywords:

High-Volume Fly Ash Concrete, Conventional Concrete, Bond Strength, Experimental Study

Introduction

Concrete is the most widely used man-made material in the world, and cement is an essential ingredient in the production of Portland cement concrete. The cement industry plays a key role in the world, from both an economic and an environmental perspective. In 2011, world cement output was estimated at 3.4 billion metric tons [1]. Cement production is also a relatively significant source of global carbon dioxide (CO₂) emissions, accounting for approximately 4.5% of global CO₂ emissions from industry in 2007 [2]. According to the World Business Council for Sustainable Development (WBCSD), the manufacture of cement emissions varies across worldwide regions from 0.73 to 0.99 kg of CO₂ for each kilogram of cement produced [3].

One of the solutions for this global concern is the use of supplementary cementitious materials as replacement of cement. The most available supplementary cementitious material worldwide is fly ash, a by-product of coal-burning thermal power stations [4]. ASTM C618-08 [5] defines fly ash as “the finely divided residue that results from the combustion of ground or powdered coal and that is transported by flue gasses.” Fly ash is categorized in three classes: class N, F, and C based on the chemical compositions [6].

Fly ash has been used in the U.S. since 1930; Davis et al. (1937) were the first researchers to publish their results about using fly ash in concrete [6]. Initially, fly ash was used in massive structures like the Thames Barrage in the UK and the Upper Stillwater Dam in the U.S., with about 30 to 75% mass replacement of hydraulic cement to reduce heat generation [6]. Subsequent research [7-11] has shown some beneficial aspects of using fly ash in concrete such as low permeability and high durability.

Traditionally, fly ash used in structural concrete as a replacement or supplementary material is limited to 15% to 25% cement replacement [12, 13] except in high strength concrete (HSC) where replacement levels of Portland cement at 35% are more common to control peak hydration temperature development [14]. When a significant amount of fly ash is used, how it contributes to the strength development of the concrete and the hydration characteristics of this type of material are of significant research interest. High-volume fly ash concrete (HVFA) is a concrete generally defined with at least 50% of the Portland cement replaced with fly ash. In 1986, the Canadian

Centre for Mineral and Energy Technology (CANMET) developed HVFAC for structural applications. The investigations by CANMET [15] and also other researchers [16, 17] have shown that HVFAC has lower shrinkage, creep and water permeability and higher modulus of elasticity compared with conventional concrete (CC).

Comprehensive research has been done on both the fresh and hardened properties of HVFAC, but very little research has been performed on the structural behavior of HVFAC. Naik et al. [18] performed pull-out tests on specimens with fly ash replacements of 10, 20, and 30% of the Portland cement. The researchers concluded that the bond strength improved with the increase in fly ash up to about 20% cement replacement and after that it began to decrease. Researchers at Montana State University [19] performed a series of pull-out tests on specimens utilizing 100 % Class C fly ash as a replacement of Portland cement. The specimen design involved #13 bars embedded into a concrete cylinder (150 x 300 mm). The embedment depth was varied from 200 to 300 mm for each material. Results of this study indicated lower bond strength for HVFAC compared to normal concrete. Gopalakrishnan et al. [20] conducted pull-out tests to determine the effects of using 50% fly ash replacement of cement on bond strength. Specimens had #20 bars embedded into a 150 mm concrete cube. The researchers reported identical bond strength for HVFAC and CC specimens.

The following study presents the results of an experimental investigation that compares the bond strength of 18 pull-out specimens and 9 full-scale HVFAC and CC beams. The results of this study were also compared with a bond database of CC beam specimens.

Experimental Program

Several different methods are used to study bond between steel reinforcement and concrete. The four most common methods are pull-out specimens, beam-end specimens, beam anchorage specimens, and beam splice specimens. The last three methods provide more realistic measures of bond strength compared with pull-out specimen tests [21]. However, the pull-out specimen is more popular due to ease of construction and simplicity of the test. The main drawback with this test is that the stress state does not reflect the actual stress state within a reinforced concrete member. In the pull-out

specimen test, the bar is in tension and the concrete surrounding the bar is in compression, but in most reinforced concrete members, both the bar and the surrounding concrete are in tension. For this reason, ACI 408-03 does not recommend the pull-out specimen test to determine development length of reinforcement. However, pull-out specimen tests are valid in determining relative performance between different types of concretes or different types of reinforcing bar coatings [22-27]. The current study used both pull-out specimens and beam splice specimens to evaluate HVFAC reinforcement bond strength compared with CC.

Specimen Design

The following section contains details regarding the pull-out and splice specimens used in the current study to evaluate bond between reinforcing steel and concrete.

Pull-out Specimens

The pull-out specimens were designed using RILEM 7-II-128 [28] as a guide. The bars were embedded 10 times the bar diameter into the concrete specimen based on preliminary testing, with half of the length debonded using a section of polyvinyl chloride (PVC) tubing. The RILEM report recommends casting the bars into concrete cubes that provide a clear cover of 4.5 times the bar diameter from the bar to the center of each side of the horizontal cross section. The specimens designed for this experiment exceeded the RILEM 7-II-128 requirement on clear cover and featured a 300 mm concrete cylinder to eliminate the potential for splitting and ensure that all of the specimens failed in the same manner (pull-out). Figure 1 is a schematic diagram of the pull-out test specimens.

Splice Specimens

Nine beams (three for each concrete type) were designed to preclude flexural and shear failures and satisfy the minimum and maximum longitudinal reinforcement requirements of ACI 318-08 [29]. The beams measured 3000 mm in length, with a cross section of 300 mm x 460 mm, and a splice in the longitudinal steel centered at midspan. The longitudinal steel consisted of three #19 bars while the shear reinforcement consisted of #10, U-shaped stirrups. One beam of each type was cast upside down to evaluate the

top bar effect. The test setup used a simply supported four-point loading condition in order to place the splice under a uniform stress, as shown in Figure 2, with the stirrups discontinued within the center portion of the beam to provide an unconfined splice condition. To ensure a bond failure prior to a flexural failure, the splice length was chosen as 70% of the development length calculated in accordance with Eq. 12-1 in ACI 318-08, repeated as Eq. 1.

$$l_d = \frac{3}{40} \frac{f_y}{\sqrt{f'_c}} \frac{\Psi_t \Psi_e \Psi_s}{\left(\frac{c_b + k_{tr}}{d_b} \right)} d_b \quad (1)$$

where:

l_d = the development length;

f_y = the specified yield strength of reinforcement;

f'_c = the specified compressive strength of concrete;

Ψ_t = the reinforcement location modification factor;

Ψ_e = the reinforcement coating modification factor;

Ψ_s = the reinforcement size modification factor;

c_b = the smaller of the distance from center of a bar to nearest concrete surface and one-half the center-to-center spacing of bars being developed;

K_{tr} = the transverse reinforcement index,;

d_b = the nominal diameter of the reinforcing bar.

Based on these calculations, the splice length was 360 mm.

Materials

The cementitious materials used for this study were ASTM Type I Portland cement; ASTM Class C fly ash from the Ameren Labadie Power Plant (Labadie, MO); gypsum from USA Gypsum (Reinholds, PA); and calcium hydroxide from the Mississippi Lime company (Sainte Genevieve, MO). Table 1 shows the physical properties and chemical compositions of the cement and fly ash.

The coarse aggregate consisted of crushed limestone with a maximum nominal aggregate size of 19 mm from Jefferson City Dolomite (Jefferson City, MO). The fine aggregate was natural sand from Missouri River Sand (Jefferson City, MO).

All of the reinforcing bars were from the same heat of steel, used the same deformation pattern, and met the requirements of ASTM A615-09 [30], Grade 60, 414 MPa material. Table 2 contains the tested mechanical properties of the reinforcing steel. The rib height, rib spacing, and relative rib area for each bar size was in accordance with ACI 408R-03 and ASTM A615-09, with the #13 and #19 reinforcing bars used in the pull-out and splice specimens having relative rib areas of 0.088 and 0.081, respectively.

Mixture Proportions

The concrete mixtures with a target compressive strength of 28 MPa were delivered by a ready-mix concrete supplier (Rolla, MO). The mixture proportions are given in Table 3. The HVFAC mixes used a 70% replacement of cement with fly ash – with one mix containing a relatively high total cementitious content (502 kg/m³) and the other mix containing a relatively low total cementitious content (337 kg/m³). The designations HVFA-H and HVFA-L represent the relatively high and relatively low total cementitious content HVFAC mixes, respectively. For the HVFAC, the gypsum was used to maintain the initial hydration stage by preventing sulfate depletion, while the calcium hydroxide ensured a more complete hydration of the fly ash with the low content of Portland cement in the mix [31]. The drums were charged at the ready-mix facility with the required amounts of cement, fly ash, sand, coarse aggregate, and water, while the powder activators (gypsum and lime) were added when the truck arrived at the lab, approximately 5 minutes later. After the gypsum and lime were added, the HVFAC was mixed at high speed for 10 minutes.

Fabrication and Curing of Test Specimens

Both the pull-out and beam splice specimens were constructed and tested in the Structural Engineering High-Bay Research Laboratory (SERL) at Missouri University of Science and Technology. After casting, the specimens and the quality control/quality assurance companion cylinders (ASTM C39-12 [32] and C496-11[33]) and beams

(ASTM C78-10[34]) were covered with both wet burlap and a plastic sheet. All of the full-scale specimens and companion cylinders and beams were moist cured for three days and, after formwork removal, were stored in a semi-controlled environment with a temperature range of 18 to 24°C and a relative humidity range of 30 to 50% until they were tested at an age of 28 days.

Fresh and Hardened Properties

Table 4 presents the fresh and hardened strength properties of the CC and HVFAC mixes.

Test Setup and Procedure

The following section contains details regarding the test setup for the pull-out and beam splice specimen testing.

Pull-out Test

The pull-out specimens were loaded into an 890-kN Tinius Olson machine by rotating the specimen 180°, bar side down, and threading the bar through a thin piece of rubber and the head of the machine until the specimen rested evenly on the rubber. The free end of the bar was clamped into a lower component of the Tinius Olson machine. A magnetic arm holding a Linear Variable Differential Transformer (LVDT) was then placed on top of the specimen. The LVDT was placed directly on top of the exposed rebar on the back end of the specimen to record bar slip.

The loading rate for the Tinius Olson machine was set at 2.5 mm/min. to avoid any dynamic effect and in order to insure a sufficient number of data points prior to failure. The load was recorded on a data acquisition computer linked to the test machine. The LVDT was also monitored to record bar slip as a function of load. The test protocol consisted of loading the bar in tension to the maximum capacity and then continuing to apply load in order to develop the full load-slip curve.

Splice Specimen Test

A load frame was assembled and equipped with two 490-kN, servo-hydraulic actuators intended to apply the two point loads to the beams. The load was applied in a displacement control method at a rate of 0.50 mm/min. The beams were supported on a roller and a pin support, 300 mm from each end of the beam, creating a four-point loading situation with the two actuators. An LVDT was used to measure the deflection at the beam center and strain gages were installed at both ends of each splice to monitor the strain in the longitudinal reinforcement during the test. Figure 2 shows both the beam loading pattern and the location of the strain gages. During the test, any cracks that formed on the surface of the beam were marked at load increments of approximately 22 kN, and both the deformation and strains were monitored until the beam reached failure.

Test Results and Discussions

The following section contains the results from the pull-out and splice specimen tests as well as a discussion and comparison between CC and HVFAC.

Pull-out Tests

All of the pull-out specimens experienced a bond shear failure. A bond shear failure occurs when the reinforcing bar and associated concrete located between the transverse ribs pulls out of the specimen as a cylinder without splitting the remaining concrete. Table 5 indicates the results of the pull-out tests. To compare the test results of the HVFAC and the CC, the values must be adjusted to reflect the different compressive strengths of the specimens. In the majority of design standards, bond strength is a function of the inverse square root of the compressive strength of the concrete (ACI 318-08, AASHTO LRFD-07 [35], AS 3600-09 [36], CSA-04 [37], and JSCE-07 [38]), but ACI 408R-03 recommends a relationship based on the inverse fourth root of the compressive strength of the concrete.

Consequently, to compare the bond strength of the HVFAC and CC specimens, the test results were normalized with both the square root and fourth root of the compressive strength of the concrete. As shown in Table 5, the bond strengths of the #13

bars for the HVFAC (both high and low cementitious content) were almost identical with the CC when normalized by either the square root or fourth root of compressive strength. In contrast, the bond strength of the #19 bars increased 17% and 12% for the high and low cementitious content HVFAC, respectively, compared with the CC when the test results were normalized by the square root of the compressive strength of the concrete. When comparing the HVFAC and CC pull-out tests normalized with the fourth root relationship, the bond strength for the #19 bars increased 9% and 5% for the high and low cementitious content HVFAC, respectively, compared with the CC.

Also, as shown in Figure 3a, the HVFAC (both high and low cementitious content) specimens had longer post peak portions of the load-slip curves compared with the CC specimens. This improved load-slip behavior may be the result of a decrease in bleed water observed in the HVFAC during construction of the test specimens.

Splice Specimen Tests

All of the beams failed in bond, experiencing a splitting failure. Based upon data collected from the strain gages, none of the longitudinal reinforcement reached yield at failure. Figure 3b shows the load-deflection behavior for the beams (the deflection was measured at midspan) for both the HVFAC and the CC specimens. Before the first flexural cracks occurred (point A), all of the beams displayed a steep linear elastic behavior. After the appearance of flexural cracks in the maximum moment region, by increasing the load, new flexural cracks were formed between the two point loads. Upon further increasing the applied load, a bond failure occurred. As Figure 3b reveals, the load-deflection behavior of the HVFAC and CC beams was essentially identical except for the value at failure. Similarly, the cracking patterns experienced by the HVFAC and CC were essentially identical, as shown in Figure 4. All of the beams displayed a horizontal splitting failure along the length of the longitudinal splice.

Table 6 summarizes the longitudinal reinforcement stress at bond failure as determined from the strain gages, where the specimen designation “Top” refers to the specimen cast upside down to evaluate the top bar effect. Also included in Table 6 are calculated steel stresses based on a moment-curvature approach, with the first calculated value based on the Popovic, Thorenfeldt, and Collins stress-strain curve, and the second

calculated value based on the Hognested stress-strain curve (ACI 408R-03 recommended method). Furthermore, as with the pull-out test, to compare the bond strength of the HVFAC and CC specimens, the test results were normalized with both the square root and fourth root of the compressive strength of the concrete.

Test results show that the high cementitious content HVFAC beams had 29% and 48% higher average longitudinal reinforcement stress compared with the CC beams when normalized by the square root of the compressive strength of the concrete for bottom and top reinforcement bars, respectively. When normalized with the fourth root of the concrete compressive strength, the high cementitious content HVFAC beams had 21% and 39% higher average longitudinal reinforcement stress compared with the CC beams for bottom and top reinforcement bars, respectively.

For the low cementitious content HVFAC beams, the average longitudinal reinforcement stress increased 15% and 23% compared with the CC beams when normalized by the square root of the compressive strength of the concrete for bottom and top reinforcement bars, respectively. When normalized with the fourth root of the concrete compressive strength, the low cementitious content HVFAC beams had 8% and 15% higher longitudinal reinforcement stress compared with the CC beams for bottom and top reinforcement bars, respectively.

The top bar effect didn't occur for the HVFAC specimens in this study. In fact, for all the HVFAC specimens, the top bars had either identical or even slightly higher bond strength than the bottom bars. In general, the top bar effect is caused by the accumulation of bleed water trapped beneath the underside of the reinforcing steel [21]. The trapped water reduces bond along this interfacial transition zone and, even more importantly, reduces the local strength of the concrete, in particular the tensile strength. Tensile strength of the concrete plays a critical role in bond splitting failures [21]. Fly ash, particularly large amounts of fly ash, increases the tortuosity of the capillary system within the concrete, rendering the system disconnected and decreasing the resulting capillary porosity [39, 40, 41]. This change in the capillary system results in a significant decrease in water migration during hydration, particularly for concretes with water-cementitious material ratios of 0.40 or less [40, 41], thus significantly reducing the top

bar effect. However, due to the limited number of top bar specimens used in this study – one for each concrete type – further research is needed to reach a definitive conclusion.

Table 7 presents the ratio of experimental-to-theoretical stress in the longitudinal reinforcement, with the theoretical value based on the moment-curvature analysis. The table includes analysis results based on two different stress-strain diagrams. The authors investigated both models to determine whether any noticeable differences resulted based on the assumed stress-strain diagram. The measured stresses are based on the strain gages installed at the start of each splice (see Figure 2). Even with the potential for slight inaccuracies in the strain gage readings due to localized cracking and the slight reduction in cross section required for mounting the gages, the measured readings offer a valuable basis of comparison with the moment-curvature results. Based on the strain gage measurements, results from the Popovic, Thorenfeldt, and Collins stress-strain curve underestimated the longitudinal reinforcement stress by approximately 20%, but the bar stress calculated based on the Hognested stress-strain curve had excellent agreement with the longitudinal reinforcement stress calculated based on the strain gages, with experimental-to-theoretical stress ratios ranging from 0.92 to 1.02.

Comparison of Test Results with Bond Test Database

Figure 5 presents the longitudinal steel reinforcement stress versus compressive strength of concrete for this study as well as the wealth of bond test data available in the literature (ACI 408-03). Given the significant scatter of the database of previous bond test results, it is somewhat difficult to draw definitive conclusions on the current test values. Nonetheless, visually, Figure 5 seems to indicate that the CC and HVFAC test results follow the same general trend of increasing bond strength as a function of the compressive strength of the concrete. Furthermore, statistical analysis of the data indicates that only one of the CC test results fall below a 95% confidence interval of a nonlinear regression curve fit of the database. The low cementitious content HVFAC and the other two CC test results fall within a 95% confidence interval of the nonlinear regression curve fit. However, all of the high cementitious content test results fall above a 95% confidence interval of the nonlinear regression curve fit of the database. As a result,

it would appear that the bond strength of HVFAC for the beams tested in this study is comparable or greater than CC.

Fracture Energy Testing

Based on the bond testing performed, particularly the beam splice specimens, it is evident that after normalizing for concrete strength, the HVFAC shows improved bond strength compared to the CC. As stated in ACI 408 [21], for bond failures caused by splitting of the concrete, the peak load is governed by the tensile response of the concrete, which is a function of both the tensile capacity and the energy dissipation capacity (fracture energy). In fact, ACI 408 states that for concrete that has similar tensile strengths, improved bond will result for whichever concrete exhibits higher fracture energies. As shown in Table 4, the normalized splitting tensile strength of the CC falls between that for the two HVFAC mixes, with all mixes falling within 10% of each other, indicating no discernible tensile strength benefit of the HVFAC. As a result, the researchers performed fracture energy tests on the three mixes used in the bond study to determine the potential cause of the increased bond strengths for the HVFAC.

The researchers performed fracture energy tests on both the CC and HVFAC using the standard three-point, notched specimen, bend test. The beam specimens measured 150×150×600 mm with a span length of 450 mm. The notch – which was cast into the concrete as opposed to being saw cut after the concrete hardened – had a depth of 40 mm and a thickness of 6 mm. A clip gauge measured the crack mouth opening displacement (CMOD), two linear variable differential transformers (LVDTs) measured deflection at midspan of the beam, and self-weight compensation was provided through lever arms (Figure 6). The tests were performed using a closed loop, servo-controlled MTS machine at a loading rate of 0.002 mm/s.

Results of the fracture energy tests were normalized in terms of concrete compressive strength using relationships developed by Bazant [42] and those within the CEB-FIP Model Code 2010 [43]. On average, the low and high cementitious content HVFAC mixes had normalized fracture energies 11% and 18% higher than the CC, respectively. In comparison, for the splice specimen tests, the low and high cementitious content HVFAC mixes had average, normalized bond strengths 8% and 21% higher than

the CC, respectively, when using the fourth root normalization. It would appear that the cementitious matrix formed by the HVFAC results in higher fracture energies than a conventional Portland cement matrix, leading to a corresponding increase in bond strength.

Findings and Conclusions

To study the bond strength of reinforcing steel in HVFAC, 18 pull-out specimens as well as 9 full-scale beams (both CC and HVFAC) were constructed and tested to failure. Based on the results of this study, the following findings and conclusions are presented for the pull-out tests:

The bond strength of the HVFAC (both high and low cementitious content) was virtually identical with the CC for the #13 bars.

The high cementitious content HVFAC and the CC specimens had the highest and lowest bond strength, respectively, for the #19 bars.

The HVFAC (both high and low cementitious) specimens had longer tails for the load-slip behavior compared with the CC specimens.

The following findings and conclusions are presented for the beam splice tests:

The HVFAC (both high and low cementitious content) beams had higher average longitudinal reinforcement steel stress compared with the CC beams.

The high cementitious content HVFAC beams had greater average longitudinal reinforcement steel stress than the low cementitious content HVFAC beams.

The top bar effect did not occur for the HVFAC specimens in this study, primarily as a result of the decreased capillary porosity of the mixes containing the high volumes of fly ash.

The load-deflection behavior of the HVFAC and CC beams was essentially identical except for the value at failure. Similarly, the cracking patterns experienced by the HVFAC and CC beams were essentially identical, with all of the specimens displaying a horizontal splitting failure along the length of the longitudinal splice.

The measured longitudinal reinforcement stress at bond failure had excellent agreement with the moment-curvature method based on the Hognested stress-strain-curve.

Based on the strain gage measurements, the moment-curvature method based on the Popovic, Thorenfeldt, and Collins stress-strain curve underestimated the longitudinal reinforcement stress by approximately 20% compared with the measured bar stress at bond failure.

For the specimens studied in this investigation, the HVFAC showed improved bond performance over the CC. This increase is most likely attributable to the increased fracture energies associated with the HVFAC. Further increases in bond strength for the top bar HVFAC beam splice specimens over the CC are a result of the decreased capillary porosity of the mixes containing the high volumes of fly ash. However, due to the limited nature of the data set regarding aspect ratio, mix designs, aggregate type and content, etc., investigated, the researchers recommend further testing to increase the database of test results.

Acknowledgment

The authors gratefully acknowledge the financial support provided by the Missouri Department of Transportation (MoDOT) and the National University Transportation Center at Missouri University of Science and Technology. The authors would also like to thank the support staff in the Department of Civil, Architectural and Environmental Engineering and Center for Infrastructure Engineering Studies at Missouri S&T for their efforts. The authors are also grateful for the ideas and help of Dr. David Darwin, the Deane E. Ackers Distinguished Professor of Civil Engineering, University of Kansas. The conclusions and opinions expressed in this paper are those of the authors and do not necessarily reflect the official views or policies of the funding institutions.

References

[1] USGS (2012). "Minerals Yearbook, Cement, U.S. Geological Survey," United States Department of the Interior, pp. 38-39.

- [2] Marland, G., T.A. Boden, and R.J. Andres. (2008). "Global, Regional, and National Fossil Fuel CO₂ Emissions. In Trends: A Compendium of Data on Global Change," Carbon Dioxide Information Analysis Center, Oak Ridge National Laboratory, United States Department of Energy, Oak Ridge, Tenn., <http://cdiac.ornl.gov/trends/emis/overview.html>, Accessed date March 2012.
- [3] Hanle, L., Jayaraman, K., and Smith, J. (2012) "CO₂ Emissions Profile of the U.S. Cement Industry," <http://infohouse.p2ric.org/ref/43/42552.pdf>, Accessed date March 2012.
- [4] Bilodeau, A. and Malhotra, V. M., (2000). "High-Volume Fly Ash System: Concrete Solution for Sustainable Development," ACI Material Journal V. 97, pp. 41-48.
- [5] ASTM 618-94a, (1995). "Standard Specification for Coal Fly Ash and Raw or Calcined Natural Pozzolan for Use as a Mineral Admixture in Portland Cement Concrete," Annual Book of ASTM Standards Vol. 04.02, American Society for Testing and Materials, Philadelphia, P.A., pp. 304-306.
- [6] ACI Committee 232 (2003). "Use of Fly Ash in Concrete" (ACI 232.2R-03). Farmington Hills, MI: American Concrete Institute.
- [7] Dunstan, E., (1984). "Fly Ash and Fly Ash Concrete," Report No. REC-ERC-82-1, Bureau of Reclamation, Denver, Colo., 42 pp.
- [8] Dunstan, E. R., Jr., (1976). "Performance of Lignite and Sub-Bituminous Fly Ash in Concrete," Report No. REC-ERC-76, U.S. Bureau of Reclamation, Denver, Colo., 23 pp.
- [9] Dunstan, E. R., Jr., (1980). "A Possible Method for Identifying Fly Ashes That Will Improve the Sulfate Resistance of Concretes," Cement, Concrete, and Aggregates, V. 2, No. 1, Summer, pp. 20-30.
- [10] Dunstan, M. R. H., (1981a). "Rolled Concrete for Dams-A Laboratory Study of High Fly Ash Concrete," Technical Note No. 105, Construction Industry Research and Information Association, London, 96 pp.
- [11] Dunstan, M. R. H., (1981b). "Rolled Concrete for Dams— Construction Trials Using High Fly Ash Content Concrete," Technical Note No. 106, Construction Industry Research and Information Association, London, 94 pp.
- [12] Berry, E.E., Hemmings, R.T., Zhang, M.H., Cornelious, B.J., Golden, D.M. (1994). "Hydration in High-volume Fly Ash Binders," ACI Materials Journal V. 91, pp.382-389.

- [13] ACI Committee 211, (1993). "Guide for Selecting Proportions for High-strength Concrete with Portland Cement and Fly Ash," ACI 226.4R, ACI Materials Journal, V. 90, pp. 272-283.
- [14] Myers, J.J., Carrasquillo, R.L., (1999) "Mix Proportioning for High-Strength HPC Bridge Beams," American Concrete Institute, Detroit, MI, American Concrete Institute Special Publication 189, pp. 37-56.
- [15] Malhotra, V.M. (1986). "Superplasticized Fly Ash Concrete for Structural Applications," Concrete International, V. 8, pp. 28- 31.
- [16] Li, S., Roy, D.M., Kumer, A. (1985). "Quantitative Determination of Pozzolanas in Hydrated System of Cement or $\text{Ca}(\text{OH})_2$ with Fly Ash or Silica Fume," Cement and Concrete Research, V. 15, pp.1079-1086.
- [17] Gopalan, M.K. (1993). "Nucleation and Pozzolanic Factors in Strength Development of Class F Fly Ash Concrete," ACI Materials Journal, V. 90, pp. 117-121.
- [18] Naik, T.R., Singh, S. S., Sivasundaram, V. (1989). "Concrete Compressives Strength, Shrinkage and Bond Strength As Affected by Addition of Fly Ash and Temperature." The University of Wisconsin – Milwaukee, Milwaukee, WI.
- [19] Cross, D., Stephens, J., and Vollmer, J. (n.d.). "Structural Applications of 100 Percent Fly Ash Concrete." Montana State University, Bozeman, MT.
- [20] Gopalakrishnan, S. (2005). "Demonstration of Utilising High Volume Fly Ash Based Concrete for Structural Applications." Structural Engineering Research Centre, Chennai India.
- [21] ACI Committee 408. (2003). "Bond and Development of Straight Reinforcing Bars in Tension" (ACI 408R-03). Farmington Hills, MI: American Concrete Institute.
- [22] Al-Sulaimani, G. J., Kaleemullah, M., Basunbul, I. A., and Rasheeduzzafar (1990). "Influence of corrosion and cracking on bond behavior and strength of reinforced concrete members." ACI Structural Journal, V. 87, No. 2, pp. 220-231.
- [23] Carins, J. and Abdullah, R. (1994). "Fundamental tests on the effects of an epoxy coating on bond strength" ACI Materials Journal, V. 91, No. 4, pp. 331-338.

- [24] Benmokrane, B., Challal, O., and Masmoudi, R. (1996). "Flexural response of concrete beams reinforced with FRP reinforcing bars." *ACI Structural Journal*, V. 91, No. 2, pp. 46-55.
- [25] Tighiouart, B., Benmokrane, B., and Gao, D. (1998). "Investigation of bond in concrete member with fiber reinforced polymer (FRP) bars." *Construction and Building Materials*, V. 12, pp. 453-462.
- [26] Andrade, C., Arteaga, A., Lopez-Hombrados, C., and Vazquez, A. (2001). "Tests on bonds of galvanized rebar and concrete cured in seawater." *Journal of Materials in Civil Engineering*, V. 13, No. 5, pp. 319-324.
- [27] Belaid, F., Arlique, G., and Francois, R. (2001). "Effect of bar properties on bond strength of galvanized reinforcement." *Journal of Materials in Civil Engineering*, V. 13, No. 6, pp. 454-458.
- [28] RILEM 7-II-128. (1994) "RC6: Bond Test for Reinforcing Steel. 1. Pull-Out Test." RILEM technical recommendations for the testing and use of construction materials, E & FN Spon, U.K., pp.102-105.
- [29] American Concrete Institute ACI Committee. (2008). "Building code requirements for structural concrete ACI 318-08 and commentary 318R-08." ACI 318-08/318R-08, Farmington Hills, MI: American Concrete Institute, pp. 155-168.
- [30] ASTM A615/A615M (2009). "Standard Specification for Deformed and Plain Carbon-Steel Bars for Concrete Reinforcement" ASTM, West Conshohocken, PA, 6 pp.
- [31] Bentz, D. P. (2010). "Powder Additions to Mitigate Retardation in High-Volume Fly Ash Mixtures", *ACI Materials Journal*, V. 107, No. 5, pp. 508-514.
- [32] ASTM C 39/C 39M (2012). "Standard Test Method for Compressive Strength of Cylindrical Concrete Specimens," ASTM, West Conshohocken, PA, 7 pp.
- [33] ASTM C 78/C 78M (2010). "Standard Test Method for Flexural Strength of Concrete (Using Simple Beam with Third-Point Loading)" ASTM, West Conshohocken, PA, 4 pp.
- [34] ASTM C 496/C 496M (2011). "Standard Test Method for Splitting Tensile Strength of Cylindrical Concrete," ASTM, West Conshohocken, PA, 5 pp.

- [35] American Association of State and Highway Transportation Officials (AASHTO) (2007). AASHTO LRFD Bridge Design Specifications, 4th Ed., Washington, D.C., pp. 5-(72-84).
- [36] AS 3600 (2009). "Concrete Structures," Standards Australia, Sydney, pp . 105-109.
- [37] CSA CAN3-A23.3 (2004). "Design of Concrete Standards for Buildings," Rexdale, Ontario, pp. 53-61.
- [38] Japan Society of Civil Engineers (2007). "Standard Specification for Concrete Structure" JSCE No. 15, Tokyo, pp. 154-159.
- [39] Malhotra, V.M. and Mehta, P.K. (2008). High-Performance, High-Volume Fly Ash Concrete for Building Sustainable and Durable Structures (3rd Ed.). Supplementary Cementing Materials for Sustainable Development, Inc., Ottawa, Canada.
- [40] Bentz, D.P. and Weiss, J. (2011). "Internal curing: A 2010 state of the art review." National NISTIR 7765. Institute of Standards and Technology, U.S. Department of Commerce, Gaithersburg, MD.
- [41] De la Varga, I. Castro, J., Bentz, D. and Weiss, J. (2012). "Application of internal curing for mixtures containing high volumes of fly ash." Cement & Concrete Composites, V. 34, pp. 1001-1008.
- [42] Bazant, Z.P. and Becq-Giraudon, E. (2002). "Statistical prediction of fracture parameters of concrete and implications for choice of testing standards." Cement & Concrete Research Journal, V. 32, pp. 529-556.
- [43] CEB-FIP Model Code 2010-fib (2012), V. 1, p. 120.

Table A.1- Properties and chemical compositions of cement and fly ash

Physical properties		
Property	Type I Cement	Class C Fly Ash
Fineness: Blaine, m ² /kg +325 mesh (+44 μm)	347 4.1%	not measured 14.4%
Specific gravity	3.15	2.73
Chemical compositions		
Component	Type I Cement (%)	Class C Fly Ash (%)
SiO ₂	21.98	33.46
Al ₂ O ₃	4.35	19.53
Fe ₂ O ₃	3.42	6.28
CaO	63.97	26.28
MgO	1.87	5.54
SO ₃	2.73	2.40
Na ₂ O	0.52 equivalent	1.43 equivalent
LOI	0.60	0.34

Table A. 2 - Mechanical properties of reinforcing steel

Bar No.	Modulus of elasticity	Yielding strength
	MPa	MPa
13	196,600	485
19	206,250	580

Table A. 3 - Mixture proportions of concrete

Mix	Water kg/m ³	Cement kg/m ³	Fly ash kg/m ³	Fine aggregate kg/m ³	Coarse aggregate kg/m ³	Gypsum kg/m ³	Calcium Hydroxide kg/m ³	Glenium 7500 liter/m ³
CC	201	449	-	655	1033	-	-	-
HVFAC-H	201	136	317	655	1033	14	35	-
HVFAC-L	134	92	213	735	1103	9	23	0.66

Table A. 4 - Fresh and hardened concrete properties

Property	CC	HVFAC-	HVFAC-L
Slump (mm)	114	127	139
Air content (%)	1.5	1.5	3.5
Unit weight (kg/m ³)	2390	2340	2451
Split cylinder strength* (kPa)	2650	2400	2100
Flexural strength** (kPa)	2850	2450	2950
Compressive strength* (MPa)	30.9	23.9	23.6

*: Values represent the average of three cylinders (ASTM C39-12 [32] and C496-11[34])

** : Values represent the average of three beams (ASTM C78-10[33])

Table A. 5- Pull-out test results (kN)

Section		f'_c (MPa)	P (kN)	μ^* MPa	$\frac{P}{\sqrt{\frac{f'_{c(test)}}{f'_{c(design)}}}}$	P_{ave} kN	$\frac{P}{\sqrt[4]{\frac{f'_{c(test)}}{f'_{c(design)}}}}$	P_{ave} (kN)
CC	13-1	30.9	44	17.2	42	43	43	44
	13-2		49	19.2	46		48	
	13-3		43	16.8	41		42	
HVFAc-H	13-1	23.9	44	17.2	47	44	46	43
	13-2		39	15.3	42		40	
	13-3		40	15.7	43		42	
HVFAc-L	13-1	23.6	38	14.9	41	42	40	41
	13-2		40	15.7	43		42	
	13-3		40	15.7	43		42	
CC	19-1	30.9	110	20.7	104	102	107	105
	19-2		111	20.9	105		108	
	19-3		103	19.3	97		100	
HVFAc-H	19-1	23.9	108	20.3	116	119	112	114
	19-2		108	20.3	116		112	
	19-3		115	21.6	124		119	
HVFAc-L	19-1	23.6	103	19.4	111	114	107	110
	19-2		112	21.0	121		116	
	19-3		103	19.4	111		107	

* : average bond strength

Table A. 6 - Longitudinal reinforcement stress (MPa)

Section		Measured ^I		Calculated (Moment-Curvature Method)				Measured ^I	
		Measured ^I	Ave.	(M-Φ) ^{II}	Ave.	(M-Φ) ^{III}	Ave.	$\frac{f_s}{\sqrt{\frac{f'_{c(test)}}{f'_{c(design)}}}}$	$\frac{f_s}{\sqrt[4]{\frac{f'_{c(test)}}{f'_{c(design)}}}}$
CC	1	376	356	304	292	375	363	337	346
	2	335		279		350			
	Top	332	332	278	278	348	348		
HV/FAC-H	1	430	405	333	334	397	398	436	420
	2	380		335		399			
	Top	433	433	360	360	422	422		
HV/FAC-L	1	372	358	328	314	390	376	387	372
	2	344		300		362			
	Top	356	356	326	326	388	388		

^I: Strain (from strain gages) multiplied by modulus of elasticity

^{II}: Popovic, Thorenfeldt, and Collins stress-strain curve

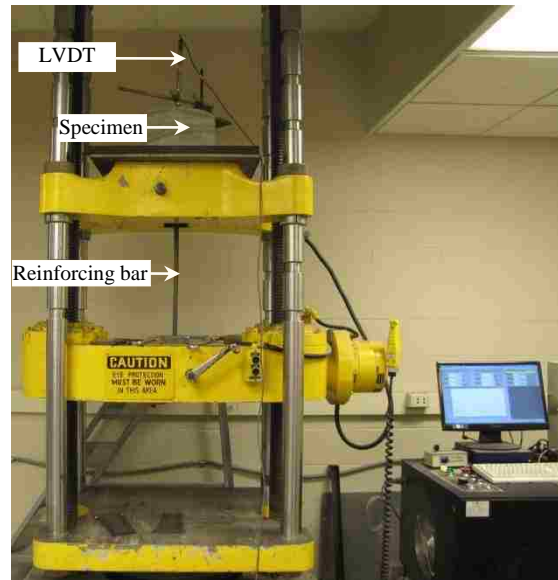
^{III}: Hognested stress-strain curve (ACI 408R-03 recommended method)

Table A. 7 - Experimental-to-theoretical ratio of longitudinal reinforcement stress

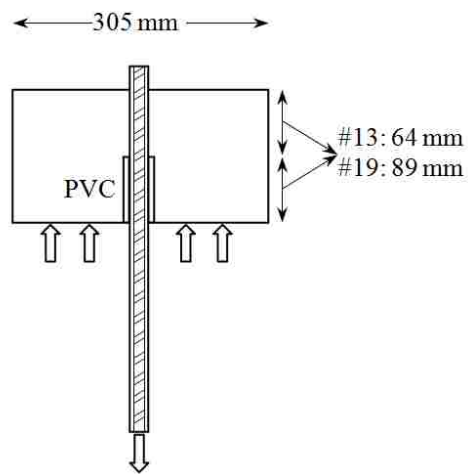
Section		$\left(\frac{f_{s(\text{test})}}{f_{s(M-\phi)}}\right)_{ave}^I$	$\left(\frac{f_{s(\text{test})}}{f_{s(M-\phi)}}\right)_{ave}^{II}$
CC	1	1.22	0.98
	2		
	Top	1.19	0.95
HVFAC-H	1	1.21	1.02
	2		
	Top	1.20	1.02
HVFAC-L	1	1.14	0.95
	2		
	Top	1.09	0.92
Ave.		1.18	0.97
COV (%)		4.2	4.3

^I: Popovic, Thorenfeldt, and Collins stress-strain curve

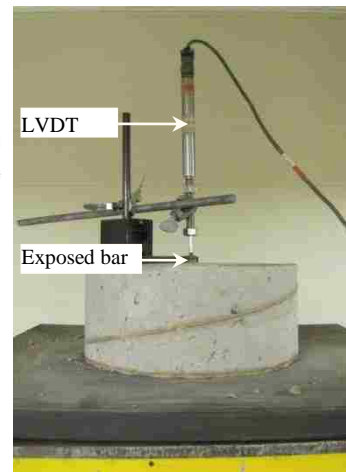
^{II}: Hognested stress-strain curve (ACI 408R-03 recommended method)



a) Direct pull-out test setup

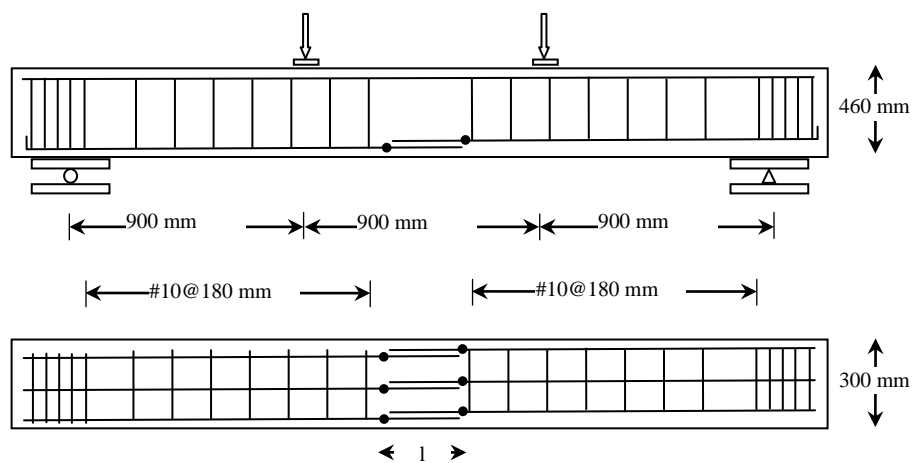


b) Pull-out test specimen details



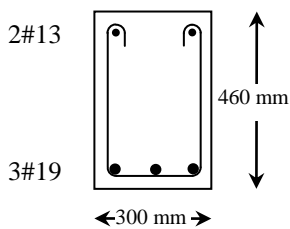
c) LVDT installation to measure bar slip

Figure A. 1- Pull out test specimen



● : Strain gage

a) Beam splice specimen reinforcing layout

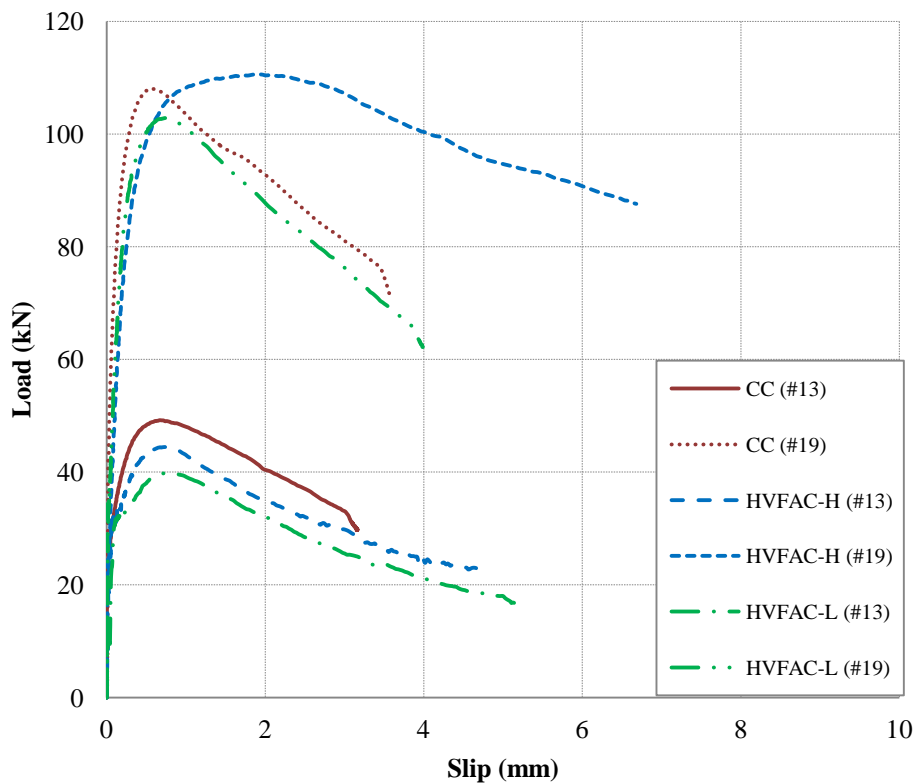


b) Beam splice specimen cross section

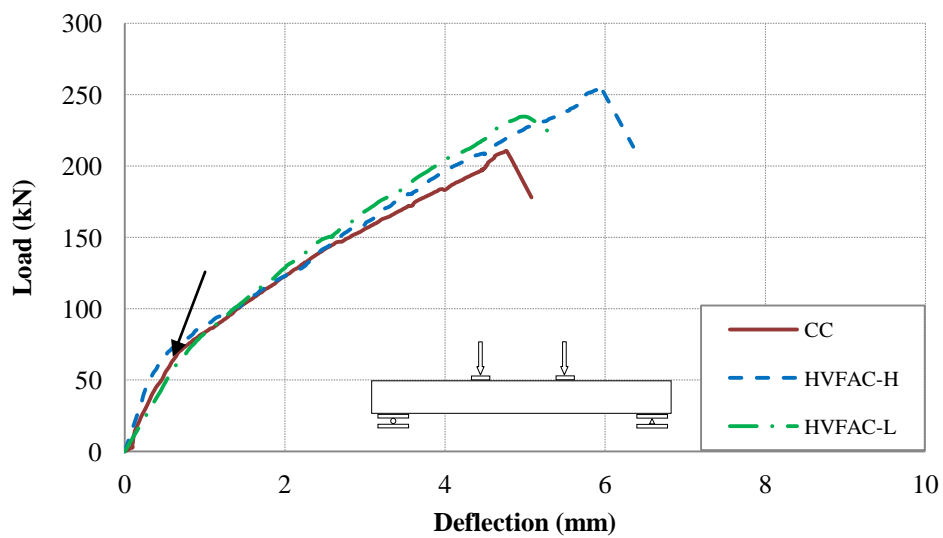


c) Splice test setup with specimen loaded

Figure A. 2 - Load pattern, cross section, and location of strain gages on the beams



a) Pull-out Test



b) Splice Specimen Test

Figure A. 3 - Load-deflections of the specimens



a) CC

b) HVFAC-H

b) HVFAC-L

Figure A. 4 - Crack pattern of the beams at bond failure

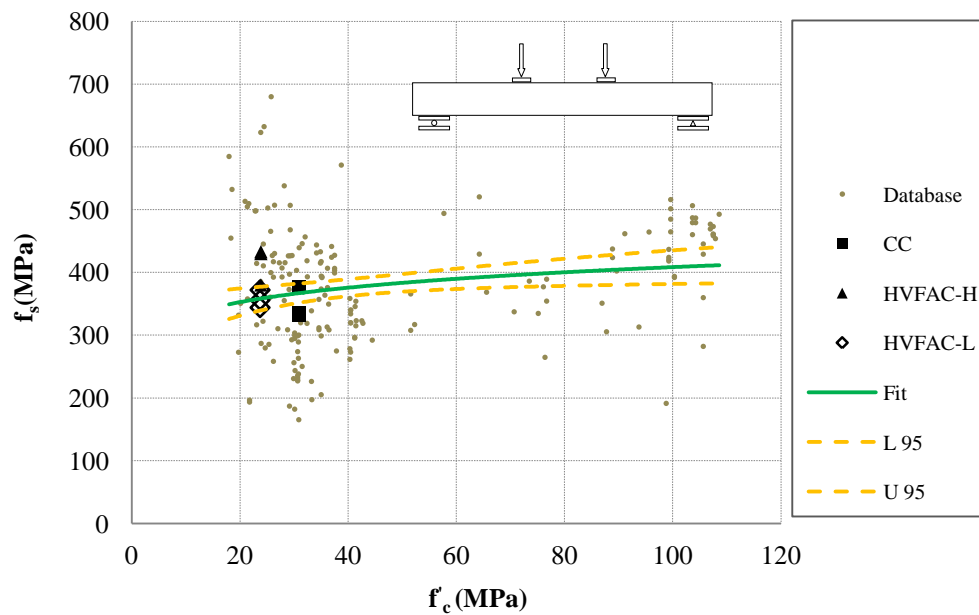


Figure A. 5 - Longitudinal steel reinforcement stress versus compressive strength of concrete (database of ACI 408-03 and test results of this study)

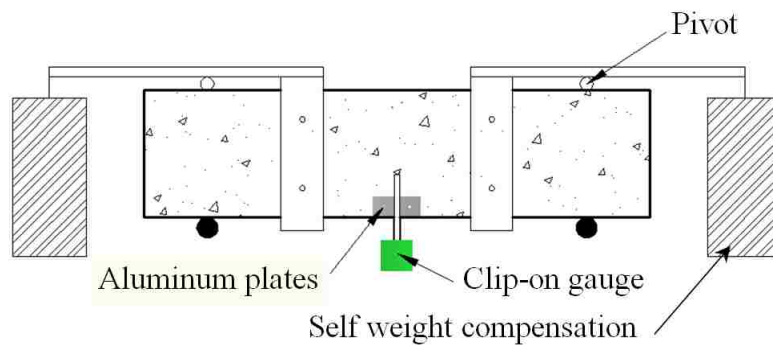


Figure A. 6 - Fracture energy specimens

APPENDIX B
AN EXPERIMENTAL STUDY ON BOND STRENGTH OF REINFORCING STEEL
IN SELF-CONSOLIDATING CONCRETE

AN EXPERIMENTAL STUDY ON BOND STRENGTH OF REINFORCING STEEL IN SELF-CONSOLIDATING CONCRETE

Trevor J. Looney, Mahdi Arezoumandi, Jeffery S. Volz, John J. Myers

Abstract

An experimental investigation was conducted to compare the bond strength of reinforcing steel in self-consolidating concrete (SCC) with conventional concrete (CC). This study investigated two different compressive strengths of SCC as well as CC. The experimental program consisted of 24 pull-out specimens as well as 12 full-scale beams (three for each concrete type and strength). The pull-out specimens were based on RILEM recommendations, and the beam specimens were tested under a simply supported four-point loading condition. The CC test results served as a control and were used to evaluate the results from the SCC pull-out and beam specimen tests. Furthermore, a comparison was performed between results of this study and a bond database of CC specimens. These comparisons indicate that SCC beams possess comparable or slightly greater bond strength than CC beams.

Keywords:

Self-Consolidating Concrete, Conventional Concrete, Bond Strength, Experimental Study

Introduction

Self-consolidating concrete (SCC) is a highly workable concrete that can spread under its own weight without segregation and bleeding. SCC was developed in Japan in the early 1980's by Okamura and colleagues at Tokyo University.¹ The motivation for this development was a lack of skilled workers for placing and consolidating concrete to make durable concrete structures.²

Like many new products, SCC was slow to gain popularity. It was used for the first time on a large scale for the Akashi-Kaikyo Bridge in Japan in 1998.³ It began to

spread in Asian and European countries before the United States. It gained acceptance in the United States around the year 2000.³ SCC has become more popular because of several advantages. It reduces labor, equipment, job noise, and time of construction. It also facilitates the filling of densely reinforced sections and complex formworks.⁴

There have been numerous studies conducted to determine the bond performance of SCC relative to conventional concrete (CC). Some researchers^{5, 6} performed direct pull-out specimens while others^{7, 8} used beam specimens to study bond strength of SCC. Both groups concluded that no significant differences were observed between SCC and CC in terms of bond strength development. However, other studies⁹⁻¹² have shown that SCC has higher bond strength and less top-bar effect compared with CC. These discrepancies merit additional research.

There are three different approaches to developing an SCC mix design. The first is material-based, the second is chemically-based, and the third is a hybrid of the first two. The first approach focuses on modifying the aggregate types and amounts. Typically, the coarse aggregate content is reduced and also rounder aggregate is used to improve the flowability of the SCC mix. The main disadvantage of this approach is that with a lower coarse aggregate content, the resulting concrete may suffer negative side effects such as reduced mechanical properties. To avoid this issue, the second approach was developed and, in this approach, the coarse aggregate and paste contents are kept the same as in a CC mix. To improve the flowability and stability of this type of mix, high-range water-reducing admixtures (HRWRA) and viscosity-modifying admixtures (VMA) are used. This current study used the third method – the hybrid approach to SCC mix design.

The following study presents the results of an experimental investigation that compares the bond strength of 24 pull-out and 12 full-scale SCC and CC beams. The results of this study were also compared with a bond database of CC beam specimens. The purpose of this study was to evaluate reinforcing bond in alternative SCC mix designs then those studied by previous researchers, as well as to add to the database of SCC bond test results in order to lead to changes or acceptance in design codes and standards.

Experimental Program

Several different methods are used to study bond between steel reinforcement and concrete. The four most common methods are pull-out specimens, beam-end specimens, beam anchorage specimens, and beam splice specimens. The last three methods provide more realistic measures of bond strength compared with pull-out specimen tests. However, the pull-out specimen is more popular due to ease of construction and simplicity of the test. The main drawback with this test is that the stress state does not reflect the actual stress state within a reinforced concrete member. In the pull-out specimen test, the bar is in tension and the concrete surrounding the bar is in compression, but in most reinforced concrete members, both the bar and the surrounding concrete are in tension. For this reason, ACI 408-0313 does not recommend the pull-out specimen test to determine development length of reinforcement. However, pull-out specimen tests are valid in determining relative performance between different types of concretes or different types of reinforcing bar coatings.¹⁴⁻¹⁹ The current study used both pull-out specimens and beam splice specimens to evaluate SCC reinforcement bond strength compared with CC.

Specimen Design

The following section contains details regarding the pull-out and splice specimens used in the current study to evaluate bond between reinforcing steel and concrete.

Pull-out Specimens

The pull-out specimens were designed using RILEM 7-II-12820 as a guide. The bars were embedded 10 times the bar diameter into the concrete specimen based on preliminary testing, with half of the length debonded using a section of polyvinyl chloride (PVC) tubing. The RILEM report recommends casting the bars into concrete cubes that provide a clear cover of 4.5 times the bar diameter from the bar to the center of each side of the horizontal cross section. The specimens designed for this experiment exceeded the RILEM 7-II-128 requirement on clear cover and featured a 305 mm concrete cylinder to

eliminate the potential for splitting and ensure that all of the specimens failed in the same manner (pull-out). Figure 1 contains details of the pull-out test specimens.

Splice Specimens

The splice specimens were designed using ACI 408 as a guide. Twelve beams (three for each concrete type and strength) were designed to preclude flexural and shear failures and satisfy the minimum and maximum longitudinal reinforcement requirements of ACI 318-08.21 Figure 2 contains details of the splice test specimens. The beams measured 3000 mm in length, with a cross section of 300 mm x 460 mm, and a splice in the longitudinal steel centered at midspan. The longitudinal steel consisted of three #19 bars for the normal strength mixes and four #19 bars for the high strength mixes, while the shear reinforcement consisted of #10, U-shaped stirrups. One beam of each type was cast upside down to evaluate the top bar effect. The test setup used a simply supported four-point loading condition in order to place the splice under a uniform stress, as shown in Figure 2, with the stirrups discontinued within the center portion of the beam to provide an unconfined splice condition. To ensure a bond failure prior to a flexural failure, the splice length was chosen as 70% of the development length calculated in accordance with Eq. 12-1 in ACI 318-08, repeated as Eq. 1.

$$l_d = \frac{3}{40} \frac{f_y}{\sqrt{f'_c}} \frac{\Psi_t \Psi_e \Psi_s}{\left(\frac{c_b + k_{tr}}{d_b} \right)} d_b \quad (1)$$

where:

l_d = the development length;

f_y = the specified yield strength of reinforcement;

λ = the lightweight concrete modification factor;

f'_c = the specified compressive strength of concrete;

Ψ_t = the reinforcement location modification factor;

Ψ_e = the reinforcement coating modification factor;

Ψ_s = the reinforcement size modification factor;

c_b = the smaller of the distance from center of a bar to nearest concrete surface and one-half the center-to-center spacing of bars being developed;

K_{tr} = the transverse reinforcement index,;

d_b = the nominal diameter of the reinforcing bar.

Based on these calculations, the splice lengths for the normal and high strength mixes were 300 mm and 360 mm, respectively.

Materials

The concrete was supplied by a local ready-mix supplier (Rolla, MO). The mixtures used ASTM Type I Portland cement and, for the high strength mixes, ASTM Class C fly ash from the Ameren Labadie Power Plant (Labadie, MO). The coarse aggregate consisted of crushed limestone with a maximum nominal aggregate size of 19 mm from Jefferson City Dolomite (Jefferson City, MO). The fine aggregate was natural sand from Missouri River Sand (Jefferson City, MO).

All of the reinforcing bars were from the same heat of steel, used the same deformation pattern, and met the requirements of ASTM A615-09,22 Grade 60, 414 MPa material. Table 1 contains the tested mechanical properties of the reinforcing steel. The rib height, rib spacing, and relative rib area for each bar size was in accordance with ACI 408R-03 and ASTM A615-09, with the #13 and #19 reinforcing bars used in the pull-out and splice specimens having relative rib areas of 0.088 and 0.081, respectively.

Mixture Proportions

The mixture proportions are given in Table 2. The normal strength concrete mixes had a target compressive strength of 41 MPa and are designated NCC and NSCC for the conventional and self-consolidating concrete, respectively. The high strength concrete

mixes had a target compressive strength of 69 MPa and are designated HCC and HSCC for the conventional and self-consolidating concrete, respectively.

Fabrication and Curing of Test Specimens

Both the pull-out and beam splice specimens were constructed and tested in the Structural Engineering High-Bay Research Laboratory (SERL) at Missouri University of Science and Technology. After casting, the specimens and the quality control/quality assurance companion cylinders (ASTM C39-1223 and C496-1124) and beams (ASTM C78-1025) were covered with both wet burlap and a plastic sheet. All of the specimens and companion cylinders and beams were moist cured for three days and, after formwork removal, were stored in the laboratory until they were tested.

Fresh and Hardened Properties

Table 3 presents the fresh and hardened strength properties of the CC and SCC mixes.

Test Setup and Procedure

The following section contains details regarding the test setup for the pull-out and beam splice specimen testing.

Pull-out Test

As shown in Figure 1, the pull-out specimens were loaded into an 890-kN Tinius Olson machine by rotating the specimen 180°, bar side down, and threading the bar through a thin piece of rubber and the head of the machine until the specimen rested evenly on the rubber. The free end of the bar was clamped into a lower component of the Tinius Olson machine. A magnetic arm holding a Linear Variable Differential Transformer (LVDT) was then placed on top of the specimen. The LVDT was placed directly on top of the exposed rebar on the back end of the specimen to record bar slip.

The loading rate for the Tinius Olson machine was set at 2.5 mm/min. to avoid any dynamic effect and in order to insure a sufficient number of data points prior to failure. The load was recorded on a data acquisition computer linked to the test machine.

The LVDT was also monitored to record bar slip as a function of load. The test protocol consisted of loading the bar in tension to the maximum capacity and then continuing to apply load in order to develop the full load-slip curve.

Splice Specimen Test

As shown in Figure 2, a load frame was assembled and equipped with two 490-kN, servo-hydraulic actuators intended to apply the two point loads to the beams. The load was applied in a displacement control method at a rate of 0.50 mm/min. The beams were supported on a roller and a pin support, 150 mm from each end of the beam, creating a four-point loading condition with the two actuators. An LVDT was used to measure the deflection at the beam center and strain gages were installed at both ends of each splice to monitor the strain in the longitudinal reinforcement during the test. Figure 2 shows both the beam loading pattern and the location of the strain gages. During the test, any cracks that formed on the surface of the beam were marked at load increments of approximately 22 kN, and both the deformation and strains were monitored until the beam reached failure.

Test Results and Discussions

The following section contains the results from the pull-out and splice specimen tests as well as a discussion and comparison between CC and SCC.

Pull-out Tests

All of the pull-out specimens experienced a bond shear failure except for one of the #19 bar HSCC specimens where the reinforcement yielded prior to a bond failure. A bond shear failure occurs when the reinforcing bar and associated concrete located between the transverse ribs pulls out of the specimen as a cylinder without splitting the remaining concrete. Table 4 indicates the results of the pull-out tests. To compare the test results of the SCC and the CC, the values must be adjusted to reflect the different compressive strengths of the specimens. In the majority of design standards, bond strength is a function of the inverse square root of the compressive strength of the concrete (e.g., ACI 318-08, AASHTO LRFD-07, 26 AS 3600-09, 27CSA-04, 28 and

JSCE-0729), but ACI 408R-03 recommends a relationship based on the inverse fourth root of the compressive strength of the concrete.

Consequently, to compare the bond strength of the SCC and CC specimens, the test results were normalized with both the square root and fourth root of the compressive strength of the concrete. As shown in Table 4, the bond strengths of the #13 and #19 bars for the NSCC were 16% and 12% higher than the NCC when normalized by the square root of compressive strength and 21% and 16% higher when normalized by the fourth root of compressive strength, respectively. In contrast, the bond strength of the #13 and #19 bars for the HSCC decreased by 6% and 9% compared with the HCC when normalized by the square root of compressive strength of concrete and decreased by 5% and 8% when normalized by the fourth root of compressive strength, respectively.

Also, as shown in Figure 3a, no significant difference was observed between the average load-slip behavior of the NCC and NSCC and also the HCC and HSCC pull-out specimens. As mentioned earlier, the only difference was that one of the #19 bar HSCC specimens yielded prior to a bond shear failure.

Splice Specimen Tests

All of the beams failed in bond, experiencing a splitting failure. Based upon data collected from the strain gages, none of the longitudinal reinforcement reached yield at failure. Figure 3b shows the load-deflection behavior for one of the beam specimens of each concrete type (the deflection was measured at midspan). Before the first flexural cracks occurred (point A), all of the beams displayed a steep linear elastic behavior. After the appearance of flexural cracks in the maximum moment region, by increasing the load, new flexural cracks were formed between the two point loads. Upon further increasing the applied load, a bond failure occurred. As Figure 3b reveals, the load-deflection behavior of the NSCC and NCC and also HSCC and HCC beams were essentially identical except for the cracking moment (point A) and value at failure. Similarly, the cracking patterns experienced by the NSCC and NCC and also HSCC and HCC were essentially identical, as shown in Figure 4. All of the beams displayed a horizontal splitting failure along the length of the longitudinal splice.

Table 5 summarizes the longitudinal reinforcement stress at bond failure as determined from the strain gages, where the specimen designation “Top” refers to the specimen cast upside down to evaluate the top bar effect. Also included in Table 5 are calculated steel stresses based on the moment-curvature approach recommended in ACI 408, with the first calculated value based on the Popovic, Thorenfeldt, and Collins stress-strain model, and the second calculated value based on the Hognestad stress-strain model (ACI 408R-03 recommended method). Furthermore, as with the pull-out test, to compare the bond strength of the NSCC and NCC and also HSCC and HCC specimens, the test results were normalized with both the square root and fourth root of the compressive strength of the concrete.

Test results show that the NSCC beams had 12% and 17% higher average longitudinal reinforcement stress compared with the NCC beams when normalized by the square root and fourth root of the compressive strength of the concrete for the bottom bars, respectively. In contrast, for the top reinforcement, the NSCC beams had 15% and 12% lower average longitudinal reinforcement stress compared with the NCC beams when normalized by the square root and fourth root of the compressive strength of the concrete, respectively. The HSCC and HCC beams had the same average longitudinal reinforcement stress in the bottom bars when normalized with both the square and fourth root of the concrete compressive strength. For the top bars, the average longitudinal reinforcement stress for the HSCC beams increased by 7% compared with the HCC beams when normalized with both the square and fourth root of the concrete compressive strength.

Contrary to previous research results for CC, a top bar effect didn't occur for the specimens studied, both CC and SCC. In fact, for all specimens except the NSCC specimens, the top bars had higher bond strength than the bottom bars, which may have been due to the very low w/c ratios (0.37 and 0.24 for the normal and high strength mixes, respectively) and the use of fly ash in the high strength mixes. In addition, the beams were not overly deep and were only slightly above the cutoff for when to consider top bar effects. These factors may have resulted in a decrease in the amount of bleed water accumulating beneath the top bars, which is the primary cause of the top bar effect. Some previous studies have also found a decrease in the top bar effect for SCC,9-12

while others have not.^{7,8} Due to the limited number of top bar specimens used in this study – one for each concrete type – further research is needed to reach a definitive conclusion.

Table 6 presents the ratio of experimental-to-theoretical stress in the longitudinal reinforcement, with the theoretical values based on the moment-curvature analysis recommended in ACI 408.13 The table includes analysis results based on two different stress-strain models – the Hognestad model recommended in ACI 408 and the Popovic, Thorenfeldt, and Collins model. The authors investigated both models to determine whether any noticeable differences resulted based on the assumed stress-strain diagram. The measured stresses are based on the strain gages installed at the start of each splice (see Figure 2). Even with the potential for slight inaccuracies in the strain gage readings due to localized cracking and the slight reduction in cross section required for mounting the gages, the measured readings offer a valuable basis of comparison with the moment-curvature results. Based on the strain gage measurements, both stress-strain curve methods underestimated the longitudinal reinforcement stress of the NCC and NSCC beams, but overestimated the longitudinal reinforcement stress for the HCC and HSCC beams. The Popovic, Thorenfeldt, and Collins stress-strain model predicts the longitudinal reinforcement stress of the NCC and NSCC beams better than the Hognestad stress-strain model. In contrast, the bar stress calculated based on the Hognestad stress-strain model had better agreement with the HCC and HSCC beam results.

Comparison of Test Results with Bond Test Database

Figure 5 presents the longitudinal steel reinforcement stress versus compressive strength of concrete for this study as well as the wealth of bond test data available in the literature (ACI 408-03). Given the significant scatter of the database of previous bond test results, it is somewhat difficult to draw definitive conclusions on the current test values. Nonetheless, visually, Figure 5 seems to indicate that the CC and SCC test results follow the same general trend of increasing bond strength as a function of the compressive strength of the concrete. Furthermore, statistical analysis of the data indicates that one of the beams of both the NCC and NSCC test results falls below a 95% confidence interval of a nonlinear regression curve fit of the database. The HCC and HSCC and the other two

NCC and NSCC test results fall within and above a 95% confidence interval of the nonlinear regression curve fit. As a result, it would appear that the bond strength of SCC for the beams tested in this study is comparable or greater than CC.

Findings and Conclusions

The purpose of this study was to evaluate reinforcing bond in alternative SCC mix designs then those studied by previous researchers, as well as to add to the database of SCC bond test results in order to lead to changes or acceptance in design codes and standards. To study the bond strength of reinforcing steel in SCC, 24 pull-out specimens as well as 12 full-scale beams (both CC and SCC) were constructed and tested to failure.

Based on the results of this study, the following findings and conclusions are presented for the pull-out tests:

Bond strength of the NSCC was higher than the NCC by approximately 15%.

Bond strength of the HCC was higher than the HSCC by approximately 7%.

No significant difference was observed in the load-slip behavior between the NSCC and NCC and also the HSCC and HCC specimens.

The following findings and conclusions are presented for the splice tests:

The average longitudinal reinforcement steel stress of the NSCC was approximately 15% higher than the NCC.

The average longitudinal reinforcement steel stress of the HSCC was virtually identical with the HCC.

The load-deflection behavior of the NSCC and NCC and also the HSCC and HCC beams was essentially identical except for the cracking moment and value at failure.

Based on the strain gage measurements, the moment curvature method based on the Popovic, Thorenfeldt, and Collins stress-strain model more accurately predicted the longitudinal reinforcement stress of the NCC and NSCC beams compared with the Hognestad stress-strain model.

Based on the strain gage measurements, the Hognestad stress-strain model had better agreement with the HCC and HSCC beam results compared with the Popovic, Thorenfeldt, and Collins stress-strain model.

Based on a comparison of the specimens studied in this investigation with a bond database of CC beam specimens, it appears that NSCC and HSCC possess reinforcement bond strength comparable or slightly greater than NCC and HCC, respectively.

However, due to the limited nature of the data set regarding aspect ratio, mix designs, aggregate type and content, etc., investigated, the researchers recommend further testing to increase the database of SCC bond test results.

Acknowledgment

The authors gratefully acknowledge the financial support provided by the Missouri Department of Transportation (MoDOT) and the National University Transportation Center at Missouri University of Science and Technology. The authors would also like to thank the support staff in the Department of Civil, Architectural and Environmental Engineering and Center for Infrastructure Engineering Studies at Missouri S&T for their efforts. The authors are also grateful for the ideas and help of Dr. David Darwin, the Deane E. Ackers Distinguished Professor of Civil Engineering, University of Kansas. The conclusions and opinions expressed in this paper are those of the authors and do not necessarily reflect the official views or policies of the funding institutions.

References

1. Ozawa, K., K. Maekawa, M. Kunishima, and H. Okamura. "Development of High Performance Concrete Based on the Durability Design of Concrete Structures." *In Proceedings of the Second East-Asia and Pacific Conference on Structural Engineering and Construction (EASEC-2)*, Vol. 1, pp. 445-450, January 1989.
2. Daczko, J., and Vachon, M., "Self Consolidating Concrete (SCC)," Significance of Tests and Properties of Concrete and Concrete-Making Materials STP 169D. *ASTM International* West Conshohocken, PA. May 2006 pp. 637-645.
3. Okamura, H. "Self-Compacting High-Performance Concrete," *Concrete International*. July 1997, pp. 50-54.

4. ACI Committee 237. "Self-Consolidating Concrete" (*ACI 237R-07*). Farmington Hills, MI: American Concrete Institute, 2007.

5. Foroughi-Asl, A., Dilmaghani, S., Famili, H. (2008). "Bond Strength of Reinforcement Steel in Self-Compacting Concrete." *International Journal of Civil Engineering*. Vol. 6, No. 1, pp. 24-33.

6. Hassan, A., Hossain, K., Lachemi, M. (2010). "Bond Strength of Deformed Bars in Large Reinforced Concrete Members Cast with Industrial Self-Consolidating Concrete Mixture." *Journal of Construction and Building Materials*, Vol 24, Issue 4, Pages 520–530.

7. Turk, K., Benli, A., Calayir, Y. (2008). "Bond Strength of Tension Lap-Splices in Full Scale Self-Consolidating Concrete Beams." *Turkish J. Eng. Env. Sci.*, Vol. 32, pp. 377 – 386.

8. Castel, A., Vidal, T., Francois, R. (2010). "Bond and Cracking Properties of Self-Consolidating Concrete." *Journal of Construction and Building Materials*, Vol 24, Issue 7, Pages 1222–1231.

9. Dehn, F., Holschemacher, K., Weibe, D. (2000). "Self-Compacting Concrete (SCC) Time Development of the Material Properties and the Bond Behavior." *Universität Leipzig*. [<http://www.wilbertprecast.com/documents/scc.pdf>], July 2012.

10. Chan, Y., Chen, Y., Liu, Y. (2003). Development of Bond Strength of Reinforcement Steel in Self-Consolidating Concrete. *ACI Structural Journal*, Vol.100, 100-S52.

11. Castel, A., Thierry, V., Kriengkai, V., Raoul, F. (2006). Effect of Reinforcing Bar Orientation and Location on Bond with Self-Consolidating Concrete. *ACI Structural Journal*, Vol.103, 103-S59.

12. Valcuende, M., Parra, C. (2009). "Bond Behavior of Reinforcement in Self-Compacting Concrete." *Journal of Construction and Building Materials*, Vol.23, pp.162–170.

13. ACI Committee 408. (2003). "Bond and Development of Straight Reinforcing Bars in Tension" (*ACI 408R-03*). Farmington Hills, MI: American Concrete Institute.

14. Al-Sulaimani, G. J., Kaleemullah, M., Basunbul, I. A., and Rasheeduzzafar (1990). "Influence of corrosion and cracking on bond behavior and strength of reinforced concrete members." *ACI Structural Journal*, V. 87, No. 2, pp. 220-231.

15. Carins, J. and Abdullah, R. (1994). "Fundamental tests on the effects of an epoxy coating on bond strength" *ACI Materials Journal*, V. 91, No. 4, pp. 331-338.
16. Benmokrane, B., Challal, O., and Masmoudi, R. (1996). "Flexural response of Concrete beams reinforced with FRP reinforcing bars." *ACI Structural Journal*, V. 91, No. 2, pp. 46-55.
17. Tighiouart, B., Benmokrane, B., and Gao, D. (1998). "Investigation of bond in concrete member with fiber reinforced polymer (FRP) bars." *Construction and Building Materials*, Vol. 12, pp. 453-462.
18. Andrade, C., Arteaga, A., Lopez-Hombrados, C., and Vazquez, A. (2001). "Tests on bonds of galvanized rebar and concrete cured in seawater." *Journal of Materials in Civil Engineering*, Vol. 13, No. 5, pp. 319-324.
19. Belaid, F., Arlique, G., and Francois, R. (2001). "Effect of bar properties on Bond strength of galvanized reinforcement." *Journal of Materials in Civil Engineering*, Vol. 13, No. 6, pp. 454-458.
20. RILEM 7-II-128. (1994) "RC6: Bond Test for Reinforcing Steel. 1. Pull-Out Test." *RILEM technical recommendations for the testing and use of construction materials*, E & FN Spon, U.K., pp.102-105.
21. American Concrete Institute ACI Committee. (2008). "Building code requirements for structural concrete ACI 318-08 and commentary 318R-08." *ACI 318-08/318R-08*, Farmington Hills, MI: American Concrete Institute, pp. 155-168.
22. ASTM A615/A615M (2009). "Standard Specification for Deformed and Plain Carbon-Steel Bars for Concrete Reinforcement" *ASTM*, West Conshohocken, PA, 6 pp.
23. ASTM C 39/C 39M (2012). "Standard Test Method for Compressive Strength of Cylindrical Concrete Specimens," *ASTM*, West Conshohocken, PA, 7 pp.
24. ASTM C 78/C 78M (2010). "Standard Test Method for Flexural Strength of Concrete (Using Simple Beam with Third-Point Loading)" *ASTM*, West Conshohocken, PA, 4 pp.
25. ASTM C 496/C 496M (2011). "Standard Test Method for Splitting Tensile Strength of Cylindrical Concrete," *ASTM*, West Conshohocken, PA, 5 pp.
26. American Association of State and Highway Transportation Officials (AASHTO) (2007). *AASHTO LRFD Bridge Design Specifications*, 4th Ed., Washington, D.C., pp. 5-(72-84).

27. AS 3600 (2009). "Concrete Structures," Standards Australia, Sydney, pp . 105-109.
28. CSA CAN3-A23.3 (2004). "Design of Concrete Standards for Buildings," Rexdale, Ontario, pp. 53-61.
29. Japan Society of Civil Engineers (2007). "Standard Specification for Concrete Structure" JSCE No. 15, Tokyo, pp. 154-159.

Table B. 1 - Mechanical properties of reinforcing steel

Bar No.	Modulus of elasticity	Yielding strength
	MPa	MPa
13	196,600	485
19	206,250	580

Table B. 2 - Mixture proportions of concrete

Mix	Water kg/m ³	Cement kg/m ³	Fly Ash kg/m ³	Fine aggregate kg/m ³	Coarse aggregate kg/m ³	AE liter/m ³	HRWR liter/m ³
NCC	165	445	-	691	955	0.33	1.04
NSCC	165	445	-	856	790	0.33	1.38
HCC	150	500	125	619	854	0.40	1.55
HSCC	150	500	125	767	707	0.31	2.23

Table B. 3 - Fresh and hardened concrete properties

Property	NCC	NSCC	HCC	HSCC
Slump (mm)	203	-	51	-
Slump flow (mm)	-	610	-	597
J- Ring (mm)	-	527	-	546
Air content (%)	6	6	2.5	3
Unit weight (kg/m ³)	2240	2330	2440	2400
Split cylinder strength*	3.0	3.6	3.9	3.9
Flexural strength** (MPa)	3.4	3.4	4.8	3.7
Compressive strength*	39.4	47.2	66.4	67.2

*: Values represent the average of three cylinders (ASTM C39-12 [32] and C496-11[34])

** : Values represent the average of three beams (ASTM C78-10[33])

Table B. 4 - Pull-out test results

Section		f'_c (MPa)	P (kN)	μ^* (MPa)	$\frac{P}{\sqrt{\frac{f'_{c(test)}}{f'_{c(design)}}}}$ (kN)	P_{ave} (kN)	$\frac{P}{\sqrt[4]{\frac{f'_{c(test)}}{f'_{c(design)}}}}$ (kN)	P_{ave} (kN)
NCC	13-1	39.9	55.2	21.0	56.5	55.6	55.7	54.7
	13-2		55.5	21.2	56.9		56.0	
	13-3		52.0	19.8	53.3		52.5	
	19-1		134.4	25.2	137.6	136.1	135.6	134.1
	19-2		132.9	24.9	136.1		134.1	
	19-3		131.4	24.6	134.6		132.6	
NSCC	13-1	47.2	69.0	26.3	64.6	63.8	66.8	66.0
	13-2		66.7	25.4	62.5		64.5	
	13-3		68.8	26.2	64.4		66.6	
	19-1		161.9	30.3	151.6	151.1	156.7	156.1
	19-2		156.5	29.3	146.6		151.4	
	19-3		165.7	31.0	155.2		160.3	
HCC	13-1	66.4	83.0	31.6	84.6	86.4	73.7	75.3
	13-2		81.6	31.1	83.1		72.5	
	13-3		89.8	34.2	91.5		79.8	
	19-1		194.2	36.4	197.9	199.4	172.5	173.9
	19-2		197.1	36.9	200.9		175.1	
	19-3		195.8	36.7	199.5		174.0	
HS CC	13-1	67.2	79.4	30.3	80.4	81.4	70.3	71.2
	13-2		80.4	30.6	81.4		71.2	
	13-3		81.5	31.1	82.6		72.2	
	19-1		182.8	34.2	185.2	182.2	161.9	159.3
	19-2		179.7	33.7	182.0		159.2	
	19-3		177.1	33.2	179.4		156.9	

*: average bond strength

Table B. 5 - Longitudinal reinforcement stress (MPa)

Section			Measured ^I		Moment-Curvature Method				Measured ^I	
		f'_c	Measured ^I	Ave.	(M- Φ) ^{II}	Ave.	(M- Φ) ^{III}	Ave.	$\frac{f_s}{\sqrt{\frac{f'_{c(test)}}{f'_{c(design)}}}}$	$\frac{f_s}{\sqrt[4]{\frac{f'_{c(test)}}{f'_{c(design)}}}}$
NCC	1	39.9	341	345	239	284	324	347	353	349
	2		350		328		370			
	Top		377	377	238	238	321	321		
NSCC	1	47.2	436	424	319	310	403	396	397	410
	2		412		301		388			
	Top		349	349	271	271	360	360		
HCC	1	66.4	427	413	499	458	554	527	421	417
	2		399		416		500			
	Top		509	509	552	552	567	567		
HSCC	1	67.2	379	416	429	454	510	526	421	419
	2		452		479		541			
	Top		546	546	562	562	624	624		

^I: Strain (from strain gages) multiplied by modulus of elasticity

^{II}: Popovic, Thorenfeldt, and Collins stress-strain model

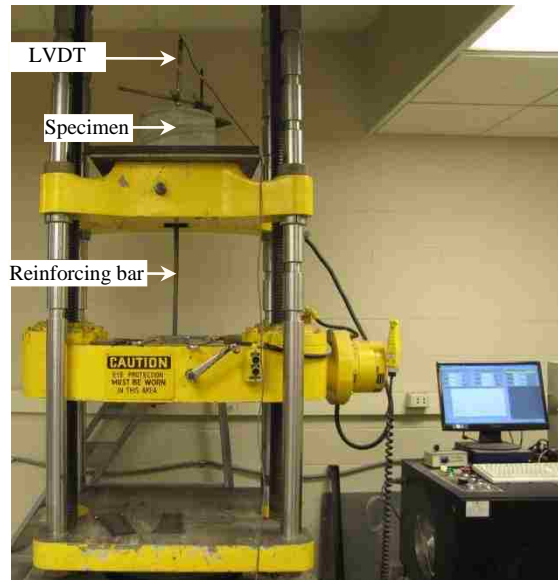
^{III}: Hognestad stress-strain model (ACI 408R-03 recommended method)

Table B. 6 - Experimental-to-theoretical ratio of longitudinal reinforcement stress

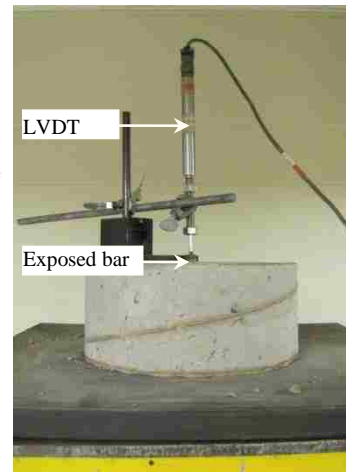
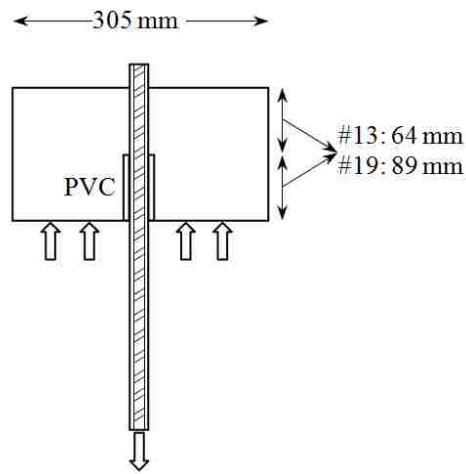
Section		$\left(\frac{f_{s(\text{test})}}{f_{s(M-\phi)}}\right)_{ave}^I$	$\left(\frac{f_{s(\text{test})}}{f_{s(M-\phi)}}\right)_{ave}^{II}$
NCC	1	1.21	0.99
	2		
	Top	1.58	1.17
NSCC	1	1.37	1.07
	2		
	Top	1.29	0.97
Ave.		1.36	1.05
COV (%)		11.7	8.7
HCC	1	0.90	0.78
	2		
	Top	0.92	0.90
HSCC	1	0.92	0.80
	2		
	Top	0.97	0.88
Ave.		0.93	0.84
COV (%)		3.2	7.0

^I: Popovic, Thorenfeldt, and Collins stress-strain curve

^{II}: Hognested stress-strain curve (ACI 408R-03 recommended method)



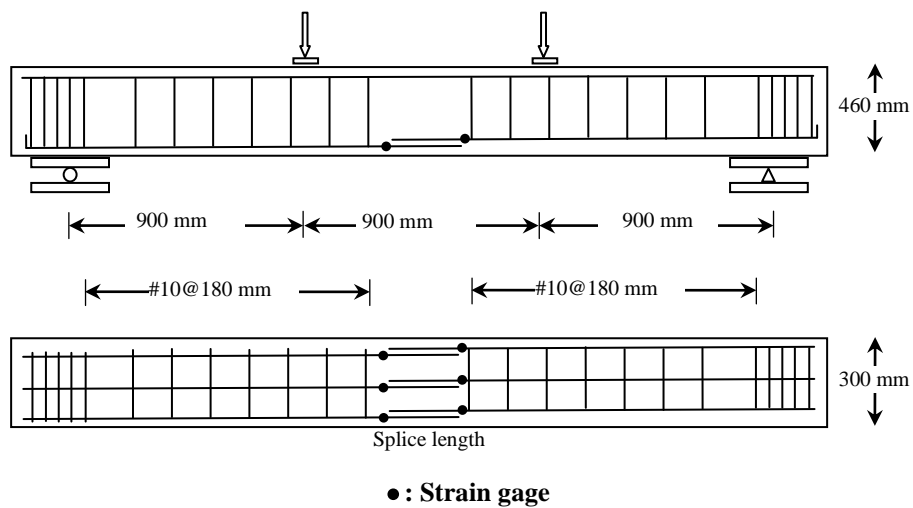
a) Direct pull-out test setup



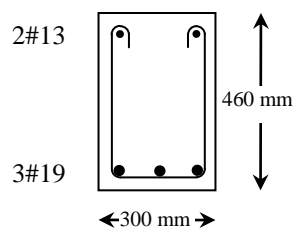
b) Pull-out test specimen details

c) LVDT installation to measure bar slip

Figure B. 1 - Pull-out test specimen



a) Beam splice specimen reinforcing layout

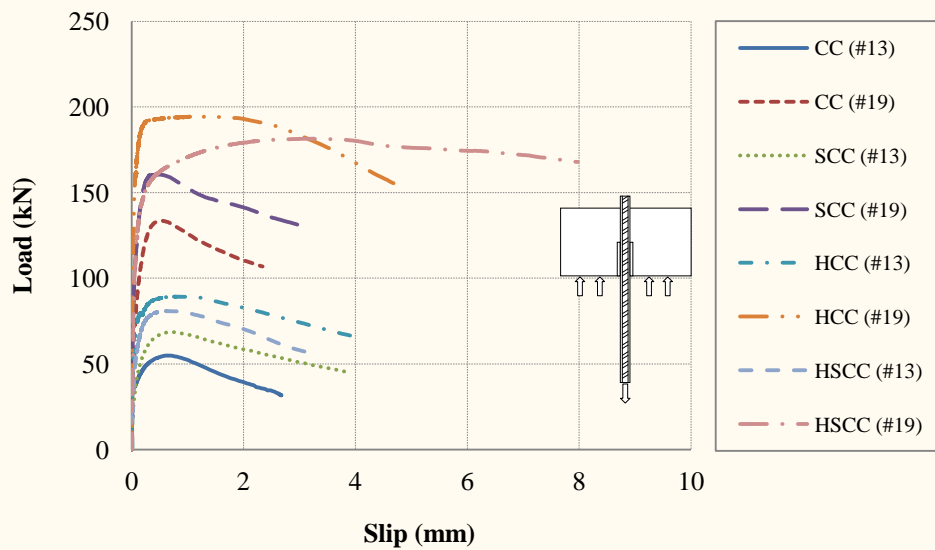


b) Beam splice specimen cross section

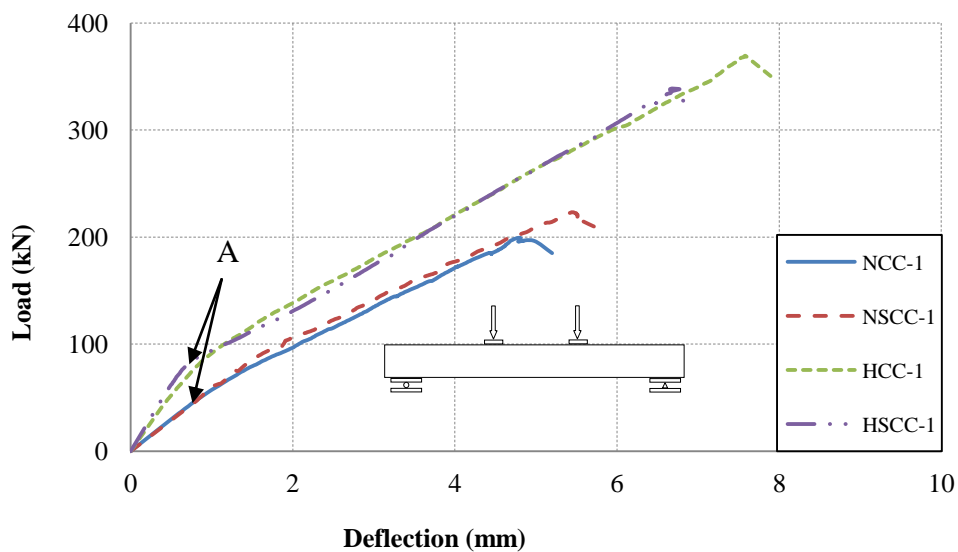


c) Splice test setup with specimen loaded

Figure B. 2 - Load pattern, cross section, and location of strain gages on the beams



a) Pull-out Test



b) Splice Specimen Test

Figure B. 3 - Load-deflections of the specimens



a) NCC

b) NSCC



c) HCC

d) HSCC

Figure B. 4 - Crack pattern of the beams at bond failure

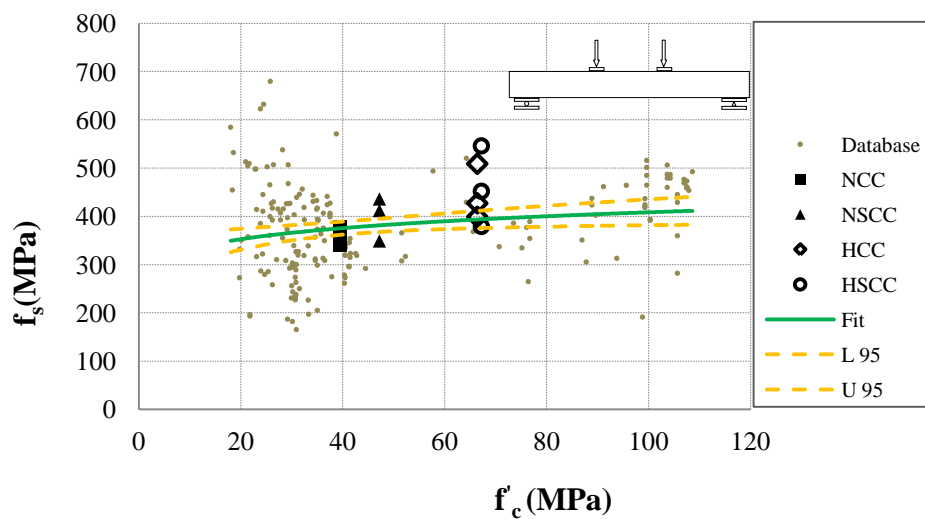


Figure B. 5 - Longitudinal steel reinforcement stress versus compressive strength of concrete (database of ACI 408-03 and test results of this study)

APPENDIX C

A COMPARATIVE STUDY OF THE BOND STRENGTH OF REINFORCING STEEL
IN HIGH-VOLUME FLY ASH CONCRETE AND CONVENTIONAL CONCRETE

A COMPARATIVE STUDY OF THE BOND STRENGTH OF REINFORCING STEEL IN HIGH-VOLUME FLY ASH CONCRETE AND CONVENTIONAL CONCRETE

Mahdi Arezoumandi, Michael H. Wolfe, Jeffery S. Volz

Abstract

The production of Portland cement – the key ingredient in concrete – generates a significant amount of carbon dioxide. However, due to its incredible versatility, availability, and relatively low cost, concrete is the most consumed man-made material on the planet. One method of reducing concrete’s contribution to greenhouse gas emissions is the use of fly ash to replace a significant amount of the cement. An experimental investigation was conducted to compare the bond strength of reinforcing steel in high-volume fly ash concrete (HVFAC) – concrete with at least 50% of the cement replaced with fly ash – with conventional concrete (CC). This experimental program consisted of 12 pull-out specimens as well as 12 full-scale beams (three unconfined and three confined by transverse reinforcement for each concrete type). The pull-out specimens were based on RILEM recommendations, and the beam specimens were tested under a simply supported four-point loading condition. The CC test results served as a control and were used to evaluate the results from the HVFAC pull-out and beam specimen tests. Furthermore, a comparison was performed between results of this study and a bond database of CC specimens. These comparisons indicate that HVFAC beams possess comparable bond strength as CC beams.

Keywords:

High-Volume Fly Ash Concrete, Conventional Concrete, Bond Strength, Experimental Study

Introduction

Concrete is the most widely used man-made material in the world, and cement is an essential ingredient in the production of Portland cement concrete. The cement industry plays a key role in the world, from both an economic and an environmental perspective. Cement production is a relatively significant source of global carbon dioxide (CO₂) emissions, accounting for approximately 4.5 percent of global CO₂ emissions from industry in 2007 [1].

One of the solutions for this global concern is the use of supplementary cementitious materials as replacement of cement. The most available supplementary cementitious material worldwide is fly ash, a by-product of coal-burning thermal power stations [2]. ASTM C618-08 [3] defines fly ash as “the finely divided residue that results from the combustion of ground or powdered coal and that is transported by flue gasses.” Fly ash is categorized in three classes: class N, F, and C based on the chemical compositions [4].

Traditionally, fly ash used in structural concrete as a replacement or supplementary material is limited to 15% to 25% cement replacement [5, 6]. When a significant amount of fly ash is used, how it contributes to the strength development of the concrete and the hydration characteristics of this type of material are of significant research interest. High-volume fly ash concrete (HVFAC) is a concrete generally defined with at least 50% of the Portland cement replaced with fly ash. In 1986, the Canadian Centre for Mineral and Energy Technology (CANMET) developed HVFAC for structural applications. The investigations by CANMET [7] have shown that HVFAC has lower shrinkage, creep and water permeability and higher modulus of elasticity compared with conventional concrete (CC).

Comprehensive research has been done on both the fresh and hardened properties of HVFAC, but very little research has been performed on the structural behavior of HVFAC. Naik et al. [8] performed pull-out tests on specimens with fly ash replacements of 10, 20, and 30 percent of Portland cement. The researchers concluded that the bond strength improved with the increase in fly ash up to about 20 percent cement replacement and after that it began to decrease. Researchers at Montana State University [9] performed a series of pull-out tests on specimens utilizing 100 percent Class C fly ash as

a replacement of Portland cement. The specimen design involved 13 mm bars embedded into a concrete cylinder (152 x 312 mm). The embedment depth was varied from 203 to 305 mm for each material. Results of this study indicated lower bond strength for HVFAC compared to normal concrete. Gopalakrishnan et al. [10] conducted pull-out tests to determine the effects of using 50 percent fly ash replacement of cement on bond strength. Specimens had 20 mm bars embedded into a 150 mm concrete cube. The researchers reported identical bond strength for HVFAC and CC specimens.

The following study presents the results of an experimental investigation that compares the bond strength of 12 pull-out and 12 full-scale HVFAC and CC beams (both confined and unconfined). The results of this study were also compared with a bond database of CC beam specimens.

Experimental Program

Several different methods are used to study bond between steel reinforcement and concrete. The four most common methods are pull-out specimens, beam-end specimens, beam anchorage specimens, and beam splice specimens. The last three methods provide more realistic measures of bond strength compared with pull-out specimen tests. However, the pull-out specimen is more popular due to ease of construction and simplicity of the test. The main drawback with this test is that the stress state does not reflect the actual stress state within a reinforced concrete member. In the pull-out specimen test, the bar is in tension and the concrete surrounding the bar is in compression, but in most reinforced concrete members, both the bar and the surrounding concrete are in tension. For this reason, ACI 408-03 [11] does not recommend pull-out specimen test to determine development length of reinforcement. However, pull-out specimen test are valid in determining relative performance between different types of concretes or different types of reinforcing bar coatings [12-14]. The current study used both pull-out and splices specimens to evaluate HVFAC reinforcement bond strength compared with CC.

Specimen Design

The following section contains details regarding the pull-out and splice specimens used in the current study to evaluate bond between reinforcing steel and concrete.

Pull-out Specimens

The pull-out specimens were designed using RILEM 7-II-128 [15] as a guide. The bars were embedded 10 times the bar diameter into the concrete specimen based on preliminary testing, with half of the length debonded using a section of polyvinyl chloride (PVC) tubing. The RILEM report recommends casting the bars into concrete cubes that provide a clear cover of 4.5 times the bar diameter from the bar to the center of each side of the horizontal cross section. The specimens designed for this experiment exceeded the RILEM 7-II-128 requirement on clear cover and featured a 305 mm concrete cylinder to eliminate the potential for splitting and ensure that all of the specimens failed in the same manner (pull-out). Figure 1 is a schematic diagram of the pull-out test specimens.

Splice Specimens

Twelve beams (six unconfined and six confined by transverse reinforcement) were designed to preclude flexural and shear failures and satisfy the minimum and maximum longitudinal reinforcement requirements of ACI 318-08 [16]. The beams measured 4270 mm in length, with a cross section of 305 mm x 457 mm, and a splice in the longitudinal steel centered at midspan. The longitudinal steel consisted of three 19 mm bars while the shear reinforcement consisted of 10 mm, closed stirrups. To ensure a bond failure prior to a flexural failure, the splice length was chosen as 75% of the development length calculated in accordance with ACI 318-08. The test setup used a simply supported four-point loading condition in order to place the splice under a uniform stress, as shown in Figure 2. The beam designation included a combination of letters: UC and C represented unconfined and confined, respectively.

Materials

The cementitious materials used for this study were ASTM Type I Portland cement; ASTM Class C fly ash from the Ameren Labadie Power Plant (Labadie, MO); gypsum from USA Gypsum (Reinholds, PA); and calcium hydroxide from the Mississippi Lime company (Sainte Genevieve, MO). Tables 1 and 2 show the physical properties and chemical compositions of the cement and fly ash.

The coarse aggregate consisted of crushed limestone with a maximum nominal aggregate size of 19 mm from Jefferson City Dolomite (Jefferson City, MO). The fine aggregate was natural sand from Missouri River Sand (Jefferson City, MO).

All of the reinforcing bars were from the same heat of steel, used the same deformation pattern, and met the requirements of ASTM A615-09 [17], Grade 60, 414 MPa material. The rib height, rib spacing, and relative rib area for each bar size was in accordance with ACI 408R-03 and ASTM A615-09, with the 13 mm and 19 mm reinforcing bars used in the pull-out and splice specimens having relative rib areas of 0.088 and 0.081, respectively.

Mixture Proportions

The concrete mixture with a target compressive strength of 35 MPa was delivered by a ready-mix concrete supplier (Rolla, MO). The concrete mixture proportions are given in Table 3. The HVFAC mix used a 70% replacement of cement with fly ash. For the HVFAC mix, the gypsum was used to maintain the initial hydration stage by preventing sulfate depletion, while the calcium hydroxide ensured a more complete hydration of the fly ash with the low content of cement in the mix [18]. The drums were charged at the ready-mix facility with the required amounts of cement, fly ash, sand, coarse aggregate, and water, while the powder activators (gypsum and lime) were added when the truck arrived at the lab, approximately 5 minutes later. After the gypsum and lime were added, the HVFAC was mixed at high speed for 10 minutes.

Fabrication and Curing of Test Specimens

Both the pull-out and beam splice specimens were constructed and tested in the Structural Engineering High-Bay Research Laboratory (SERL) at Missouri University of Science and Technology. After casting, the specimens and the quality control/quality assurance companion cylinders (ASTM C39-12 [19] and C496-11[20]) and beams (ASTM C78-10[21]) were covered with both wet burlap and a plastic sheet. All of the specimens and companion cylinders and beams were moist cured for three days and, after formwork removal, were stored in the laboratory until they were tested.

Fresh and Hardened Properties

Table 4 presents the fresh and hardened strength properties of the CC and HVFAC mixes.

Test Setup and Procedure

The following section contains details regarding the test setup for the pull-out and beam splice specimen testing

Pull-out Test

The pull-out specimens were loaded into an 890-kN Tinius Olson machine by rotating the specimen 180°, bar side down, and threading the bar through a thin piece of rubber and the head of the machine until the specimen rested evenly on the rubber. The free end of the bar was clamped into a lower component of the Tinius Olson machine. A magnetic arm holding a Linear Variable Differential Transformer (LVDT) was then placed on top of the specimen. The LVDT was placed directly on top of the exposed rebar on the back end of the specimen to record bar slip.

The loading rate for the Tinius Olson machine was set at 2.5 mm/min. to avoid any dynamic effect and in order to insure a sufficient number of data points prior to failure. The load was recorded on a data acquisition computer linked to the test machine. The LVDT was also monitored to record bar slip as a function of load. The test protocol

consisted of loading the bar in tension to the maximum capacity and then continuing to apply load in order to develop the full load-slip curve.

Splice Specimen Test

A load frame was assembled and equipped with two 490-kN, servo-hydraulic actuators intended to apply the two point loads to the beams. The load was applied in a displacement control method at a rate of 0.50 mm/min. The beams were supported on a roller and a pin support, 300 mm from each end of the beam, creating a four-point loading situation with the two actuators. An LVDT was used to measure the deflection at the beam center and strain gages were installed at both ends of each splice to monitor the strain in the longitudinal reinforcement during the test. Figure 2 shows both the beam loading pattern and the location of the strain gages. During the test, any cracks that formed on the surface of the beam were marked at load increments of approximately 22 kN, and both the deformation and strains were monitored until the beam reached failure.

Test Results and Discussions

The following section contains the results from the pull-out and splice specimen tests as well as a discussion and comparison between CC and HVFAC.

Pull-out Tests

All of the pull-out specimens experienced a bond shear failure. Table 5 indicates the results of the pull-out tests. To compare the test results of the HVFAC and the CC, the values must be adjusted to reflect the different compressive strengths of the specimens. In the majority of design standards, bond strength is a function of the inverse square root of the compressive strength of the concrete (ACI 318-08, AASHTO LRFD-07 [22], AS 3600-09 [23], CSA-04 [24], and JSCE-07 [25].), but ACI 408R-03 recommends a relationship based on the inverse fourth root of the compressive strength of the concrete.

Consequently, to compare the bond strength of the HVFAC and CC specimens, the test results were normalized with both the square root and fourth root of the compressive strength of the concrete. As shown in Table 5, the bond strength of the

HVFAC was 7% higher and 4% lower than that for the CC for the 13 mm and 19 mm bars, respectively, when normalized by the square root of the compressive strength of the concrete. When comparing the HVFAC and CC pull-out tests normalized with the fourth root relationship, the bond strength was essentially identical for the 13 mm bars, while for the 19 mm bars, the HVFAC had 11% lower bond strength than the CC. As shown in Figure 3a, no significant difference was observed in the load-slip behavior of the CC and HVFAC specimens, and it is also worth noting that they had almost identical slopes in the post peak portions of the graph.

Splice Specimen Tests

All of the beams failed in bond, experiencing a splitting failure. Based upon data collected from the strain gages, none of the longitudinal reinforcement reached yield at failure. Figure 3b shows the load-deflection behavior for the beams (the deflection was measured at midspan) for both the HVFAC and the CC specimens. Before the first flexural cracks occurred (point A), all of the beams displayed a steep linear elastic behavior. After the appearance of flexural cracks in the maximum moment region, by increasing the load, new flexural cracks were formed between the two point loads. Upon further increasing the applied load, a bond failure occurred. As Figure 3b reveals, the load-deflection behavior of the HVFAC and CC beams was essentially identical except for the value at failure. Similarly, the cracking patterns experienced by the HVFAC and CC were essentially identical, as shown in Figure 4. All of the beams displayed a horizontal splitting failure along the length of the longitudinal splice, for both the confined and unconfined specimens.

Table 6 summarizes the longitudinal reinforcement stress at bond failure as determined from the strain gages. As with the pull-out tests, in order to compare the bond strength of the HVFAC and CC specimens, the test results were normalized with both the square root and fourth root of the compressive strength of the concrete. When normalized with the square root of compressive strength, test results show that the HVFAC beams had 17% and 19% higher average steel stress compared with the CC beams for the unconfined and confined sections, respectively. When normalized with the fourth root of

compressive strength, the HVFAC beams had 6% and 7% higher average steel stress compared with the CC beams for unconfined and confined sections, respectively.

Comparison of Test Results with Bond Test Database

Figure 5 presents the longitudinal steel reinforcement stress versus compressive strength of concrete for both unconfined and confined beams of this study as well as the wealth of bond test data available in the literature (ACI 408-03). Given the significant scatter of the database of previous bond test results, it is somewhat difficult to draw definitive conclusions on the current test values. Nonetheless, visually, Figure 5 seems to indicate that the CC and HVFAC test results follow the same general trend of increasing bond strength as a function of the compressive strength of the concrete. Furthermore, statistical analysis of the data indicates that the CC and HVFAC test results fall above a 95% confidence interval of a nonlinear regression curve fit of the database for both confined and unconfined beams. As a result, it would appear that the bond strength of HVFAC for the beams tested in this study is comparable or greater than CC.

Conclusions and Recommendations

To study the bond strength of reinforcing steel in HVFAC, 12 pull-out specimens as well as 12 full-scale beams (both CC and HVFAC) were constructed and tested to failure. For the specimens studied in this investigation, it appears that HVFAC possesses reinforcement bond strength comparable or slightly greater than CC. However, due to the limited nature of the data set regarding aspect ratio, mix designs, aggregate type and content, etc., investigated, the researchers recommend further testing to increase the database of test results.

Acknowledgment

The authors gratefully acknowledge the financial support provided by the Missouri Department of Transportation (MoDOT) and the National University Transportation Center at Missouri University of Science and Technology. The authors would also like to thank the support staff in the Department of Civil, Architectural and Environmental Engineering and Center for Infrastructure Engineering Studies at Missouri

S&T for their efforts. The authors are also grateful for the ideas and help of Dr. David Darwin, the Deane E. Ackers Distinguished Professor of Civil Engineering, University of Kansas. The conclusions and opinions expressed in this paper are those of the authors and do not necessarily reflect the official views or policies of the funding institutions.

References

- [1] Marland, G., T.A. Boden, and R.J. Andres. (2008). "Global, Regional, and National Fossil Fuel CO₂ Emissions. In Trends: A Compendium of Data on Global Change," Carbon Dioxide Information Analysis Center, Oak Ridge National Laboratory, United States Department of Energy, Oak Ridge, Tenn., <http://cdiac.ornl.gov/trends/emis/overview.html>, Accessed date March 2012.
- [2] Bilodeau, A. and Malhotra, V. M., (2000). "High-Volume Fly Ash System: Concrete Solution for Sustainable Development, ACI Material Journal V.97, pp. 41-48.
- [3] ASTM 618-94a, (1995). "Standard Specification for Coal Fly Ash and Raw or Calcined Natural Pozzolan for Use as a Mineral Admixture in Portland Cement Concrete," Annual Book of ASTM Standards Vol. 04.02, American Society for Testing and Materials, Philadelphia, P.A., pp. 304-306.
- [4] ACI Committee 232. (2003). "Use of Fly Ash in Concrete" (ACI 232.2R-03). Farmington Hills, MI: American Concrete Institute.
- [5] E.E. Berry, R.T. Hemmings, M.H. Zhang, B.J. Cornelious, D.M. Golden, (1994). "Hydration in High-volume Fly Ash Binders," ACI Materials Journal V.91, pp.382-389.
- [6] ACI Committee 211, (1993). "Guide for Selecting Proportions for High-strength Concrete with Portland Cement and Fly Ash," ACI 226.4R, ACI Materials Journal, V. 90 ,pp. 272-283.
- [7] Malhotra, V.M. (1986). "Superplasticized Fly Ash Concrete for Structural Applications," Concrete International, V.8, pp. 28- 31.
- [8] Naik, T.R., Singh, S. S., Sivasundaram, V. (1989). "Concrete Compressives Strength, Shrinkage and Bond Strength As Affected by Addition of Fly Ash and Temperature." The University of Wisconsin – Milwaukee, Milwaukee, WI.
- [9] Cross, D., Stephens, J., and Vollmer, J. (n.d.). "Structural Applications of 100 Percent Fly Ash Concrete." Montana State University, Bozeman, MT.

- [10] Gopalakrishnan, S. (2005). "Demonstration of Utilising High Volume Fly Ash Based Concrete for Structural Applications." Structural Engineering Research Centre, Chennai India.
- [11] ACI Committee 408. (2003). "Bond and Development of Straight Reinforcing Bars in Tension" (ACI 408R-03). Farmington Hills, MI: American Concrete Institute.
- [12] Al-Sulaimani, G. J., Kaleemullah, M., Basunbul, I. A., and Rasheeduzzafar (1990). "Influence of corrosion and cracking on bond behavior and strength of reinforced concrete members." ACI Structural Journal, V. 87, No. 2, pp. 220-231.
- [13] Carins, J. and Abdullah, R. (1994). "Fundamental tests on the effects of an epoxy coating on bond strength" ACI Materials Journal, V. 91, No. 4, pp. 331-338.
- [14] Benmokrane, B., Challal, O., and Masmoudi, R. (1996). "Flexural response of Concrete beams reinforced with FRP reinforcing bars." ACI Structural Journal, V. 91, No. 2, pp. 46-55.
- [15] RILEM 7-II-128. (1994) "RC6: Bond Test for Reinforcing Steel. 1. Pull-Out Test." RILEM technical recommendations for the testing and use of construction materials, E & FN Spon, U.K., pp.102-105.
- [16] American Concrete Institute ACI Committee. (2008). "Building code requirements for structural concrete ACI 318-08 and commentary 318R-08." ACI 318-08/318R-08, Farmington Hills, MI: American Concrete Institute, pp. 155-168.
- [17] ASTM A615/A615M (2009). "Standard Specification for Deformed and Plain Carbon-Steel Bars for Concrete Reinforcement" ASTM, West Conshohocken, PA, 6 pp.
- [18] Bentz, D. P. (2010). "Powder Additions to Mitigate Retardation in High-Volume Fly Ash Mixtures", ACI Materials Journal, V. 107, No. 5, pp. 508-514.
- [19] ASTM C 39/C 39M (2012). "Standard Test Method for Compressive Strength of Cylindrical Concrete Specimens," ASTM, West Conshohocken, PA, 7 pp.
- [20] ASTM C 78/C 78M (2010). "Standard Test Method for Flexural Strength of Concrete (Using Simple Beam with Third-Point Loading)" ASTM, West Conshohocken, PA, 4 pp.
- [21] ASTM C 496/C 496M (2011). "Standard Test Method for Splitting Tensile Strength of Cylindrical Concrete," ASTM, West Conshohocken, PA, 5 pp.

[22] American Association of State and Highway Transportation Officials (AASHTO) (2007). AASHTO LRFD Bridge Design Specifications, 4th Ed., Washington, D.C., pp. 5-(72-84).

[23] AS 3600 (2009). "Concrete Structures," Standards Australia, Sydney, pp . 105-109.

[24] CSA CAN3-A23.3 (2004). "Design of Concrete Standards for Buildings," Rexdale, Ontario, pp. 53-61.

[25] Japan Society of Civil Engineers (2007). "Standard Specification for Concrete Structure" JSCE No. 15, Tokyo, pp. 154-159.

Table C. 1 - Physical Properties of Cement and Fly Ash

Property	Type I Cement	Class C Fly Ash
Fineness: Blaine, m ² /kg	347	not measured
+325 mesh (+44 μm)	4.1%	14.4%
Specific gravity	3.15	2.73

Table C. 2 - Chemical Composition of Cement and Fly Ash

Component	Type I Cement, %	Class C Fly Ash, %
SiO ₂	21.98	33.46
Al ₂ O ₃	4.35	19.53
Fe ₂ O ₃	3.42	6.28
CaO	63.97	26.28
MgO	1.87	5.54
SO ₃	2.73	2.40
Na ₂ O	0.52 equivalent	1.43 equivalent
LOI	0.60	0.34

Table C. 3 - Mixture proportions of concrete

Mix	Water kg/m ³	Cement kg/m ³	Fly ash kg/m ³	Fine aggregate kg/m ³	Coarse aggregate kg/m ³	Gypsum kg/m ³	Calcium Hydroxide kg/m ³
CC	201	449	-	655	1033	-	-
HVFAC	201	136	317	655	1033	14	35

Table C. 4 - Fresh and Hardened Concrete Properties

Property	CC	HVFAC
Slump (mm)	114	127
Air content (%)	1.5	1.5
Unit weight (kg/m ³)	2390	2340
Split cylinder strength* (kPa)	3290	3160
Flexural strength** (kPa)	3820	3610
Compressive strength* (MPa)	38.7	30.5

*: Values represent the average of three cylinders

**: Values represent the average of three beams

Table C. 5 - Pull-out test results (kN)

Section		P	$\sqrt{\frac{P}{f'_{c(\text{design})}}}$ $\sqrt{f'_{c(\text{test})}}$	P _{ave}	$\sqrt[4]{\frac{P}{f'_{c(\text{design})}}}$ $\sqrt[4]{f'_{c(\text{test})}}$	P _{ave}
CC	13-1	53	50	49	51	50
	13-2	53	50		51	
	13-3	51	48		49	
HVFAC	13-1	48	51	52	50	51
	13-2	50	53		51	
	13-3	50	53		51	
CC	19-1	143	133	135	138	140
	19-2	145	135		140	
	19-3	146	136		141	
HVFAC	19-1	127	135	129	131	125
	19-2	121	128		125	
	19-3	116	124		120	

Table C. 6 - Longitudinal reinforcement stress (MPa)

Section		Measured ¹			
		Measured ¹	Ave.	$\frac{f_s}{\sqrt{\frac{f'_{c(test)}}{f'_{c(design)}}}}$	$\frac{f_s}{\sqrt[4]{\frac{f'_{c(test)}}{f'_{c(design)}}}}$
CC	UC-1	500	518	429	472
	UC-2	535			
	UC-3	520			
	C-1	535	546	462	502
	C-2	511			
	C-3	593			
HVFAC	UC-1	465	495	504	500
	UC-2	489			
	UC-3	532			
	C-1	534	524	552	535
	C-2	524			
	C-3	513			

¹: Strain (from strain gauges) multiplied by modulus of elasticity

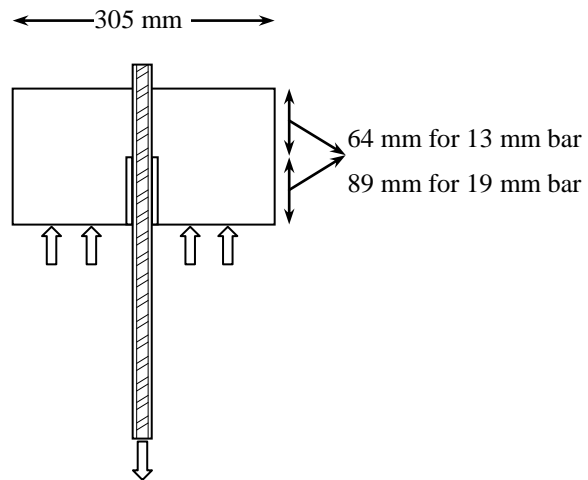
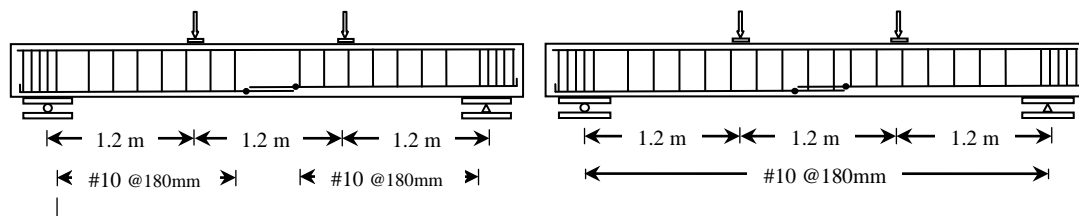


Figure C. 1- Pull out test specimen



a) Without stirrups in test region

b) With stirrups in test region

: Strain gauge

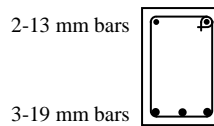
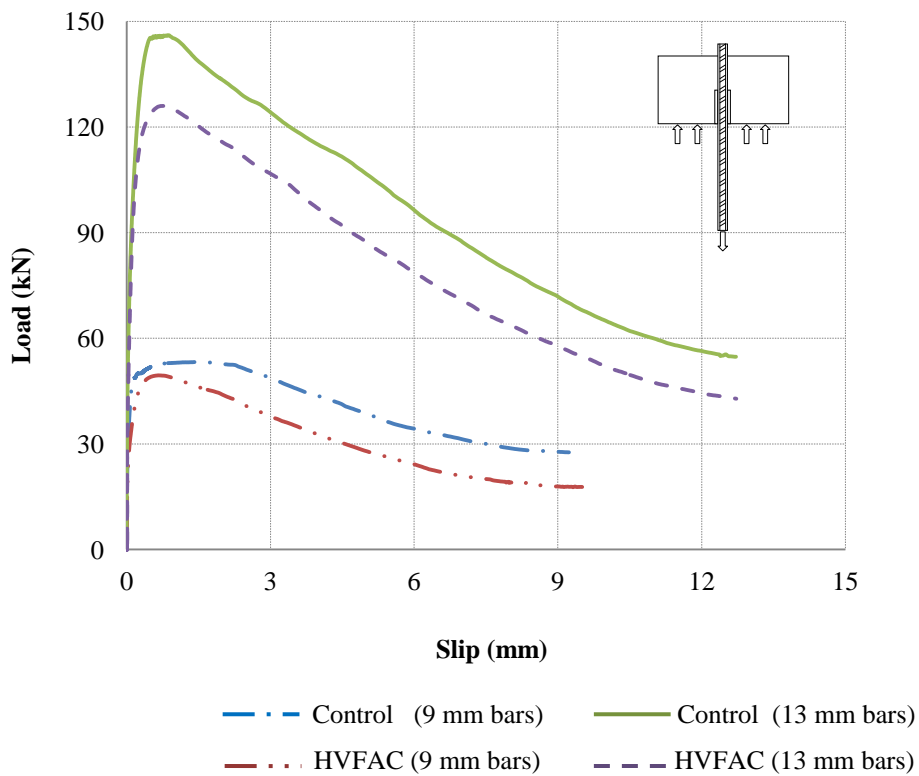
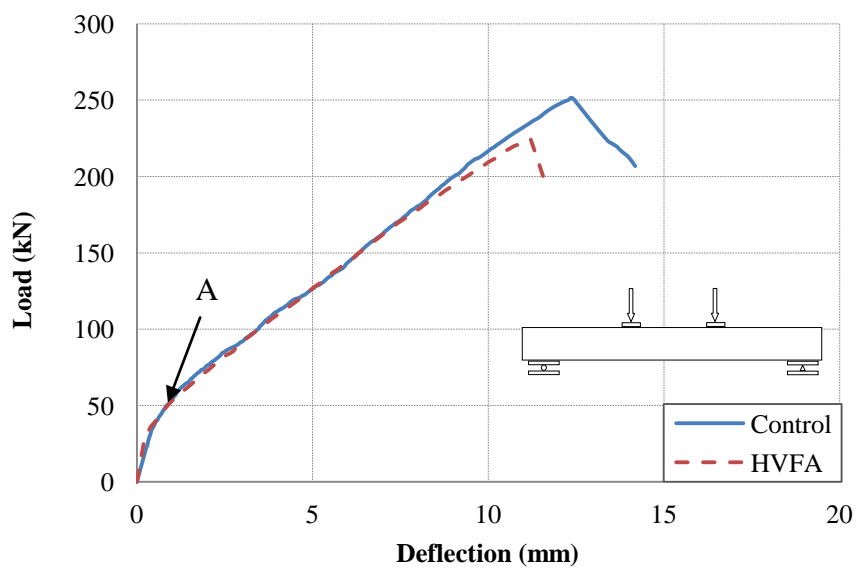


Figure C. 2 - Load pattern, cross section, and location of strain gauges on the beams



a) Pull out Test



b) Splice Specimen Test

Figure C. 3 - Load-deflections of the specimens



Control unconfined



Control confined

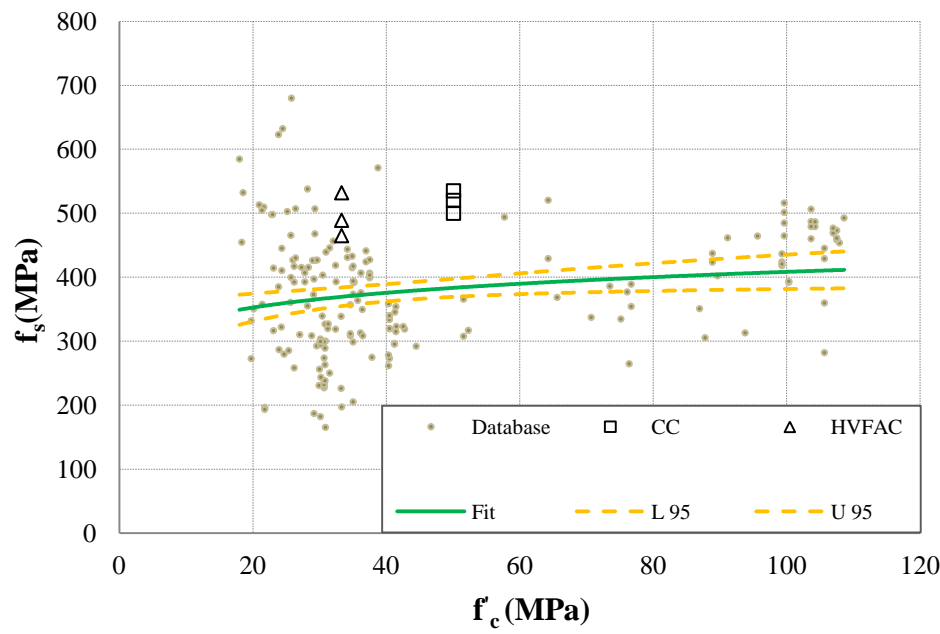


HVFA unconfined

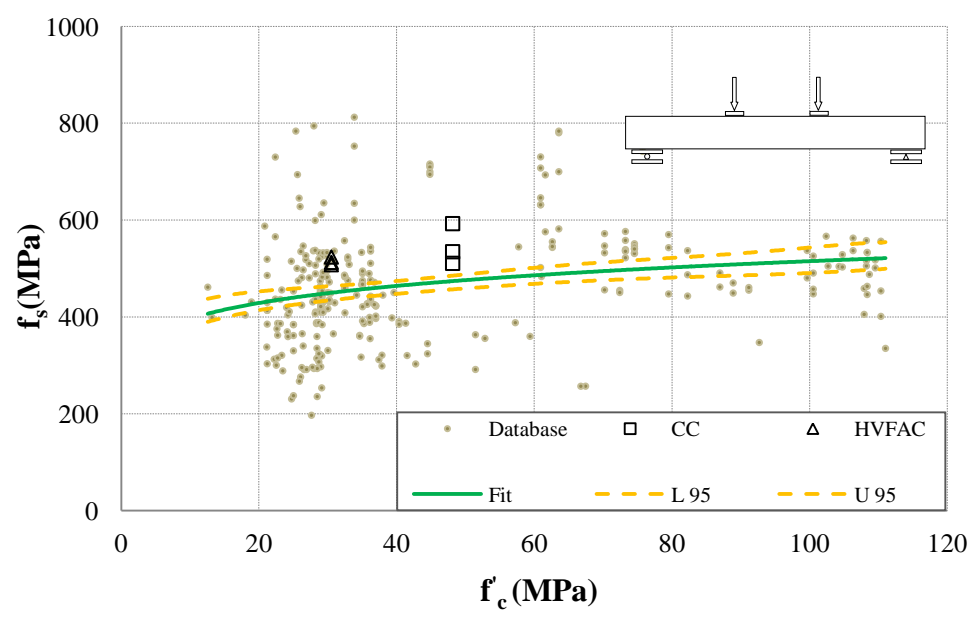


HVFA confined

Figure C. 4 - Crack pattern of the beams at bond failure



a) Unconfined



b) Confined

Figure C. 5 - Longitudinal steel reinforcement stress versus compressive strength of concrete (database of ACI 408-03 and test results of this study)

APPENDIX D
MECHANICAL PROPERTIES OF HVFAC

MECHANICAL PROPERTIES OF HVFAC

The following section includes the results and discussion on the compressive strength, tensile splitting strength, and flexural strength of the CC and HVFAC mixes.

Compressive Strength

Results of the compressive strength tests of the CC and HVFAC at 1, 3, 7, 28, and 90 days are presented in Figure D.1. Each data point represents the average of three replicate specimens tested in accordance with ASTM C39-12 using 100 mm×200 mm cylindrical specimens. The compressive strength of the HVFAC mix was lower than the compressive strength of the CC until 28 days, after that HVFAC mix showed slightly higher strength.

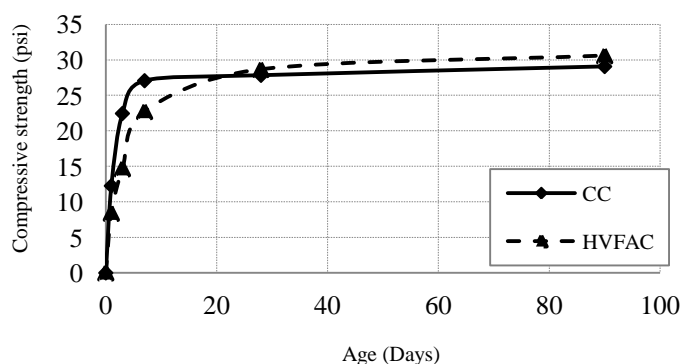


Figure D. 1 - Development of compressive strength of CC vs. HVFAC

Tensile Splitting Strength

Results of the tensile splitting strength testing performed in accordance with ASTM C496-10 are presented in Table D.1. The values are normalized by dividing by the square root of compressive strength. For both HVFAC mixes, the normalized values fall below the predictive relationship proposed by ACI 318-11, shown as Equation D-1. It has also been reported by other researchers that the ACI 318-11 provision overestimates the tensile splitting strength of concrete at low compressive strength (Neville 1997). Furthermore, the results of testing for tensile splitting strength tend to vary considerably, typically ranging from 0.35 to 0.63 times the square root of compressive strength

(Kosmatka, S. H. et al. 2011), and the results for both mixes are within this range and also compare favorably with previous research (Bouzoubaa et al.2001, Atis 2003).

$$f_{ct} = 0.56\sqrt{f'_c} \quad (D-1)$$

where:

- f_{ct} = average tensile splitting strength (MPa);
 f'_c = specified compressive strength of concrete (MPa).

Flexural Strength

Results of the flexural strength testing performed in accordance with ASTM C78-10 are also presented in Table D.1. The results indicate that both the CC and HVFAC mixes showed higher value compared with the provisions in ACI 318-11, shown as Equation D-2.

$$f_r = 0.62\sqrt{f'_c} \quad (D-2)$$

where:

- f_r = modulus of rupture of concrete (MPa).

Table D.1 - Tensile splitting strength and Flexural strength

Mix	f'_c	f_{ct}	f_r	$f_{ct}/\sqrt{f'_c}$	$f_r/\sqrt{f'_c}$
CC	22.00	1.40	2.70	0.30	0.58
	23.20	1.90	2.60	0.40	0.54
	26.50	1.90	3.90	0.37	0.76
	27.70	2.10	4.40	0.40	0.84
	28.80	2.30	4.30	0.43	0.80
	27.00	2.10	4.10	0.40	0.79
	26.70	2.20	3.20	0.43	0.62
	27.50	2.50	3.00	0.48	0.57
	30.50	2.80	3.90	0.51	0.71
	28.60	2.90	4.40	0.54	0.82
	Ave.			0.42	0.70
	COV (%)			16.52	16.39
HVFAC	20.20	2.20	3.50	0.49	0.78
	20.30	2.10	3.60	0.47	0.80
	23.10	2.00	2.90	0.42	0.60
	23.10	2.00	2.90	0.42	0.60
	24.00	2.10	2.90	0.43	0.59
	24.00	2.10	2.90	0.43	0.59
	24.90	2.20	3.10	0.44	0.62
	24.90	2.20	3.20	0.44	0.64
	28.60	2.90	3.90	0.54	0.73
	28.80	3.10	4.30	0.58	0.80
	Ave.			0.46	0.68
	COV (%)			11.99	13.30

References

American Concrete Institute ACI Committee. (2011). "Building code requirements for structural concrete ACI 318-08 and commentary 318R-11." ACI 318-11/318R-11, Farmington Hills, MI: American Concrete Institute.

ASTM C 39/C 39M (2012). "Standard Test Method for Compressive Strength of Cylindrical Concrete Specimens," ASTM, West Conshohocken, PA, 7 pp.

ASTM C 78/C 78M (2010). "Standard Test Method for Flexural Strength of Concrete (Using Simple Beam with Third-Point Loading)" ASTM, West Conshohocken, PA, 4 pp.

ASTM C 496/C 496M (2011). "Standard Test Method for Splitting Tensile Strength of Cylindrical Concrete," ASTM, West Conshohocken, PA, 5 pp.

Atis, C. D., (2003). "High-Volume Fly Ash Concrete with High Strength and Low Drying Shrinkage," *Journal of Materials in Civil Engineering ASCE*, Vol. 15, No. 2, pp. 153-156.

Bouzoubaa, N., Zhang, M. H., and Malhorta, V.M., (2001). "Mechanical properties and durability of concrete made with high-volume fly ash blended cement using a coarse fly ash," *Cement and Concrete Research*, V. 31, pp. 1393-1402.

Kosmatka, S. H. and Wilson, M. L. (2011) "Design and Control of Concrete Mixtures", 15th edition, Portland cement Association.

Neville, A. M. (1997). "Properties of Concrete", 4th edition, John Wiley & Sons Inc., New York.

APPENDIX E
MECHANICAL PROPERTIES OF SCC

MECHANICAL PROPERTIES OF SCC

The following section includes the results and discussion on the compressive strength, tensile splitting strength, and flexural strength of the CC and SCC mixes.

Compressive Strength

Results of the compressive strength tests of the CC and SCC at 1, 3, 7, 28, and 90 days are presented in Figure E.1. Each data point represents the average of three replicate specimens tested in accordance with ASTM C39-12 using 100 mm×200 mm cylindrical specimens. The compressive strength of the CC mix was lower than the compressive strength of the SCC mix at all ages. Furthermore, the difference in compressive strengths was very consistent throughout the testing phase. At one day after casting, the CC compressive strength was 21% lower than the SCC, while at an age of 90 days, the CC was 24% lower than the SCC. However, the only difference between the two mixes involved the chemical admixtures used to convert the CC mix to a SCC mix. With the w/cm ratios being equal, as well as all of the constituents, it is believed that the high amount of HRWRA used to provide the flowable characteristics of the SCC accounts for the strength differences. The HRWRA allows more water to be effective in the hydration process by dispersing the cement particles. This characteristic in turn hydrates more of the Portland cement, creating a denser overall microstructure, thus improving the compressive strength of the SCC.

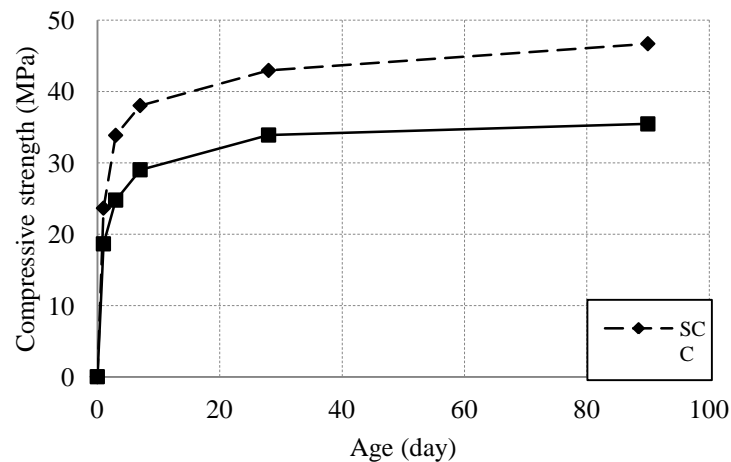


Figure E.1 - Development of compressive strength of CC vs. SCC

Tensile Splitting Strength

Results of the tensile splitting strength tests of the CC and SCC are presented in Table E.1 along with the corresponding compressive strengths. The specimens were tested in accordance with ASTM C496-11 using 100 mm×200 mm cylindrical specimens. The values are normalized by dividing by the square root of compressive strength. As shown in Table E.1, the average of the normalized tensile splitting strengths for the CC and SCC mixes are virtually identical. However, these values fall approximately 10% below the predictive relationship proposed in ACI 318-11, shown as Equation E-1. One potential explanation for the slightly lower values is that splitting tensile strengths traditionally show a large amount of scatter, typically ranging from 0.35 to 0.63 times the square root of compressive strength (Kosmatka, S. H. et al. 2011), and the results for both mixes are well within this range.

$$f_{ct} = 0.56\sqrt{f'_c} \quad (\text{E-1})$$

As a further evaluation, the test results were compared with values from previous research studies on SCC (Aslani et al. 2012). As shown in Figure E.2, the CC and SCC test results from the current study fall within the middle portion of the data and follow the same general trend of increasing tensile splitting strength as a function of the compressive strength of the concrete. In addition, statistical analysis of the data indicates that the CC and SCC test results fall well within a 95% confidence interval of a nonlinear regression curve fit of the database. This result indicates that the test values are very consistent with the wealth of tensile splitting strength test data available in the literature.

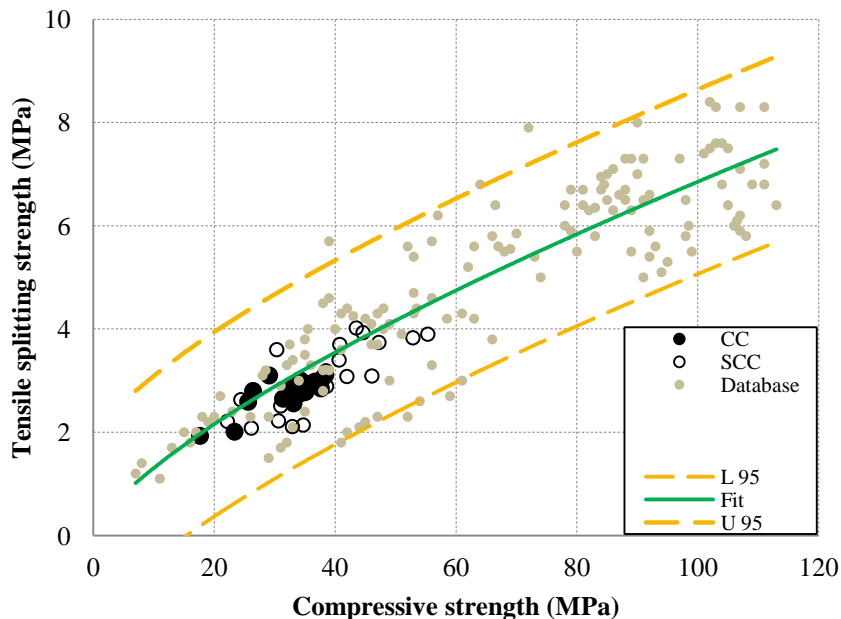


Figure E.2 - Tensile splitting strength vs. compressive strength of concrete; results from literature (Aslani et al. 2012) and test results of this study

Flexural Strength

Results of the flexural strength tests of the CC and SCC are presented in Table E.2 along with the corresponding compressive strengths. Each value represents the average of three replicate specimens tested in accordance with ASTM C78-10 using 150×150×600 mm prism specimens (flexural strength) or ASTM C39-12 using 100 mm×200 mm cylindrical specimens (compressive strength). The values are normalized by dividing by the square root of compressive strength. As shown in Table E.2, the average of the normalized flexural strengths for the CC and SCC mixes are virtually identical. Furthermore, both values are within approximately 4% of the prediction equation from ACI 318-08, shown as Equation E-2.

$$f_r = 0.62\sqrt{f'_c} \quad (\text{E-2})$$

Table E. 1 - Tensile splitting strength (MPa)

CC			SCC		
f_c^*	f_{ct}^*	$f_{ct}/\sqrt{f_c}$	f_c^*	f_{ct}^*	$f_{ct}/\sqrt{f_c}$
17.65	1.93	0.46	26.14	2.08	0.41
23.36	2.01	0.42	43.50	4.02	0.61
25.61	2.59	0.51	30.63	2.22	0.40
26.42	2.80	0.54	31.00	2.51	0.45
29.09	3.10	0.57	30.34	3.60	0.65
31.38	2.65	0.47	47.25	3.74	0.54
32.38	2.80	0.49	46.08	3.09	0.46
33.11	2.88	0.50	38.50	3.19	0.51
33.12	2.56	0.45	34.72	2.14	0.36
33.52	2.79	0.48	32.93	2.11	0.37
33.53	2.80	0.48	38.59	2.89	0.47
34.20	3.01	0.52	41.95	3.08	0.48
34.44	2.76	0.47	55.33	3.90	0.52
34.84	2.96	0.50	40.66	3.40	0.53
35.10	2.78	0.47	52.87	3.83	0.53
36.62	2.98	0.49	44.62	3.93	0.59
37.64	2.85	0.46	24.40	2.63	0.53
37.80	3.03	0.49	22.17	2.21	0.47
38.37	3.11	0.50	40.77	3.70	0.58
Ave.		0.49			0.50
COV (%)		7.13			16.18

*: Values represent the average of three cylinders

Table E. 2 - Flexural strength (MPa)

CC			SCC		
f_c^*	f_r^*	f_r/f_c	f_c^*	f_r^*	f_r/f_c
31.38	3.92	0.70	47.25	4.62	0.67
32.38	4.09	0.72	46.08	4.66	0.69
33.28	3.50	0.61	52.87	5.39	0.74
33.53	3.21	0.56	56.74	5.12	0.68
34.20	3.26	0.56	55.01	5.54	0.75
34.44	3.85	0.66	45.96	4.08	0.60
35.10	4.25	0.72	43.50	3.73	0.56
35.81	3.06	0.51	55.33	4.83	0.65
36.62	4.28	0.71	48.08	3.71	0.53
38.37	4.21	0.68	45.23	3.94	0.59
Ave.		0.64			0.65
COV (%)		12.05			11.20

*: Values represent the average of three cylinders or three beams

References

American Concrete Institute ACI Committee. (2011). "Building code requirements for structural concrete ACI 318-08 and commentary 318R-11." ACI 318-11/318R-11, Farmington Hills, MI: American Concrete Institute.

Aslani, F. and Nejadi, S. (2012) " Mechanical properties of conventional and self-compacting concrete: An analytical study" Construction and Building Material Journal, Vol. 36, pp. 330-347.

ASTM C 39/C 39M (2012). "Standard Test Method for Compressive Strength of Cylindrical Concrete Specimens," ASTM, West Conshohocken, PA, 7 pp.

ASTM C 78/C 78M (2010). "Standard Test Method for Flexural Strength of Concrete (Using Simple Beam with Third-Point Loading" ASTM, West Conshohocken, PA, 4 pp.

ASTM C 496/C 496M (2011). "Standard Test Method for Splitting Tensile Strength of Cylindrical Concrete," ASTM, West Conshohocken, PA, 5 pp.

Kosmatka, S. H. and Wilson, M. L. (2011) "Design and Control of Concrete Mixtures", 15th edition, Portland cement Association.

APPENDIX F
SHEAR TEST DATA OF HVFAC

SHEAR TEST DATA OF HVFAC

Strain-Load Curves

Figure F.1 shows both the beam loading pattern and the location of the strain gauges. Strain gauges were used to measure the strain in the reinforcements. The strain gauges were installed on the lower layer of the bottom longitudinal reinforcement at midspan (maximum flexural moment location) and quarter point along the span (middle of the shear test region). For the sections with stirrups, 10 additional strain gauges were installed on the stirrups.

All of the beams failed in shear. Based upon data collected from the strain gauges, none of the longitudinal reinforcement reached yield at failure, as expected, all of the stirrups yielded. Figures F.2 through F.5 show strain-load curves for both longitudinal and shear reinforcement strains of the CC and HVFAC beams, respectively.

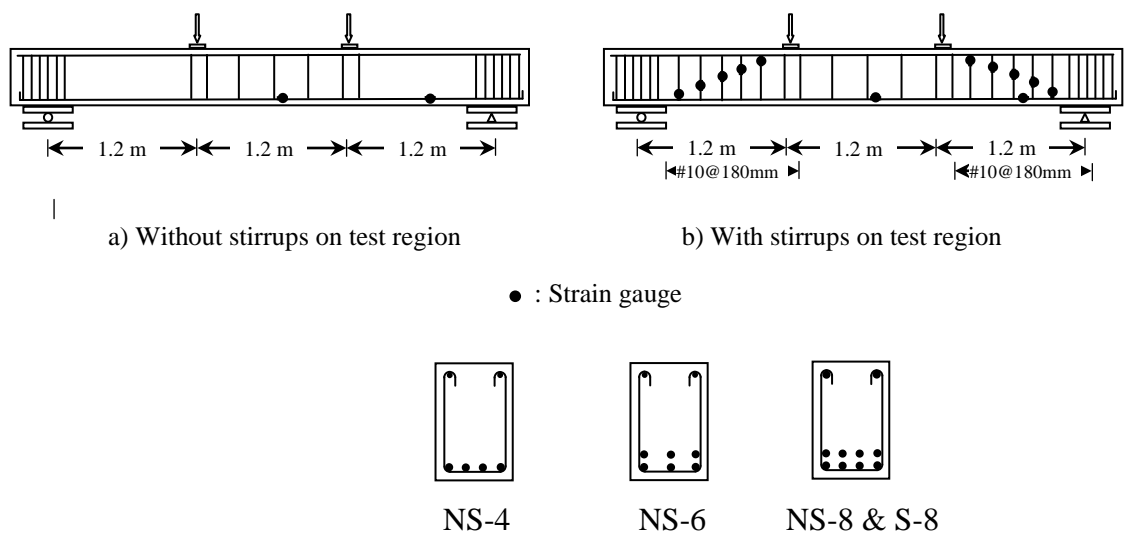
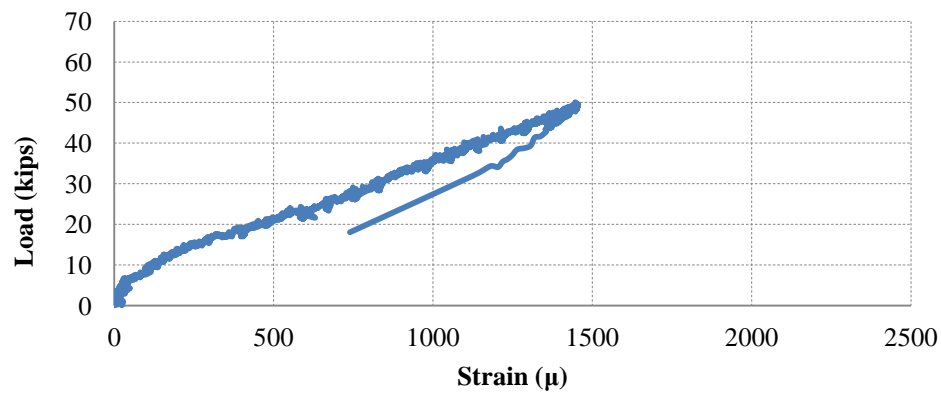
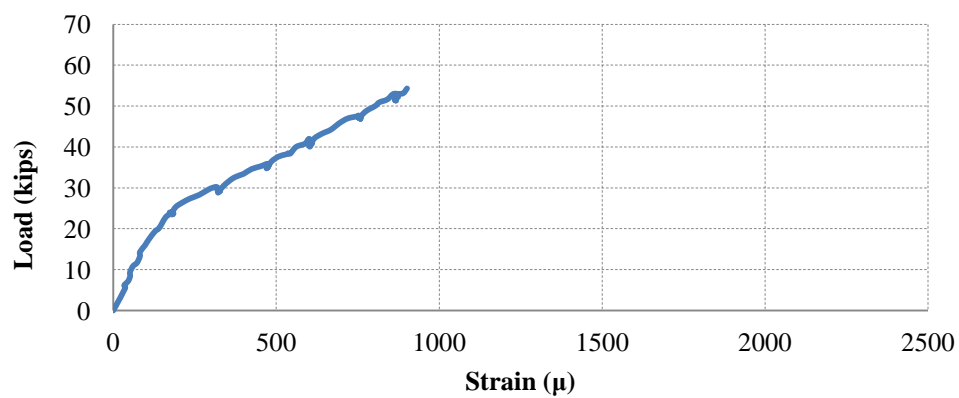


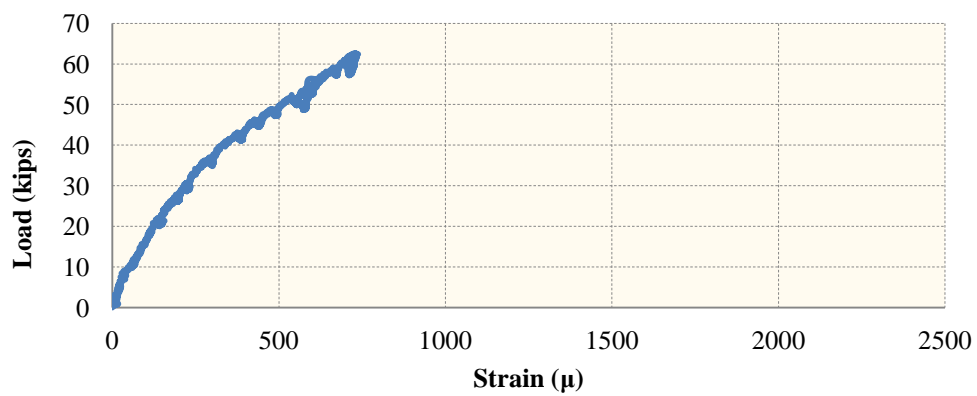
Figure F.1- Load pattern, cross sections, and location of strain gauges on the test beams



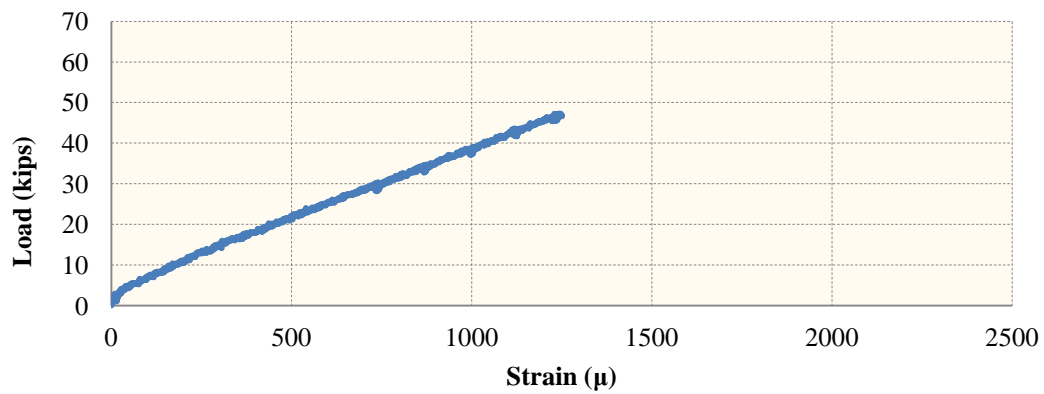
a) CC-NS-4-1



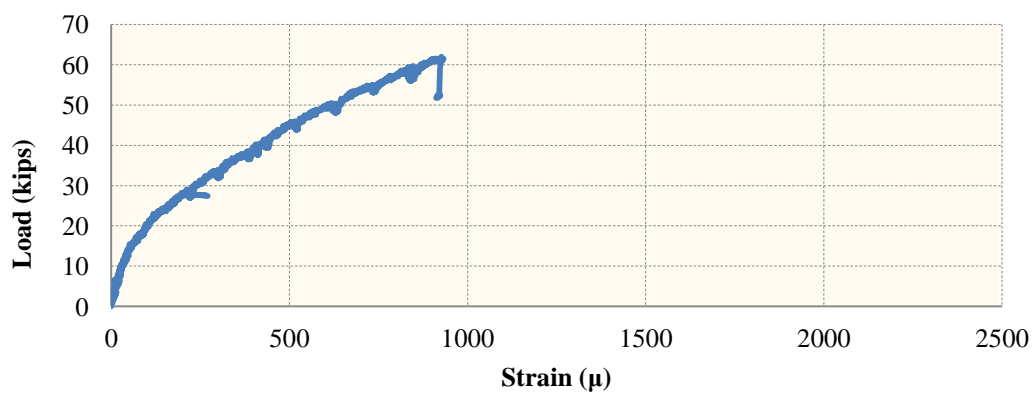
b) CC-NS-6-1



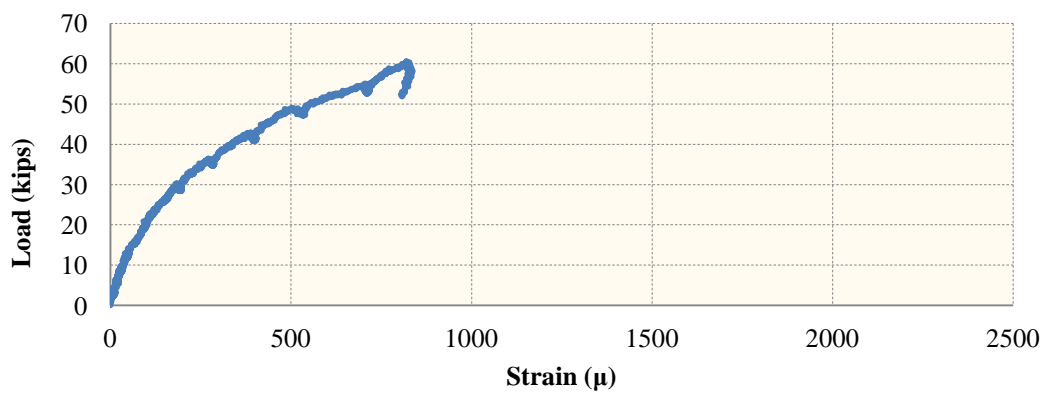
c) CC-NS-8-1



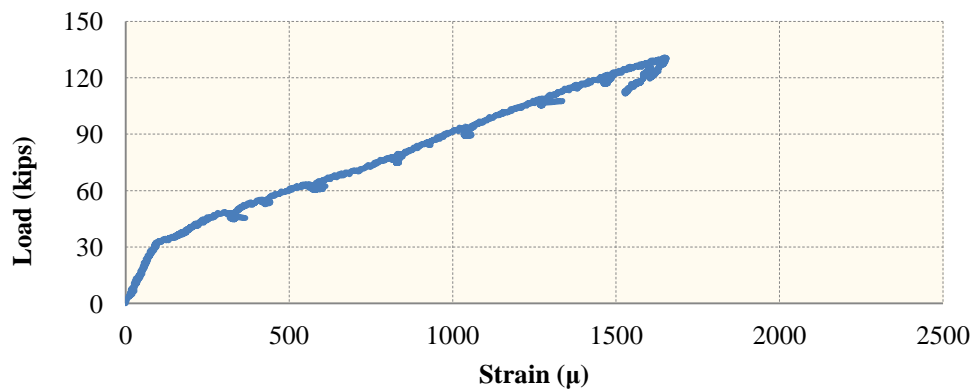
d) CC-NS-4-2



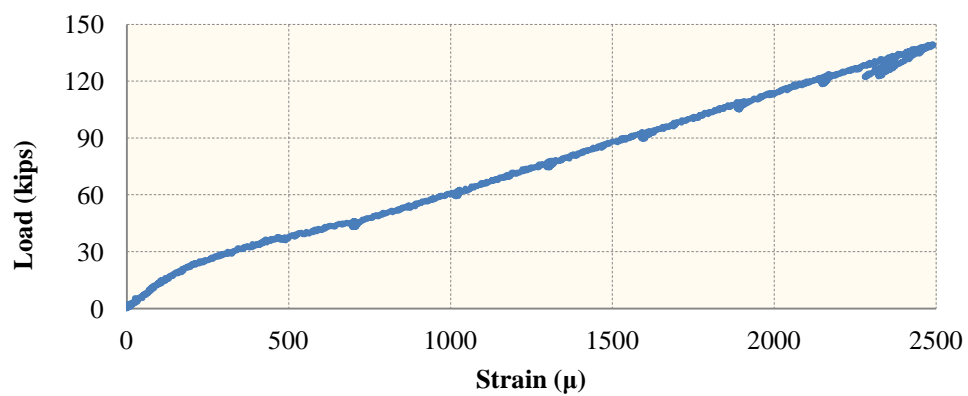
e) CC-NS-6-2



f) CC-NS-8-2

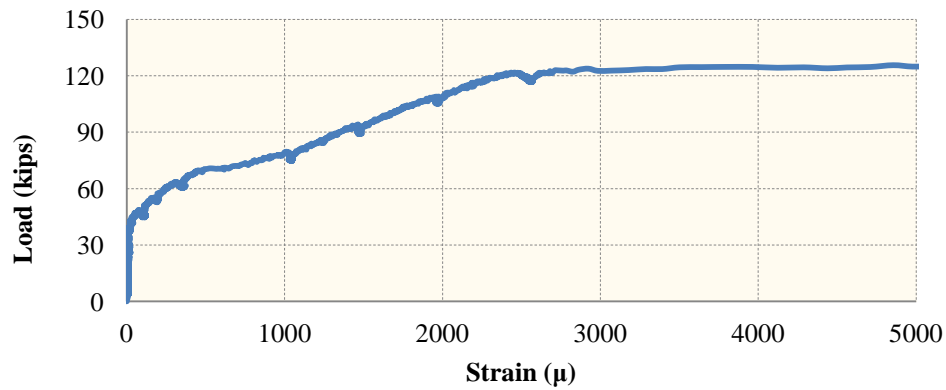


g) CC-S-8-1

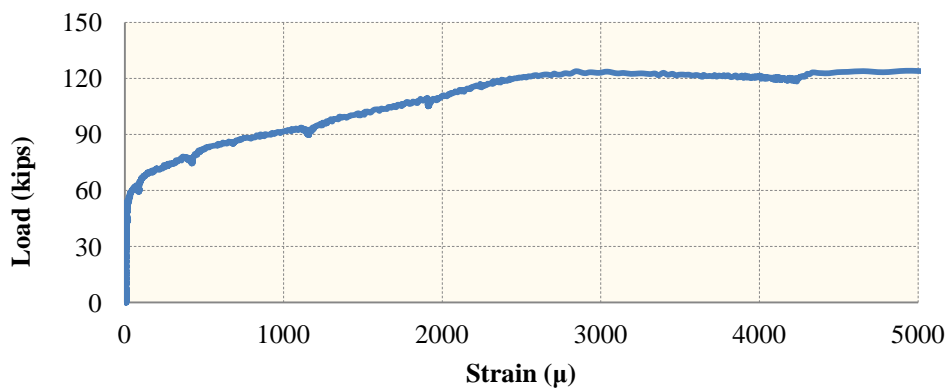


h) CC-S-8-2

Figure F.2 - Load –strain curves of the longitudinal reinforcement of the CC beams

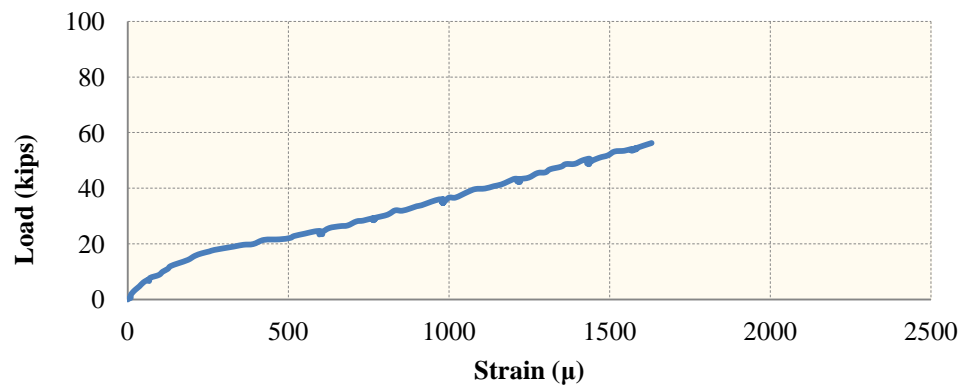


a) CC-S-8-1

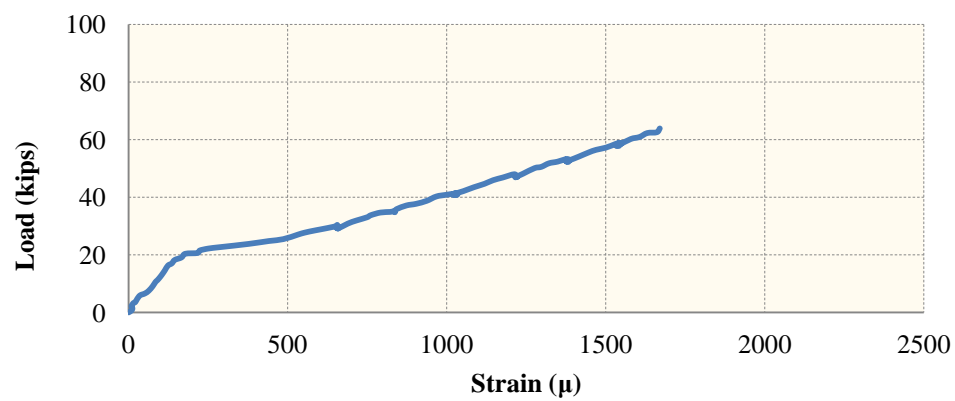


b) CC-S-8-2

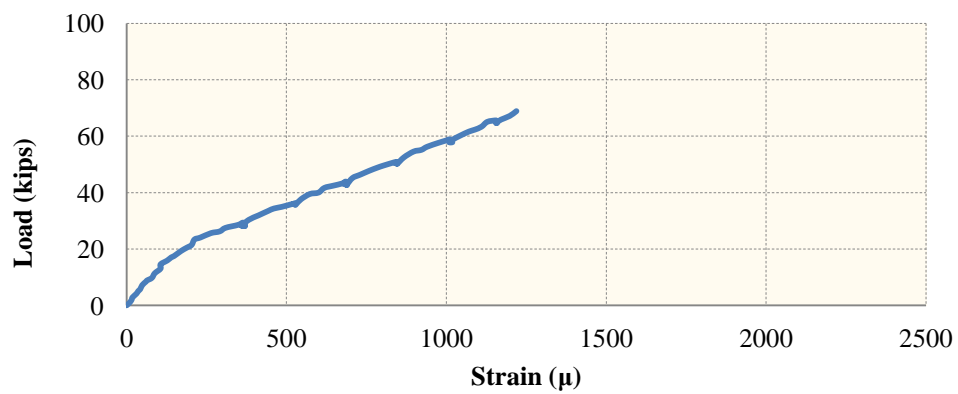
Figure F.3 - Load –strain curves of the shear reinforcement of the CC beams



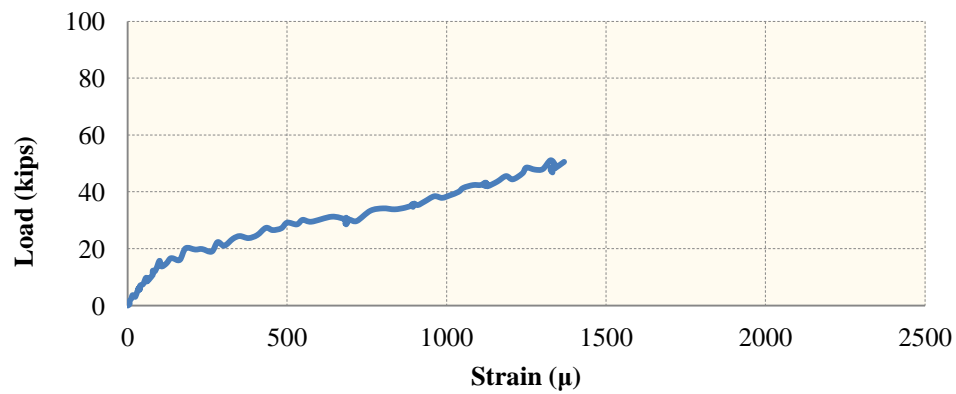
a) HVFAC-NS-4-1



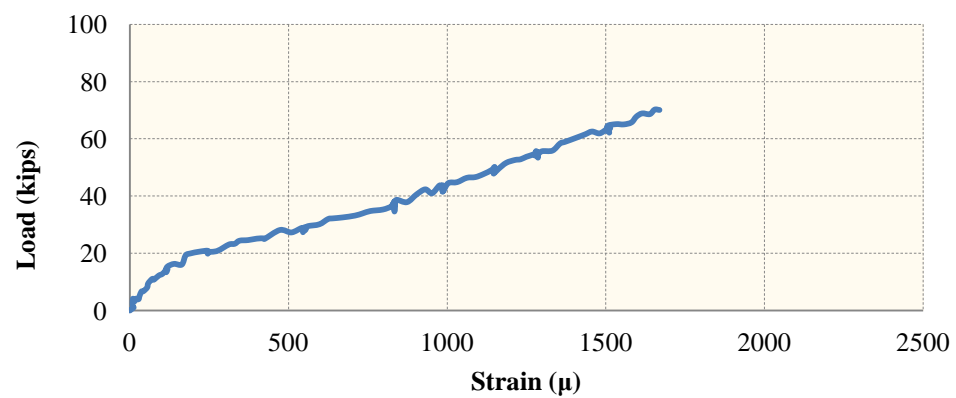
b) HVFAC-NS-6-1



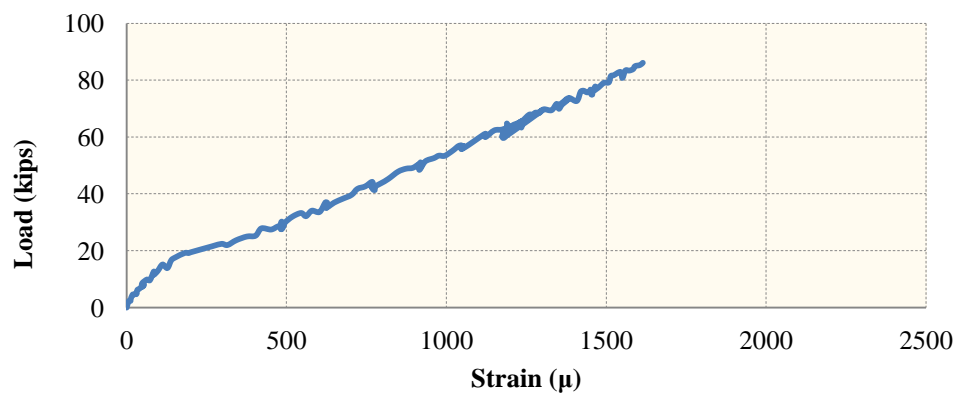
c) HVFAC-NS-8-1



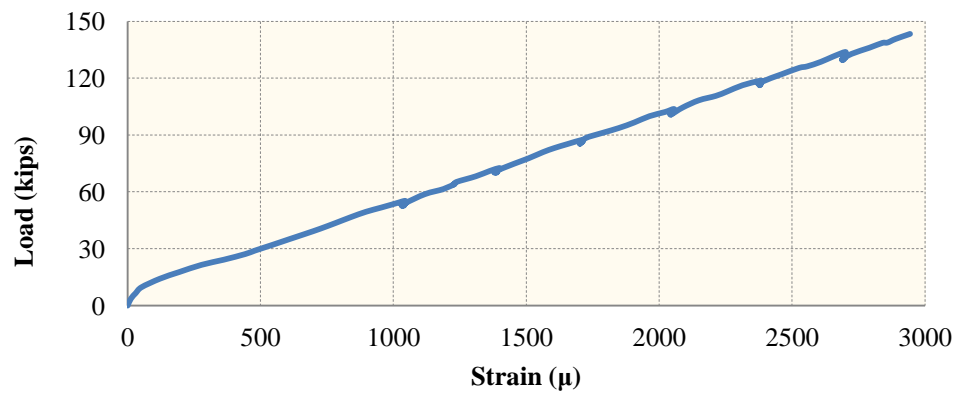
d) HVFAC-NS-4-2



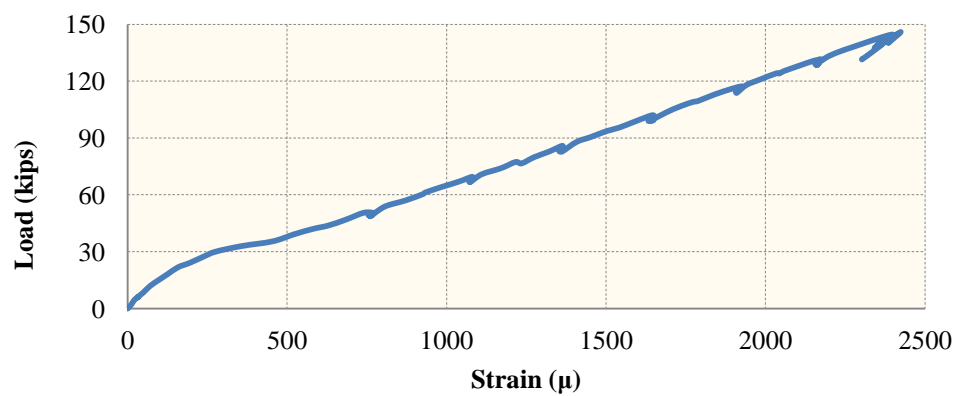
e) HVFAC-NS-6-2



f) HVFAC-NS-8-2

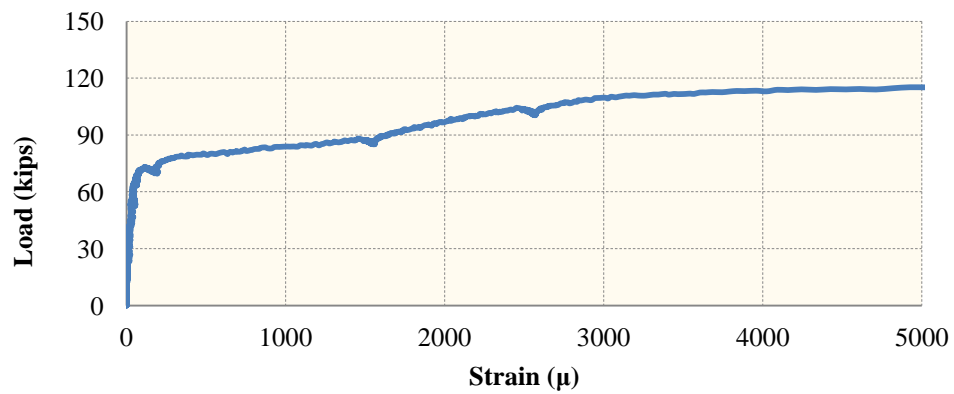


g) HVFAC-S-8-1

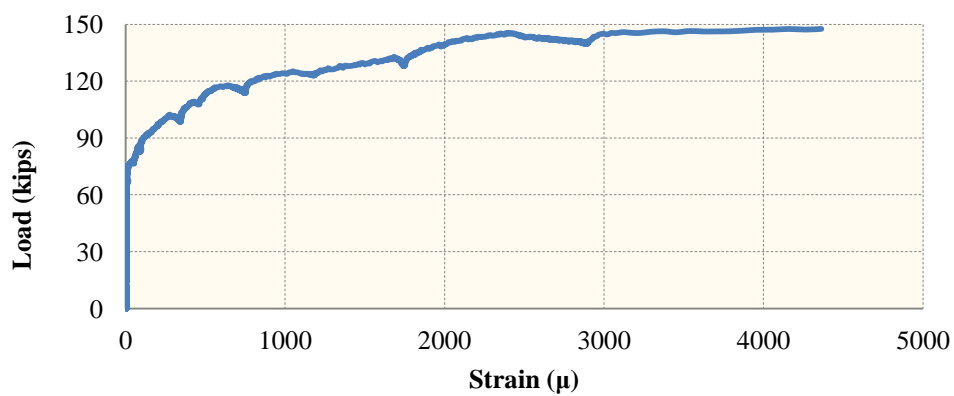


h) HVFAC-S-8-2

Figure F.4 - Load –strain curves of the longitudinal reinforcement of the HVFAC beams



a) HVFAC-S-8-1



b) HVFAC-S-8-2

Figure F.5 - Load –strain curves of the shear reinforcement of the HVFAC beams

APPENDIX G
SHEAR TEST DATA OF SCC

SHEAR TEST DATA OF SCC

Strain-Load Curves

Figure G.1 shows both the beam loading pattern and the location of the strain gauges. Strain gauges were used to measure the strain in the reinforcements. The strain gauges were installed on the lower layer of the bottom longitudinal reinforcement at midspan (maximum flexural moment location) and quarter point along the span (middle of the shear test region). For the sections with stirrups, 10 additional strain gauges were installed on the stirrups.

All of the beams failed in shear. Based upon data collected from the strain gauges, none of the longitudinal reinforcement reached yield at failure, as expected, all of the stirrups yielded. Figures G.2 through G.5 show strain-load curves for both longitudinal and shear reinforcement strains of the CC and SCC beams, respectively.

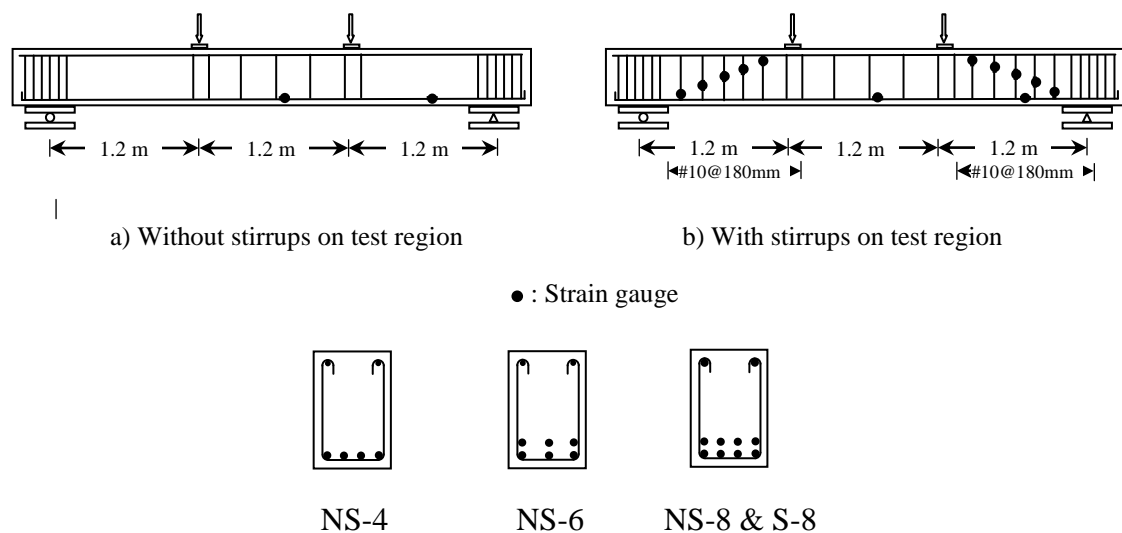
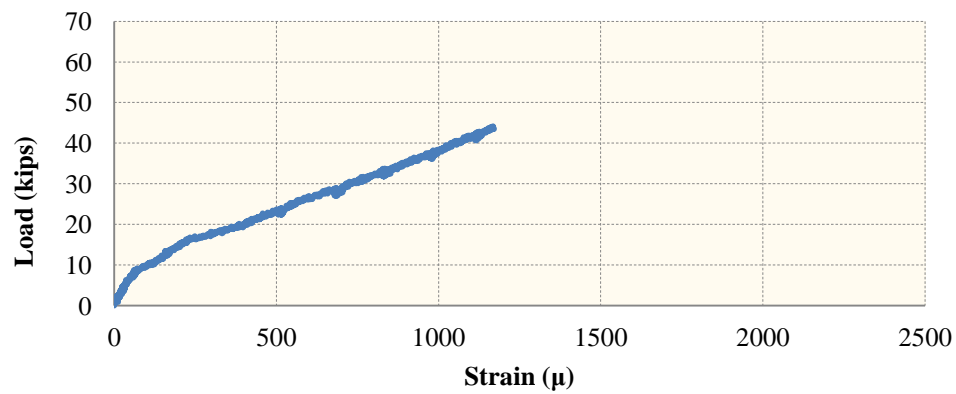
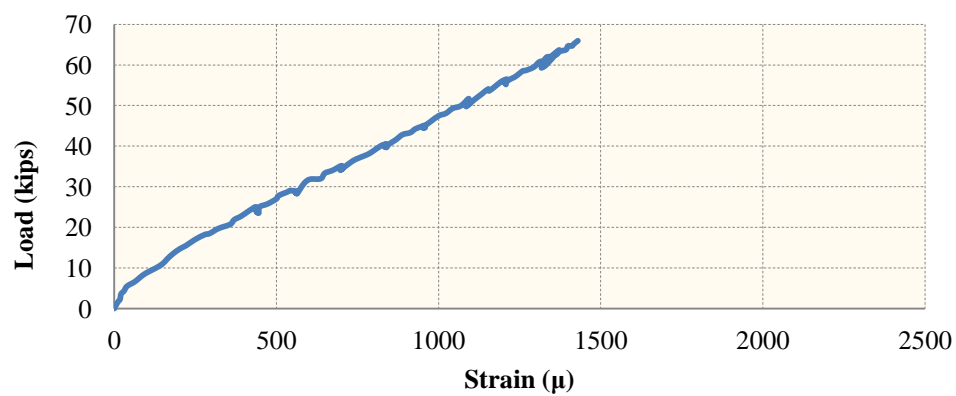


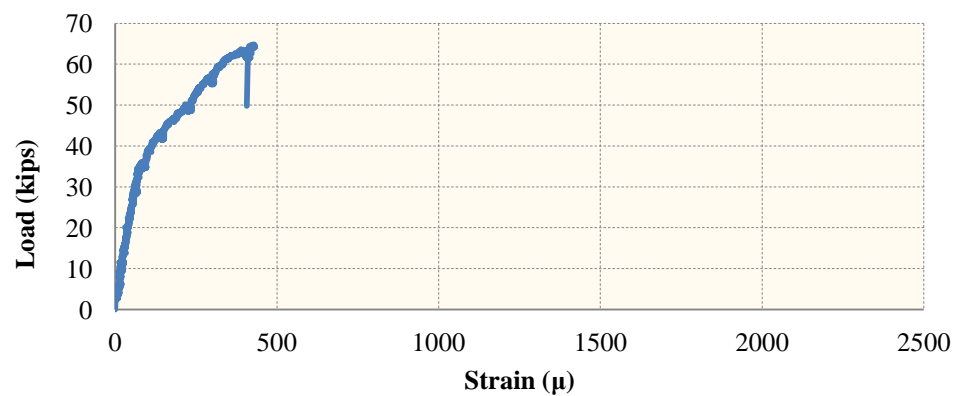
Figure G.1- Load pattern, cross sections, and location of strain gauges on the test beams



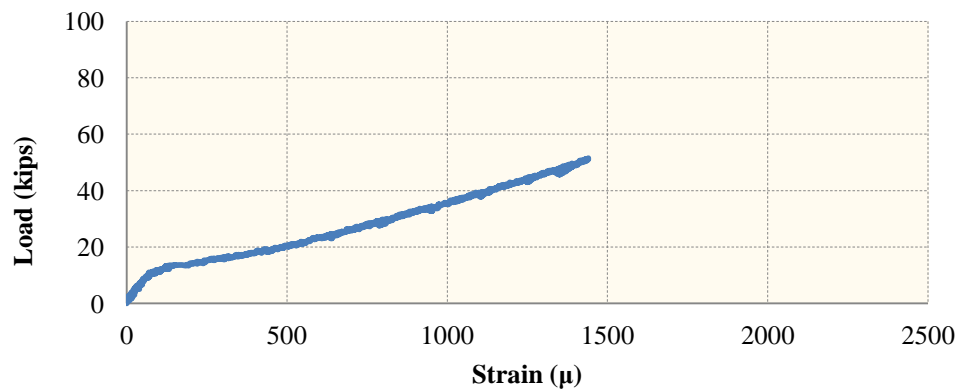
a) CC-NS-4-1



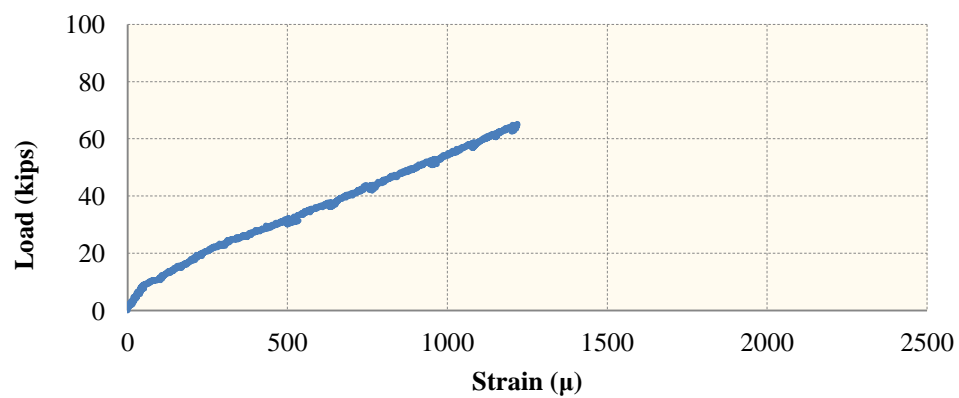
b) CC-NS-6-1



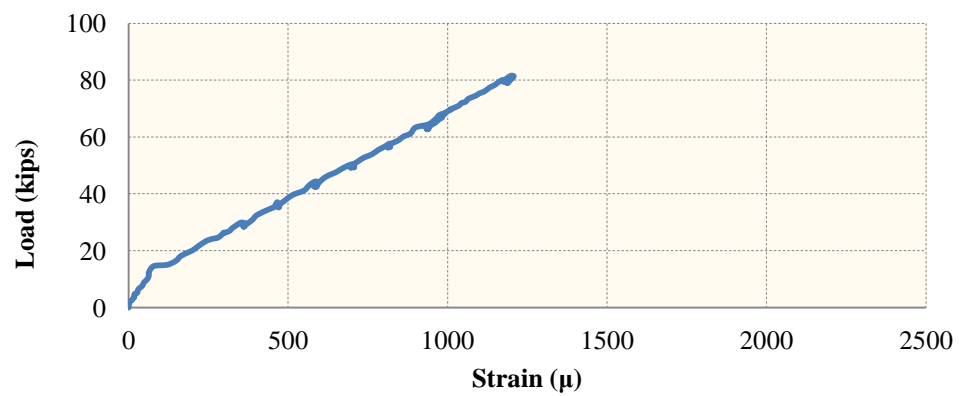
c) CC-NS-8-1



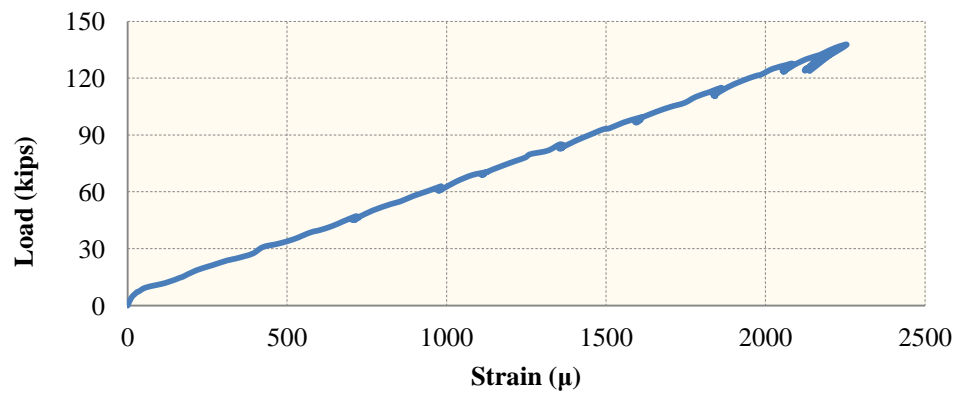
d) CC-NS-4-2



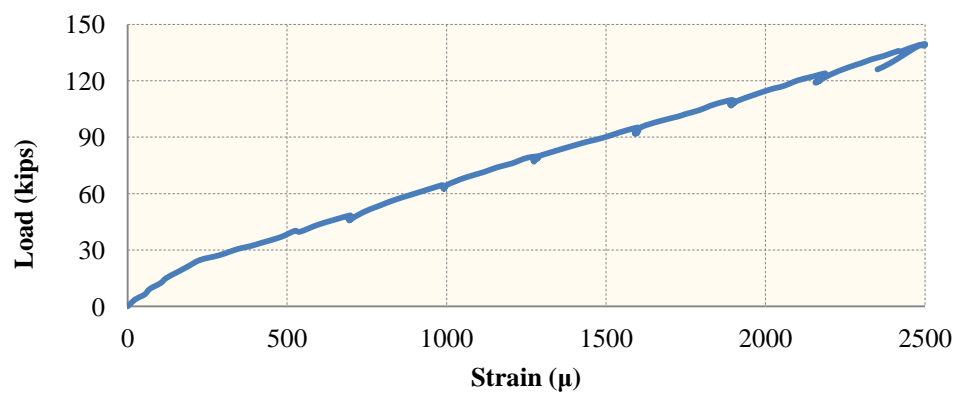
e) CC-NS-6-2



f) CC-NS-8-2

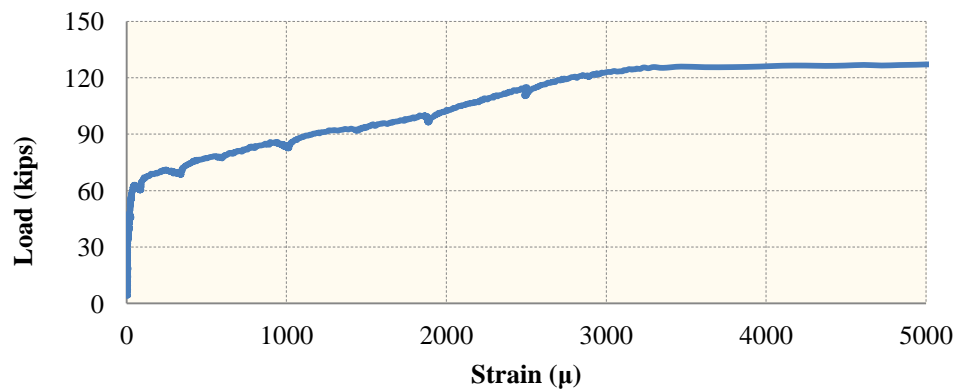


g) CC-S-8-1

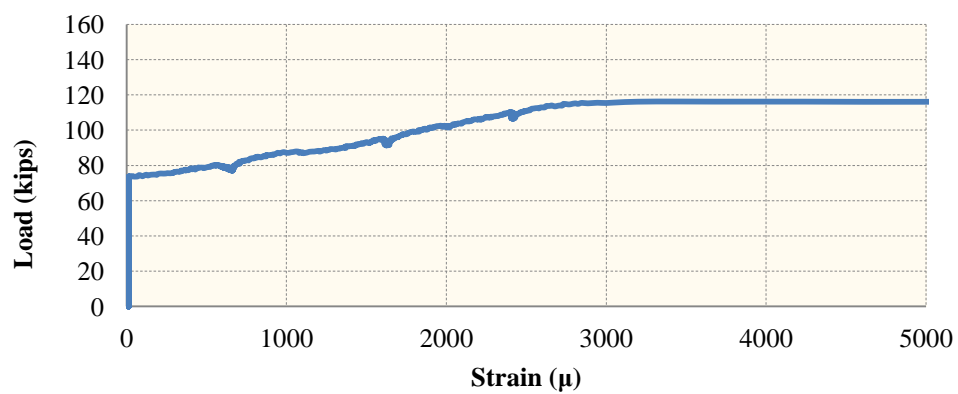


h) CC-S-8-2

Figure G.2 - Load –strain curves of the longitudinal reinforcement of the CC beams

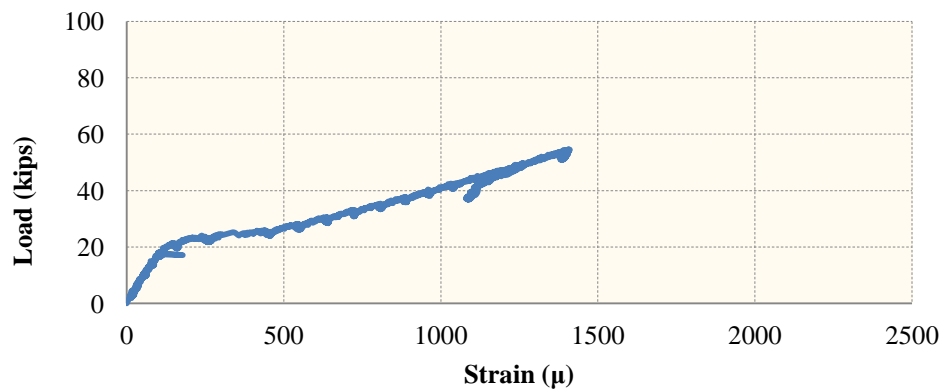


a) CC-S-8-1

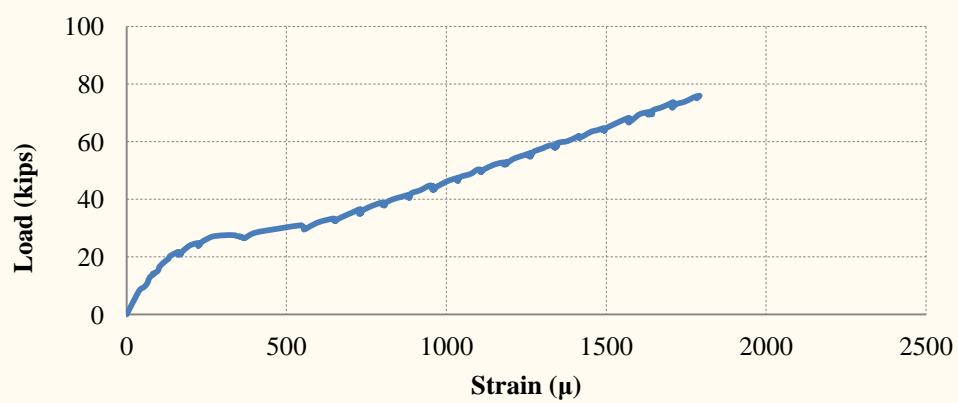


b) CC-S-8-2

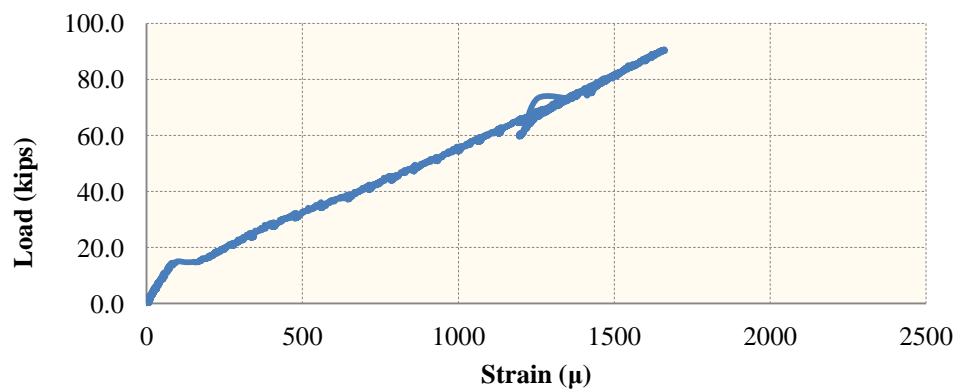
Figure G.3 - Load –strain curves of the shear reinforcement of the CC beams



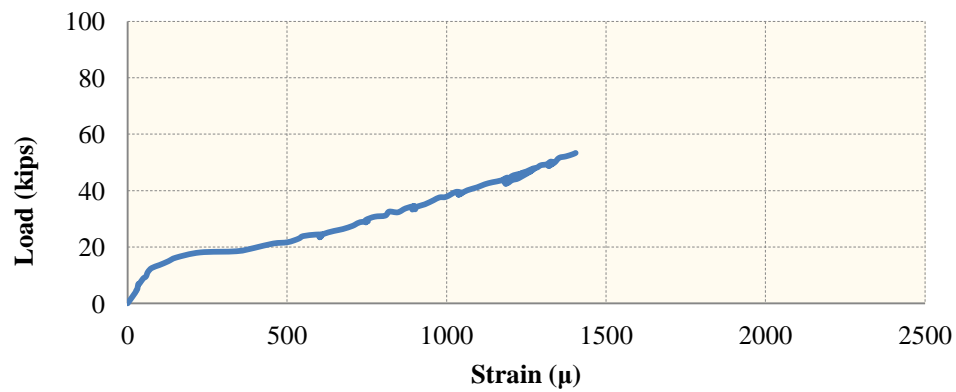
a) SCC-NS-4-1



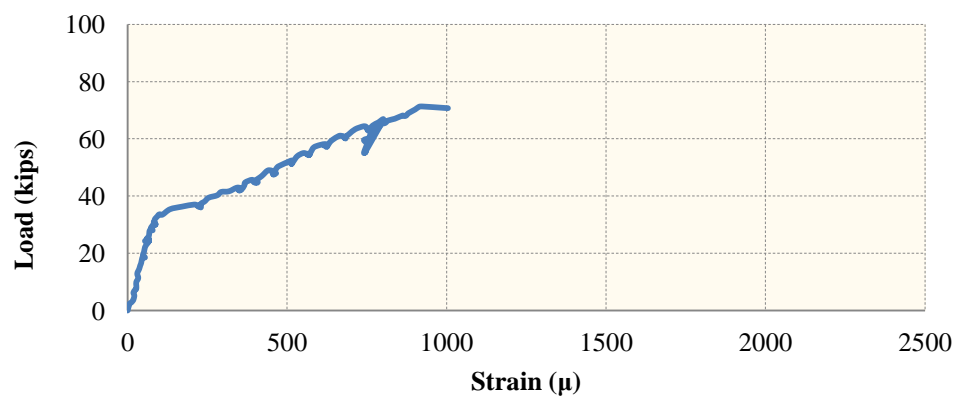
b) SCC-NS-6-1



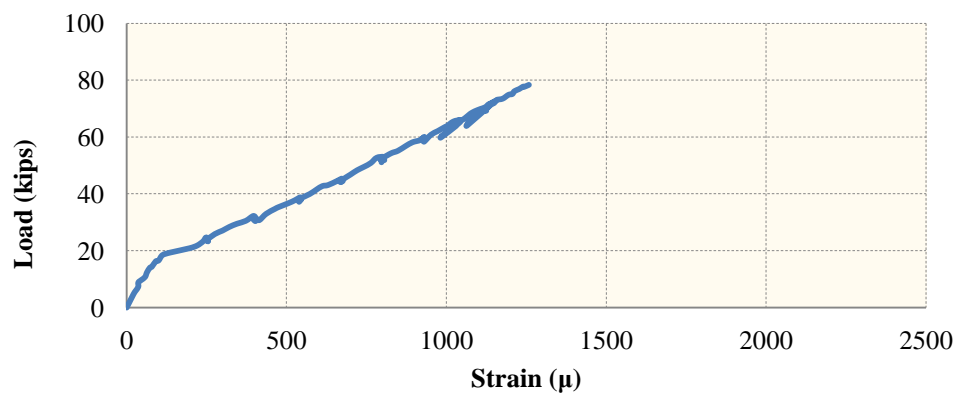
c) SCC-NS-8-1



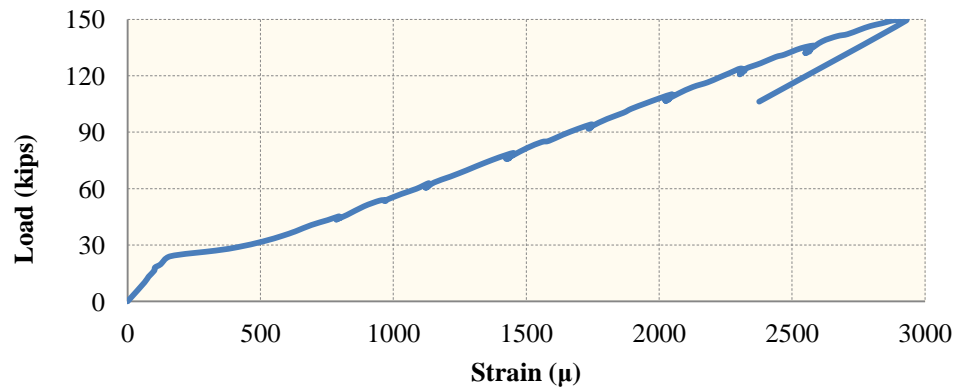
d) SCC-NS-4-2



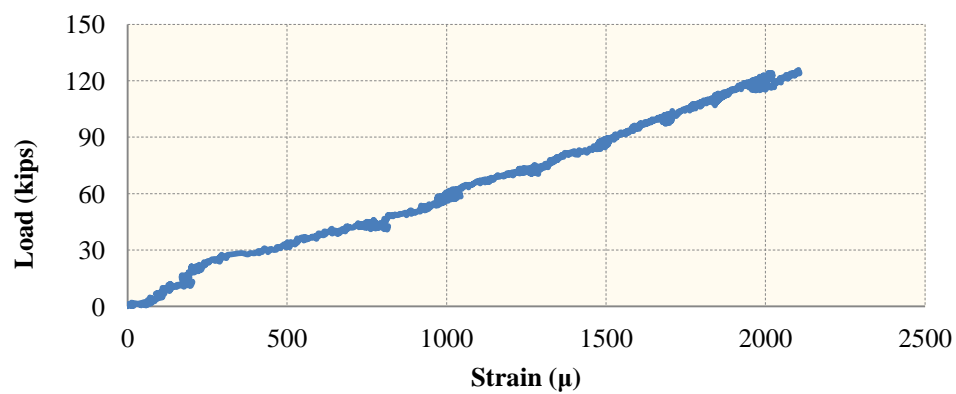
e) SCC-NS-6-2



f) SCC-NS-8-2

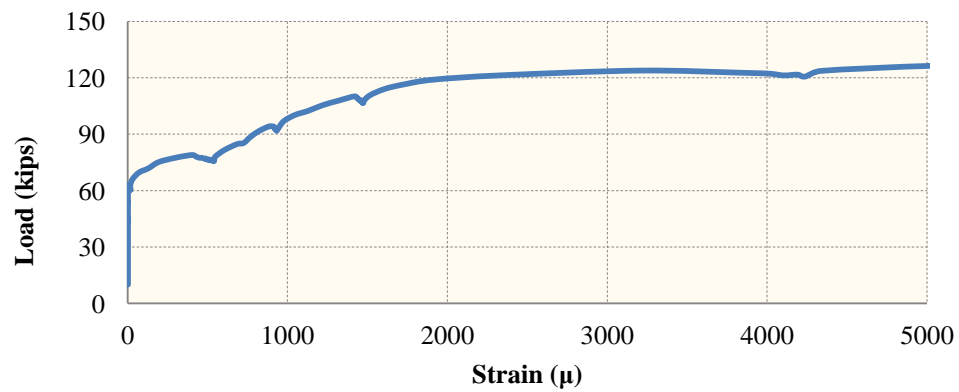


g) SCC-S-8-1

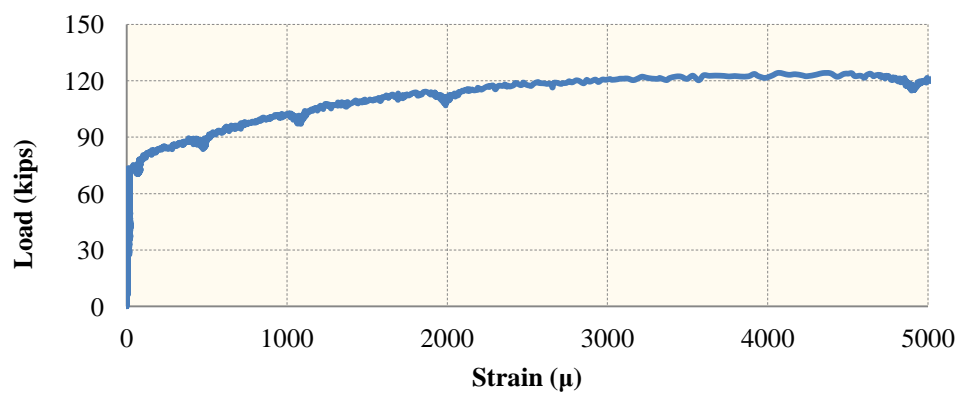


h) SCC- S-8-2

Figure G.4 - Load –strain curves of the longitudinal reinforcement of the SCC beams



a) SCC-S-8-1



b) SCC- S-8-2

Figure G.5 - Load-strain curves of the shear reinforcement of the SCC beams

APPENDIX H
FRACTURE ENERGY TEST DATA OF HVFAC

FRACTURE ENERGY

Fracture energy is defined as the amount of energy necessary to create a crack of unit surface area projected in a plane parallel to the crack direction. Hillerborg (1985) provided a theoretical basis for a concrete fracture energy testing procedure, often referred to as the work-of-fracture method (WFM), in which the fracture energy is computed as the area under the experimental load-deflection response curve – for a notched concrete beam subjected to three-point bending – divided by the projected area of the fractured concrete. In other words, when conducting a three-point bending test on a notched beam, as the beam splits into two halves, the fracture energy (G_F) can be determined by dividing the total dissipated energy by the projected surface area of the crack as shown in Equation H-1.

$$G_F = \frac{W}{b(d-a_o)} \quad (\text{H-1})$$

where W is the total energy dissipated in the test, and b , d , and a_o are the thickness, height, and notch depth of the beam, respectively. The same approach was adopted by the RILEM standard.

For the current study, the researchers performed fracture energy tests on both the CC and SCC using the three-point, notched specimen, bend test. The beam specimens measured 150×150×600 mm with a span length of 450 mm. The notch – which was cast into the concrete as opposed to being saw cut after the concrete hardened – had a depth of 40 mm and a thickness of 6 mm. Two linear variable differential transformers (LVDTs) measured deflection at midspan of the beam, and self-weight compensation was provided through lever arms (Figure H.1). The tests were performed using a closed loop, servo-controlled MTS machine at a loading rate of 0.002 mm/s.

A total of 16 specimens were constructed for fracture energy testing, eight for each concrete type. After casting, the beam specimens and companion compressive strength cylinders were covered with both wet burlap and a plastic sheet. The specimens and cylinders were moist cured for three days and, after formwork removal, were stored in the laboratory until they were tested at 28 days.

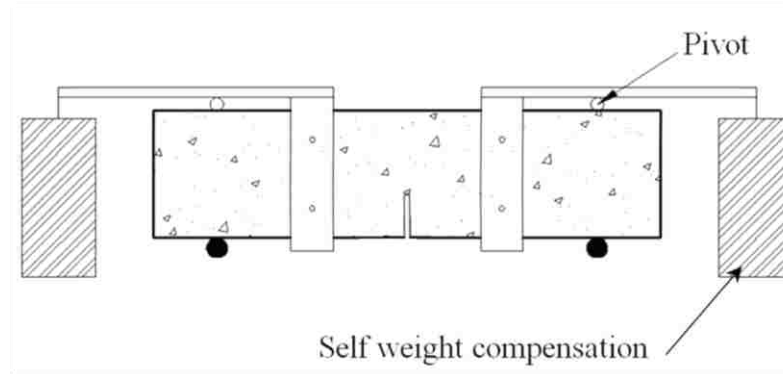


Figure H.1- Fracture energy specimens

Test Results

Results of the fracture energy tests for the CC and HVFAC are presented in Table H.1 along with the corresponding compressive strengths at time of testing. Also included in Table F.1 are theoretical fracture energies based on relationships proposed by Bazant et al.(2005), the JSCE-07 “Standard Specifications for Concrete Structures,” and the CEB-FIP Model Code 2010. The Bazant expression, shown as Equation H-2, is a function of compressive strength, type and maximum size of the aggregate and water-to-cement ratio, while the JSCE-07 relationship, shown as Equation H-3, is a function of compressive strength and maximum aggregate size, and the CEB-FIP Model Code 2010 relationship, shown as Equation H-4, is only a function of compressive strength. As shown in Table H.1, the Bazant equation showed excellent agreement with the test data, with most of the test values falling within 10% of the predicted fracture energies. The JSCE-07 expression, on the other hand, noticeably underestimated the fracture energies.

$$G_F = 2.5 \alpha_o \left(\frac{f_c'}{0.051} \right)^{0.46} \left(1 + \frac{d_a}{11.27} \right)^{0.22} \left(\frac{w}{c} \right)^{-0.30} \quad (\text{N/m}) \quad (\text{H-2})$$

$$G_F = 10 d_{\max}^{0.33} f_{ck}^{0.33} \quad (\text{N/m}) \quad (\text{H-3})$$

$$G_F = 73 f_{cm}^{0.18} \quad (\text{N/m}) \quad (\text{H-4})$$

where $\alpha_o=1$ for rounded aggregate and 1.44 for crushed or angular aggregate.

Figure H.2 is a plot of fracture energy as a function of compressive strength. Included in the plot are the results of the current study as well as the wealth of fracture energy test data available in the literature (Bazant et al. 2005). Given the significant scatter of the database of fracture energy test results, it is somewhat difficult to draw definitive conclusions on the current test values. Nonetheless, visually, Figure H.2 seems to indicate that the CC and HVFAC test results fall within the upper portion of the data and follow the same general trend of increasing fracture energy as a function of compressive strength. More importantly, the CC and HVFAC fracture energies from the current study are very consistent with each other when accounting for compressive strength, offering a valuable comparison between the two concrete types. Furthermore, statistical analysis of the data indicates that the CC and HVFAC test results fall within and slightly above a 95% confidence interval of a nonlinear regression curve fit of the database. This result indicates that the test values are also consistent with the wealth of fracture energy test data available in the literature.

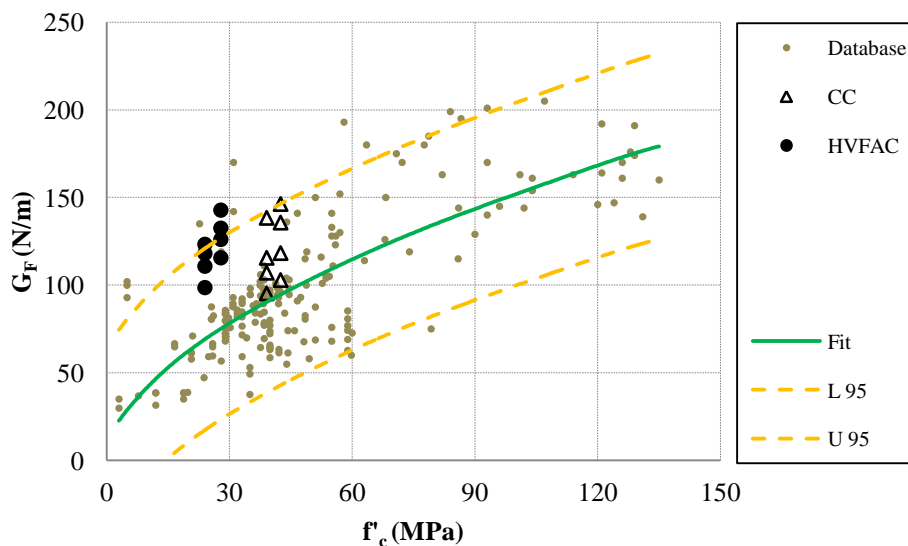


Figure H.2 - Fracture energy vs. compressive strength; results from literature (Bazant et al. 2005) and test results of this study

Table H.1- Fracture energy (G_F)

Mix	CC		HVFAC	
	First Batch	Second Batch	First Batch	Second Batch
f_c^*	42.5	39.1	24.0	27.9
G_F^{**}	146.3	138.4	123.3	115.6
	135.7	107.1	110.8	126.1
	102.9	95.3	118.1	132.5
	118.3	115.6	98.6	142.8
$G_{F(AVE.)}$	125.8	114.1	112.7	129.3
$G_{F(Bazant.)}$	129.9	125.0	99.9	107.0
$G_{F(JSCE)}$	91.1	88.6	75.4	79.3
$G_{F(CEB-FIP)}$	143.4	141.2	129.3	132.9
$\left(\frac{G_{F(test)}}{G_{F(Bazant)}} \right)$	0.94	1.01	0.87	1.10
$\left(\frac{G_{F(test)}}{G_{F(JSCE)}} \right)$	1.30	1.30	1.31	1.80
$\left(\frac{G_{F(test)}}{G_{F(CEB-FIP)}} \right)$	0.83	0.82	0.76	1.07

* MPa, ** N/m

References

Bazant, Z.P., and Becq-Giraudon, E., (2002), Statistical prediction of fracture parameters of concrete and implications for choice of testing standards. *Cement and Concrete Research Journal*, Vol. 32, No. 4, pp. 529-556.

CEB-FIP Model Code 2010-fib (2012), Vol. 1, p.120.

Japan Society of Civil Engineers (2007). "Standard Specifications for Concrete Structures" JSCE No. 15, Tokyo, pp. 154-159.

Hillerborg, A. (1985) "The Theoretical Basis of a Method to Determine the Fracture Energy G_F of Concrete," *Materials and Structures*, V. 18, No. 106, pp. 291-296.

RILEM, 1985, TC 50-FMC, Fracture Mechanics of Concrete, "Determination of the Fracture Energy of Mortar and Concrete by Means of Three-Point Bend Tests on Notched Beams," RILEM Recommendation, *Materials and Structures*, V. 18, No. 16, pp. 287-290.

APPENDIX I
FRACTURE ENERGY TEST DATA OF SCC

FRACTURE ENERGY TEST DATA OF SCC

Fracture energy is defined as the amount of energy necessary to create a crack of unit surface area projected in a plane parallel to the crack direction. Hillerborg (1985) provided a theoretical basis for a concrete fracture energy testing procedure, often referred to as the work-of-fracture method (WFM), in which the fracture energy is computed as the area under the experimental load-deflection response curve – for a notched concrete beam subjected to three-point bending – divided by the projected area of the fractured concrete. In other words, when conducting a three-point bending test on a notched beam, as the beam splits into two halves, the fracture energy (G_F) can be determined by dividing the total dissipated energy by the projected surface area of the crack as shown in Equation I-1.

$$G_F = \frac{W}{b(d-a_o)} \quad (I-1)$$

where W is the total energy dissipated in the test, and b , d , and a_o are the thickness, height, and notch depth of the beam, respectively. The same approach was adopted by the RILEM standard.

For the current study, the researchers performed fracture energy tests on both the CC and SCC using the three-point, notched specimen, bend test. The beam specimens measured 150×150×600 mm with a span length of 450 mm. The notch – which was cast into the concrete as opposed to being saw cut after the concrete hardened – had a depth of 40 mm and a thickness of 6 mm. Two linear variable differential transformers (LVDTs) measured deflection at midspan of the beam, and self-weight compensation was provided through lever arms (Figure I.1). The tests were performed using a closed loop, servo-controlled MTS machine at a loading rate of 0.002 mm/s.

A total of 16 specimens were constructed for fracture energy testing, eight for each concrete type. After casting, the beam specimens and companion compressive strength cylinders were covered with both wet burlap and a plastic sheet. The specimens and cylinders were moist cured for three days and, after formwork removal, were stored in the laboratory until they were tested at 28 days.

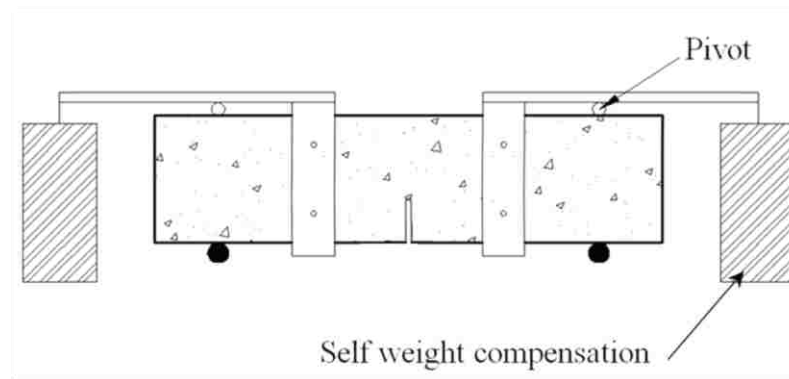


Figure I.1 - Fracture energy specimens

Test Results

Results of the fracture energy tests for the CC and SCC are presented in Table I.1 along with the corresponding compressive strengths at time of testing. Also included in Table I.1 are theoretical fracture energies based on relationships proposed by Bazant et al.(2005), the JSCE-07 “Standard Specifications for Concrete Structures,” and the CEB-FIP Model Code 2010. The Bazant expression, shown as Equation I-2, is a function of compressive strength, type and maximum size of the aggregate and water-to-cement ratio, while the JSCE-07 relationship, shown as Equation I-3, is a function of compressive strength and maximum aggregate size, and the CEB-FIP Model Code 2010 relationship, shown as Equation I-4, is only a function of compressive strength. As shown in Table I.1, the Bazant and CEB-FIP equations showed excellent agreement with the test data, with most of the test values falling within 10% of the predicted fracture energies. The JSCE-07 expression, on the other hand, noticeably underestimated the fracture energies, with predicted values ranging from 70 to 74% of the test values.

$$G_F = 2.5 \alpha_o \left(\frac{f_c'}{0.051} \right)^{0.46} \left(1 + \frac{d_a}{11.27} \right)^{0.22} \left(\frac{w}{c} \right)^{-0.30} \quad (\text{N/m}) \quad (\text{I-2})$$

$$G_F = 10 d_{\max}^{0.33} f_{ck}^{0.33} \quad (\text{N/m}) \quad (\text{I-3})$$

$$G_F = 73 f_{cm}^{0.18} \quad (\text{N/m}) \quad (\text{I-4})$$

where $\alpha_o=1$ for rounded aggregate and 1.44 for crushed or angular aggregate.

Figure I.2 is a plot of fracture energy as a function of compressive strength. Included in the plot are the results of the current study as well as the wealth of fracture energy test data available in the literature (Bazant et al. 2005). Given the significant scatter of the database of fracture energy test results, it is somewhat difficult to draw definitive conclusions on the current test values. Nonetheless, visually, Figure I.2 seems to indicate that the CC and SCC test results fall within the upper portion of the data and follow the same general trend of increasing fracture energy as a function of compressive strength. More importantly, the CC and SCC fracture energies from the current study are very consistent with each other when accounting for compressive strength, offering a valuable comparison between the two concrete types. Furthermore, statistical analysis of the data indicates that the CC and SCC test results fall within and slightly above a 95% confidence interval of a nonlinear regression curve fit of the database. This result indicates that the test values are also consistent with the wealth of fracture energy test data available in the literature.

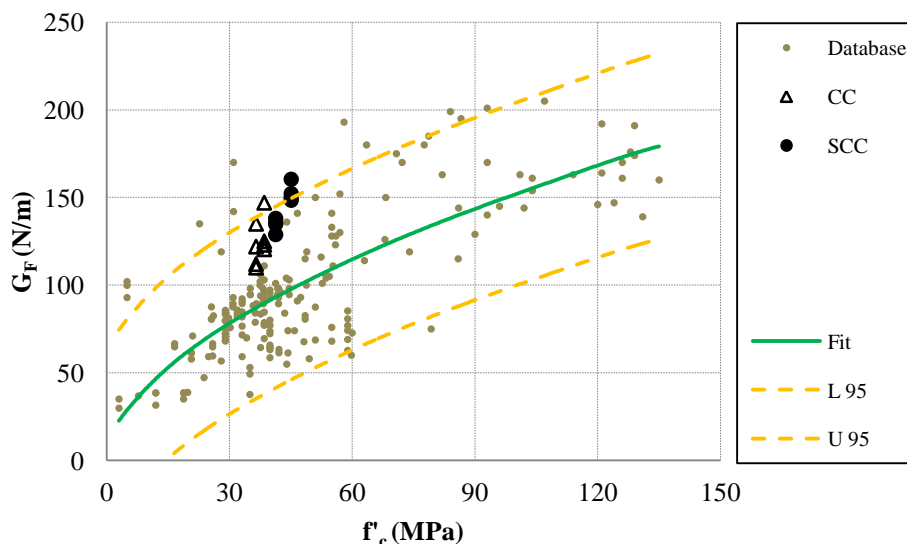


Figure I.2 - Fracture energy vs. compressive strength; results from literature (Bazant et al. 2005) and test results of

Table I.1- Fracture energy (G_F)

Mix	CC		SCC	
	First Batch	Second Batch	First Batch	Second Batch
f_c^*	36.5	38.5	41.3	45.1
G_F^{**}	135	123	136	150
	122	147	135	148
	112	125	138	152
	110	120	129	160
$G_{F(AVE.)}$	120	129	135	153
$G_{F(Bazant.)}$	121	124	128	134
$G_{F(JSCE)}$	87	88	90	93
$G_{F(CEB-FIP)}$	139	141	143	145
$\left(\frac{G_{F(test)}}{G_{F(Bazant)}} \right)$	0.99	1.04	1.05	1.14
$\left(\frac{G_{F(test)}}{G_{F(JSCE)}} \right)$	1.39	1.46	1.50	1.65
$\left(\frac{G_{F(test)}}{G_{F(CEB-FIP)}} \right)$	0.86	0.92	0.95	1.06

* MPa, ** N/m

References

Bazant, Z.P., and Becq-Giraudon, E., (2002), Statistical prediction of fracture parameters of concrete and implications for choice of testing standards. *Cement and Concrete Research Journal*, Vol. 32, No. 4, pp. 529-556.

CEB-FIP Model Code 2010-fib (2012), Vol. 1, p.120.

Japan Society of Civil Engineers (2007). "Standard Specifications for Concrete Structures" JSCE No. 15, Tokyo, pp. 154-159.

Hillerborg, A. (1985) "The Theoretical Basis of a Method to Determine the Fracture Energy G_F of Concrete," *Materials and Structures*, V. 18, No. 106, pp. 291-296.

RILEM, 1985, TC 50-FMC, *Fracture Mechanics of Concrete*, "Determination of the Fracture Energy of Mortar and Concrete by Means of Three-Point Bend Tests on Notched Beams," RILEM Recommendation, *Materials and Structures*, V. 18, No. 16, pp. 287-290.

APPENDIX J
STATISTICAL DATA ANALYSIS OF HVFAC

STATISTICAL DATA ANALYSIS OF HVFAC

To compare the tensile splitting strength, flexural strength, and fracture energy test results of both the CC and the HVFAC mixes, the results must be adjusted to reflect the different compressive strengths. The tensile splitting and flexural strength of the mix is a function of the square root of the compressive strength of the concrete. Also, fracture energy is a function of the compressive strength with powers of 0.46, 0.33, and 0.18 based on the Bazant et al., the JSCE-07, and the CEB-FIP Model Code 2010, respectively. Therefore, to normalize the data for comparison, the tensile splitting and flexural strengths were divided by the square root of the compressive strengths, while the fracture energies were divided by the aforementioned powers of the compressive strengths.

Statistical tests (both parametric and nonparametric) were used to evaluate whether there is any statistically significant difference between the tensile splitting strength, flexural strength, and fracture energy test results for the CC and HVFAC mixes.

Parametric Test

The paired t-test is a statistical technique used to compare two population means. This test assumes that the differences between pairs are normally distributed. If this assumption is violated, the paired t-test may not be the most powerful test. The hypotheses for the paired t-tests for tensile splitting strength, flexural strength, and fracture energy are as follows:

H_0 : The mean of the normalized tensile splitting strength of the CC mix is equal to the HVFAC mix [$f_{ct}(\text{CC}) = f_{ct}(\text{HVFAC})$].

H_a : Not H_0

H_0 : The mean of the normalized flexural strength of the CC mix is greater than the HVFAC mix [$f_r(\text{CC}) > f_r(\text{HVFAC})$].

H_a : Not H_0

H_0 : The mean of the normalized fracture energy of the HVFAC mix is greater than the CC mix [$G_F(\text{HVFAC}) > G_F(\text{CC})$].

H_a : Not H_0

The statistical computer program SAS 9.2 was employed to perform these statistical tests. Both Kolmogorov-Smirnov (K-S) and Anderson-Darling (A-D) tests showed the data – the differences between the tensile splitting strength, flexural tensile strength, and fracture energy of the mixes – follow a normal distribution. Therefore, the paired t-tests could be performed. Table J.1 summarizes the result of the paired t-test (p-values at the 0.05 significance level). All the p-values were greater than 0.05, which means the null hypotheses at the 0.05 significance level are confirmed.

Nonparametric Test

Unlike the parametric tests, nonparametric tests are referred to as distribution-free tests. These tests have the advantage of requiring no assumption of normality, and they usually compare medians rather than means. The Wilcoxon signed-rank test is usually identified as a nonparametric alternative to the paired t-test. The hypothesis for this test is the same as those for the paired t-test except median is used instead of mean value. The Wilcoxon signed rank test assumes that the distribution of the difference of pairs is symmetrical. This assumption can be checked; if the distribution is normal, it is also symmetrical. As mentioned earlier, the data follows normal distribution and the Wilcoxon signed ranks test can be used. Table J.1 summarizes the result of the paired t-test (p-values at the 0.05 significance level). All the p-values were greater than 0.05 that means the null hypothesis at the 0.05 significance level are confirmed.

Results of the statistical data analyses showed that in term of tensile splitting strength there is no statistically significant difference between the mean of the normalized tensile splitting strength of the CC and HVFAC mix. While for flexural strength statistical tests indicated that the CC mix had higher normalized flexural strength compared with the HVFAC mix.

In term of fracture energy, normalized results based on Bazant, JSCE-07, and CEB-FIP Model Code 2010 equations showed that the HVFAC mix had higher fracture energy compared with the CC mix.

Table J.1- P-values for statistic tests

Hypothesis	P*	NP**
Tensile Splitting Strength		
$f_{ct(CC)} = f_{ct(HVFAC)}$	0.895	0.838
Flexural Strength		
$f_{r(CC)} > f_{r(SCC)}$	0.954	0.970
Fracture Energy		
Bazant Equation		
$G_{F(HVFAC)} > G_{F(CC)}$	0.684	0.637
JSCE-07 Equation		
$G_{F(HVFAC)} > G_{F(CC)}$	0.658	0.688
CEB-FIP Model Code 2010 Equation		
$G_{F(HVFAC)} > G_{F(CC)}$	0.612	0.637

*: parametric test

** : non- parametric test

APPENDIX K
STATISTICAL DATA ANALYSIS OF SCC

STATISTICAL DATA ANALYSIS OF SCC

To compare the tensile splitting strength, flexural strength, and fracture energy test results of both the CC and the SCC mixes, the results must be adjusted to reflect the different compressive strengths. The tensile splitting and flexural strength of the mix is a function of the square root of the compressive strength of the concrete. Also, fracture energy is a function of the compressive strength with powers of 0.46, 0.33, and 0.18 based on the Bazant et al., the JSCE-07, and the CEB-FIP Model Code 2010, respectively. Therefore, to normalize the data for comparison, the tensile splitting and flexural strengths were divided by the square root of the compressive strengths, while the fracture energies were divided by the aforementioned powers of the compressive strengths.

Statistical tests (both parametric and nonparametric) were used to evaluate whether there is any statistically significant difference between the tensile splitting strength, flexural strength, and fracture energy test results for the CC and SCC mixes.

Parametric Test

The paired t-test is a statistical technique used to compare two population means. This test assumes that the differences between pairs are normally distributed. If this assumption is violated, the paired t-test may not be the most powerful test. The hypotheses for the paired t-tests for tensile splitting strength, flexural strength, and fracture energy are as follows:

H_0 : The mean of the normalized tensile splitting strength (flexural strength) of the CC mix is equal to the SCC mix [$f_{ct}(CC) = f_{ct}(SCC)$ or $f_r(CC) = f_r(SCC)$].

H_a : Not H_0

H_0 : The mean of the normalized fracture energy of the SCC mix is greater than the CC mix [$G_F(SCC) > G_F(CC)$].

H_a : Not H_0

The statistical computer program SAS 9.2 was employed to perform these statistical tests. Both Kolmogorov-Smirnov (K-S) and Anderson-Darling (A-D) tests showed the data – the differences between the tensile splitting strength, flexural tensile strength, and fracture energy of the mixes – follow a normal distribution. Therefore, the paired t-tests could be performed. Table K.1 summarizes the result of the paired t-test (p-values at the 0.05 significance level). All the p-values were greater than 0.05, which means the null hypotheses at the 0.05 significance level are confirmed.

Nonparametric Test

Unlike the parametric tests, nonparametric tests are referred to as distribution-free tests. These tests have the advantage of requiring no assumption of normality, and they usually compare medians rather than means. The Wilcoxon signed-rank test is usually identified as a nonparametric alternative to the paired t-test. The hypothesis for this test is the same as those for the paired t-test except median is used instead of mean value. The Wilcoxon signed rank test assumes that the distribution of the difference of pairs is symmetrical. This assumption can be checked; if the distribution is normal, it is also symmetrical. As mentioned earlier, the data follows normal distribution and the Wilcoxon signed ranks test can be used. Table K.1 summarizes the results of the paired t-test (p-values at the 0.05 significance level). All the p-values were greater than 0.05, which means the null hypotheses at the 0.05 significance level are confirmed.

Results of the statistical data analyses showed that in terms of tensile splitting strength and flexural tensile strength, there is no statistically significant difference between the mean of the normalized values of the SCC and CC mixes.

For fracture energy, on the other hand, the normalized results based on the Bazant, JSCE-07, and CEB-FIP Model Code 2010 equations indicated that the SCC mix had higher fracture energy compared with the CC mix.

Table K.1 - P-values for statistic tests

Hypothesis	P*	NP**
Tensile Splitting Strength		
$f_{ct(CC)} = f_{ct(SCC)}$	0.60	0.748
Flexural Strength		
$f_{r(CC)} = f_{r(SCC)}$	0.945	0.998
Fracture Energy		
Bazant Equation		
$G_{F(SCC)} > G_{F(CC)}$	0.963	0.960
JSCE-07 Equation		
$G_{F(SCC)} > G_{F(CC)}$	0.965	0.971
CEB-FIP Model Code 2010 Equation		
$G_{F(SCC)} > G_{F(CC)}$	0.978	0.971

* : parametric test

** : non- parametric test

VITA

Mahdi Arezoumandi was born in Tehran, Iran in 1977. He received his Bachelor of Civil Engineering degree in 2000 and his Master of Science in Earthquake Engineering degree in 2002 from the Tehran Polytechnic University. He began his PhD at Missouri University of Science and Technology in August 2009.

After graduation with master degree, he worked as a structural design engineer at Small Industries and Industrial Park Organization (SIIPO) for five years. He was involved in the design and construction of a wide range of civil engineering structures such as buildings, bridges, industrial structures, and water reservoirs. As a structural engineer, he was also involved in the design of steel and concrete buildings (both residential and commercial). In December 2013, he received his Ph.D. in Civil Engineering from Missouri University of Science and Technology.